THE IMPACT OF COST AND FOULING ON HEAT EXCHANGER INVENTORY IN POWER AND REFRIGERATION SYSTEMS

BY

BILAL AHMED QURESHI

A Dissertation Presented to the

DEANSHIP OF GRADUATE STUDIES

KING FAHD UNIVERSITY OF PETROLEUM & MINERALS

DHAHRAN, SAUDI ARABIA

In Partial Fulfillment of the

Requirements for the Degree of

DOCTOR OF PHILOSOPHY

In

MECHANICAL ENGINEERING

MARCH 2014

KING FAHD UNIVERSITY OF PETROLEUM & MINERALS

DHAHRAN, SAUDI ARABIA

DEANSHIP OF GRADUATE STUDIES

This dissertation, written by **Bilal Ahmed Qureshi** under the direction of his dissertation advisor and approved by his dissertation committee, has been presented to and accepted by the Dean of Graduate Studies, in partial fulfillment of the requirements for the degree of **DOCTOR OF PHILOSOPHY** in ***Mechanical Engineering***.

Dissertation Committee

May 4, 2014
Thesis Advisor
Prof. Dr. Syed M. Zubair

4 May 2014
Co-Advisor
Dr. Mostafa H. Sharqawy

Department Chairman
Dr. Zuhair M. Gasem

4/may/2014
Member
Prof. Dr. Shahzada Z. Shuja

Dean of Graduate Studies
Dr. Salam A. Zummo

May 4, 2014
Member
Prof. Dr. Mohamed A. Antar

20/5/14
Date

4-May-2014 Member
Dr. Faizur Rahman

[*This work is dedicated to my wife and children.*]

ACKNOWLEDGEMENTS

All praises and thanks are due to Allah (subhaanahu wa ta'aala) for bestowing me with knowledge, health and patience to complete this work. After that, acknowledgement is due to KFUPM and NSTIP (project # 08-ENE50-4) for the support given to this research project through its funding and excellent facilities.

I acknowledge, with deep gratitude and appreciation, the inspiration, encouragement, valuable time and continuous guidance given to me by my Committee Chairman, Dr. Syed M. Zubair. Secondly, I am grateful to my Committee Co-Chairman, Dr. Mostafa H. Sharqawy and Committee members Dr. Mohamed A. Antar, Dr. S. Z. Shuja and Dr. Faizur Rahman for their constructive guidance and technical support. Thanks are also due to the Department secretaries, Mr. Qamar Zaman, Mr. Jaleel and Mr. Lateef for their help and assistance. Special thanks are due to Mr. Syed Younus Ahmed and Mr. Peter Varghese for their continued technical support for the experimental work.

My heart-felt gratitude to my wife and children for the sacrifices they made. Also, my sincerest appreciation for the support and encouragement from my parents, my wife's parents and my brothers. I would also like to thank my friends Usama Siddiqui, Haris Malik, Usman Kaleem, Ameer Hamza, Osama Hasan, Khalid and all others who provided wonderful company and good memories that will last a life time.

Table of Contents

LIST OF TABLES

LIST OF FIGURES

ABSTRACT

Name: Bilal Ahmed Qureshi

Title of Study: The Impact of Cost and Fouling on Heat Exchanger Inventory in Power and Refrigeration Systems

Major Field: Mechanical Engineering

Date of Degree: March, 2014

The first part of this study focuses on predicting the effect of variation in inventory (overall conductance) allocated on power and refrigeration systems wherein fouling, which results in decrease of this inventory, is considered as a main application. Experimental work was performed on a 1.5 ton vapor compression system which showed that system parameters and properties varied logarithmically when overall conductance was reduced. Then specific examples of power and refrigeration systems were simulated beginning with endoreversible single-stage cycles and then the Rankine and simple vapor compression cycles. Based upon these simulations and the experimental work, an equation was proposed to predict effect of reduction in overall conductance on all system properties and performance parameters using non-dimensional quantities. Agreement was found to be within 1.15% of simulated and predicted values. Such an equation helps to reduce the number of experiments and/or numerical simulations.

The second part of this study focused on thermoeconomic optimization of different power and refrigeration systems for endoreversible and irreversible cases using the allocated heat exchanger inventories. The systems investigated include a thermodynamic model of a vapor compression cycle with dedicated mechanical subcooling as well as endoreversible cases of the dedicated and integrated mechanical subcooling cycles along with an endoreversible power cycle with one feedwater heater. It was found that a practical minimum with respect to the dimensionless cost equations for the fluid to ambient high-side absolute temperature ratio existed for all cost equations. The connection between endoreversible and irreversible cycles for this ratio was shown to establish viability of the endoreversible results. Furthermore, it was found that the cost functions for simpler cycles can be derived from those of more complex systems. Also, if the only difference between a power and refrigeration cycle is that the cycle is flowing in the opposite direction, then multiplying a minus sign on one side of the cost equations of a system would provide the cost equations for the other system. Finally, a holistic view of cost optimization in power and refrigeration systems is presented, which constitutes a step forward in thermoeconomic optimization theory as it resulted in generalized cost equations.

DOCTOR OF PHILOSOPHY IN MECHANICAL ENGINEERING

KING FAHD UNIVERSITY OF PETROLEUM AND MINERALS

DHAHRAN, SAUDI ARABIA

ملخص بحث

درجة الدكتوراة في الفلسفة

الاسم : بلال أحمد قريشي

العنوان: أثر التكلفة والإفساد في مبادل حراري المخزون في الطاقة وأنظمة التبريد

التخصص : الهندسة الميكانيكية

تاريخ التخرج : مارس 2014

يركز الجزء الأول من هذه الدراسة على تأثير الكمية (UA) والتي تعبر عن المخزون الحراري على الاتساخ في المبادلات الحرارية في محطات القوي الكهربائية وأنظمة التبريد و التي يؤدي تزايد الاتساخ فيها إلى تناقص المخزون الحراري. وقد تم اجراء دراسة معملية على وحدة تبريد سعة طن ونصف تبريد تعمل بضغط البخار حيث أوضحت الدراسة أن متغيرات التشغيل والخصائص تتغير بشكل لوغاريثمي مع تغير المخزون الحراري. وبناء على ذلك تمت محاكاة دائرة تبريد ذات أطراف مرتجعة أحادية المرحلة بالإضافة إلى دائرة مبسطة تعمل بضغط البخار. وقد تم استنباط معادلة للتنبؤ بالانخفاض في المخزون الحراري وذلك من الدراسة المعملية ونتائج المحاكاة. وتقوم المعادلة المستنبطة بحساب التغير المتوقع في المخزون الحراري حسب ظروف التشغيل وخواص المواد المستخدمة بنمط لا يعتمد على نظام الوحدات المستخدم وقد تم حساب التغير في نتائج المعادلة بالمقارنة بالنتائج المعملية وكانت متوافقة حيث لا يتعدى الخطأ فيها 1.15%. ومن المتوقع أن تسهم هذه المعادلة في توفير الكثير من التجارب المعملية والمحاكاة في المستقبل.

وتم في الجزء الثاني من الدراسة التركيز على الوضع الأمثل على أساس مباديء كل من الديناميكا الحرارية والاقتصاد لمختلف النظم التي تمت دراستها. واشتملت الدراسة على نموذج مبني على الديناميكا الحرارية لوحدة

تبريد تعمل بضغط البخار مزودة بنظام تبريد ميكانيكي دوني بالإضافة لمنظومة قوى حرارية مع نظام سخان المياه المغذي. وقد تبين وجود حد أدنى عملي فيما يتعلق بمعادلات التكلفة ذات نمط لا يعتمد على نظام الوحدات المستخدم لنسبة درجة حرارة السوائل المستخدمة مقسومة على درجة الحرارة المطلقة وذلك لكل المعادلات.كما تبينت الصلة بين الدورات مرتجعة النهايات والأخرى الغير مرتجعة وعلاوة على ذلك، فقد وجد أن وظائف التكلفة للدورات والأنظمة المعقدة يمكن استخلاصها من الأنظمة البسيطة .أيضا، إذ كان الفرق الوحيد بين دورات توليد القدرة ودورات التبريد هو ان اتجاه التدفق يكون معاكسا لبعضهم البعض وبالتالي فإن ضرب علامة السالب فى جانب واحد من معادلات التكلفة من شأنه أن يوفر معادلات التكاليف للنظام الآخر. أخيرا، تم تقديم نظرة شمولية لتحسين التكلفة في أنظمة الطاقة والتبريد، الأمر الذي يشكل خطوة إلى الأمام في أيجاد ظروف التشغيل الأمثل حراريا واقتصاديا كما بينت الدراسة أنه يمكن تعميم معادلات التكلفة على لعديد من المنظومات.

درجة الدكتوراة في الفلسفة في الهندسة الميكانيكية

جامعة الملك فهد للبترول والمعادن

الظهران– المملكة العربية السعودية

CHAPTER 1

INTRODUCTION

In this chapter, the main points of discussion will be the motivation, objectives and method of solution of this research work.

1.1 Motivation

Heat exchanger inventory is an expensive commodity. The effects of its allocation, reduction during operation (due to fouling) as well as optimizing the heat exchanger inventory of these cycles has been a subject of much discussion. Conductances are not unlimited in availability and thus have a certain dollar value attached to them that must be distributed wisely. This entails not only distribution with consideration of best performance but also of lowest cost. Thermoeconomics is a known method for this type of optimization. Furthermore, experimental and numerical work related to fouling consumes time and money. If a mathematical model can be presented that can help to

predict necessary parameters of the system, this can help to reduce the number of experiments and numerical simulations.

1.2 General Background

The heat exchanger inventory is defined as the sum of the conductances of the condenser and evaporator in a power or refrigeration cycle. One of the cornerstones of sustainable development is the cost-effective fuel saving of systems that use or produce useful energy. This, in turn, calls for more intensive and extensive system analysis while the system is still in its design phase. Such analysis has to be multi-disciplinary. Accessing the analysis from the discipline of thermodynamics is the advantage of thermoeconomics. Thermoeconomics was first developed during the sixties. The name was coined by professor M. Tribus [1]. Development of thermoeconomics to handle energy-intensive systems in general was initiated by R. Gaggioli [2-3]. In the last 25 years, the development of thermoeconomics has been impressive. Works related to endoreversible thermoeconomics by De Vos [4-5] constitutes one approach.

Where there are heat exchangers, fouling will often inevitably follow. Fouling studies are performed to ascertain the effect on performance parameters so that contingency plans can be adopted for times of failure or clean up schedules drawn up to avoid the former. Heat exchangers are one of the main components of these systems. Therefore, even a small performance degradation, due to fouling, has the potential to cause further energy consumption and/or decrease cooling capacity along with the

efficiency. This results in higher costs of running the equipment. Foulants vary in nature from mold compounds, human hair and textile fibers to airborne particulate matter and dust [6] but they all result in an overall decrease in the ability of the heat exchanger to transfer heat. Heat exchanger design is based on best practice values and experience related to fouling resistance. Experimental and numerical studies on fouling, when done correctly, often take a great amount of time and incur high costs. Reducing the number of experiments, thus, becomes a matter of great interest as this will result in saving of both time and money.

1.3 Thesis Objectives

The overall objective of this thesis dissertation is to examine the impact of fouling and cost-based optimization on both power and refrigeration systems. In this regard, the following specific objectives are proposed:

- To investigate a model, applicable to both power and refrigeration systems, that can predict the effect of reduction in conductance (UA), due to fouling, on these systems.
- Application of the proposed performance degradation model on vapor compression and power cycles using thermodynamic models.
- Experimental evaluation of the performance characteristics of a vapor compression cycle, under fouled conditions.

- Thermoeconomic optimization using a thermodynamic model for a vapor compression refrigeration system.
- Thermoeconomic optimization for a Carnot representation of a mechanical subcooling system.
- Thermoeconomic optimization of a vapor compression cycle with mechanical subcooling using a thermodynamic model.

1.4 Inventory Reduction due to Fouling: Research Approach

The first objective mentioned is to develop a model to predict effect of fouling resulting in UA-degradation on all system (properties and performance) parameters. A model will be presented that is to be used to connect three types of cases: 1) Fouling in the HX on high temperature-side only, 2) Fouling in the HX on low temperature-side only, and 3) Fouling (equally) in the HX on both high and low-temperature-side. The UA-value, which represents the conductance affected due to fouling, will be decreased from 0 to 50% to simulate the three cases mentioned. Using these simulations, an attempt will be made to develop a relationship between these three types of cases. Once this is achieved, thermodynamic models of both power and refrigeration cycles will be simulated to ascertain practical applicability of the proposed model.

Experimental evaluation of the performance characteristics of a vapor compression cycle, under fouled conditions, will also be done. For this purpose, a 1.5 ton

residential system will be bought from the local market and installed. Fouling will be simulated by appropriately blocking the required percentage of surface area of the condenser.

1.5 Optimal Allocation for Cost Minimization: Research Approach

Thermoeconomic optimization of refrigeration systems by minimizing the heat exchanger inventory cost for cases involving constant work rate, constant cooling load and constant heat rejection rate, based on a Carnot refrigerator model, was studied in the past. Therefore, in this work, initially, a simple vapor compression cycle (SVCC) based on a thermodynamic model will be simulated in EES [6] to ascertain the practical application of their cost functions and to understand how they behave in real systems. Then, the same approach is used for the case of vapor compression cycles with mechanical subcooling. One type is the dedicated mechanical subcooling system and its schematic (See Fig. 1.1) is given below while the other is the integrated mechanical subcooling system. This will result in non-dimensional cost functions that are minimized by taking derivatives with respect to relevant variables. Thermoeconomic optimization of a Carnot power cycle with one feedwater heater will also be performed as the Carnot-based simple power plant has already been studied. Finally, a holistic view of thermoeconomic optimization will be presented based on these cycles.

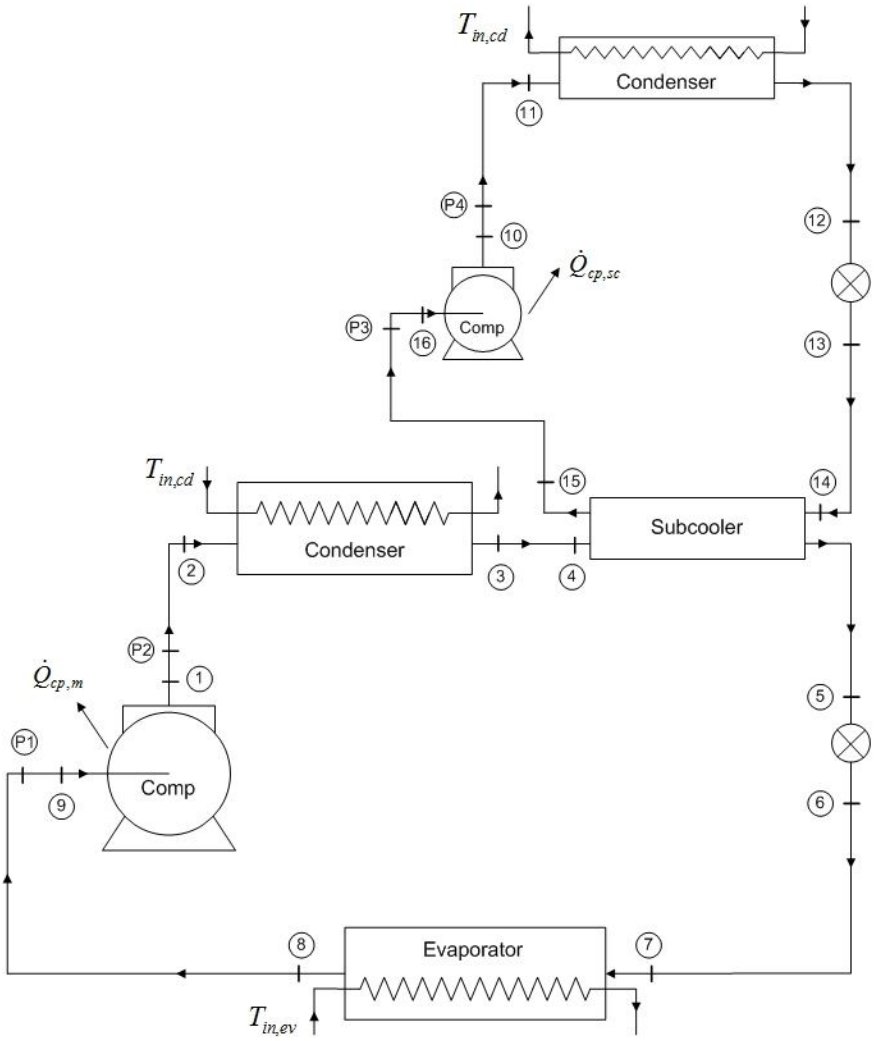

Figure 1.1. Schematic of a dedicated mechanical subcooling system

1.6 Organization

Chapter 2 summarizes the literature survey carried out during the current work. The mathematical modeling of the various systems used in the thesis is outlined in chapter 3. Details regarding the experimental work with the vapor compression system are presented in chapter 4. Details regarding the experimental and numerical work with the vapor compression system with dedicated mechanical subcooling are explained in chapter 5. Chapter 6 explains how to predict fouling in power and refrigeration systems. Chapter 7 outlines the cost optimization in power and refrigeration systems. Finally, conclusions and recommendations are presented in chapter 8.

CHAPTER 2

LITERATURE REVIEW

In this chapter, literature review is presented, which focuses on the effects of heat exchanger inventory allocation, its reduction and optimization.

2.1 Optimal Allocation for Cost Minimization

The Theory of Exergetic Cost was first developed by Valero *et al*. [7-8] and Lozano *et al*. [9]. The first to use thermoeconomics to diagnose a refrigeration plant was d'Accadia and de Rossi [10]. The case of a simple vapor compression cycle was used to demonstrate what would happen if one of the components malfunctioned and what its effect would be on the other components. The highest impact on fuel was due to the electric motor running the compressor. d'Accadia and de Rossi [11] also presented an optimization process to a refrigeration plant based on the theory of exergetic cost to evaluate the costs of all plant components unit-by-unit, leading to a simplified cost minimization methodology for the whole plant.

Optimization of endoreversible and irreversible vapor compression refrigeration systems and heat pumps subject to finite time and finite size constraints have been the subject of much interest in the past. As far as heat exchanger inventory allocation is concerned, authors such as Bejan [12-15] and Chen *et al*. [16] have addressed the issue as it pertains to minimizing the heat exchanger inventory for a constant work rate, or a constant cooling load. The opposite has also been investigated (minimizing the work rate or maximizing the cooling load for a constant heat exchanger inventory) by Bejan [14], Klein [17], Wu [18], Chen *et al*. [19] and Sahin and Kodal [20].

Wall [21] performed thermoeconomic optimization of a heat pump system. He chose efficiencies of the compressor, condenser, evaporator and electric motor as variables to be optimized. It was shown that the efficiency of the electric motor is the most important variable. Wu *et al*. [22] investigated the operation of a Carnot heat pump and derived the relation between optimal profit and coefficient of performance of an endoreversible Carnot heat pump based on a relatively general heat transfer law: $q \propto \Delta(T^n)$. The exponent *n* represented cases of convection heat transfer (n = 1), radiation heat transfer (n = 4) and the linear phenomenological law in irreversible thermodynamics (n = -1). The optimization process was explained for different values of the ratio of work input and energy output prices.

El-Sayed [23] performed thermoeconomic optimization of three mechanical vapor-compression seawater distillation units. He found that increased unit size is achieved at the expense of a tolerable decrease in efficiency. Taking the cooling load per

unit total cost as objective function, Sahin and Kodal [24] performed finite time thermoeconomic analysis for an endoreversible refrigerator and heat pump while Kodal *et al*. [25] did for irreversible single stage vapor compression refrigeration system and heat pump. Antar and Zubair [26] investigated minimizing the heat exchanger inventory cost in refrigeration and heat pump systems for cases involving constant work rate, constant cooling load and constant heat rejection rate. They found that the total inventory reached a minimum when the unit cost ratio attained unity. That investigation was based on a Carnot refrigerator model developed by Bejan [14], which concluded that optimal distribution of heat exchanger area required equal allocation. The same conclusion was reached by Klein and Reindl [27].

Sahin and Kodal [28] performed finite size thermoeconomic optimization for endoreversible heat engines using a new thermoeconomic optimization criterion i.e. power output per unit total cost. Analytical equations for optimum working fluid temperatures, thermal efficiency, distribution of heat exchanger areas and specific power output were determined. The effect of relative fuel cost was also discussed. The Carnot model developed by Bejan [14] was used by Antar and Zubair [29] to study cost optimization of power plant heat exchanger inventory for a specified power output. The total inventory reached a minimum when the unit cost ratio attained unity. Kodal and Sahin [30] performed finite size thermoeconomic optimization for irreversible heat engines using a new thermoeconomic optimization criterion i.e. power output per unit total cost. They showed that the optimal performance characteristics depend on the

relative fuel cost parameter but since this parameter varies for different countries, the economical condition of a country should be considered for the optimal design of a heat engine.

Thermoeconomic optimization of combined cycle power plants was performed by Bandyopadhyay *et al*. [31]. Flexibility in selecting different working fluids at different operating pressures were identified for optimal design and operation of the combined cycle power plant. Thermoeconomic optimization of heat recovery steam generators of combined cycle gas turbine power plants considering off-design operation was performed by Rovira *et al*. [32]. The results of the optimizations were compared to those obtained with usual thermoeconomic models based on design conditions performance. The differences between the optimum designs reached with both optimization models in the 400MW configurations were almost negligible but the amortization cost and the efficiency of the design obtained with the new model become slightly lower. Silveira and Tuna [33] presented a thermoeconomic functional analysis method based on the Second Law of Thermodynamics and applied it to analyze four cogeneration systems. The cogeneration system consisting of a gas turbine with a heat recovery steam generator, without supplementary firing, was found to have the lowest exergetic production cost. Abusoglu and Kanoglu [34] provided a review of exergoeconomic analysis and optimization of combined heat and power production. Main thermoeconomic methodologies available in literature were described and their advantages and disadvantages with respect to one another were compared and discussed.

Sahin *et al*. [35] studied the thermoeconomical performance optimization of a two-stage irreversible combined refrigeration system. The cooling load per unit total cost was taken as the objective function as before wherein performance and design parameters were analytically derived. The irreversibility of heat transfer across finite temperature differences, the heat leak loss between the external heat reservoirs and the internal dissipation of the working fluids were considered. Results were also compared with a single-stage system and it was found that the ratio of the optimal performance coefficients increased as the level of internal irreversibility increased. Additionally, Sahin and Kodal [36] studied an endoreversible two-stage combined refrigeration system, which was optimized with respect to the cooling load per total cost. That study, however, involved only one evaporator. The study performed by Morales [37] involved a two-stage Carnot refrigerator which expanded the work done by Antar and Zubair [26] to a two-stage Carnot refrigerator system with two evaporators. In his work, cost optimization was performed for constant rate of work, heating and cooling. He found that only two variables had a significant minimum with respect to the dimensionless Heat Exchanger Inventory Cost Equation (HEICE): θ (the ratio between the condenser temperature to average coolant temperature), and Φ (the ratio between the evaporator temperature to condenser temperature). Also, it was found that all the dimensionless cost functions were minimized at the same θ.

Misra *et al*. [38] performed a thermoeconomic optimization of a single effect water/LiBr vapour absorption refrigeration system for air-conditioning application.

Sequential local optimization of the system was carried out unit by unit in which the total cost consisted of both the capital investment as well as operation and maintenance cost. The authors performed a similar analysis on an aqua-ammonia vapour-absorption refrigeration system [39] as well. Rosen and Dincer [40] carried out a thermoeconomic analysis of a coal fired electrical generating station based on capital cost only. They emphasized that the reason for this is that the capital cost is often the most significant cost component and costs other than that are often proportional to it. Thus, qualitative agreement is expected. They showed that an important parameter is the ratio of the thermodynamic loss rate to capital cost. Furthermore, a systematic correlation exists for capital cost and exergy loss. It should be noted that objective function originally proposed by Sahin and Kodal [24] was modified by Chen *et al*. [41] to include the maintenance cost.

Durmayaz *et al*. [42] provided an extensive review on optimization of thermal systems based on finite-time thermodynamics and thermoeconomics that considered various objective functions. They concluded that finite-time thermoeconomic analysis was still in its early stages and needed more work in fundamental theory development and applications. Therefore, the finite-time exergoeconomic performance optimization of a Carnot engine was investigated using the profit maximization criterion as the objective by Chen *et al*. [43]. The focus of this paper is to search the compromised optimization between economics (profit) and the utilization factor (efficiency) for finite-time irreversible cycles. The analytical formulae concerning optimal profit versus efficiency,

the maximum profit and the corresponding efficiency are derived. Tyagi *et al*. [44] proposed a new thermoeconomic approach and parametric study of an irreversible regenerative Brayton refrigeration cycle. The objective function, i.e. cooling load per unit cost, was optimized with respect to the state point temperatures for a typical set of operating conditions. The power input and cooling load were found to be decreasing functions of the expansion outlet temperature, while it is the reverse in the case of COP. Selbas *et al*. [45] carried out an exergoeconomic optimization of subcooled and superheated vapor compression refrigeration cycles. Beyer's method [46] was used in order to optimize the system components for different refrigerants. The cost function consisted of unit cost of input exergy and capital cost of each element of the system. Optimum subcooling and superheating temperatures were found along with the optimum heat exchanger areas. Results were compared with manufacturers' values and it was seen that results were parallel with them. Kizilkan *et al*. [47] performed an exergoeconomic optimization of a LiBr-water absorption refrigeration system similar to that of Misra *et al*. [38] with the difference that these authors used the structural method [46] instead of using an average cost approach. Optimum heat exchanger areas with corresponding system component temperatures were determined for a 20 kW cooling load. Kim [48] introduced a new thermoeconomic methodology for energy systems. The method states that the number of the proposed equation is only one in each field, and it is developed with a wonergy newly introduced in this paper. The wonergy is defined as an energy that can equally evaluate the worth of each product. For cost optimization, the cost of fuel and capital cost were used. It was concluded that exergy is the most reasonable in cost

allocation and cost analysis, and all of exergy, enthalpy and profit are reasonable in cost optimization. Silveira *et al*. [49] presented a thermoeconomic optimization methodology for the analysis and design of energy systems. The objective was to minimize the exergetic production cost, which includes capital and operational cost for a given amount and type of exergy, depending on the analyzed energy system. One of the systems analyzed was a steam compression refrigeration system. Sayyaadi and Nejatolahi [50] performed a multi-objective optimization of a cooling tower assisted vapor compression refrigeration system. The total exergy destruction of the system (as a thermodynamic criterion) and the total product cost of the system (as an economic criterion) were considered as two objective functions simultaneously. A thermodynamic model based on energy and exergy analyses and an economic model according to the Total Revenue Requirement (TRR) method were developed. The results show that the multi-objective design more acceptably satisfies generalized engineering criteria than the other two single-objective optimized designs. A review of the performance optimization criteria based on the finite-time thermodynamics for absorption refrigerator systems was been presented by Wouagfack and Tchinda [51]. The coefficient of performance, the cooling load, the thermo-economic objective function, the thermo-ecological objective function and the new thermo-ecological objective function were discussed. The authors aimed to stimulate interest in defining of new performance criteria for the optimization of absorption refrigerators.

Mumanachit [52] carried out a comparison of the performance and economic viability of an ammonia compound system to an NH_3/CO_2 cascade system applied to a low-temperature freezer application with a load of 680 Tons. Component-based system-level simulations provide the basis for identifying the relative operating costs of the two systems and, therefore, the life cycle savings associated with the operating costs. The simulations indicated that the cascade heat exchanger that appropriately balanced performance with cost should be designed to have a pinch point temperature difference of 10 ^{o}F at its nominal operating conditions. Rezayan and Behbahaninia [53] performed a thermoeconomic optimization and exergy analysis of a NH_3/CO_2 cascade refrigeration system. The objective function was the total annual cost of the system which included costs of input exergy to the system and annualized capital cost of the system. The condensing temperature of ammonia, evaporating temperature of carbon dioxide, condensing temperature of carbon dioxide and temperature difference in the cascade condenser were chosen as decision variables. The optimization process was carried out using Direct Search Method. The annual cost of the system was reduced by 9.34 percent compared to the base case design. Thermoeconomic optimization of an ammonia-water power/cooling cogeneration cycle was investigated by Zare *et al*. [54] in order to determine the thermodynamic performance of the cycle and assess the unit cost of products. The results show that the sum of the unit cost of the cycle products obtained through thermoeconomic optimization is less than by around 18.6% and 25.9% compared to the cases when the cycle is optimized from the viewpoints of first and second laws of thermodynamics, respectively. It was also found that for each increase of $3/ton in unit

cost of the steam as the heat source, the unit cost of the output power and cooling is increased by around $7.6/GJ and $15-19/GJ, respectively.

Thermoeconomic cost analysis of a 600 MWe oxy-combustion pulverized-coal-fired power plant was performed by Xiong *et al*. [55]. It was found that, in comparison to the corresponding conventional supercritical plant with the same gross output, the additional power consumption in the oxy-combustion system increases the unit exergy costs (or unit thermoeconomic costs) of products by about 10%. On the other hand, the additional monetary cost, including investment cost, interest, and operation and maintenance cost, in the oxy-combustion system increases the unit thermoeconomic costs of products by nearly another 10%. Bassily [56] performed numerical cost optimization and irreversibility analysis of the triple-pressure reheat steam-air cooled GT commercial combined cycle power plants. It was determined that optimizing the net revenue could result in an annual saving of about $29.2 million for a 400 MW power plant.

It was noted that thermoeconomic optimization of mechanical subcooling systems and Carnot power cycles with one feedwater heater have not been performed; neither on the Carnot level nor using a thermodynamically modeled system. Furthermore, a holistic view combining these analyses was also not present for the particular methodology to be considered in this study.

2.2 Inventory Reduction due to Fouling

Fouling of heat transfer surfaces is a serious problem that affects the design and operation of heat exchangers. Fouling involves the formation of deposits of low thermal conductivity on heat transfer surfaces, leading to degradation in the rate of heat transfer. At the design stage fouling is accounted for by increasing the heat transfer surface area. According to Garrett-Price *et al*. [57], the general practice is to design heat exchangers with an average oversize of about 35%. Heat exchangers designed with excess surface area tend to be larger and heavier. This evidently results in extra costs to cover additional material, transportation and installation. To maintain the desired heat transfer rates during the operational stage of a heat exchanger periodic cleaning of heat transfer surfaces is a necessity. Periodic cleaning results in additional costs arising from loss of production and additional maintenance activities. It is not surprising that fouling related costs constitute a significant portion of the industry's running costs [58]. The nature of the fouling curve with time is usually logarithmic, linear or asymptotic [59] as shown in Fig. 2.1. The practical effect of these different curves is the time taken to achieve a certain amount of inventory reduction.

Fouling is usually classified into six categories depending on the key physical or chemical process essential to the particular fouling mechanism. The categories are crystallization, particulate, chemical, corrosion, biological and solidification [59]. Crystallization fouling accounts for over 25% of the fouling problems encountered. Crystallization fouling, or scaling, occurs when inverse solubility salts that are originally dissolved in the process fluid, deposit on heat transfer surfaces. A notable feature of

inverse solubility salts is that their solubilities decrease with increase in temperature. Salts that normally lead to scaling are usually sulfates, phosphates and carbonates of calcium.

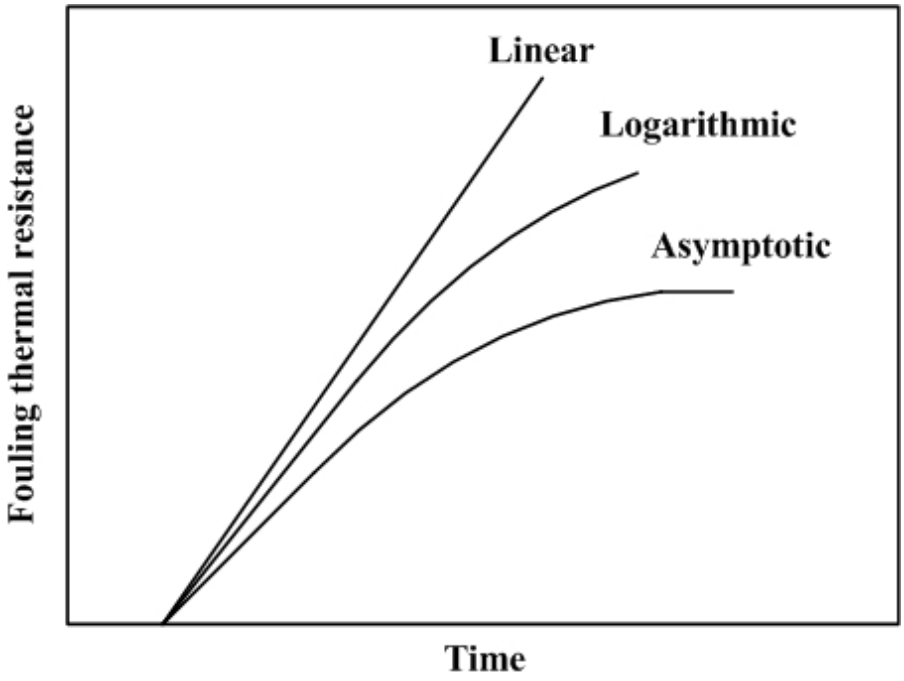

Figure 2.1. Various fouling models

Mwaba *et al*. [60] performed crystallization fouling experiments on heat exchanger surfaces. They noticed an asymptotic behavior in the development of the fouling resistance. The fouling resistance was calculated from measured temperatures and the applied heat flux. A new correlation was proposed that can assist heat exchanger operators to plan cleaning schedules. Merheb *et al*. [61] showed that low-frequency waves can be used to detect fouling in plate heat exchangers by comparing evolution of acoustic wave parameters such as power and delay.

Pahlavanzadeh *et al*. [62] experimentally investigated the effect of two tube inserts on the heat transfer enhancement, pressure drop and mineral salts fouling mitigation in tube of a heat exchanger. The pressure drop increased substantially by 46% for wire coil and 500% for wire mesh. Wire coil insert with vibration mitigate mineral salts fouling (scaling) about 34%, and wire mesh have no effect on scaling, however, it sometimes increased deposit rate. Cussac [63] studied particulate fouling on Alloy-800 heater tubes. The influence of bubbles on the deposition of Iron Oxides on the tube surface was studied by using a high-speed movie camera. Zhenhua *et al*. [64] performed an experimental study to investigate calcium carbonate fouling on the heat transfer surface, during forced convective heat transfer. A dynamic monitoring apparatus of fouling resistance was set up which measured required temperatures and flow rates. The fouling behaviors were examined under different factors including fluid velocity, hardness, alkalinity, solution temperature, and wall temperature. Asymptotic fouling curves varying with time were obtained. Perez *et al*. [65] developed a probe for cross

flow heat exchangers in order to accurately estimate in situ convective exchange coefficient as well as the fouling thickness of heat exchangers from a reliable transient state estimation method. The probe accurately predicted the deposit thickness. The device was cheap and technologically simple associated with adapted data processing. On the other hand, Lalot and Palsson [66] employed a neural network based technique to achieve the same. Lim [67] performed experiments of duration 31-53 days to study fouling on water side brazed type of condensers in cooling tower application. This test facility was built because even though BPHEs are widely used in the refrigeration cycles used as water-cooled condensers, fouling characteristics of BPHE are not well understood. Outlet water temperature and refrigerant pressure measurements were found to be the critical measurements as small drifts result in high errors in fouling resistances. Fouling resistances were found to exhibit asymptotic behaviour. Sun [68] investigated the effects of coating and CO_2 sparging on fouling prevention and cooling water use reduction. Four bench-scale experiments were performed. Fouling rates were evaluated by analyzing daily cooling water samples and fouling materials on the tested condenser tubes. The coating on the condenser tubes prevented fouling to some extent. Comparisons of fouling rates between experiments with and without CO_2 indicated that CO_2 was effective in fouling control. Vessakosol and Charoensuk [69] studied the heat transfer and flow field around a cross-flow heat exchanger tube with fouling. Finite element method was used on concentric and eccentric fouling cases. They found that the heat transfer rate of cross-flow heat exchanger depends on the eccentricity and thermal conductivity ratio between the fouling material and fluid. Lei *et al*. [70] experimentally studied the surface

morphology effect, using different roughness and textures, on calcium carbonate fouling in plate heat exchangers. A strong correlation between the surface roughness and the amount of crystallization fouling deposit was reported. Through detailed image analysis, four stages of the formation of crystallization fouling were identified. Albert *et al*. [71] carried out fouling experiments in a double pipe heat exchanger with supersaturated aqueous $CaSO_4$ solution at a Reynolds number of 17,500 corresponding to a flow velocity of 0.65 m/s. Roughness and constriction effects on heat transfer were considered. Mohanty and Singru [72] showed that the Cleanliness Factor can be used as an effective tool for investigation of performance of a shell and tube heat exchanger under fouled conditions. The fouling parameters were predicted by measurements of flow rate and pressure drop. Hence, it can assist the exchanger operators to plan cleaning schedules. Izadi [73] performed an experimental and numerical investigation of fouling in heat exchangers in which an on-line fouling monitoring system was developed. The fouling thermal resistance for selected solutions was measured in real time by this system. Experiments with durations of two to seven days were performed. Multiple contaminants and various effects were studied. The resistance due to fouling was determined by calculating the difference in heat transfer resistance between fouled and clean conditions. Results show flow velocity has the greatest effect on calcium carbonate scale formation. Mayer *et al*. [74] studied the impact of crystallization fouling on a microscale heat exchanger. Fouling experiments with $CaCO_3$ were analyzed regarding thermal and fluid dynamic behavior. It was observed that the fouling behavior in microscale is comparable to that in macroscale.

Work related to fouling in the literature [75-80] shows that such studies are still being done even though there has been a great amount of advancement in technology. Even state space models have been applied to detect fouling in heat exchangers [81]. Pak *et al*. [75] investigated experimentally the effects of air-side fouling on the performance of various condenser coils found in unitary air-conditioning systems and established that, under fouled conditions, the heat transfer performance degraded by 7 – 12% at the standard air face velocity of 1.53 m/s. Yang, Braun and Groll [76], in their experimental work, obtained the fouled conditions after injection of 600 g of dust upstream of the filter–coil combination, which was meant to simulate a year of operation in the field. Depending upon the filter and coil, the coil pressure drops increased in the range of 6–30% for an air velocity of 2.54 m/s. The largest relative effect of fouling on pressure drop occurs for coils with fewer rows, primarily due to higher fin densities. The impact of fouling on air-side effective heat transfer coefficients was found to be relatively small, which ranged from −14% to 4%. Ali and Ismail [78] experimentally investigated evaporator air-side fouling of room air-conditioners showing that COP decreased by more than 57% due to 300 g of real foulant collected from various evaporator coils. Although it was noticed that 110 g of this material did not deposit onto the coils and R12 was used as the refrigerant, which has now been phased out of use. Pu *et al*. [79] studied the effects of biofouling on air-side heat transfer and pressure drop for finned tube heat exchangers by artificially accelerating microorganism growth. Their results indicated that the air-side heat transfer coefficient decreased by 7.2% at 2.0 m/s when the biofouled area ratio was 10%, while it decreased by 15.9% at 2.0 m/s when the biofouled area ratio

was 60%. Furthermore, it caused a 21.8% - 41.3% increase in pressure drop when the air velocity was between 0.5 and 2.0 m/s. Bell and Groll [80] experimentally studied air-side pressure drop in plate-fin and microchannel coils under clean and fouled conditions applicable to residential systems. In terms of pressure drop, they found that both heat exchangers were practically insensitive to Arizona Road Test Dust. Furthermore, in an experimental setup whose results were applicable to residential and small commercial systems, Siegel [82] experimentally found that the doubling in pressure drop due to air-side fouling reduced the air flow by 6.5% only. Bultman *et al*. [83] simulated the effect of partially blocked condensers of a 3-ton vapor compression system and reported that the COP was predicted to decrease by 7.6% when the airflow across the condenser was reduced by 40% for a constant-speed fan. Yang, Braun and Groll [77] developed simulation models for three packaged air conditioners and showed that the equipment cooling capacity is reduced with fouling primarily because of a decrease in air flow due to the increased pressure drop. In most cases, EER (energy efficiency ratio) was reduced (in the range of 1–10%) with fouling primarily due to increased fan power. Also, the impact of the evaporator side fan efficiency was found to be significant. Yang *et al*. [84] developed dimensionless Pi-groups to predict performance of fin-and-tube condensers. Neural network approach was used wherein standard deviation of the trained dimensionless neural networks were 0.66%, 4.83% and 0.11% for the capacity, refrigerant pressure drop and air pressure drop, respectively. Qureshi and Zubair [85-87] have done numerical simulation of different systems under fouled conditions.

Performance degradation (0 to 50%), using various refrigerants, from a first- and second-law standpoint was investigated.

All such studies are time consuming and/or expensive and, thus, any reduction in either one or both is important. One way of doing this is to introduce a new equation that will help predict the effect of UA degradation on properties and performance parameters in such a way as to diminish the computational or experimental work.

CHAPTER 3

MATHEMATICAL MODELS

In this chapter, five models are presented: i) Curzon-Ahlborn cycle, i) Reversed Curzon-Ahlborn cycle, iii) Simple vapor compression system, iv) Rankine power cycle, and v) Vapor compression cycle with dedicated mechanical subcooling. These are used in chapters 5 and 6.

3.1 Curzon-Ahlborn Cycle

In this section, the modeling related to the first objective is outlined. It is known that practical heat engines are less efficient than the classical Carnot cycle. Inefficiencies occur due to heat leaks, finite heat transfer etc. Furthermore, heat capacitances are finite as opposed to infinite. Consider an endoreversible cycle for a heat engine (i.e. Curzon-Ahlborn (CA) model [88]) but with finite heat capacitance (See Fig. 3.1). The following assumptions were made:

- The heat and pressure losses are negligible in the lines

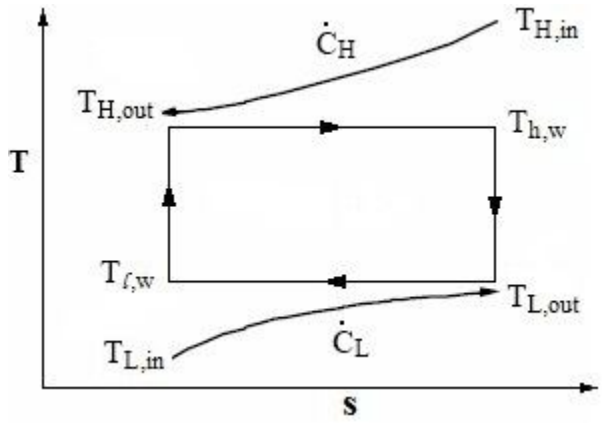

Figure 3.1. Temperature - specific entropy plot for a heat transfer-limited power cycle with finite capacitance rate source and sink temperatures

Heat transfer between the heat source and working fluid is given by:

$$\dot{Q}_H = \alpha\left(T_{H,in} - T_{h,w}\right) \tag{3.1}$$

where

$$\alpha = \varepsilon_H \dot{C}_H \quad ; \quad \varepsilon_H = 1 - \exp(-NTU_H) \quad ; \quad NTU_H = \frac{(UA)_H}{\dot{C}_H}$$

Similarly, the heat transfer between the heat sink and working fluid is given by:

$$\dot{Q}_L = \beta\left(T_{l,w} - T_{L,in}\right) \tag{3.2}$$

where

$$\beta = \varepsilon_L \dot{C}_L \qquad ; \qquad \varepsilon_L = 1 - \exp(-NTU_L) \; ; \qquad NTU_L = \frac{(UA)_L}{\dot{C}_L}$$

The First Law, in this case, is given by:

$$\dot{W} = \dot{Q}_H - \dot{Q}_L \tag{3.3}$$

For the internally reversible cycle, we have

$$\frac{\dot{Q}_L}{\dot{Q}_H} = \frac{T_{l,w}}{T_{h,w}} \tag{3.4}$$

The efficiency of the CA-cycle is, in general, given by:

$$\eta = 1 - \frac{\dot{Q}_L}{\dot{Q}_H} \tag{3.5}$$

and, based on Eq. (3.4), can also be written as [88]

$$\eta = 1 - \frac{T_{l,w}}{T_{h,w}} \tag{3.6}$$

There is a clear similarity to the Carnot efficiency:

$$\eta_{Carnot} = 1 - \frac{T_{L,in}}{T_{H,in}} \tag{3.7}$$

Percentage decrease in conductance (UA) due to fouling is given by:

$$UA_p = \left(1 - \frac{UA}{(UA)_{cl}}\right) x100 \tag{3.8}$$

A similar model for reversed CA-cycle can be made as well, which is done in the next section.

3.2 Reversed Curzon-Ahlborn Cycle

In this section, the modeling related to the first objective is outlined. It is known that practical refrigeration cycles are less efficient than the classical reversed Carnot cycle. Inefficiencies occur due to heat leaks, finite heat transfer etc. Furthermore, heat capacitances are finite as opposed to infinite. Consider an endoreversible cycle for a refrigerator (i.e. reversed Curzon-Ahlborn (CA) model) but with finite heat capacitance (See Fig. 3.2). The following assumptions were made:

- The heat losses are negligible in the lines
- The pressure losses are negligible in the lines

Heat transfer between the heat sink and working fluid is given by:

$$\dot{Q}_H = \alpha \left(T_{h,w} - T_{H,in}\right) \tag{3.9}$$

where

$$\alpha = \varepsilon_H \dot{C}_H \quad ; \quad \varepsilon_H = 1 - \exp(-NTU_H) \quad ; \quad NTU_H = \frac{(UA)_H}{\dot{C}_H}$$

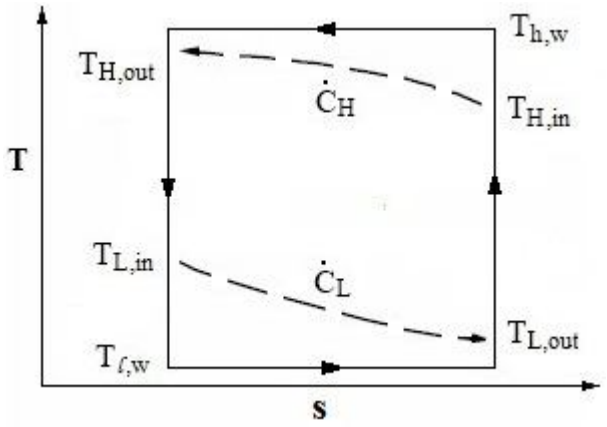

Figure 3.2. Temperature - specific entropy plot for a heat transfer-limited refrigeration cycle with finite capacitance rate source and sink temperatures

Similarly, the heat absorption process is given by:

$$\dot{Q}_L = \beta\left(T_{L,in} - T_{l,w}\right) \tag{3.10}$$

where

$$\beta = \varepsilon_L \dot{C}_L \quad ; \quad \varepsilon_L = 1 - \exp(-NTU_L) \; ; \quad NTU_L = \frac{(UA)_L}{\dot{C}_L}$$

The First Law, in this case, is given by:

$$\dot{W} = \dot{Q}_H - \dot{Q}_L \tag{3.11}$$

For the internally reversible cycle, we have

$$\frac{\dot{Q}_L}{\dot{Q}_H} = \frac{T_{l,w}}{T_{h,w}} \tag{3.12}$$

The coefficient of performance of the reverse CA-cycle is, thus, given by:

$$COP = \frac{T_{l,w}}{T_{h,w} - T_{l,w}} \tag{3.13}$$

Percentage decrease in conductance (UA) due to fouling is given by:

$$UA_p = \left(1 - \frac{UA}{(UA)_{cl}}\right) x100 \tag{3.14}$$

3.3 Simple Rankine Power Cycle

The following assumptions were made in the model:

- The heat losses are negligible in the lines
- The pressure losses are negligible in the lines

3.3.1 Description and modeling

A simple Rankine power cycle consists of a pump, condenser, turbine and boiler that are connected in a closed loop through piping (See Fig. 3.3) that has heat transfer with the surroundings. The working fluid, in this case, is water/steam. At state 1, the water enters the pump as a low-pressure saturated liquid, where its pressure is increased

to that of the boiler. At state 2, it leaves the pump as a high-pressure subcooled liquid and enters the boiler where it absorbs heat irreversibly at constant pressure to state 3. Depending on the amount of heat absorbed, state 3 may be a saturated or a superheated vapor. The vapor then enters the turbine as a high-pressure, high-temperature vapor and exits as a low-pressure, low-temperature two-phase liquid-vapor during which it produces power that is transmitted to a generator (not shown). After this, the fluid enters the condenser, where heat is rejected to a sink (usually the atmosphere) until it achieves a saturated liquid state. The First Law is given by:

$$\dot{W} = \dot{Q}_H - \dot{Q}_L \tag{3.16}$$

In the heat exchangers, the heat transfer occurs by convection to flowing fluid streams having finite mass flow rate and specific heats. Therefore, the rate of heat transfer from the cycle at the low temperature, in the condenser, can be written as

$$\dot{Q}_{cd} = \left(\varepsilon \dot{C}_{\min}\right)_{cd} (T_4 - T_{L,in}) = \dot{m}(h_4 - h_1) \tag{3.17}$$

where ε is the heat exchanger effectiveness. Similarly, the rate of heat transfer between the Rankine cycle and the flue gas in the boiler is

$$\dot{Q}_{bl} = \left(\varepsilon \dot{C}_{\min}\right)_{bl} (T_{H,in} - T_2) = \dot{m}(h_3 - h_2) \tag{3.18}$$

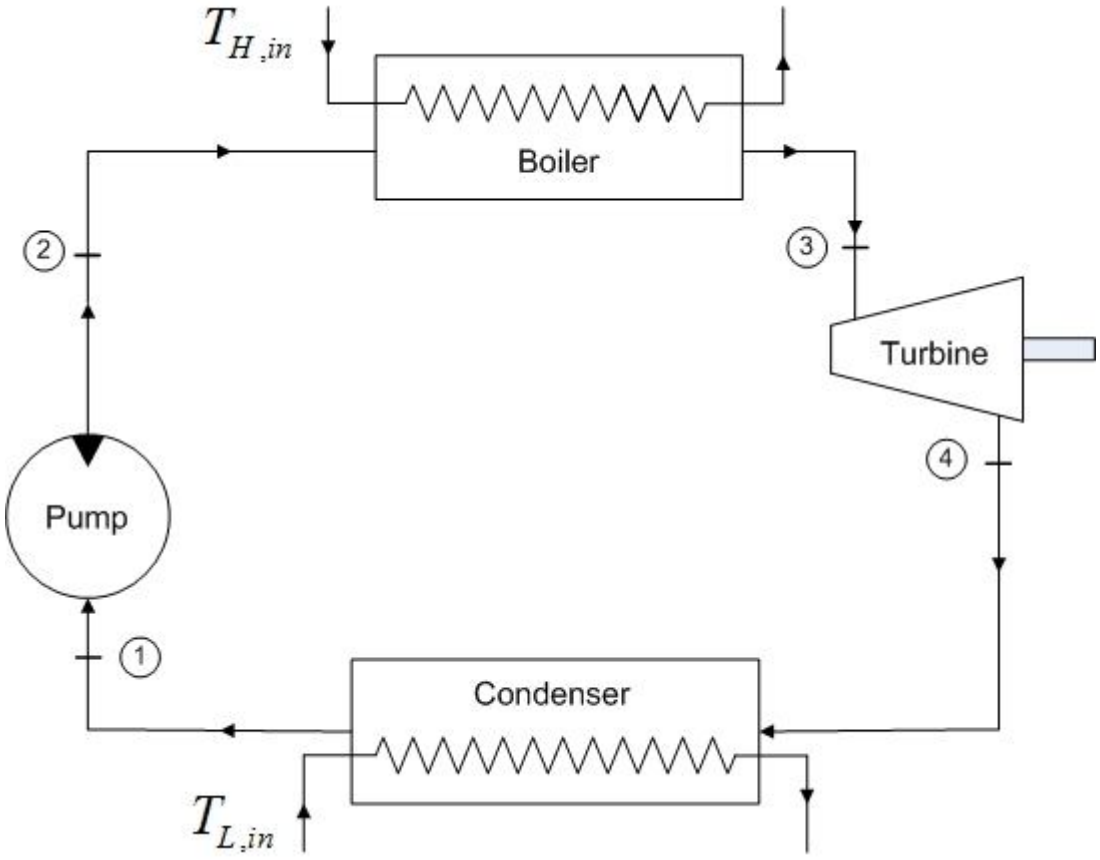

Figure 3.3. Schematic of a simple Rankine cycle

Pump operation is defined in terms of an isentropic efficiency, so that its power requirement is given by

$$\dot{W}_{pp} = \frac{\dot{W}_{pp,is}}{\eta_{pp,is}} \tag{3.19a}$$

where

$$\dot{W}_{pp,is} = v_1(P_2 - P_1) \tag{3.19b}$$

Ignoring any heat exchange between the pump and the surrounding, the energy balance can be expressed as

$$\dot{W}_{pp} = \dot{m}(h_2 - h_1) \tag{3.20}$$

Ignoring any heat exchange between the turbine and the surrounding, the energy balance can be expressed as

$$\dot{W}_t = \dot{m}(h_3 - h_4) \tag{3.21}$$

The efficiency of the Rankine power cycle is, in general, given by:

$$\eta = \frac{\dot{W}_t - \dot{W}_{pp}}{\dot{Q}_H} = 1 - \frac{\dot{Q}_L}{\dot{Q}_H} \tag{3.22}$$

We know that when one of the fluids is undergoing a phase change, based on the fact that a major portion of the heat exchange in a Rankine system is in two-phase region, we can write from heat exchanger theory [89]

$$UA = \dot{C}_{\min} \ln\left[\frac{1}{1-\varepsilon}\right] \tag{3.23}$$

This equation was applied to the condenser and the boiler for a specified value of $\dot{C}_{\min}$. It should be noted that $\dot{C}_{\min}$ is the thermal capacitance rate of that fluid in the heat exchanger which is not undergoing the phase change. For the boiler, Eq. (3.23) is a close

approximation despite the presence of subcooled and superheat regions in it [90]. Now, the reduction in *UA* value is due to the increase in fouling on the flue gas/air-side and can be represented as a percentage, UA_p, in the following manner:

$$UA_p = \left(1 - \frac{UA}{UA_{cl}}\right)100 \tag{3.24}$$

In the current work, the percentage decrease in the *UA* value due to fouling was varied from 0 to 50% for each heat exchanger where a zero value refers to clean conditions. Furthermore, heat leakages in the lines and pressure drop in the heat exchangers were considered as negligible in all the calculations. A computer program was written in Engineering Equation Solver (EES) for solving the above set of equations. In this program, thermophysical properties of the working fluid is needed at each step of the calculation, which are obtained from the built-in functions provided by EES [6]. It should be noted that EES solves the above equations by making blocks of simultaneously solvable equations and then applying a variant of the Newton's method [91].

3.3.2 Model validation

The Rankine power cycle model has been validated from the numerical data provided by various authors [92-93]. Firstly, the results from Demirel [92] for an ideal Rankine cycle with superheating were used to verify the above model where the net work done and thermal efficiency were predicted with an error of less than 1%. Secondly, the results of two numerical examples for simple ideal Rankine cycles given by Cengel and Boles [93] were also compared and the errors associated with net work output and

thermal efficiency predictions were found to be less than 0.05%. These results are summarized in Table 3.1.

Table 3.1: Percentage error in calculated values for Rankine power cycle model

Source	Fluid	P_{bl} (MPa)	P_{cd} (kPa)	T_{sup} (°C)	$W_{net,err}$ (%)	ε_{err} (%)
Demirel [92]	Steam	4.1	40	425	0.83	0.97
Cengel and Boles [93][a]	R134a	1.4	700	-	0	0
Cengel and Boles [93][b]	Steam	10	20	-	0.046	0

a problem 10-21
b problem 10-24

3.4 Simple Vapor Compression Cycle

The following assumptions were made in the model:

- The heat losses are negligible in the lines
- The pressure losses are negligible in the lines

3.4.1 Description and modeling

A simple vapor compression refrigeration system consists of a compressor, condenser, expansion valve and evaporator that are connected in a closed loop through piping that has heat transfer with the surroundings, as shown in Fig. 3.4. At state 1, the refrigerant leaves the condenser as a high-pressure, medium-temperature, saturated liquid and enters the expansion valve, where it expands in an isenthalpic manner. At state 2, it leaves the expansion valve as a low-quality vapor and enters the evaporator where it absorbs heat irreversibly at constant pressure to state 3. The refrigerant leaves the evaporator at state 3

as a low-pressure, low-temperature, saturated vapor and enters the compressor. At state 4, it leaves the compressor as a high-pressure, high-temperature, superheated vapor and enters the condenser.

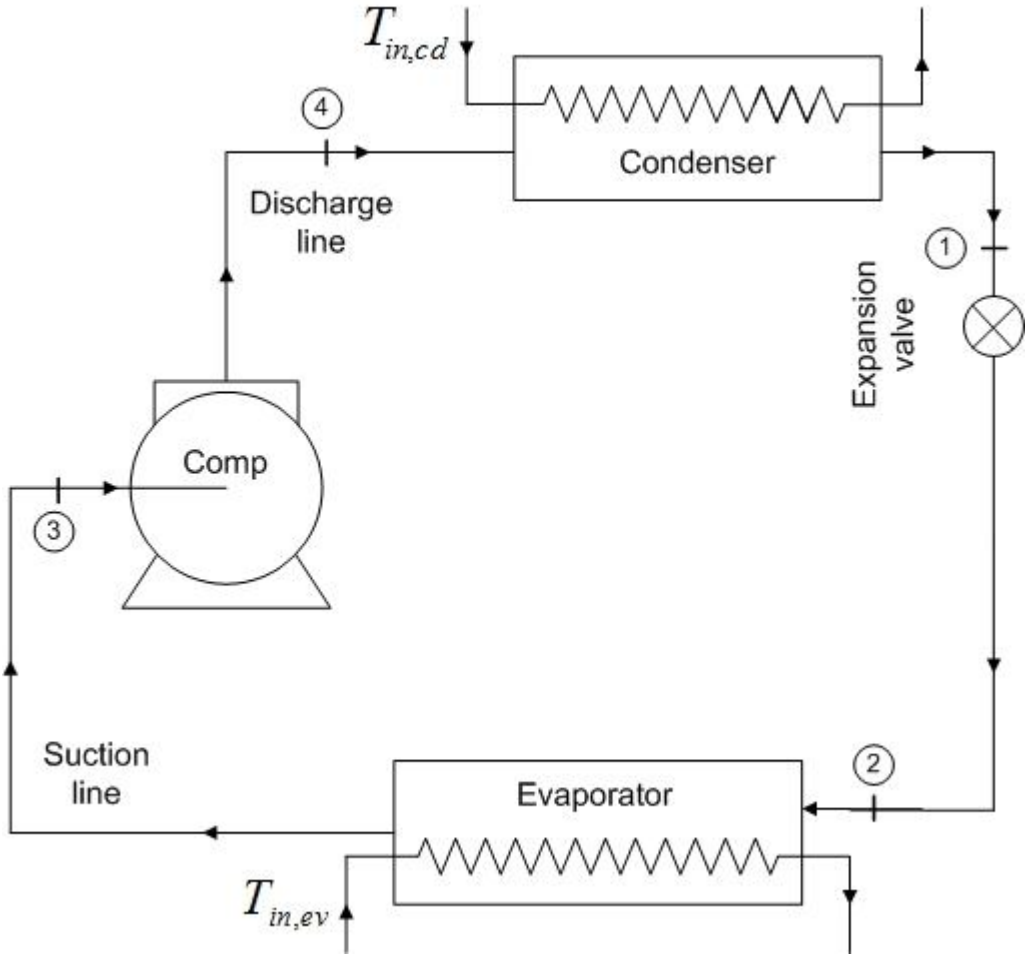

Figure 3.4. Schematic of a simple vapor compression cycle

In the heat exchangers, the heat transfer occurs by convection to flowing fluid streams having finite mass flow rate and specific heats. Therefore, the rate of heat transfer to the cycle at the low temperature, in the evaporator, can be written as

$$\dot{Q}_{ev} = \left(\varepsilon \dot{C}_{\min}\right)_{ev} (T_{in,ev} - T_2) = \dot{m}_{rfg} (h_3 - h_2) \tag{3.25}$$

where ε is the heat exchanger effectiveness. Similarly, the rate of heat transfer between the refrigeration cycle and the sink in the condenser is

$$\dot{Q}_{cd} = \left(\varepsilon \dot{C}_{\min}\right)_{cd} (T_1 - T_{in,cd}) = \dot{m}_{rfg} (h_4 - h_1) \tag{3.26}$$

Compressor operation is defined in terms of an isentropic efficiency, so that its power requirement is given by

$$\dot{W}_{cp} = \frac{\dot{W}_{cp,is}}{\eta_{cp,is}} \tag{3.27}$$

By applying the first law of thermodynamics, work input to the compressor can also be expressed as

$$\dot{Q}_w - \dot{W}_{cp} = \dot{m}_{rfg} (h_4 - h_3) \tag{3.28}$$

where $\dot{Q}_w$ is the heat transfer across the shell of the compressor. It should be noted that heat loss from the shell was considered negligible. Compressors operate at approximately fixed speeds such that the volumetric displacement rate remains nearly constant for a specified compressor but it should be noted that the volumetric flow rate varies with

operating conditions. The volumetric flow rate is commonly written in terms of the volumetric efficiency, $\eta_{cp,v}$, defined by [94]

$$\eta_{cp,v} = 1 - R\left(\frac{v_3}{v_4} - 1\right) \tag{3.29}$$

where R is the ratio of the clearance volume to the displacement volume and v_3 and v_4 are the specific volumes of the refrigerant at the compressor inlet and outlet, respectively. Furthermore, the volumetric efficiency can also be written as [94]

$$\eta_{cp,v} = \frac{\dot{V}_{in,cp}}{Piston\ Displacement} \tag{3.30}$$

where $\dot{V}_{in,cp}$ is the refrigerant volumetric flow rate at the inlet of the compressor.

Defining the COP as the refrigeration effect over the compressor work, we get

$$COP = \frac{\dot{Q}_{ev}}{\dot{W}_{cp}} \tag{3.31}$$

It should be noted that in the present study, the fan power requirement was not considered in the calculation of COP. The reason is that, in commercial systems, fan energy use typically represents only 9% of the total; however, in residential systems, it is much less [95]. Furthermore, experimental work applicable to residential and small commercial systems by Siegel [82] showed that the fan power increased by 1.4% only due to air-side fouling.

The deviation of an actual refrigeration system from a reversible one can be written in the form of the second-law efficiency as

$$\eta_{II} = \frac{COP}{COP_{rev}} \tag{3.32}$$

where

$$COP_{rev} = \frac{T_{in,ev}}{T_{in,cd} - T_{in,ev}} \tag{3.33}$$

We know that when one of the fluids is undergoing a phase change, based on the fact that a major portion of the heat exchangers in a vapor-compression system, is in two-phase region, we can write from the heat exchanger theory [89]

$$UA = \dot{C}_{\min} \ln\left[\frac{1}{1-\varepsilon}\right] \tag{3.34}$$

This equation was applied separately to the evaporator and the condenser for a specified value of $\dot{C}_{\min}$ as air-side fouling does not substantially reduce the air flow [82]. It should be noted that $\dot{C}_{\min}$ is the thermal capacitance rate of that fluid in the heat exchanger which is not undergoing the phase change. Now, the reduction in *UA* value is due to the increase in fouling on the air-side and can be represented as a percentage, UA_p, in the following manner:

$$UA_p = \left(1 - \frac{UA}{UA_{cl}}\right)100 \tag{3.35}$$

In the current work, the model is solved in the same way as described at the end of section 3.3.1.

3.4.2 Model validation

Stoecker and Jones [96] determined performance data for components of a vapor compression refrigeration system in which the data was represented by fitted equations using nine constants (See Eqs. below). This was done for the refrigeration capacity and power consumed for a York hermetic reciprocating compressor (H62SP-22E, R22, 1750 *rpm*).

$$\dot{Q}_{ev} = c_1 + c_2 T_2 + c_3 T_2^2 + c_4 T_1 + c_5 T_1^2 + c_6 T_1 T_2 + c_7 T_1 T_2^2 + c_8 T_1^2 T_2 + c_9 T_1^2 T_2^2 \tag{3.36}$$

$$\dot{W}_{cp} = d_1 + d_2 T_2 + d_3 T_2^2 + d_4 T_1 + d_5 T_1^2 + d_6 T_1 T_2 + d_7 T_1 T_2^2 + d_8 T_1^2 T_2 + d_9 T_1^2 T_2^2 \tag{3.37}$$

The condenser performance, assuming constant heat exchanger parameters for Bohn heat transfer division air-cooled condenser, refrigerant 22, model number 36 was represented by [96]:

$$\dot{Q}_{cd} = 9.39(T_1 - T_{in,cd}) \tag{3.38a}$$

where the number 9.39 represents the value of $\left(\varepsilon \dot{C}_{\min}\right)_{cd}$ in kW K^{-1}.

The cooling capacity for a Dunham-Bush, refrigerant 22, direct-expansion, inner-fin liquid chiller (CH660B) was given by [96]:

$$\dot{Q}_{ev} = 6\left[1 + 0.046(T_{in,ev} - T_2)\right](T_{in,ev} - T_2) \qquad (3.38b)$$

It should be noted that, in Eq. (3.38b), the term $6[1 + 0.046(T_{in,ev} - T_2)]$ represents $\left(\varepsilon \dot{C}_{\min}\right)_{ev}$. Considering the above model of Stoecker and Jones [96], the following data set was used to generate results for comparison purpose: $T_{in,cd} = 40\ ^{o}C$, $\left(\varepsilon \dot{C}_{\min}\right)_{cd} = 9.39\ kW\ K^{-1}, \eta_{cp,is} = 0.65$ wherein $T_{in,ev}$ was varied from 0 – 15 °C. It should be noted that, in this range, the cooling capacity varied from 57.24 kW – 90.56 kW and $\left(\varepsilon \dot{C}_{\min}\right)_{ev}$ from 7.98 – 8.83 kW K^{-1} in the model of Stoecker and Jones [96]. These values of the cooling capacity and $\left(\varepsilon \dot{C}_{\min}\right)_{ev}$ were then used in our thermodynamic model to compare the prediction of the heat rejected, compressor power and COP along with the condenser and evaporator temperatures (See Table 3.2). It shows that all relevant quantities can be predicted by the thermodynamic model accurately wherein the maximum error encountered was 2.05% while the absolute mean error was 1.05%.

Table 3.2: Comparison of performance data from Stoecker and Jones [96] and current model

$T_{in,ev}$ (°C)	$\dot{Q}_{cd}^{**}$ (kW)	$\dot{Q}_{cd,\mathrm{mod}}$ (kW)	Err (%)	$\dot{W}_{cp}^{**}$ (kW)	$\dot{W}_{cp,\mathrm{mod}}$ (kW)	Err (%)	T_1^{**} (°C)	$T_{1,mod}$ (°C)	Err (%)	COP^{**}	$\mathrm{COP}_{\mathrm{mod}}$	Err (%)
0	82.16	82.23	*0.09*	24.92	24.98	*0.24*	48.75	48.76	*0.01*	2.30	2.29	*0.26*
1	84.58	84.65	*0.08*	25.39	25.46	*0.28*	49.01	49.02	*0.01*	2.33	2.33	*0.26*
2	87.03	87.12	*0.10*	25.86	25.94	*0.31*	49.27	49.28	*0.02*	2.37	2.36	*0.34*
3	89.52	89.63	*0.12*	26.32	26.42	*0.38*	49.53	49.55	*0.03*	2.40	2.39	*0.42*
4	92.04	92.17	*0.14*	26.77	26.90	*0.49*	49.80	49.82	*0.03*	2.44	2.43	*0.53*
5	94.59	94.77	*0.19*	27.21	27.39	*0.66*	50.07	50.09	*0.04*	2.48	2.46	*0.65*
6	97.18	97.39	*0.22*	27.65	27.87	*0.80*	50.35	50.37	*0.04*	2.52	2.50	*0.80*
7	99.80	100.10	*0.30*	28.08	28.35	*0.96*	50.63	50.66	*0.05*	2.55	2.53	*0.94*

8	102.50	102.80	*0.29*	28.51	28.82	*1.09*	50.91	50.94	*0.07*	2.59	2.57	*1.08*
9	105.10	105.50	*0.38*	28.94	29.30	*1.24*	51.20	51.24	*0.07*	2.63	2.60	*1.22*
10	107.90	108.30	*0.37*	29.36	29.77	*1.40*	51.49	51.53	*0.08*	2.67	2.64	*1.38*
11	110.60	111.10	*0.45*	29.78	30.25	*1.58*	51.78	51.83	*0.10*	2.72	2.67	*1.55*
12	113.40	113.90	*0.44*	30.20	30.71	*1.69*	52.08	52.13	*0.10*	2.76	2.71	*1.71*
13	116.20	116.80	*0.52*	30.62	31.18	*1.83*	52.38	52.44	*0.11*	2.80	2.75	*1.82*
14	119.10	119.70	*0.50*	31.03	31.64	*1.97*	52.69	52.75	*0.11*	2.84	2.78	*1.90*
15	122.00	122.70	*0.57*	31.45	32.10	*2.07*	52.99	53.06	*0.14*	2.88	2.82	*2.05*

** Stoecker and Jones [96]

Data from the work of Aprea and Greco [97] related to experiments, using R407C as one of the working fluids, was also used for verification of the model for a single set of data, which is as follows: $\dot{Q}_{ev} = 5\ kW, \eta_{cp,is} = 0.61, T_{cd} = 35\ °C, T_{ev} = -5\ °C, T_{ev} = -5\ °C,$ $T_{in,ev} = 28.1\ °C$ for a volumetric air flow rate of 812 m^3/h. It should be noted that $\left(\varepsilon \dot{C}_{\min}\right)_{ev}$ and $\left(\varepsilon \dot{C}_{\min}\right)_{cd}$ values were not reported in the paper, therefore these were determined by the EES program as 0.151 $kW.K^{-1}$ and 0.996 $kW.K^{-1}$, respectively. The percentage error for the prediction of the COP and the difference between the discharge and suctions temperatures was found to be 5.1% and 3.1%, respectively.

3.5 Vapor Compression Cycle with Dedicated Mechanical Subcooling

The following assumptions were made in the model:

- The heat losses are negligible in the lines
- The pressure losses are negligible in the lines

3.5.1 Description and modeling

The main components of the system under consideration include two compressors, two expansion valves, two condensers, one evaporator and a sub-cooler. The system consists of two simple cycles coupled to each other via a sub-cooler as shown in Fig. 1.1, while its pressure-enthalpy diagram is shown in Fig. 3.5 below. In Fig. 1.1, the lower cycle is known as the main cycle and the upper cycle is known as the sub-cooler cycle. The components of the two cycles are connected in a closed loop through a piping system that has heat transfer with the surroundings. The system can have either the same refrigerant or different refrigerants flowing through the two cycles.

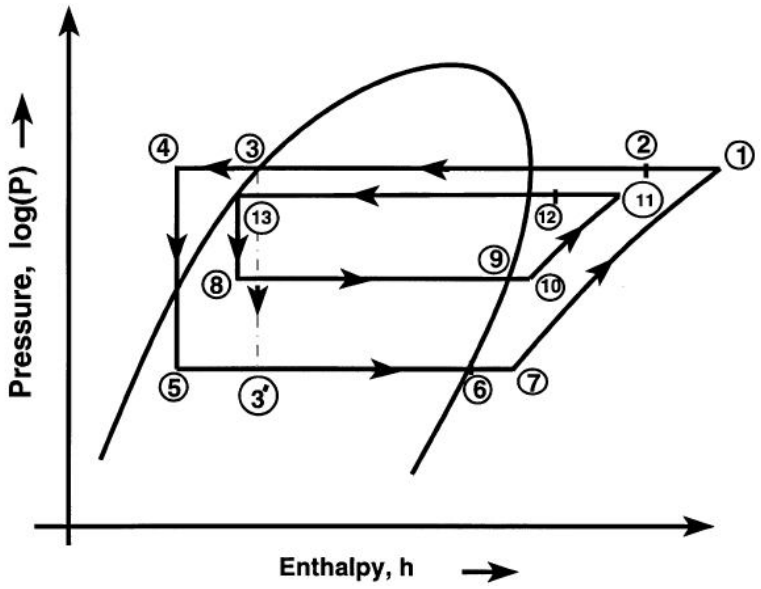

Figure 3.5. Pressure-enthalpy diagram of a refrigeration cycle with dedicated sub-cooling

Although a complete cycle description is available in Khan and Zubair [98], it should be kept in mind that, the refrigerant leaves the main-cycle evaporator at state 6 as a low-pressure low-temperature saturated vapor and enters the main-cycle compressor at

state 7. The refrigerant from state 6 to 7 takes heat from the surroundings in the suction line. At state 1, it leaves the compressor as a high-temperature high-pressure superheated vapor and enters the main-cycle condenser. The refrigerant from state 1 to 2 rejects heat to the surroundings in the discharge line. At state 3, the refrigerant leaves the main-cycle condenser as a high pressure saturated liquid which enters the subcooler. In the subcooler, it is cooled below the saturated liquid state at a constant pressure and enters the main-cycle expansion valve. At state 5, it leaves the expansion valve as a low-quality vapor and enters the evaporator, where it is evaporated at constant pressure to the saturated vapor state.

The subcooler-cycle refrigerant after cooling the main cycle refrigerant in the subcooler leaves as a low-pressure low-temperature saturated vapor at state 9 and enters the subcooler-cycle compressor at state 10. The refrigerant from state 9 to 10 takes heat from the surroundings. At state 11, it leaves the compressor as a superheated vapor and enters the subcooler-cycle condenser. The refrigerant from state point 11 to 12 rejects heat to the surrounding in the subcooler discharge line. At state 13, it leaves the condenser as a saturated liquid and enters the subcooler cycle expansion valve. At state 8, it leaves the expansion valve as a low-quality vapor and enters the subcooler.

In the heat exchangers, the heat transfer occurs by convection to flowing fluid streams having finite mass flow rate and specific heats. Therefore, the rate of heat transfer to the cycle at the low temperature in the evaporator can be written as

$$\dot{Q}_{ev} = \left(\varepsilon \dot{C}_{\min}\right)_{ev} (T_{in,ev} - T_5) = \dot{m}_m (h_6 - h_5) \tag{3.39a}$$

where ε is the heat exchanger effectiveness. Similarly, the rate of heat transfer from the main cycle condenser is

$$\dot{Q}_{cd} = \left(\varepsilon \dot{C}_{\min}\right)_{cd} (T_3 - T_{in,cd}) = \dot{m}_m (h_2 - h_3) \tag{3.39b}$$

It should be noted that Stoecker and Jones [96] have stated that the large majority of heat exchange occurs in the two-phase region.

For the sub-cooler loop, the rate of heat transfer between the refrigerant flowing through the sub-cooler and that coming from the main condenser is given as

$$\dot{Q}_{sc} = \varepsilon_{sc}\, \dot{Q}_{\max} = \dot{m}_m c_{p,m} \varepsilon_{sc} (T_3 - T_8) \tag{3.40}$$

where $c_{p,m}$ was calculated at the average of the values at states 3 and 4.

Furthermore, an energy balance on the sub-cooler provides us with the following relation

$$\dot{m}_{sc} (h_9 - h_8) = \dot{m}_m (h_3 - h_4) \tag{3.41}$$

Similarly, the rate of heat transfer from the sub-cooler cycle condenser is

$$\dot{Q}_{cd} = \left(\varepsilon \dot{C}_{\min}\right)_{cd} (T_{13} - T_{in,cd}) = \dot{m}_{sc} (h_{12} - h_{13}) \tag{3.42}$$

Compressor operation is defined in terms of an isentropic efficiency, so that its power requirement is given by

$$\dot{W}_{cp} = \frac{\dot{W}_{cp,is}}{\eta_{cp,is}} \tag{3.43}$$

The above equation was applied to each compressor. By applying the first law of thermodynamics, work input to the main compressor can also be expressed as

$$\dot{Q}_{cp,m} - \dot{W}_{cp,m} = \dot{m}_m (h_1 - h_7) \tag{3.44}$$

where $\dot{Q}_{cp,m}$ is the heat transfer across the shell of the main compressor. Similarly, work input to the sub-cooler cycle compressor can be written as

$$\dot{Q}_{cp,sc} - \dot{W}_{cp,sc} = \dot{m}_{sc} (h_{11} - h_{10}) \tag{3.45}$$

where $\dot{Q}_{cp,sc}$ is the heat transfer across the shell of the sub-cooler cycle compressor.

It should be noted that heat losses from the shells were considered negligible in the current work. Defining the COP as the refrigeration effect divided by the compressor work, we get

$$COP = \frac{\dot{Q}_{ev}}{\dot{W}_{cp,m} + \dot{W}_{cp,sc}} \tag{3.46}$$

It should be noted that the fan power requirement was not considered in the calculation of the COP. The reason is that, in commercial systems, fan energy consumption in commercial building energy use typically represents only 9% of the total but, in residential systems, it is much less [95].

3.5.2 Model validation

A numerical study of dedicated mechanical sub-cooling systems, using R-134a as the refrigerant in both the upper and lower cycles, showed two point calculations in Table 1 of Khan and Zubair [98]. The following outputs were compared: COP, the heat transfer in the sub-cooler and the temperature of the main cycle refrigerant after exiting the sub-cooler. For the case when the compressor efficiencies were 68%, the percentage differences were found to be 0.24%, 0.85% and -0.02%, respectively. When the compressor efficiencies were taken as 100%, the percentage differences were found to be 0.08%, 0.001% and 0.03%, respectively.

Stoecker and Jones [96] supplied performance data for each component of a simple vapor compression refrigeration system. The details of the performance equations were also provided for a York hermetic reciprocating compressor (H62SP-22E, R22, 1750 *rpm*). Assuming a constant heat exchanger effectiveness for the Bohn heat transfer division air-cooled condenser that uses R22 (model number 36), the condenser performance was represented by [96]:

$$\dot{Q}_{cd} = 9.39(T_3 - T_{in,cd}) \tag{3.47}$$

where 9.39 refers to the value of $\left(\varepsilon \dot{C}_{\min}\right)_{cd}$ in kW K^{-1}. The evaporator refrigeration capacity for a Dunham-Bush inner-fin liquid chiller (CH660B), using R22, was given by [96]:

$$\dot{Q}_{ev} = \left(\varepsilon \dot{C}_{\min}\right)_{ev} (T_{in,ev} - T_6) \tag{3.48}$$

where $\left(\varepsilon \dot{C}_{\min}\right)_{ev} = 6\left[1 + 0.046(T_{in,ev} - T_6)\right]$.

A comparison was conducted between the thermodynamic model used in the current work and the model presented in Stoecker and Jones [96]. In this case, the current model was modified, by commenting out the sub-cooler portion of the program. The following was used as input to generate the data: $T_{in,cd} = 40\ ^{o}C$, $\left(\varepsilon \dot{C}_{\min}\right)_{cd} = 9.39\ kW\ K^{-1}, \eta_{cp,is} = 0.65$ in which $T_{in,ev}$ was varied from 0 to 15 °C. It should be noted that, in this range, the cooling capacity varied from 57.24 kW to 90.56 kW and $\left(\varepsilon \dot{C}_{\min}\right)_{ev}$ from 7.98 to 8.83 kW K^{-1} in the Stoecker and Jones model [96]. These values of $\left(\varepsilon \dot{C}_{\min}\right)_{ev}$ and cooling capacity were then used in the current modified model to compare the prediction of the compressor power, heat rejected and COP as well as the condenser and evaporator temperatures. It was found that all quantities were predicted accurately as the maximum error was less than 2.1% but most errors were less than 1%.

Experimental data related to a simple vapor compression cycle is available in Table 1 of Cabello *et al*. [99]. This data was used to compare the accuracy of the current model after modification, as before. For our model, a representative value for the isentropic efficiency of the compressor was determined as 41.16% from the first data set, which was then used for the remaining runs. A comparison of the (modified) thermodynamic model used in the current work and the experimental data [99] shows that the maximum error found was 1.81%, though most errors were less than 0.5%.

The two-stage system which is closest to the one under study is the cascade refrigeration system. Table 1 of Dopazo and Fernandez-Seara [100] contains experimental data for a cascade refrigeration system at design operating conditions where Ammonia and Carbon Dioxide constitute the high- and low-temperature system, respectively. The model described in the previous section was modified to represent a cascade refrigeration system and the four heat exchanger pressures along with the compressor isentropic efficiencies and cooling load were used as input. The prediction of the mass flow rate and electric power consumption of the Carbon Dioxide as well as Ammonia system, the rate of heat transfer in the cascade heat exchanger and the COP were compared with the experimental values provided. The results are summarized in Table 3.3. It should be noted that the overall transmission efficiency, which is determined by multiplying the mechanical transmission and motor efficiencies, needed to determine the conversion of thermodynamic power required by the compressors into their respective electric powers were found from the experimental data as 0.95 and 0.82 for the high- and low-temperature systems, respectively.

Table 3.3: Comparison of experimental data of Dopazo and Fernandez-Seara [100] and the current (modified) model

Quantity	Experimental Value	Current Model	Error (%)
Mass flow rate of CO_2 (kg h^{-1})	124.4	124.7	0.26
Compressor power of CO_2 (kW)	3.93	3.94	0.35
Volume flow rate of NH_3 (L min^{-1})	1.23	1.16	-5.82

Compressor power of NH_3 (kW)	6.32	5.99	-5.27
Cascade heat exchange (kW)	13.2	12.6	-4.55
COP	0.92	0.95	3.43

CHAPTER 4

VAPOR COMPRESSION SYSTEM: EXPERIMENTAL WORK

In this chapter, details of the experimental work performed using a simple vapor compression cycle are presented. The purpose of this experimental work is to complement theoretical studies, which indicate that the effect of fouling on various parameters of a vapor compression system have a logarithmic characterization. Experimental data will show the effect of fouling on compressor power consumption, COP, condenser pressure and superheat temperature at the compressor exit.

4.1 Experimental Setup and Procedure

The experimental vapor compression system is shown in Fig. 4.1(a) while the schematic of the system is illustrated in Fig. 4.1(b). Major system components include a condenser, expansion valve, compressor and an evaporator. It should be noted that the

cycle uses R22 as a working fluid. The system is a 1.5 ton split air-conditioning system used to cool a room of a residence. It consists of a finned serpentine condenser having a face area of 0.514 m^2 (5/16" copper tube with aluminum fins – 16 FPI) for heat transfer after which there is a thermal expansion valve (State 4, Fig. 4.1(b)). The refrigeration system uses a three cylinder 2.14 kW hermetic reciprocating compressor for the cycle. The refrigerant, after compression is condensed and, before expanding, passes through a sight-glass so that its liquid state can be verified. The evaporator is a finned serpentine heat exchanger having a surface area of 0.22 m^2 (7 mm copper tubes with aluminum fins – 16 FPI) for heat transfer. At the evaporator exit (State 7, Fig. 4.1(b)), the superheat vapor is compressed to the condenser pressure (State 1, Fig. 4.1(b)).

To determine the temperature of the refrigerants at required locations, 8 type K surface mount thermocouples were used (See Appendix A for thermocouple calibration). They were placed over the surface of the pipes while keeping them isolated from the environment using insulation. The locations of the thermocouples are the same as the states mentioned in Fig. 4.1(b).

Figure 4.1(a). Experimental plant

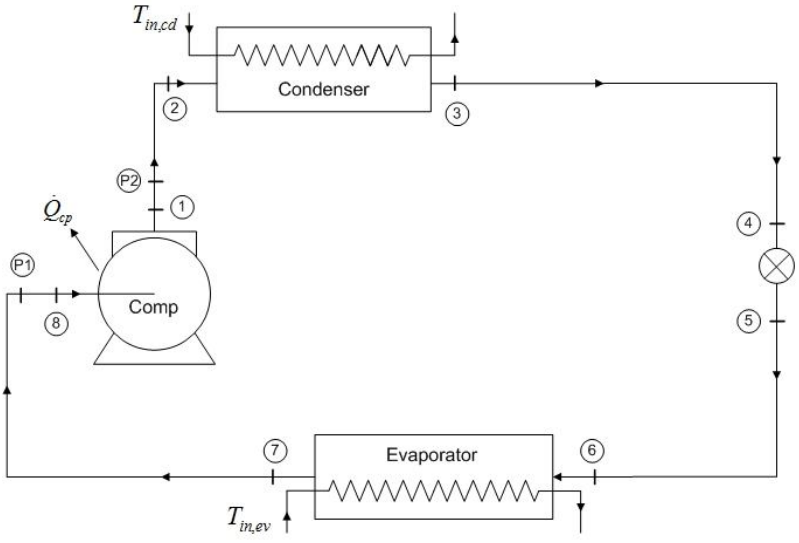

Figure 4.1(b). Schematic of a vapor compression cycle

Furthermore, two general purpose pressure transducers (P1 and P2 in Fig. 4.1(b)) were employed at the suction and discharge of the compressor accompanied by Bourdon tube gauges for independent verification (See Appendix B for calibration of pressure transducers). A wattmeter is used to determine the power consumption of the compressor. Table 4.1 should be consulted for uncertainties in the sensors used. Finally, the validity of the results is assessed by applying the first law of thermodynamics on the cycle (i.e. summation of the heat and work transfers should be equal).

Table 4.1: Uncertainties in measuring devices.

Physical variable	Measuring device	Measurement and calibration range	Uncertainty
Temperature	Type K thermocouples	0-100°C	±0.2 °C
Pressure	Pressure gauges	0-100 psig	±2 psig
		0-500 psig	±10 psig
Compressor power consumption	Wattmeter	0-3 kW	±60 W

Beginning with the clean condition (see Fig. 4.1(a)), the system was blocked by 10% intervals, which was calculated based on the length of the heat transfer area. Fig. 4.2 shows the experimental system when it is (partially) blocked to simulate fouling.

Figure 4.2. Experimental plant with partially blocked condenser

The system characteristics were studied at an (average) ambient condition of 31.6 °C while the room temperature was kept at approximately 21 °C. It should be noted that data was recorded for 2 to 3 hours wherein the data acquisition system recorded all relevant quantities at an interval of 30 seconds (See Appendix C for complete set of raw data recorded for all relevant quantities). Approximately one hour was needed to allow the system to reach steady state. After this, a 40-minute section of data from the second hour was selected for all relevant quantities, which constituted 80 points each. The average of these 80 points for each quantity was then taken and considered as a representative of the condition of the system. This procedure constitutes one averaged data point for each relevant quantity. In this way, the system was blocked up to 50% resulting in six averaged data points.

4.2 Data Analysis

The results from the experiments are discussed in this section. The following assumptions were made during the analysis:

- The pressure losses are negligible in the lines

Now, the heat transfer rate in the evaporator can be determined form the following equation:

$$\dot{Q}_{ev} = \left(\varepsilon \dot{C}_{\min}\right)_{ev} (T_{in,ev} - T_6) = \dot{m}(h_7 - h_6) \tag{4.1}$$

The heat transfer rate from the condenser is similarly defined as follows:

$$\dot{Q}_{cd} = \left(\varepsilon \dot{C}_{\min}\right)_{cd} (T_3 - T_{in,cd}) = \dot{m}(h_2 - h_3) \tag{4.2}$$

An energy balance on the compressor provides the following equation:

$$\dot{Q}_{cp} - \dot{W}_{cp} = \dot{m}(h_1 - h_8) \tag{4.3}$$

where $\dot{Q}_{cp}$ is the heat transfer rate across the compressor shell and was assumed to be 5% of the power consumption of the compressor. It should be noted that various researchers [101-103] have modeled the compressor shell heat loss by assuming a constant value for the compressor shell thermal conductance (UA). This implies that losses are not constant and vary with temperature difference.

It should be noted that the COP is defined as the cooling load divided by the work from the compressor. The reason for not including the fan power requirement in the COP calculation is that, in commercial building energy usage, fan energy consumption is usually only 9% of the total and it is much less in residential systems [95].

$$COP = \frac{\dot{Q}_{ev}}{\dot{W}_{cp}} \tag{4.4}$$

We know that when one of the fluids is undergoing a phase change, based on the fact that a major portion of the heat exchangers in this system is in two-phase region, we can write from the heat exchanger theory [89]

$$UA = \dot{C}_{\min} \ln\left[\frac{1}{1-\varepsilon}\right] \tag{4.5}$$

It should be kept in mind that $\dot{C}_{\min}$ is the thermal capacitance rate of that fluid in the heat exchanger which is not undergoing a phase change.

Fig. 4.3 shows the change in normalized compressor power consumption with percentage increase in condenser blockage. It should be noted that the power consumption is normalized with respect to the clean condition. For the experimental data obtained from Federov [104] as well as the current experiment, condenser blockage represents physically blocking the condenser by covering part of it. For the simulation work of Bultman *et al*. [83], it represents a decrease in the air mass flow due to blockage/fouling. It should be kept in mind that decrease in the air mass flow rate reduces the overall UA-value as was shown in Table 1 of Bultman *et al*. [83]. Furthermore, in reality, when fouling does occur, there is both blockage and change in air mass flow rate. For the work of Qureshi and Zubair [85], it is the percentage decrease in overall UA-value due to blockage/fouling. The important point to observe is that all these works show a consistent behavior; that is, the nature of change of the normalized power consumption due to fouling is logarithmic. Figs. 4.4-4.6 show the change in normalized COP, condenser pressure and superheat temperature at the compressor exit, respectively, with percentage increase in condenser blockage. The relevant clean condition is used to normalize the COP, pressure and temperature. This consistent behavior is seen in these figures as well. The reason for this behavior is understood from Eq. (4.5), which contains

the logarithm function. As fouling/blockage occurs, the change in the effectiveness of the heat exchanger is logarithmic in nature (See Fig. 2(a) of Qureshi and Zubair [85]) and this, in turn, varies the heat transfer in the heat exchanger in the same manner. The power consumption is directly connected to the nature of the heat transfer in the heat exchanger through the first law of thermodynamics (See Eq. (4.6) below) and, hence, we see a logarithmic behavior in the compressor power consumption as well.

$$\dot{Q}_{cd} - \dot{Q}_{ev} = \dot{W}_{cp} \tag{4.6}$$

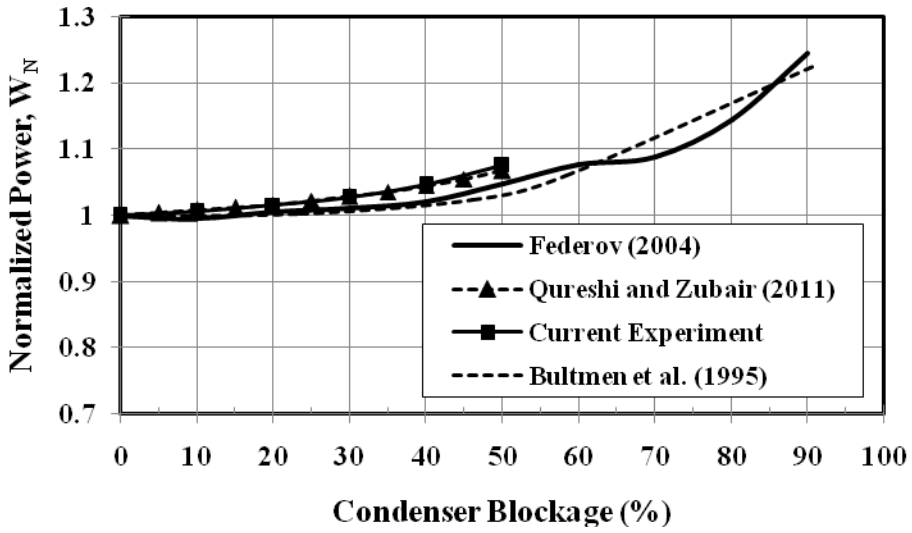

Figure 4.3. Variation of normalized compressor power with percentage increase in condenser blockage

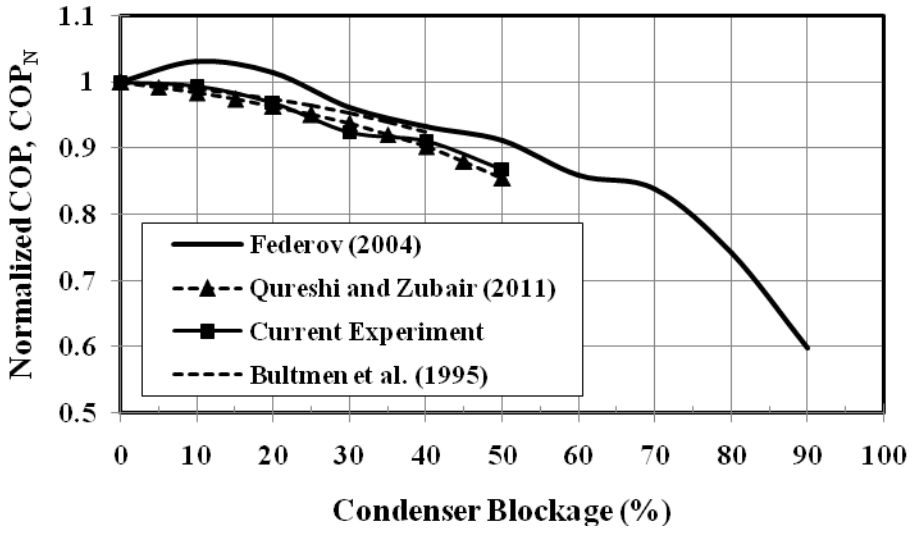

Figure 4.4. Variation of normalized COP with percentage increase in condenser blockage

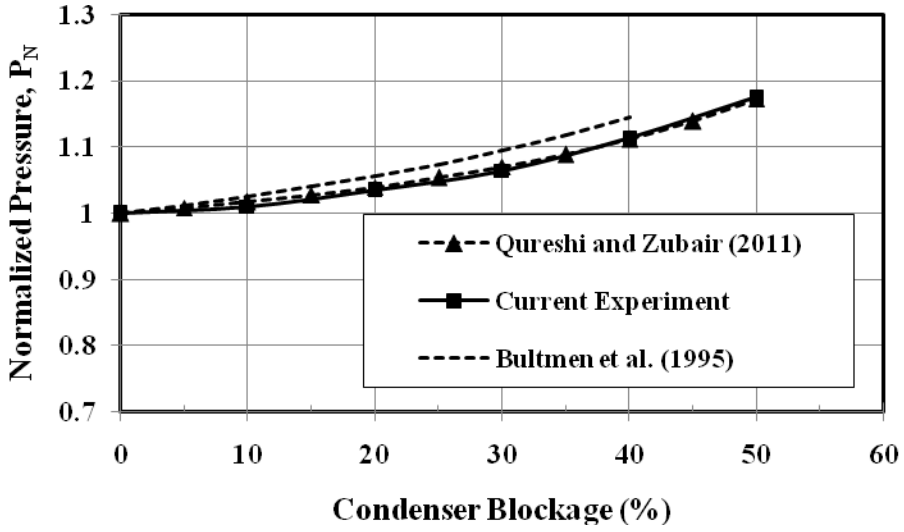

Figure 4.5. Variation of normalized condenser pressure with percentage increase in condenser blockage

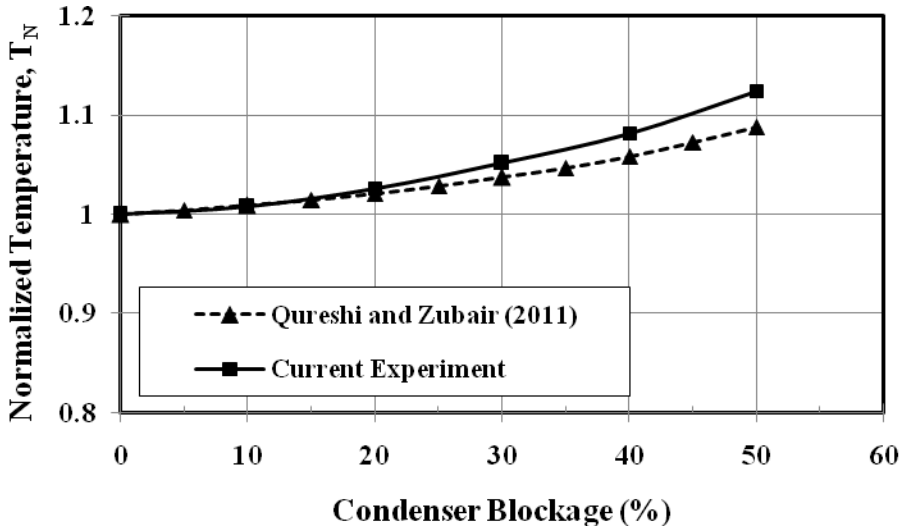

Figure 4.6. Variation of normalized superheat temperature at compressor exit with percentage increase in condenser blockage

To substantiate the nature of these curves in a rigorous manner, all of them were fitted to see how close each resembles the logarithmic behavior. It should be noted that these curves consist of performance parameters as well as properties based on both experimental and numerical data. Figs. 4.7(a) - (b) show samples of these fits on an unblocked/unfouled percentage basis since logarithm of zero does not exist. In Figs. 4.7(a) and 4.7(b), the R^2 value is 0.972 and 0.983, respectively. A complete list is shown in Table 2 wherein the R^2 values range from 0.969 to 0.996 and the average is 0.982.

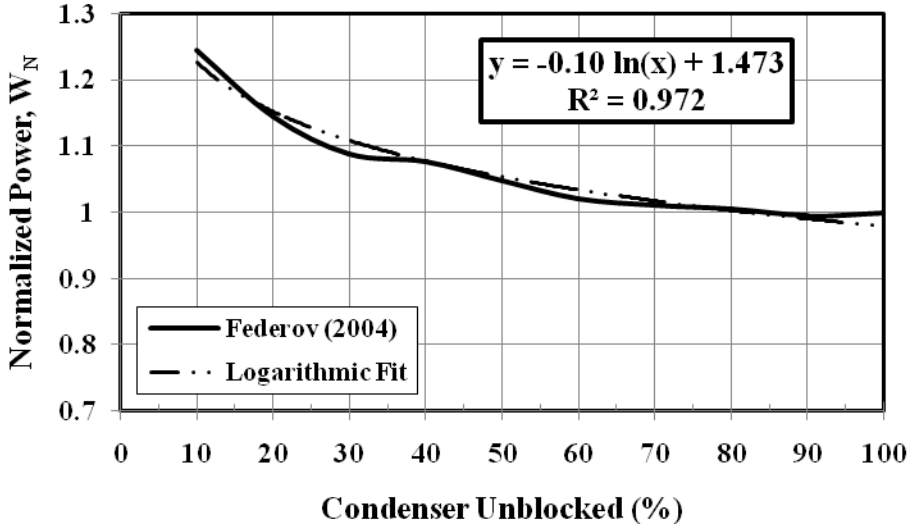

Figure 4.7(a). Logarithmic fitting of normalized power consumption for data of Federov [104]

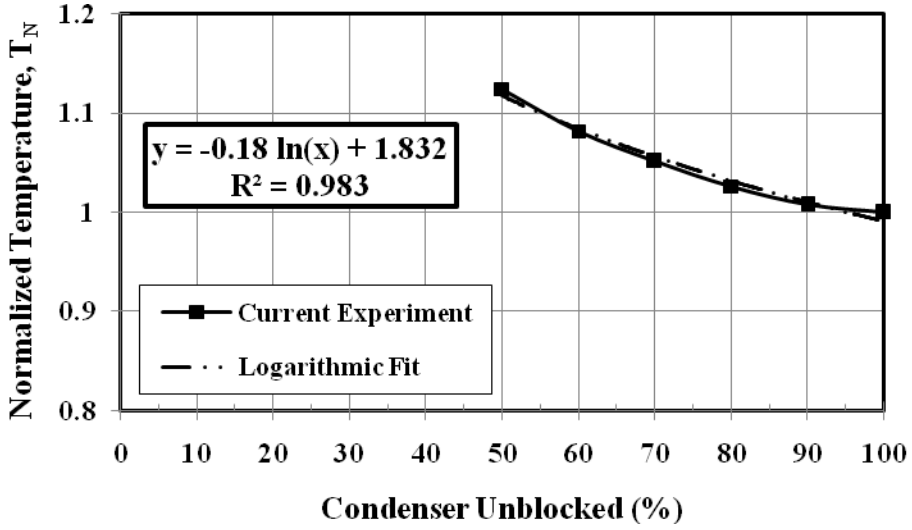

Figure 4.7(b). Logarithmic fitting of normalized superheat temperature at compressor exit for data of current work

Table 4.2: List of R^2-values and logarithmic fit equations for plotted lines in Figs. 4.3-4.6.

Fig. #	Reference	R^2-value	Logarithmic fit Eq.
4.3	Federov [104]	0.972	-0.1 ln(x) +1.473
4.3	Qureshi and Zubair [85]	0.989	-0.09 ln(x) +1.437
4.3	Current Experiment	0.969	-0.1 ln(x) +1.489
4.3	Bultman *et al*. [83]	0.977	-0.09 ln(x) +1.435
4.4	Federov [104]	0.982	0.183 ln(x) +0.187
4.4	Qureshi and Zubair [85]	0.991	0.207 ln(x) +0.051
4.4	Current Experiment	0.976	0.198 ln(x) +0.094
4.4	Bultmen *et al*. [83]	0.987	0.146 ln(x) +0.327
4.5	Qureshi and Zubair [85]	0.984	-0.24 ln(x) +2.12
4.5	Current Experiment	0.973	-0.26 ln(x) +2.182
4.5	Bultmen *et al*. [83]	0.996	-0.28 ln(x) +2.3
4.6	Qureshi and Zubair [85]	0.988	-0.12 ln(x) +1.578
4.6	Current Experiment	0.983	-0.18 ln(x) +1.832

CHAPTER 5

VAPOR COMPRESSION SYSTEM WITH DEDICATED MECHANICAL SUBCOOLING: EXPERIMENTAL AND NUMERICAL WORK

In this chapter, details of the experimental and numerical work performed using a vapor compression system with dedicated mechanical subcooling are presented. The purpose of this chapter is to establish the logarithmic nature of the variation of properties and performance parameters in comparatively more complex refrigeration systems.

5.1 Experimental Work

This experimental work is aimed at complementing theoretical studies on dedicated mechanical subcooling cycles. Experimental data will be used to show the effects of the use of dedicated subcooling on important parameters of the system (such as coefficient of

performance and cooling capacity) over a period of several hours. Furthermore, with this work, the aim is to provide proof of concept for this system in particular.

5.1.1 Experimental setup and procedure

Two refrigerant loops are employed in the experimental system used (See Fig. 5.1). Major system components include two condensers, two expansion valves, two compressors, one sub-cooler and an evaporator. Fig. 5.2(a) shows two simple cycles connected to each other through a sub-cooler, in which the bottom cycle is the main cycle and the top cycle is the sub-cooler cycle. Fig. 5.2(b) illustrates the corresponding pressure-enthalpy diagram. Khan and Zubair [98] provided a complete cycle description. It must be noted that the main cycle uses R22 and the dedicated subcooling cycle uses R12 as a working fluid. Also, the two condensers work with the same inlet temperatures of the cooling medium.

The base system is a 1.5 ton split air-conditioning system used to cool a room of a residence. It consists of a finned serpentine condenser having a face area of 0.514 m^2 (5/16” copper tube with aluminum fins – 16 FPI) for heat transfer after which there is a thermal expansion valve (State 5, Fig. 5.2(a) located at the exit of the subcooler, which acts as the evaporator of the dedicated subcooling loop. The refrigeration system uses a three cylinder 2.14 kW hermetic reciprocating compressor for the main cycle. The refrigerant, after compression is condensed. The subcooler receives liquid refrigerant from the condenser and, before expanding, passes through a sight-glass so that its liquid state can be verified.

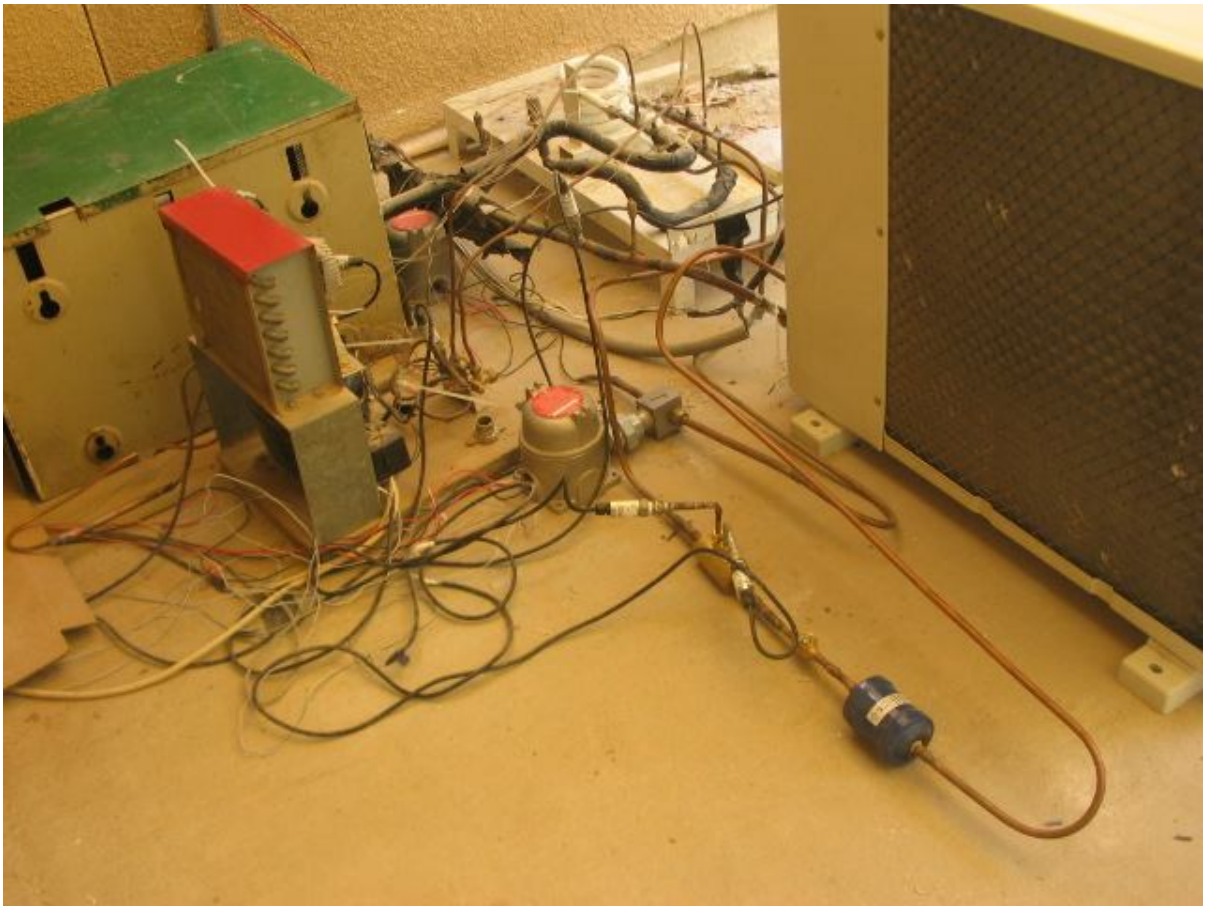

Figure 5.1. Experimental plant

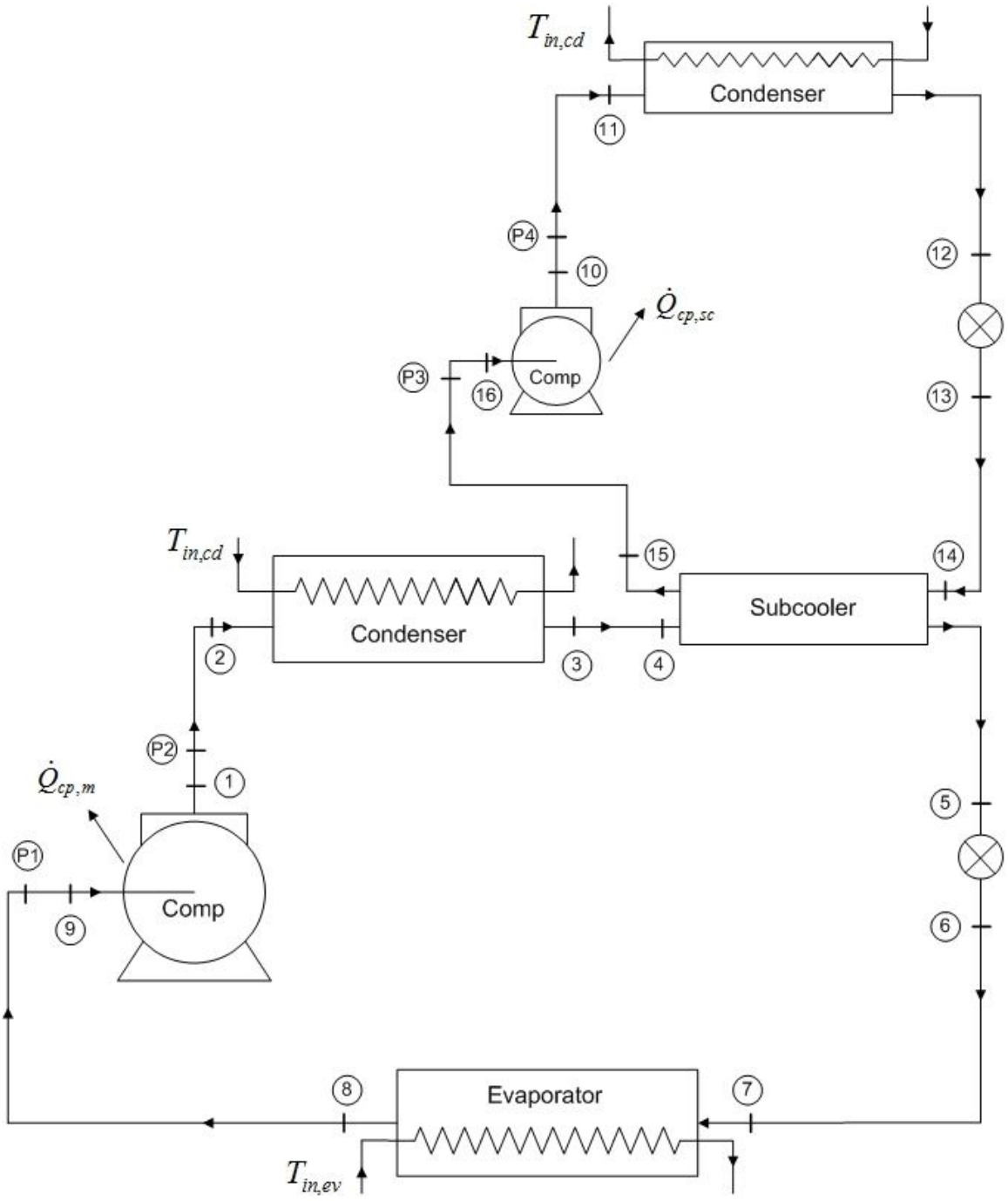

Figure 5.2(a). Schematic of a vapor compression cycle with dedicated mechanical sub-cooling

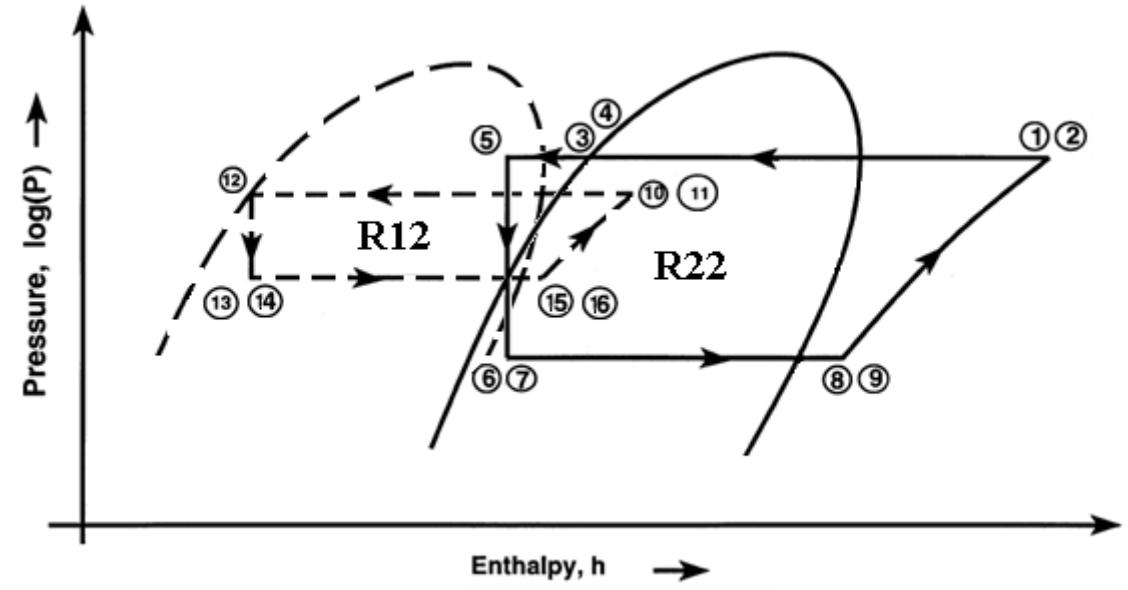

Figure 5.2(b). Pressure-enthalpy diagram of a refrigeration cycle with dedicated sub-cooling

The evaporator is a finned serpentine heat exchanger having a surface area of 0.22 m^2 (7 mm copper tubes with aluminum fins – 16 FPI) for heat transfer. At the evaporator exit (State 8, Fig. 5.2(a)), the superheat vapor is compressed to the condenser pressure (State 1, Fig. 5.2(a)). It should be noted that the dedicated subcooling cycle uses a 0.186 kW hermetic reciprocating compressor.

To determine the temperature of the refrigerants at required locations, 16 type K surface mount thermocouples were used (See Appendix A for thermocouple calibration). They were placed over the surface of the pipes while keeping them isolated from the environment using insulation. The locations of the thermocouples are the same as the states mentioned in Fig. 5.2(a). Furthermore, four general purpose pressure transducers (P1 to P4 in Fig. 5.2(a)) were employed at the suction and discharge of the compressors accompanied by Bourdon tube gauges for independent verification. The refrigerant mass flow rate is determined by applying energy balance on the main cycle compressor. A wattmeter is used to determine the power consumption of the compressor. Table 4.1 should be consulted for uncertainties in the sensors used. Other required refrigerant properties such as enthalpy are determined using the Engineering Equation Solver (EES) software [6], in which relevant functions are incorporated.

An energy balance is applied on the subcooler (See Eq. (5.1)) to calculate the mass flow rate of the refrigerant in the dedicated subcooling cycle. Finally, the validity of the results is assessed by applying the first law of thermodynamics on the cycle (i.e. summation of the heat and work transfers should be equal).

$$\dot{m}_{sc} = \dot{m}_m \frac{h_5 - h_4}{h_{15} - h_{14}} \tag{5.1}$$

It should be noted that results are based on experimental data recorded over several hours for two situations i.e. with and without subcooling. The data acquisition system recorded all relevant quantities at intervals of one minute. The system characteristics were studied with the subcooler loop as well as without it as the ambient conditions varied over time. In this work, the split unit working alone is called the *base configuration*, while the same system using the dedicated subcooling loop is referred as the *subcooler configuration*.

5.1.2 Data analysis

The results from the experiments on the two configurations mentioned in the previous sections are discussed in this section (See Appendix D for complete set of raw data recorded for all relevant quantities). The following assumptions were made during the analysis:

- The pressure losses are negligible in the lines

Now, the heat transfer rate in the evaporator can be determined form the following equation:

$$\dot{Q}_{ev} = \dot{m}_m (h_8 - h_7) \tag{5.2}$$

The heat transfer rate from the main condenser is similarly defined.

The heat exchanged, in the subcooling cycle, by the fluid moving through the subcooler and the refrigerant flowing through the condenser can be written as

$$\dot{Q}_{sc} = \dot{m}_m (h_4 - h_5) \tag{5.3}$$

The heat transfer rate from the subcooler condenser is similarly defined as:

$$\dot{Q}_{cd,sc} = \dot{m}_{sc} (h_{11} - h_{12}) \tag{5.4}$$

The main cycle mass flow rate was determined by applying an energy balance on the cycle compressor.

$$\dot{Q}_{cp,m} - \dot{W}_{cp,m} = \dot{m}_m (h_1 - h_9) \tag{5.5}$$

where $\dot{Q}_{cp,m}$ is the heat transfer rate across the main compressor shell and was assumed to be 5% of the power consumption of the compressor. The compressor power requirement of the sub-cooler cycle compressor was defined similarly.

The COP was taken as the cooling load divided by the power from both the compressors. The two configurations were tested over a long period of time one day after the other. The ambient conditions were not the same while running each configuration when corresponding hours are compared. Therefore, the second-law efficiency was employed to evaluate the two configurations instead of the COP, which is defined in Eq. (5.6) below.

$$\eta_{II} = \frac{COP}{COP_{\max}} \tag{5.6a}$$

where

$$COP_{\max} = \frac{T_{amb}}{T_{amb} - T_{room}} \tag{5.6b}$$

and

$$COP = \frac{\dot{Q}_{ev}}{\dot{W}_{cp,m} + \dot{W}_{cp,sc}} \tag{5.6c}$$

Currently, to solve the set of equations shown above, a simple program in Engineering Equation Solver (EES) was written. It should be noted that thermophysical properties of R22 and R12 are already built into the software [6].

For the base configuration test performed over a period of several hours, the variation in the main compressor discharge temperature and the ambient temperature is presented in Figs. 5.3(a)-(b). Experimental results show that the discharge temperature reaches its highest point when the ambient temperature reaches its peak. The variation in the discharge and suction pressures for the base configuration are presented in Fig. 5.4(a)-(b). The data indicates that these pressures follow the pattern of the ambient temperature. Variation in the compressor power as well as the cooling capacity requirement of the system (See Fig. 5.5) shows that the average cooling capacity throughout the day was 3.5 kW and the average compressor power requirement was 1.8 kW. Fig. 5.6 shows that the average COP for the test period was 1.9 and was at its

minimum when the ambient temperature was at its maximum. The COP variation is a mirror image of the ambient temperature pattern.

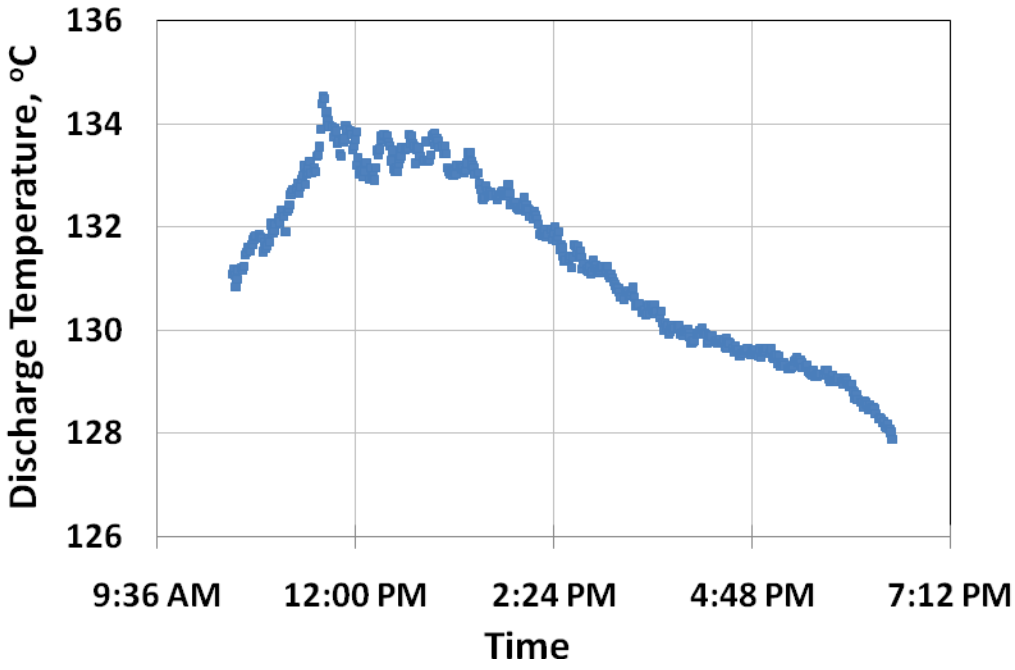

Figure 5.3(a). Variation of compressor discharge temperature – Base configuration

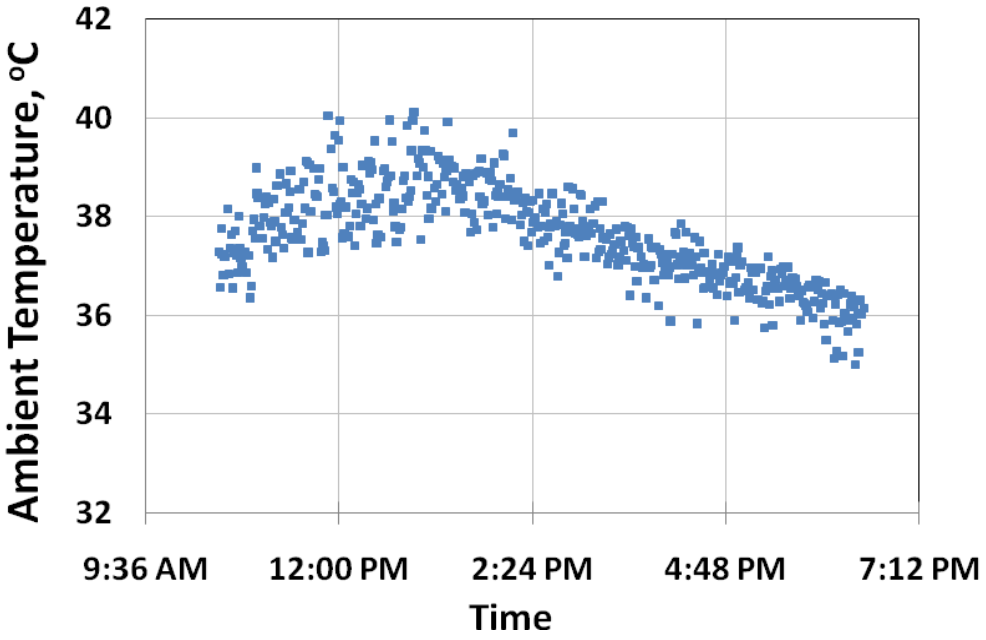

Figure 5.3(b). Variation of ambient temperature – Base configuration

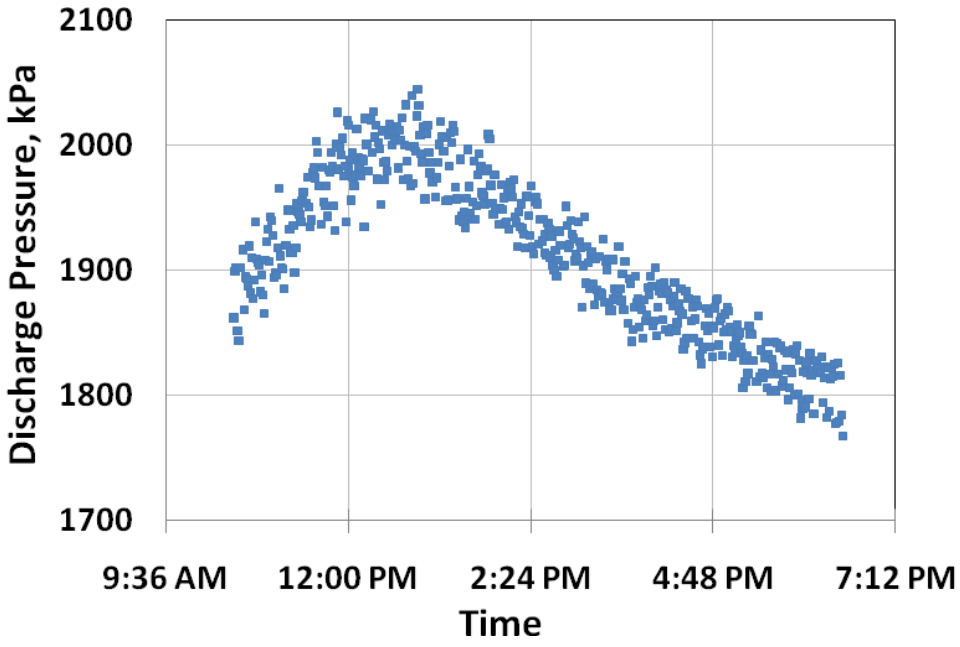

Figure 5.4(a). Variation of discharge pressure – Base configuration

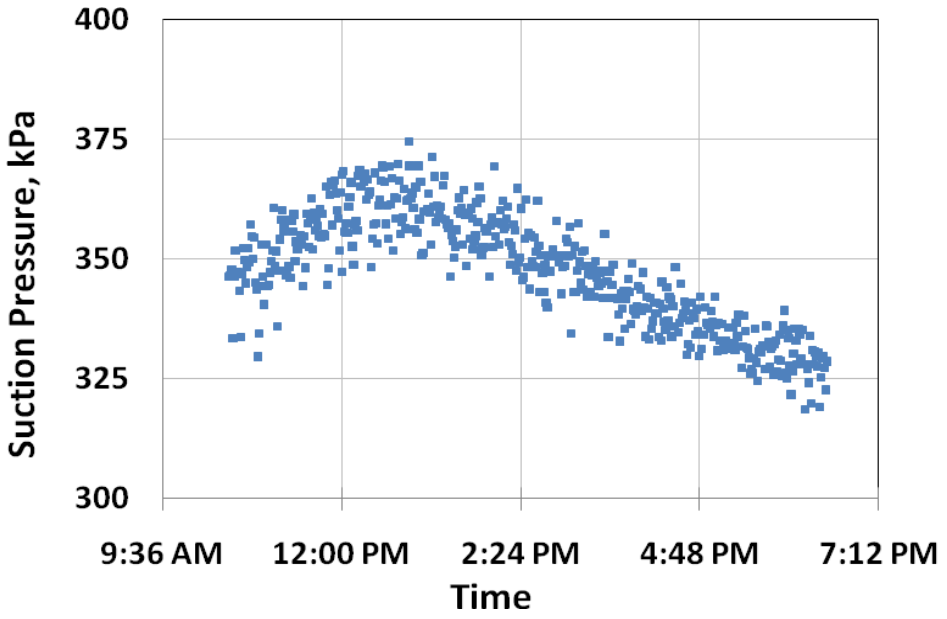

Figure 5.4(b). Variation of suction pressure – Base configuration

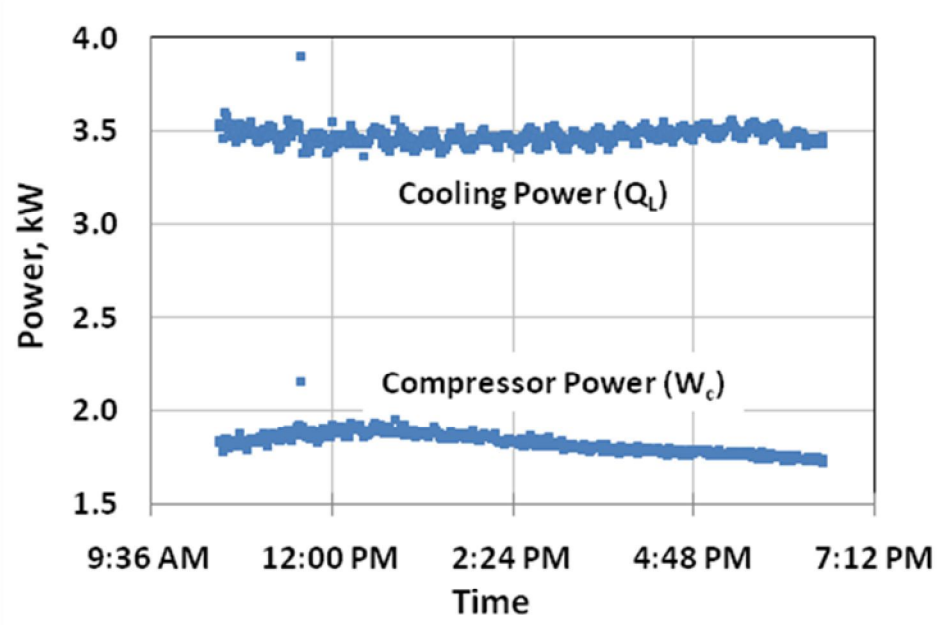

Figure 5.5. Variation of cooling capacity and compressor power requirement – Base configuration

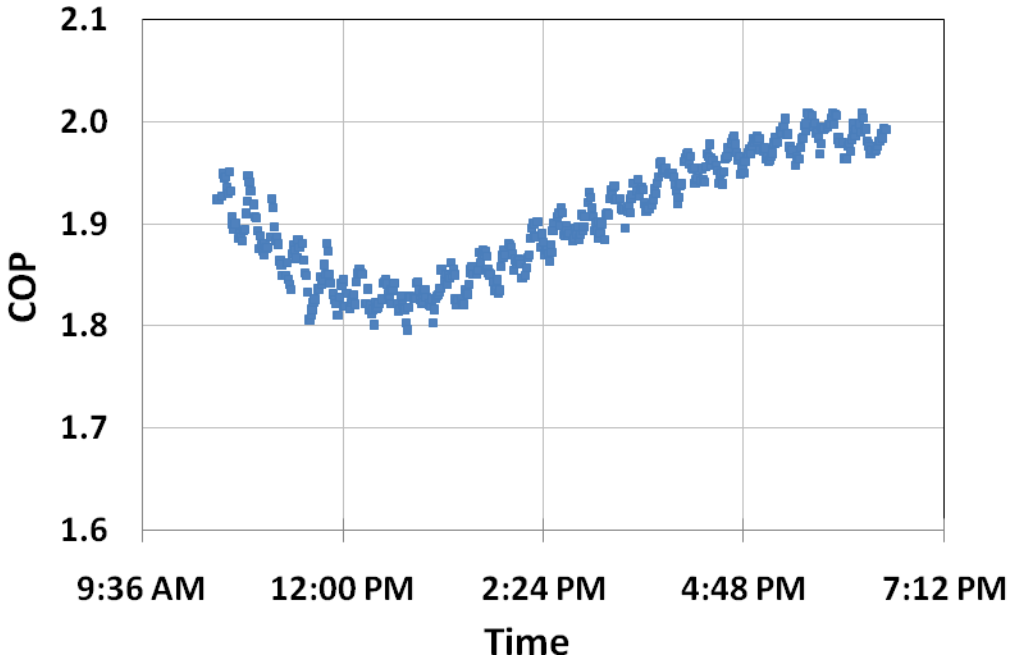

Figure 5.6. Variation of COP – Base configuration

For the subcooler configuration, Figs. 5.7-5.10 present the variation in the discharge temperatures for both compressors, pressure variations for the main and small cycle and compressor power requirement for both compressors. The data indicates that these quantities, in general, follow the pattern of the ambient temperature. In Fig. 5.7(a), it is observed that the discharge temperature of the main cycle compressor reaches its peak at noon time while that of the small cycle does so much later in the day. This seems to be due to the fact that the discharge pressure of the subcooler cycle compressor increased, which is evident from Fig. 5.8(a).

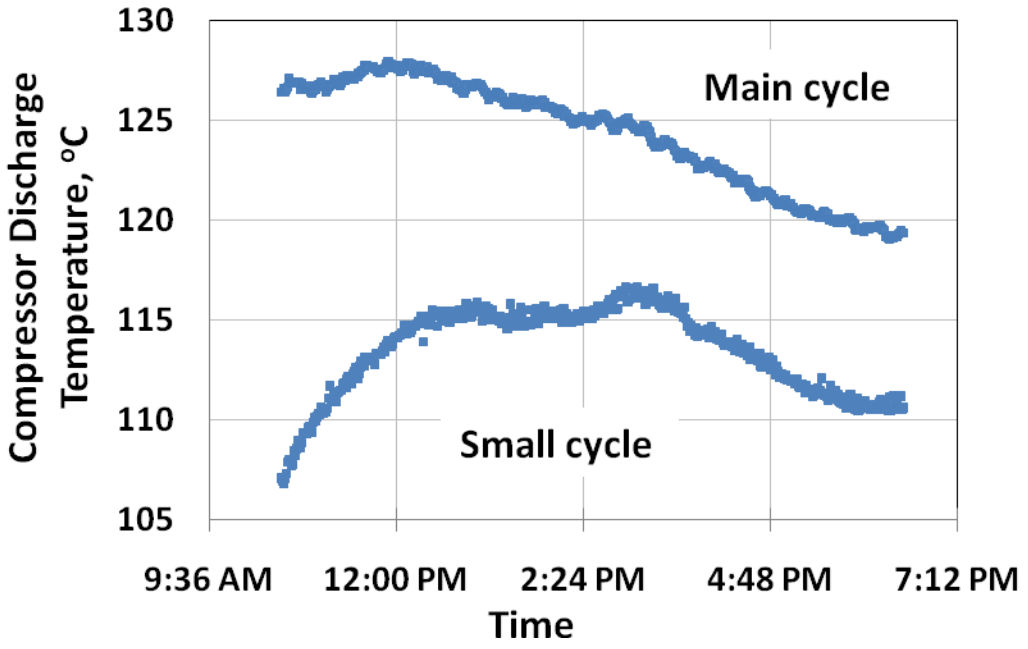

Figure 5.7(a). Variation of compressor discharge temperatures – Subcooler configuration

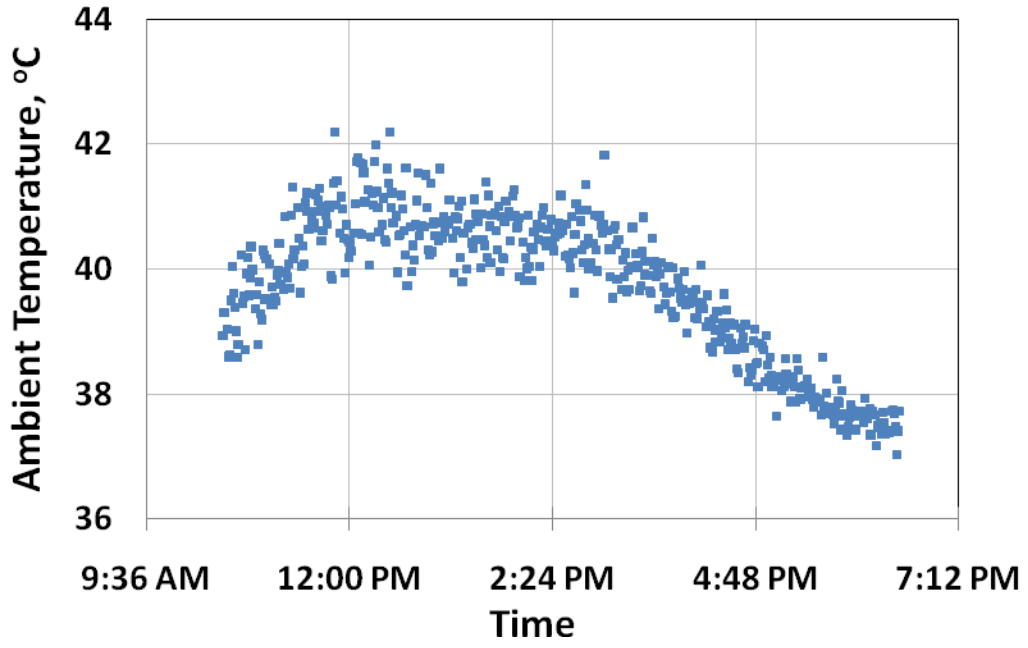

Figure 5.7(b). Variation of ambient temperature – Subcooler configuration

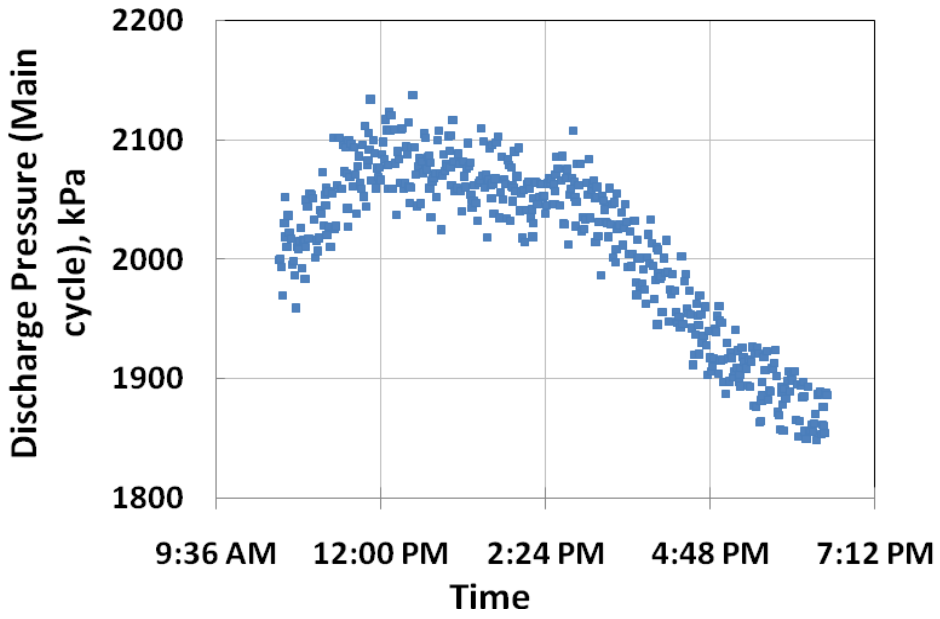

Figure 5.8(a). Variation of main cycle discharge pressure – Subcooler configuration

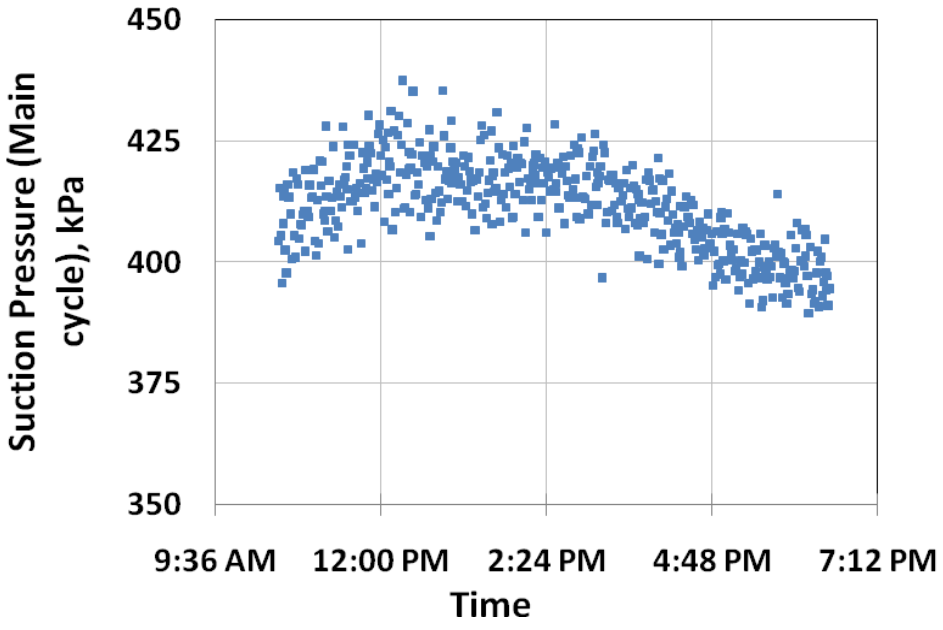

Figure 5.8(b). Variation of main cycle suction pressure – Subcooler configuration

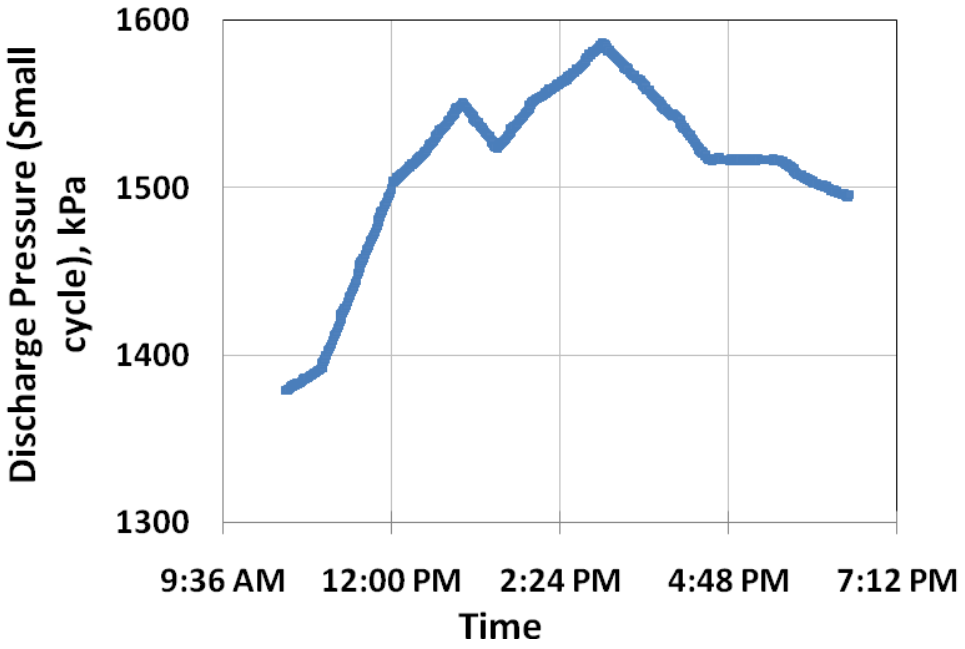

Figure 5.9(a). Variation of small cycle discharge pressure – Subcooler configuration

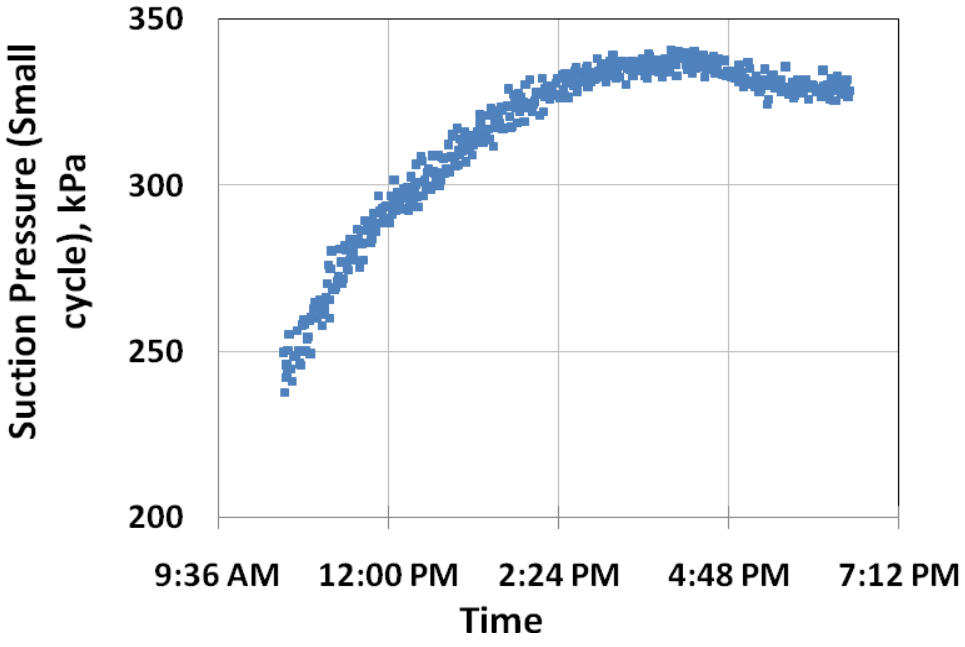

Figure 5.9(b). Variation of small cycle suction pressure – Subcooler configuration

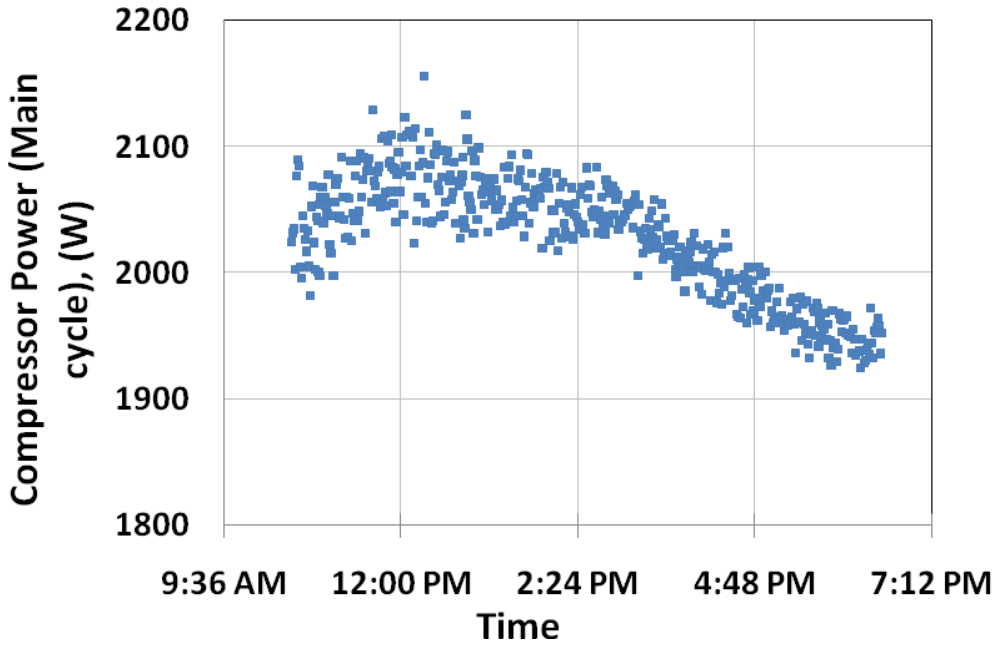

Figure 5.10(a). Variation of compressor power (Main cycle) – Subcooler configuration

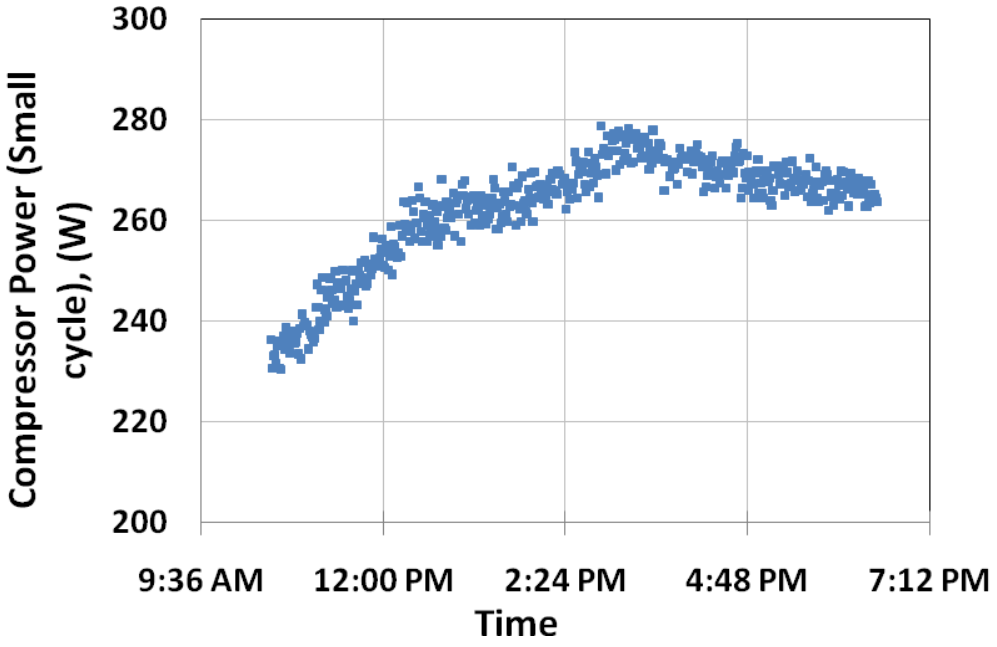

Figure 5.10(b). Variation of compressor power (Small cycle) – Subcooler configuration

An appreciable amount of subcooling (5 - 8 °C) was noticed during the experiment (See Fig. 5.11(a)). The least amount of subcooling was seen during the hottest time of the day, which is probably because the main cycle condenser temperature at the inlet is at its highest at this time. Thus, more heat transfer is required to achieve the saturated liquid state after which subcooling can begin. Fig. 5.11(b)-(c) shows the variation of subcooler effectiveness and the amount of heat transferred in the subcooler (i.e. subcooling power), respectively, over the day. The average effectiveness was calculated as 0.157 whereas the highest was seen to be 0.203 when ambient temperature was lowest. The average subcooling power was found to be 0.253 kW while the maximum was seen to be 0.299 when ambient temperature was at its minimum value. Fig. 5.12(a) indicates that average cooling capacity for this configuration is 4 kW, which is 0.5 kW higher compared to the base configuration. Fig. 5.12(b) shows the COP following the pattern of the variation in the cooling capacity.

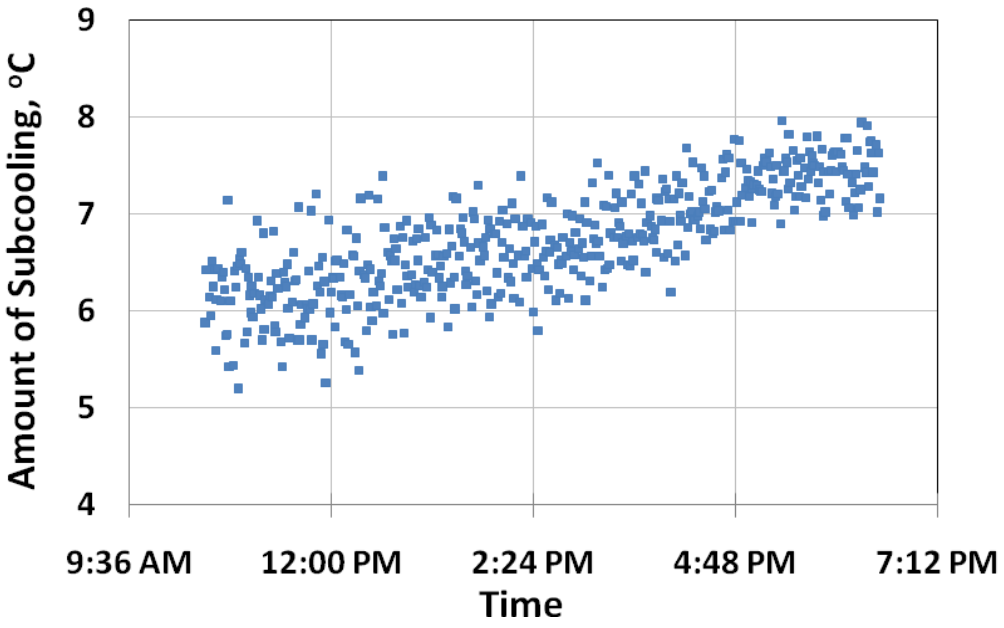

Figure 5.11(a). Variation in amount of subcooling – Subcooler configuration

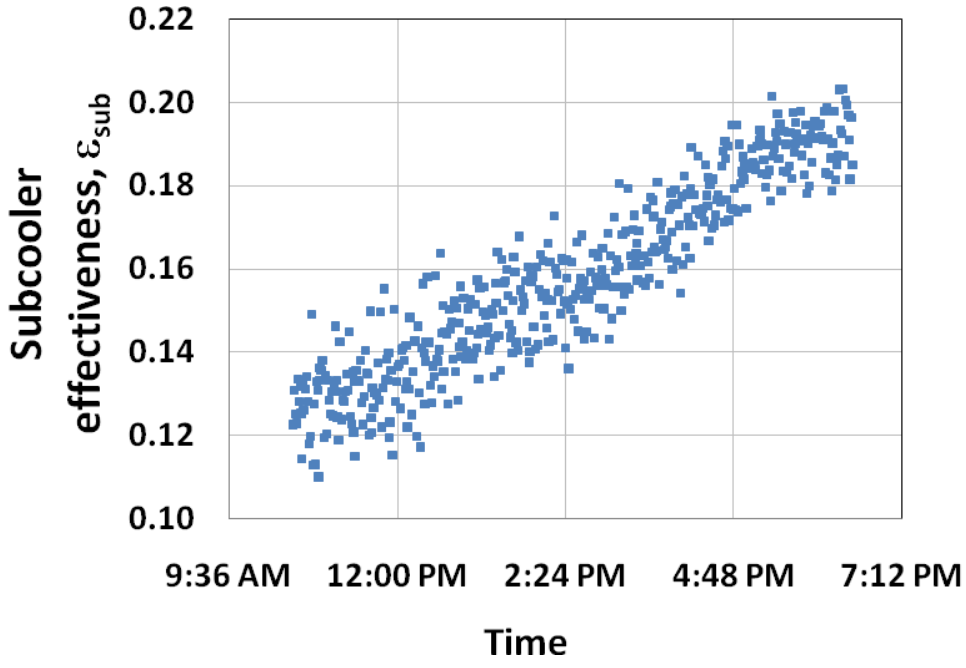

Figure 5.11(b). Variation in subcooler effectiveness – Subcooler configuration

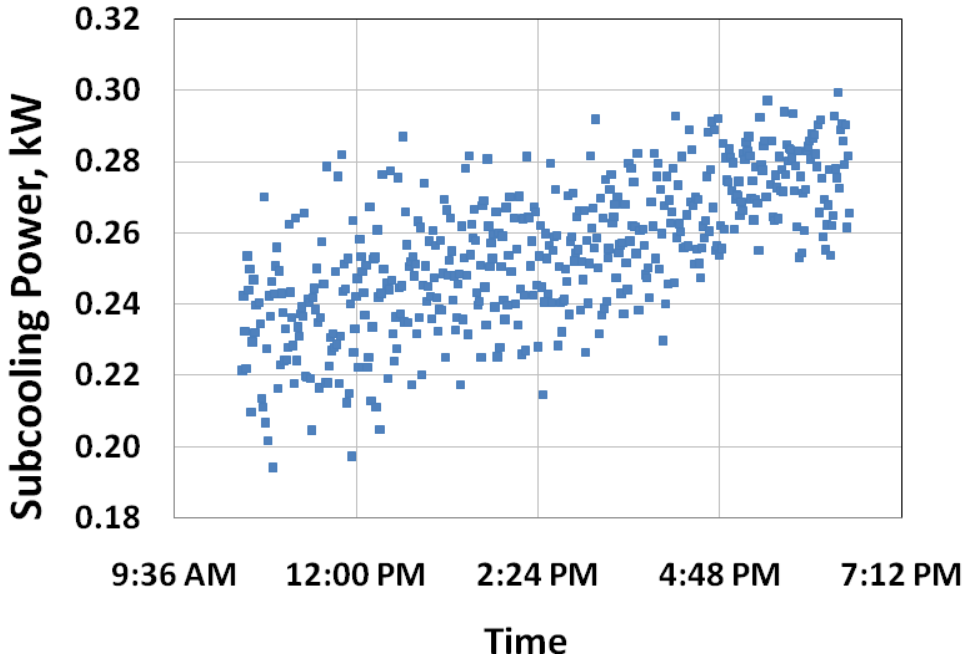

Figure 5.11(c). Variation in subcooler power – Subcooler configuration

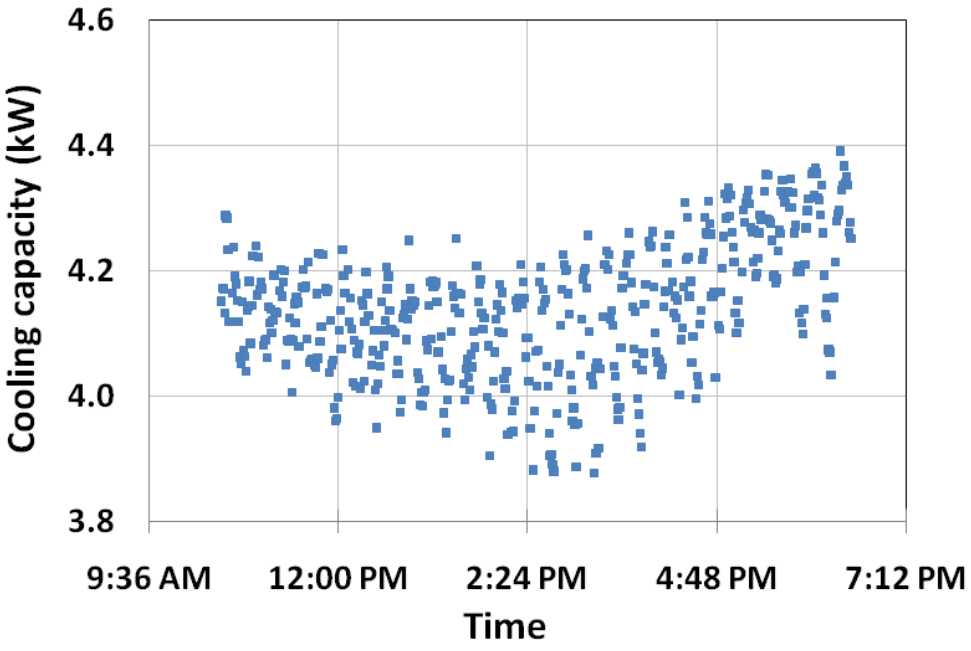

Figure 5.12(a). Variation in cooling capacity – Subcooler configuration

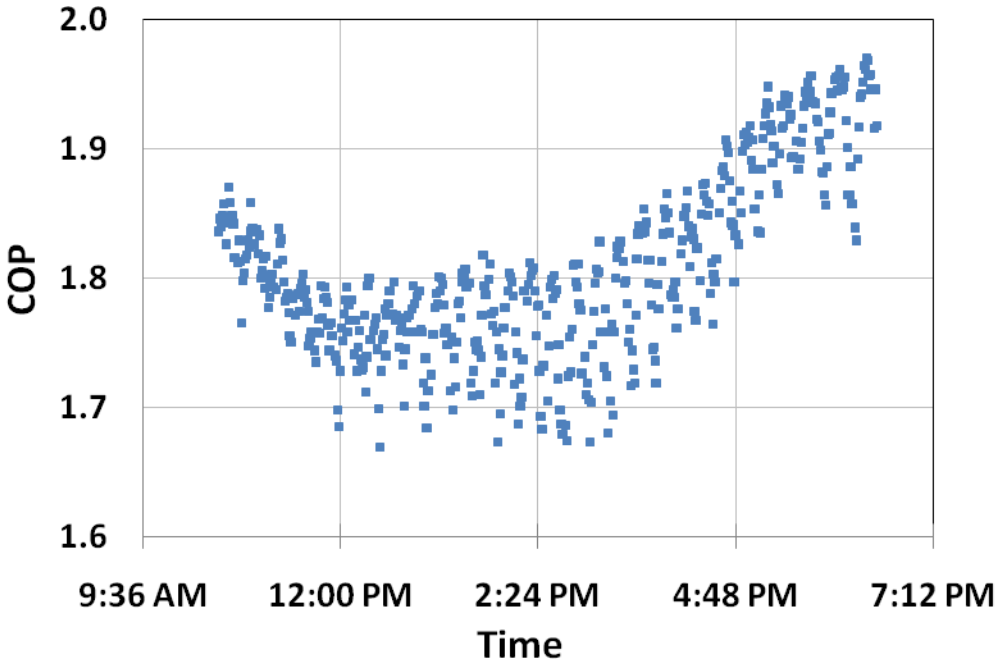

Figure 5.12(b). Variation in COP – Subcooler configuration

A comparison of second-law efficiency variation for both configurations for the test period and the percentage increase in it due to use of dedicated subcooling are illustrated in Figs. 5.13 and 5.14, respectively. The general trend that is visible from both figures is that use of subcooling is consistently better than the simple vapor compression cycle. Also, the difference in the second-law efficiency seems to reach a minimum around the hottest time of the day and then increases again with the ambient temperature decreasing as the day progresses. The average value for the second-law efficiency of the subcooler configuration was 0.116 while it was 0.096 for the base configuration, which constitutes a percentage increase of 18.4% with respect to the base configuration. The

maximum value for the second-law efficiency of the subcooler configuration was 0.124 while it was 0.109 for the base configuration. From Fig. 5.14, the average increase in second-law efficiency, due to use of subcooling, was found to be 21%. It should be noted that the complete period was divided into 30 minute time slots and the average determined for each of them to ascertain overall behavior more appropriately (See Table 5.1). Table 5.1 shows that the minimum advantage provided by the subcooler configuration is 14.58%. It is expected that larger systems would provide a greater advantage [87]. Table 5.2 contains a summary of the average uncertainty found in the quantities plotted in the figures.

5.2 Numerical Work

The results from Qureshi and Zubair [87] indicate that dedicated mechanical sub-cooling is more suited to cycles using R134a than R717 as the main cycle refrigerant. Therefore, the effect of fouling resulting in UA-degradation on the main and sub-cooling cycle will now be discussed briefly using R134a as the main cycle refrigerant. Section 3.5 should be consulted for modeling and validation of this system. The following conditions were used for Figs. 5.15(a) and (b) using R134a, R407C and R410A, one by one, as the sub-cooler cycle refrigerant: $\eta_{cp,is,m} = 0.65, \eta_{cp,is,sc} = 0.65, \dot{C}_{\min,m} = 12\ kW\ K^{-1}$ and $\dot{C}_{\min,sc} = 3.6\ kW\ K^{-1}$.

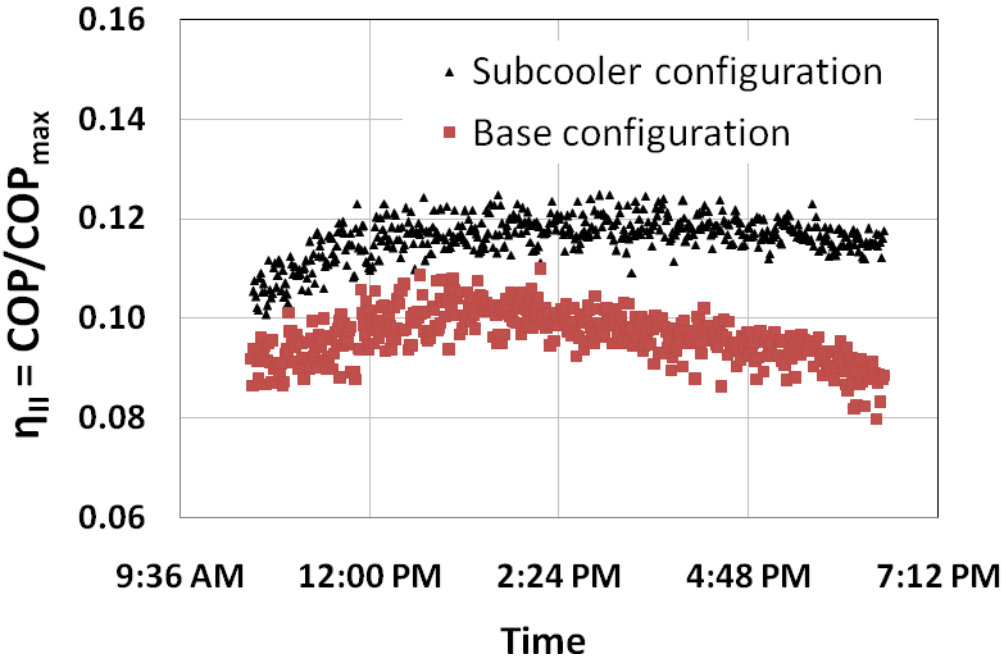

Figure 5.13. Comparison of second-law efficiency variation for both configurations

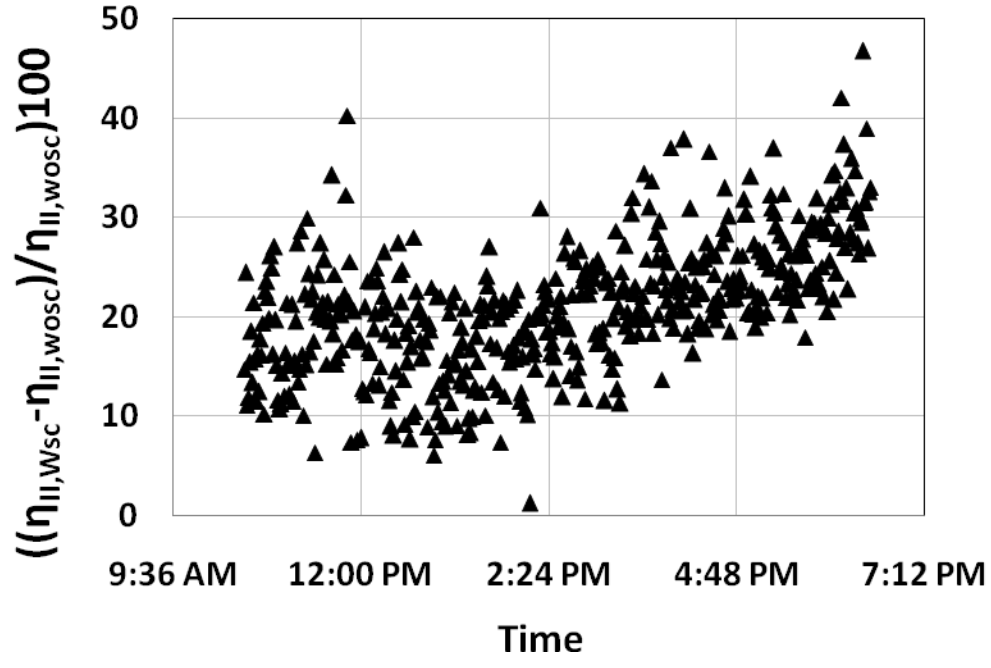

Figure 5.14. Percentage change in second-law efficiency due to use of subcooling

Table 5.1: Average percentage increase in second-law efficiency.

Time slot	Average difference (%)
10:30 - 11:00 am	16.89
11:00 - 11:30 am	18.65
11:30 - 12:00 pm	20.20
12:00 - 12:30 pm	18.02
12:30 - 1:00 pm	16.20
1:00 - 1:30 pm	14.58
1:30 - 2:00 pm	18.33
2:00 - 2:30 pm	17.52
2:30 - 3:00 pm	20.96
3:00 - 3:30 pm	20.88
3:30 - 4:00 pm	23.80
4:00 - 4:30 pm	23.69
4:30 - 5:00 pm	24.96
5:00 - 5:30 pm	25.41
5:30 - 6:00 pm	25.76
6:00 - 6:30 pm	31.31

Table 5.2: Average uncertainty calculated for plotted quantities.

Quantity	Uncertainty	
	Base configuration	Subcooler configuration
Cooling capacity	0.162 kW	0.196 kW
COP	0.054	0.075
Second-law efficiency	0.0042	0.0057
Amount of subcooling	-	0.63 °C
Subcooler effectiveness	-	0.013
Subcooling power	-	0.013 kW

It is assumed that, at the clean condition, the effectiveness of both the condensers and the main evaporator is 80% and cooling capacity is 100 kW. Also, it is assumed that the refrigerant at the suction of the compressors is a saturated vapor while it is a saturated liquid at the condenser exit. In each case, before proceeding, the system was optimized with respect to the COP at the clean condition. In Figs. 5.15(a) and (b), equal degradation of the *UA* value due to fouling of both condensers and the main evaporator is considered. The COP and the cooling capacity of evaporator and sub-cooler were degraded by approximately 12%, 14% and 4%, respectively, irrespective of the sub-cooler cycle refrigerant. Furthermore, the power requirement of the main compressor decreased by 3.7% while it increased by 12% for the sub-cooler cycle compressor. The power decrease in the main compressor may be understood from the fact that both the heat exchangers of the main cycle are being fouled equally, which, keeping the First Law in mind, reduces the difference between them. It is also noticed that the smallest variation (only 2.5%) in the saturation temperature of the sub-cooler occurred when R134a was used as the sub-

cooler cycle refrigerant. The most important point to note is that, in these figures, the nature of the change of all the quantities shown is similarly logarithmic as was seen from various sources in Chapter 4 for comparatively simpler systems. This indicates that, even though the system is more complex especially with the presence of more heat exchangers, the nature of the behavior has, in essence, not changed.

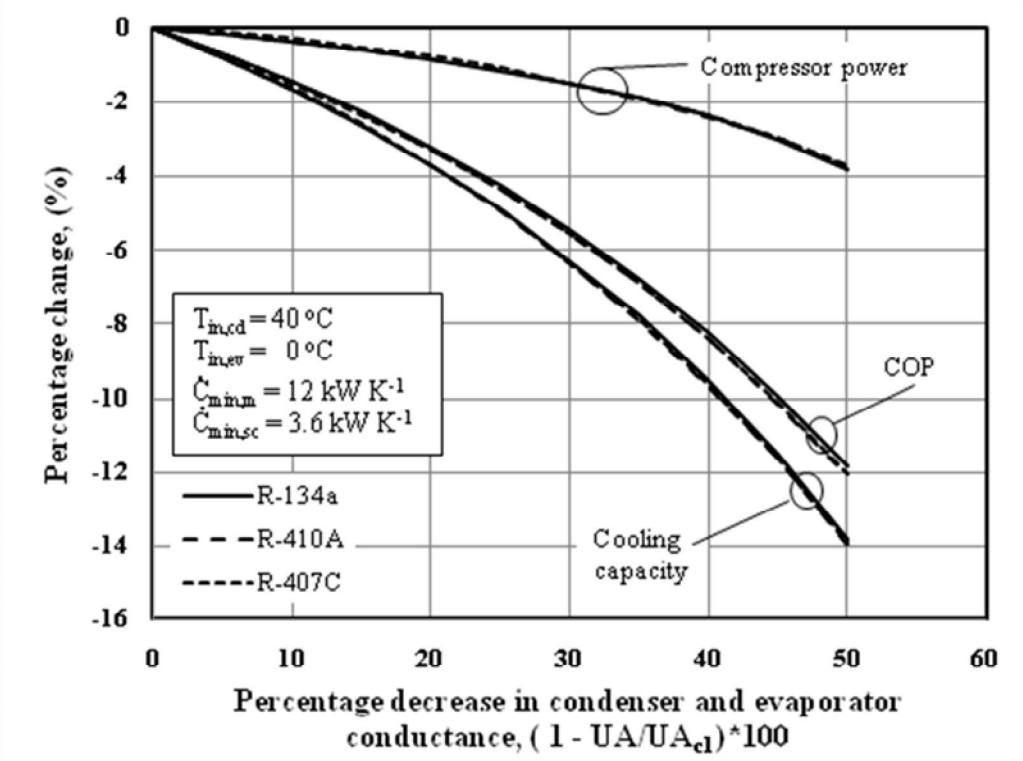

Figure 5.15(a). Effect of equal UA degradation (in both condensers and the main evaporator) on main cycle – for R134a$_m$- R134a$_{sc}$, R410A$_{sc}$, R407C$_{sc}$

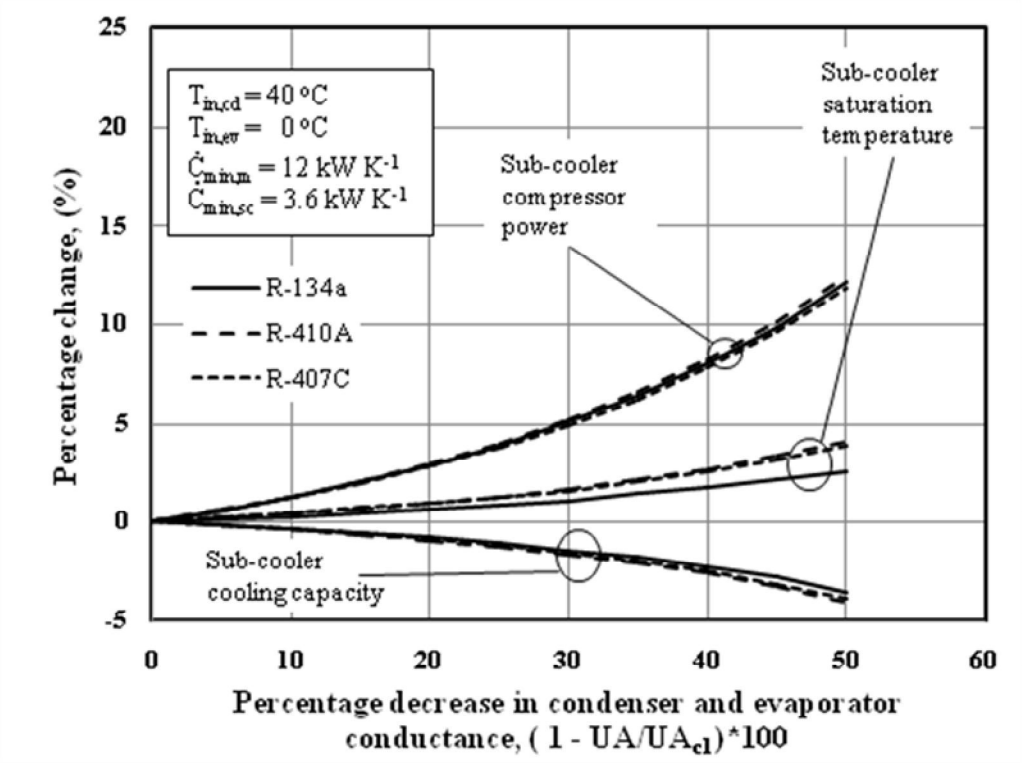

Figure 5.15(b). Effect of equal UA degradation (in both condensers and the main evaporator) on dedicated sub-cooler section – for R134a$_m$- R134a$_{sc}$, R410A$_{sc}$, R407C$_{sc}$

CHAPTER 6

PREDICTING EFFECT OF FOULING ON UA-DEGRADATION IN POWER AND REFRIGERATION SYSTEMS

In this chapter, a model will be presented to predict properties and performance parameters of power and refrigeration systems under fouled conditions.

6.1 Methodology and Procedure

Having established that the effect of fouling on properties and performance parameters is governed by a logarithmic process, the CA and reversed CA cycles will now be used to establish a prediction model by observing the behavior of some important parameters. These two cycles are used as they are the basis for all power and refrigeration systems. The prediction model will then be checked against simulated data using models

for a simple vapor compression cycle and a Rankine cycle. These two cycles are used as they are the simplest of all refrigeration and power systems and proof of applicability in these cases will serve as the basis for more complicated configurations for them in the future.

6.2 Determining the Fouling Prediction Model

The CA and reversed CA cycles will now be used to help establish a prediction model by observing the behavior of some important variables consisting of both performance parameters and properties.

6.2.1 Observations from Curzon-Ahlborn cycle

An example of a power cycle undergoing fouling will be simulated in the heat exchangers present in the above model for:

- Case 1: Fouling in HX on high temperature-side only
- Case 2: Fouling in HX on low temperature-side only
- Case 3: Fouling in both HX (equally)

The following conditions were used:

$$T_{H,in} = 327\ ^{o}C, T_{L,in} = 20\ ^{o}C, \dot{C}_H = \dot{C}_L = 12\,kW.K^{-1}, UA_p = 0\ to\ 50\%$$

The results obtained for the three cases described above are shown in Figs. 6.1(a)-(c).

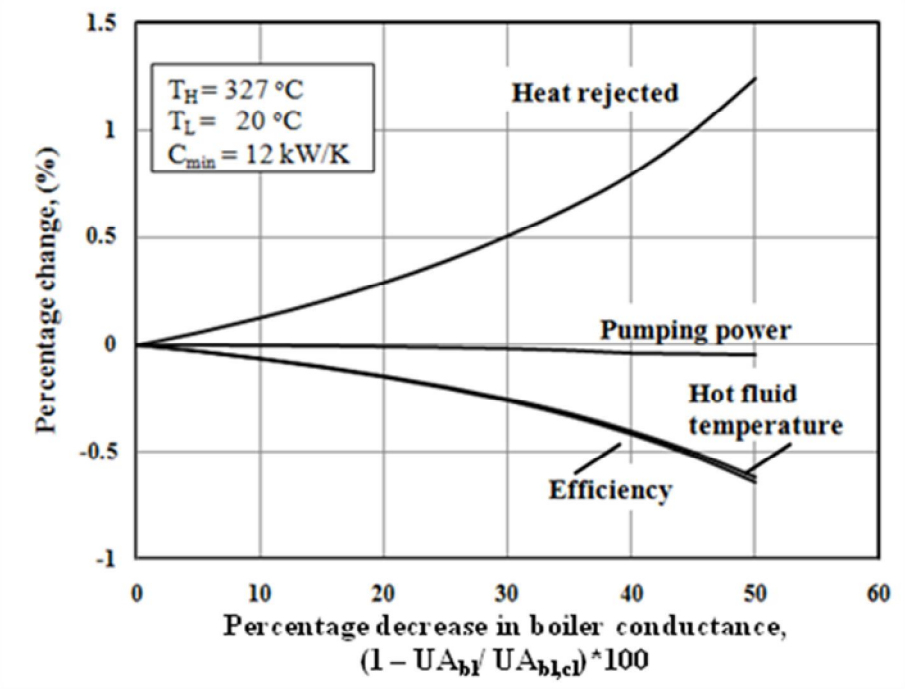

Figure 6.1(a). Effect of reduction in boiler conductance only: CA cycle

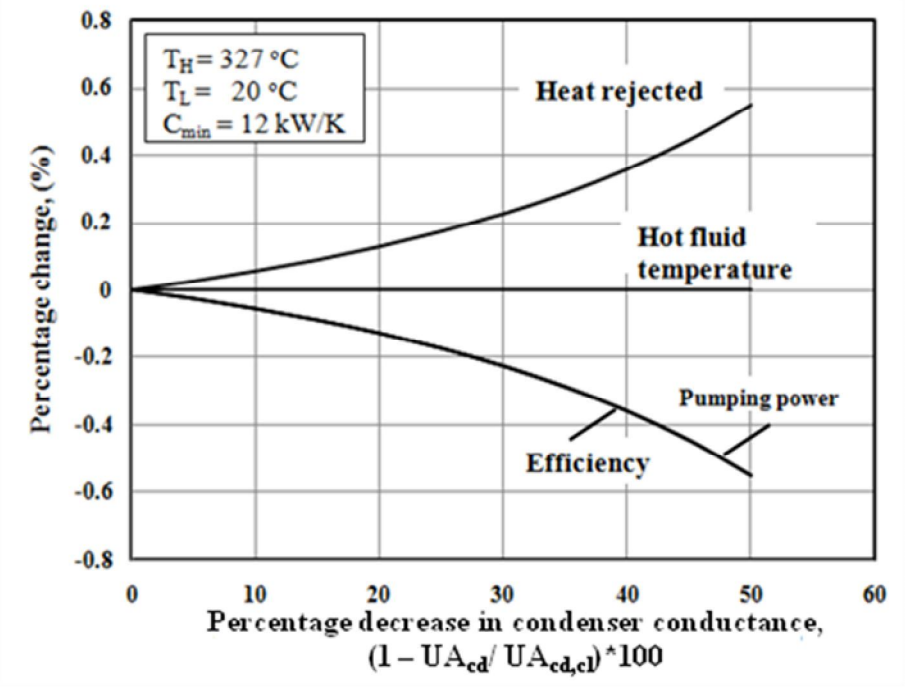

Figure 6.1(b). Effect of reduction in condenser conductance only: CA cycle

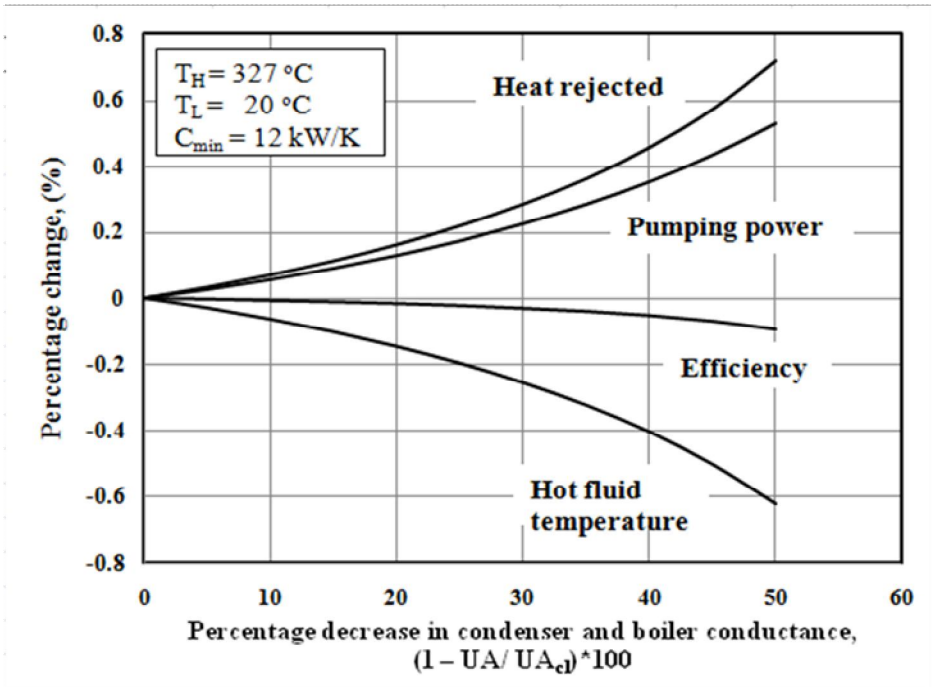

Figure 6.1(c). Effect of reduction in (equal) condenser and boiler conductance: CA cycle

For the case of maximum power production, similar behavior was noticed. It is seen from comparison of the above three figures that the results exhibit a logarithmic behavior. Furthermore, the plotted lines of Fig. 6.1(c) seem to be the results of an addition or subtraction process of some kind from the first two figures i.e. 6.1(a) and 6.1(b).

6.2.2 Observations from reversed Curzon-Ahlborn cycle

Following a similar path, an example of a refrigeration cycle undergoing fouling will be simulated in the heat exchangers present in the reversed CA model for:

- Case 1: Fouling in HX on high temperature-side only
- Case 2: Fouling in HX on low temperature-side only
- Case 3: Fouling in both HX (equally)

The following conditions were used:

$$T_{H,in} = 40\ ^{o}C, T_{L,in} = 0\ ^{o}C, \dot{C}_H = \dot{C}_L = 12\,kW.K^{-1}, UA_p = 0\ to\ 50\%$$

The following results were obtained due to fouling for the three situations described above (See Figs. 6.2(a)-(c)):

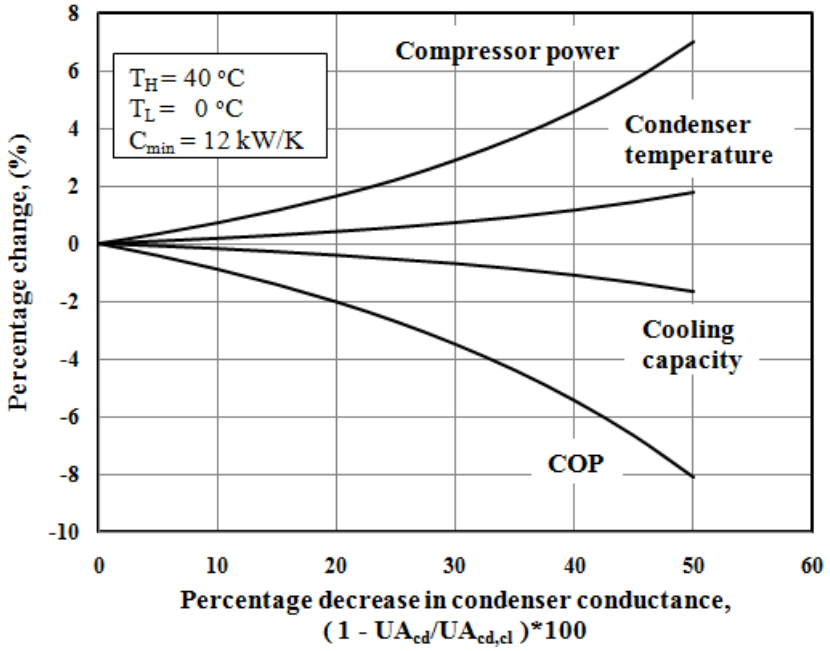

Figure 6.2(a). Effect of reduction in condenser conductance only: Reversed CA cycle

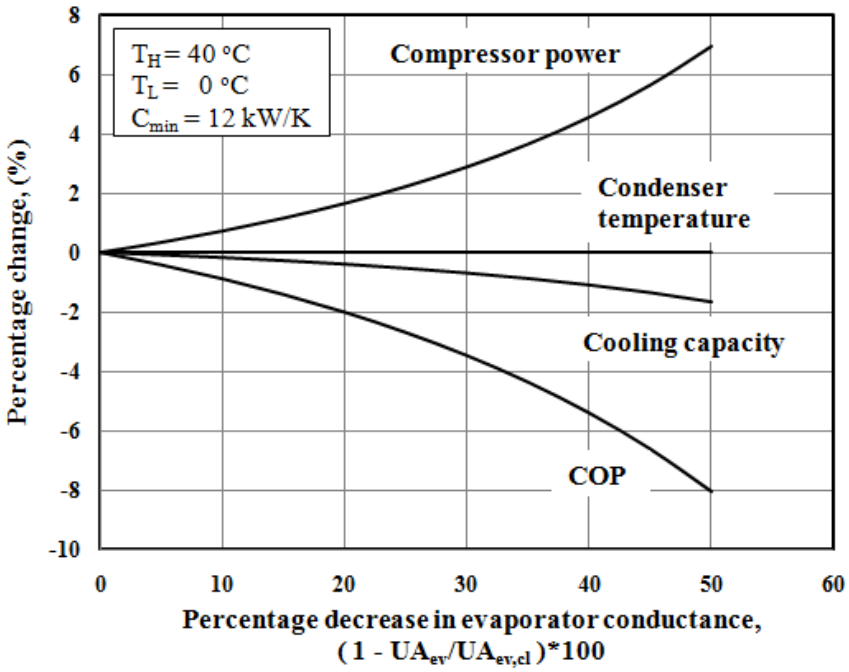

Figure 6.2(b). Effect of reduction in evaporator conductance only: Reversed CA cycle

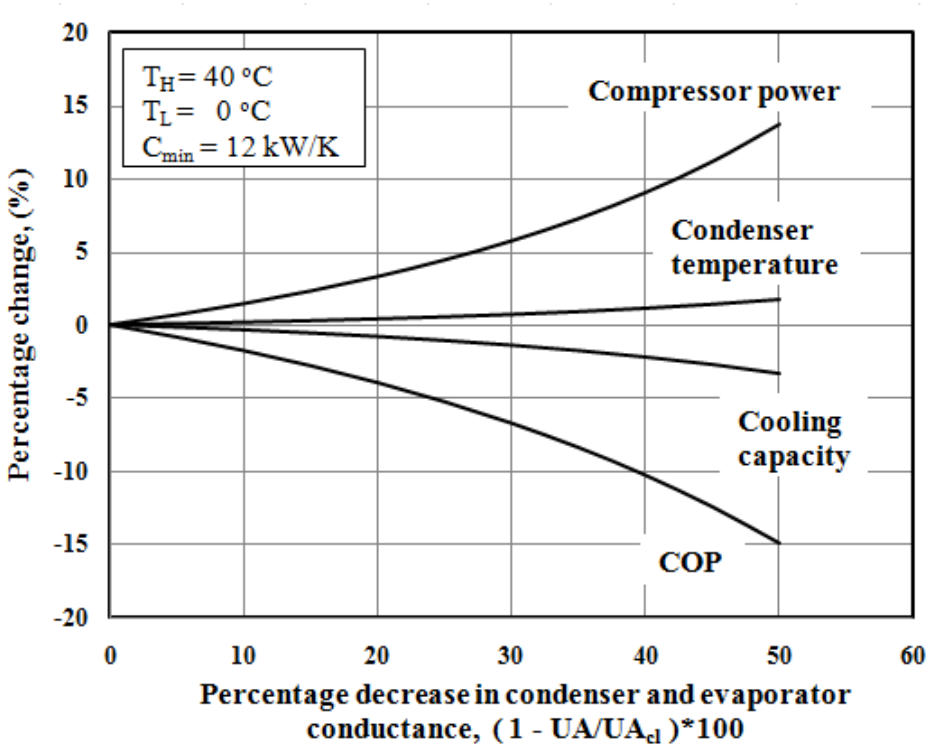

Figure 6.2(c). Effect of reduction in (equal) condenser and evaporator conductance:

Reversed CA cycle

As was seen in the Carnot based results for the power cycle, similar trends and observations are seen here. This type of relationship among these simulated cases was first noted by Qureshi and Zubair [85] for a vapor compression refrigeration system and then again by Qureshi and Zubair [86] for a vapor compression refrigeration system with integrated mechanical subcooling. In these works, an equation was proposed to predict the impact of fouling on performance parameters and properties which was linear in nature. This often resulted in significant errors and, therefore, the proposed equation left room for improvement.

6.2.3 Fouling model

Based on what has been proven in Chapter 4, indicated in Chapter 5 and the above observations, the following fouling model is proposed:

$$\sum_{i=1}^{k} c_{f,i} \left(\ln \frac{X_i}{X_{i,ref}} \right) = \ln \frac{X_{comb}}{X_{comb,ref}} \tag{6.1}$$

where k is the total number of externally irreversible heat exchangers, $c_{f,i}$ is a constant that depends on system configuration, X is any quantity e.g. properties or performance characteristics, *ref* is the reference condition and *comb* refers to the combined effect of more than one heat exchanger fouling simultaneously. The proposed model can predict relevant parameters in any one of the previous three situations provided information is available on the other two along with the reference condition.

As an example, applying Eq. (6.1) to a simple heat engine that contains only two external heat exchangers (i.e. $k = 2$), we get

$$c_1 \ln\left(X_H \Big|_{\substack{UA_{p,L}=x \\ UA_{p,H}=z_1}} \right) - c_1 \ln\left(X_{H,ref} \Big|_{\substack{UA_{p,L}=x \\ UA_{p,H}=a_1}} \right) + c_2 \ln\left(X_L \Big|_{\substack{UA_{p,H}=y \\ UA_{p,L}=z_2}} \right) - c_2 \ln\left(X_{L,ref} \Big|_{\substack{UA_{p,H}=y \\ UA_{p,L}=a_2}} \right) = \ln\left(X_{comb} \Big|_{\substack{UA_{p,H}=z_1 \\ UA_{p,L}=z_2}} \right) - \ln\left(X_{comb,ref} \Big|_{\substack{UA_{p,H}=a_1 \\ UA_{p,L}=a_2}} \right) \quad (6.2a)$$

The question may be asked as to what is the best choice for the variables x, y, a_1 and a_2? On inspection, it seems that taking a value of zero for all of them is the best. Using these values, we get

$$c_1 \ln\left(X_H \Big|_{\substack{UA_{p,L}=0 \\ UA_{p,H}=z_1}} \right) - c_1 \ln\left(X_{H,ref} \Big|_{\substack{UA_{p,L}=0 \\ UA_{p,H}=0}} \right) + c_2 \ln\left(X_L \Big|_{\substack{UA_{p,H}=0 \\ UA_{p,L}=z_2}} \right) - c_2 \ln\left(X_{L,ref} \Big|_{\substack{UA_{p,H}=0 \\ UA_{p,L}=0}} \right) = \ln\left(X_{comb} \Big|_{\substack{UA_{p,H}=z_1 \\ UA_{p,L}=z_2}} \right) - \ln\left(X_{comb,ref} \Big|_{\substack{UA_{p,H}=0 \\ UA_{p,L}=0}} \right) \quad (6.2b)$$

In Eq. (6.2b), the second, fourth and sixth terms are identical except for the constants and refers to the condition of the system when it is clean which is known from manufacturer. This helps to simplify the calculation.

For the prediction of case 3 from data of case 1 and case 2 in CA as well reversed CA cycle model simulations, the required constants were found by regression and most errors are less than 0.01%. This indicates excellent agreement between predicted and simulated values.

6.3 Determining the Constants for the Fouling Prediction Model

Now, the constants (c_f) were found using regression since the purpose uptil now was to demonstrate the usage of the model. In reality, we must be able to predict these constants beforehand. This entails modeling the prediction constants (c_f) for both heat exchangers i.e. condenser and evaporator. Therefore, in the following sections, it is shown how to achieve this using the classical Buckingham Pi Theorem.

6.3.1 Steps for deriving model constants

The fouling constants will be determined in the following manner:

1. The first step is to determine constants for an endoreversible CA-cycle as well as reversed CA-cycle by studying their nature and behavior. The reason for doing this is that it is well-known in Thermodynamics that trends found in the reversible cycle are often seen in real cycles.
2. Considering the complexity of the problem, the Buckingham Pi theorem will be used to determine dimensionless groups that would affect the determination of the constants (See Appendix E and section 6.3.2 for steps of derivation):
3. For the endoreversible case, data will be generated with NTU ranging from 0.5 to 5 ($\varepsilon = 0.393 - 0.993$) and thermal capacitance ratio from 1 to 0.7. This covers the large majority of heat exchangers used in these systems.
4. Data will be generated for the three cases mentioned in 6.2.2 for the range mentioned above. For any particular value of NTU and C_r, the three cases would

start with the same clean condition and allowed to foul down to 50% of its original UA-value.

5. Excel will then be used to determine the best fit. This would act as a first guess for determining the value of the set of constants for the evaporator and condenser. Then through a process of trial and error, the best fit would be used. The best fit is the one that balances between simplicity and least error. Any prediction within 1% of the calculated value is considered correct.
6. Next, the complete model will be checked using data generated from a simulation model of a simple vapor compression cycle (SVCC) as application to a real system is important to demonstrate.
7. For the case of SVCC, data will be generated for R134a with NTU ranging from 0.5 to 5 (ε = 0.393 – 0.993) and thermal capacitance ratio from 1 to 0.7. This covers the large majority of heat exchangers used in this system.
8. For SVCC case, the quantities that will be fitted are rate of cooling$\left(\dot{Q}_L\right)$, COP, superheat temperature$\left(T_{\text{sup}}\right)$ and condenser temperature$\left(T_{cd}\right)$ as these cover both performance parameters and properties.

6.3.2 Buckingham Pi applied to a reversed CA cycle

Keeping in mind the points outlined in Appendix E, we get:

Step 1:

We define the problem in terms of the following 11 important variables.

$$c_f = f(U_{H,cl}, A_{H,cl}, U_{L,cl}, A_{L,cl}, \Delta T_L, T_{avg}, \dot{m}_H, \dot{m}_L, c_{p,H}, c_{p,L}) \quad (6.3a)$$

where

$$\Delta T_L = T_{L,in} - T_{ev,cl} \quad (6.3b)$$

$$T_{avg} = \left(T_{H,in} + T_{L,in}\right)/2 \quad (6.3c)$$

Step 2:

Using both MLtT and FLtT system to check regarding repeating parameters. This is summarized in tabular form below:

Table 6.1: Selected variables in terms of MLtT and FLtT system for reversed CA cycle

	c_f	$U_{H,cl}$, $U_{L,cl}$	$A_{H,cl}$, $A_{L,cl}$	ΔT_L, T_{avg}	$\dot{m}_L, \dot{m}_H$	$c_{p,L}, c_{p,H}$
MLtT	-	$\frac{M}{t^3 T}$	L^2	T	$\frac{M}{t}$	$\frac{L^2}{t^2 T}$
FLtT	-	$\frac{F}{L^2 t T}$	L^2	T	$\frac{Ft}{L}$	$\frac{L^2}{t^2 T}$

It is seen that there are 4 repeating parameters that are chosen as follows:

$$\dot{m}_H, A_{H,cl}, \Delta T_L, U_{H,cl}$$

Step 3:

Therefore, we have 7 dimensionless Pi groups. The remaining independent parameters will now be used one by one. According to dimensional analysis, it can be written

$$\pi_1 = \dot{m}_H^a A_{H,cl}^b \Delta T_L^c U_{H,cl}^d U_{L,cl} \tag{6.4a}$$

To equalize units on both sides, we may write

$$\pi_1 = \left(\frac{M}{t}\right)^a \left(L^2\right)^b T^c \left(\frac{M}{t^3 T}\right)^d \left(\frac{M}{t^3 T}\right) \tag{6.4b}$$

which leads to

$$\pi_1 = \frac{U_{L,cl}}{U_{H,cl}} \tag{6.4c}$$

The other six dimensionless groups are found similarly. A summary of all π groups has been provided in Table 6.2.

Table 6.2: Summary of dimensionless Pi groups for determining fouling constants

Group #	**Parameter form**	**Dimensional form**	**π group**
π_1	$\dot{m}_H^a A_{H,cl}^b \Delta T_L^c U_{H,cl}^d U_{L,cl}$	$\left(\frac{M}{t}\right)^a \left(L^2\right)^b T^c \left(\frac{M}{t^3 T}\right)^d \left(\frac{M}{t^3 T}\right)$	$\frac{U_{L,cl}}{U_{H,cl}}$
π_2	$\dot{m}_H^a A_{H,cl}^b \Delta T_L^c U_{H,cl}^d c_f$	$\left(\frac{M}{t}\right)^a \left(L^2\right)^b T^c \left(\frac{M}{t^3 T}\right)^d$	c_f
π_3	$\dot{m}_H^a A_{H,cl}^b \Delta T_L^c U_{H,cl}^d A_{L,cl}$	$\left(\frac{M}{t}\right)^a \left(L^2\right)^b T^c \left(\frac{M}{t^3 T}\right)^d \left(\mathrm{L}^2\right)$	$\frac{A_{L,cl}}{A_{H,cl}}$
π_4	$\dot{m}_H^a A_{H,cl}^b \Delta T_L^c U_{H,cl}^d T_{avg}$	$\left(\frac{M}{t}\right)^a \left(L^2\right)^b T^c \left(\frac{M}{t^3 T}\right)^d T$	$\frac{\Delta T_L}{T_{avg}}$
π_5	$\dot{m}_H^a A_{H,cl}^b \Delta T_L^c U_{H,cl}^d \dot{m}_L$	$\left(\frac{M}{t}\right)^a \left(L^2\right)^b T^c \left(\frac{M}{t^3 T}\right)^d \left(\frac{M}{t}\right)$	$\frac{\dot{m}_L}{\dot{m}_H}$

π_6	$\dot{m}_H^a A_{H,cl}^b \Delta T_L^c U_{H,cl}^d c_{p,H}$	$\left(\frac{M}{t}\right)^a \left(L^2\right)^b T^c \left(\frac{M}{t^3 T}\right)^d \left(\frac{L^2}{t^2 T}\right)$	$\frac{U_{H,cl} A_{H,cl}}{\dot{m}_H c_{p,H}} = NTU_{H,cl}$
π_7	$\dot{m}_H^a A_{H,cl}^b \Delta T_L^c U_{H,cl}^d c_{p,L}$	$\left(\frac{M}{t}\right)^a \left(L^2\right)^b T^c \left(\frac{M}{t^3 T}\right)^d \left(\frac{L^2}{t^2 T}\right)$	$\frac{c_{p,L}}{c_{p,H}}$

Therefore, we may write:

$$c_f = f\left(\frac{U_{L,cl}}{U_{H,cl}}, \frac{A_{L,cl}}{A_{H,cl}}, \frac{\Delta T_L}{T_{avg}}, NTU_{H,cl}, \frac{\dot{m}_L}{\dot{m}_H}, \frac{c_{p,L}}{c_{p,H}}\right) \tag{6.5}$$

It is known from theory that the UA-value of a heat exchanger is important. Therefore, π_1 and π_3 will be used in a combined form i.e. $\left(U_{L,cl} A_{L,cl}\right) / \left(U_{H,cl} A_{H,cl}\right)$ and similarly, for π_6 and π_7, we will have $\left(\dot{m}_L c_{p,L}\right) / \left(\dot{m}_H c_{p,H}\right)$, which represents a thermal capacitance ratio (C_r), due to the significance of thermal capacitance rate in heat exchangers. It is known from theory that the UA-value of a heat exchanger is important. Therefore, π_1 and π_3 will be used in a combined form i.e. $\left(U_{L,cl} A_{L,cl}\right) / \left(U_{H,cl} A_{H,cl}\right)$ and similarly, for π_6 and π_7, we will have $\left(\dot{m}_L c_{p,L}\right) / \left(\dot{m}_H c_{p,H}\right)$, which represents a thermal capacitance ratio (C_r), due to the significance of thermal capacitance rate in heat exchangers. Now, this result will be applied to data generated using the reversed CA cycle to show that the required constants can be predicted using the above dimensionless quantities. It is noted that the Pi-groups shown in Eq. (6.5) have a similarity with those developed independently by Yang *et al.* [84] for predicting condenser performance using neural networks wherein the objective function was the heat transfer.

6.3.3 Buckingham Pi applied to a CA cycle

Keeping in mind the points outlined in Appendix E, we get:

Step 1:

We define the problem in terms of the following 11 important variables.

$$c_f = f(U_{H,cl}, A_{H,cl}, U_{L,cl}, A_{L,cl}, \dot{W}_{cl}, T_{avg}, \dot{m}_H, \dot{m}_L, c_{p,H}, c_{p,L}) \tag{6.6}$$

where T_{avg} is defined in Eq. (6.3c).

Step 2:

Using both MLtT and FLtT system to check regarding repeating parameters. This is summarized in tabular form below:

Table 6.3: Selected variables in terms of MLtT and FLtT system for CA cycle

	c_f	$U_{H,cl}$, $U_{L,cl}$	$A_{H,cl}$, $A_{L,cl}$	$\dot{W}_{cl}$	T_{avg}	$\dot{m}_L, \dot{m}_H$	$c_{p,L}, c_{p,H}$
MLtT	-	$\frac{M}{t^3 T}$	L^2	$\frac{ML^2}{t^3}$	T	$\frac{M}{t}$	$\frac{L^2}{t^2 T}$
FLtT	-	$\frac{F}{L^2 t T}$	L^2	$\frac{FL}{t}$	T	$\frac{Ft}{L}$	$\frac{L^2}{t^2 T}$

It is seen that there are 4 repeating parameters that are chosen as follows:

$$\dot{m}_L, A_{L,cl}, \dot{W}_{cl}, U_{L,cl}$$

Step 3:

Therefore, we have 7 dimensionless Pi groups. All dimensionless Pi groups are the same as in Table 6.2 except for π_4 and, thus, its derivation is shown below:

$$\pi_4 = \dot{m}_L^a A_{L,cl}^b \dot{W}_{cl}^c U_{L,cl}^d T_{avg} \tag{6.7a}$$

To equalize units on both sides, we may write

$$\pi_4 = \left(\frac{M}{t}\right)^a \left(L^2\right)^b \left(\frac{ML^2}{t^3}\right)^c \left(\frac{M}{t^3 T}\right)^d T \tag{6.7b}$$

which leads to

$$\pi_4 = \frac{\dot{W}_{cl}}{U_{L,cl} A_{L,cl} T_{avg}} \tag{6.7c}$$

Furthermore, all 'H' subscripts are replaced with 'L' subscripts.

6.3.4 Reversed Curzon-Ahlborn cycle

As mentioned in section 6.3.1, for the endoreversible case, data was generated for NTU ranging from 0.5 to 5 (ε = 0.393 – 0.993) and thermal capacitance ratio (C_r) from 1 to 0.7 for the three cases mentioned in 6.2.2. The clean conditions consist of varying the evaporator temperature from 253.7 to 263.7 in 2 °C steps. In real systems, the compressor size is determined for a given load during the design phase and then it is fixed during performance. In the endoreversible case, the compressor does not exist. Therefore, for simulating the performance case, the evaporator temperature is kept constant for each of the three cases. Initially, it is preferred that, if it is possible to ignore the effect of one of

the dimensionless quantities such as NTU and a prediction within 1% is still possible, then it will be used since it provides a simpler expression. To achieve this, an NTU (=1.609 in this case) is chosen from around the middle of the range used. Then an attempt is made to fit the data according to Eq. (6.1) for the effect of C_r only.

We have three performance parameters i.e. COP, load and power consumption while one property i.e. condenser temperature (T_{cd}), that can be checked for modeling the constants. Let us first take the condenser temperature. It was found that, for NTU = 1.609 at $C_r = 1$, the set of constants for the evaporator and condenser both produced zero value for the constants. The reason for this is that when only the condenser or evaporator was being fouled (Case 1 or 2, respectively), the condenser temperature varied but it remained constant when both the heat exchangers were equally fouled (i.e. Case 3). The behavior in Case 3 is understood from the fact that the heat transfer ratio remains constant irrespective of the UA-value since the effectiveness for both heat exchangers decreases by the same amount (See Eqs. (3.9), (3.10) and (3.12)). Next, for $C_r = 0.7$, the constants for both the evaporator and condenser produced a wavy curve but was, in general, decreasing as π_5 increased. Linear best fit curves (and their corresponding equations) were determined using Excel and the constants were re-determined using them to produce a set of straight lines providing corresponding constants for the evaporator and condenser. The correction to the original curve proved useful as it resulted in negligible error in prediction and yet provided a linear curve, which is easy to model (See Figs. 6.3(a) and (b)).

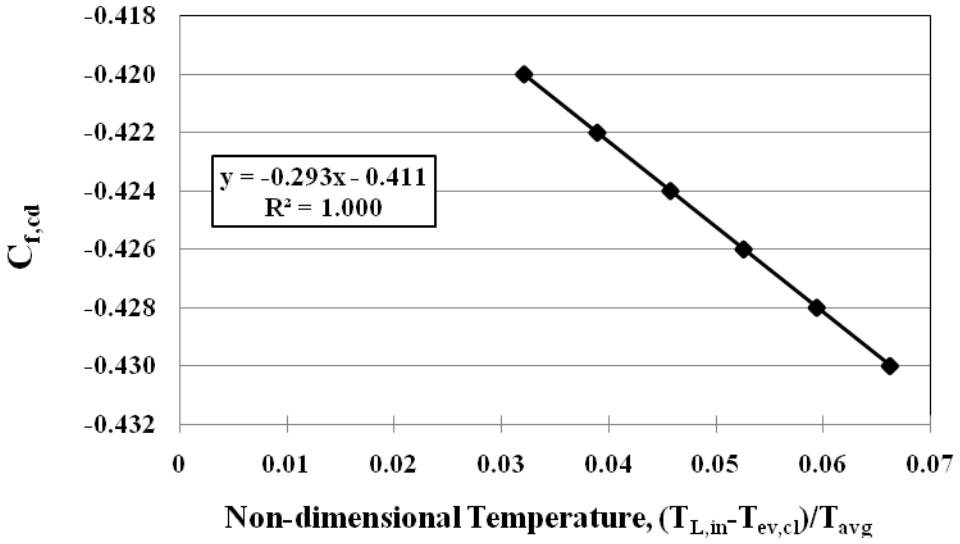

Figure 6.3(a). Determining fouling data constants for T_{cd} variation for Case 1 (for C_r=0.7): ER

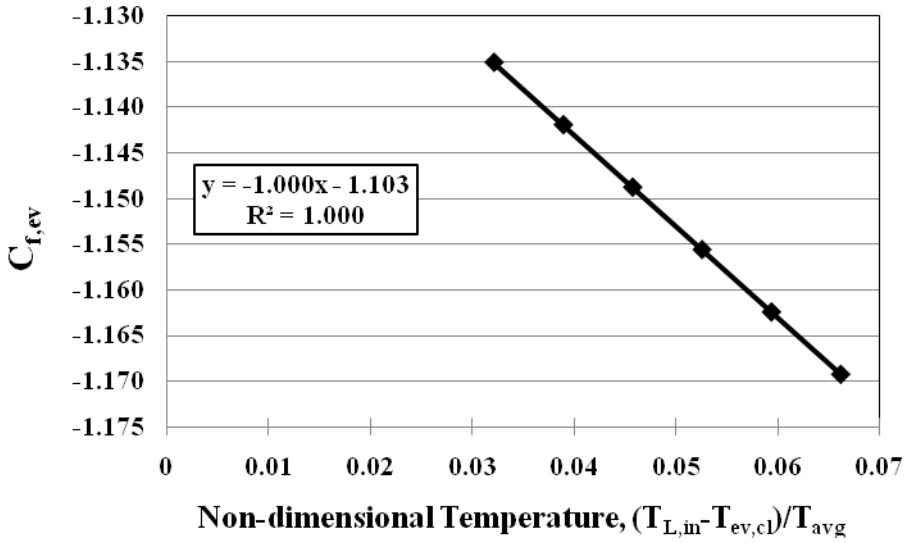

Figure 6.3(b). Determining fouling data constants for T_{cd} variation for Case 2 (for C_r=0.7): ER

For the sake of simplicity, it is initially assumed that the slope and intercept of the fit equations shown in Figs. 6.3 (a)-(b) vary linearly from 1 to 0.7. Such an assumption results in the following two sets of equations for C_r = 0.9 and 0.8, respectively:

@C_r = 0.9

Evaporator side: $c_{f,ev} = -0.333x - 0.367$

Condenser side: $c_{f,cd} = -0.097x - 0.137$

@C_r = 0.8

Evaporator side: $c_{f,ev} = -0.667x - 0.735$

Condenser side: $c_{f,cd} = -0.195x - 0.274$

Constants for each heat exchanger are generated using these equations and applied to the fouling data generated for C_r values of 0.8 and 0.9. All prediction errors are found to be less than 1% and, thus, considered as acceptable. Now, all the slopes and intercepts can be generated for each heat exchanger based on the value of C_r using the following equations:

Evaporator side slope: $c_{f,ev,slp} = 3.334C_r - 3.334$

Evaporator side intercept: $c_{f,ev,icpt} = 3.677C_r - 3.677$

Condenser side slope: $c_{f,cd,slp} = 0.977C_r - 0.977$

Condenser side intercept: $c_{f,cd,icpt} = 1.37C_r - 1.37$

Now, we check the constants generated at NTU = 1.609 for the other NTU values to determine whether they can be used for them. After applying the constants, it is found that all errors are less than 1% and, thus, considered as acceptable. Therefore, the final prediction equation for each heat exchanger comes out as:

$$c_{f,ev} = (3.334C_r - 3.334)\frac{\Delta T_L}{T_{avg}} + (3.677C_r - 3.677) \tag{6.3a}$$

$$c_{f,cd} = (0.977C_r - 0.977)\frac{\Delta T_L}{T_{avg}} + (1.37C_r - 1.37) \tag{6.3b}$$

We now use the calculated COPs under fouled conditions and determine the constants for both heat exchangers needed to predict this performance parameter. It should be noted that, at $C_r = 1$, both constants are zero as for T_{cd} for the same reason. Following a similar procedure as for T_{cd}, we find that, incidentally, Eq. (6.3a) provides a good fit for COP on the evaporator side at a NTU of 1.609. But it was also found that Eq. (6.3b) does not provide an acceptable fit as prediction errors were as high as 4%. Therefore, the next step is to assume a non-linear profile for the intercept part only of the condenser-side equation and check whether this is enough to predict the constants or not. So, a second-degree polynomial solution with respect to C_r is assumed and tested for NTU = 1.609. All errors are reduced to less than 0.2% and, thus, this solution is found to be valid at this NTU. Therefore, for a NTU of 1.609, the condenser-side equation for the constants takes the following form:

$$c_{f,cd} = \left(0.977C_r - 0.977\right)\frac{\Delta T_L}{T_{avg}} + \left(3.225C_r^2 - 4.11C_r + 0.885\right) \quad (6.4)$$

Now, we check whether these solutions are valid for the complete range of NTU values. Testing reveals that this is not the case and, therefore, we are forced to take the effect of NTU into account for both the evaporator side and condenser side equations. First, we determine the effect of NTU for the evaporator-side equation. To achieve this, we determine constants manually that would provide less than 1% errors for each NTU at a C_r value of 0.7. Once these were determined, a linear solution was assumed for C_r values between 1 and 0.7. This easily provides the necessary solution equations for each NTU. Then these are checked for C_r values of 0.9 and 0.8 for each NTU to see if all errors are less than 1%. This is found to be the case for all NTU values and, thus, accepted as the final solution for the evaporator-side equation.

A similar procedure is followed for the condenser-side equation but it is found that assuming a linear solution for each NTU was not suitable as errors were greater than 1% in many cases. Therefore, a second-degree polynomial solution was assumed for each NTU and through a process of trial and error, an acceptable solution was found to fit all the constants to be predicted. Therefore, the final prediction equation for each heat exchanger comes out as:

$$c_{f,ev} = \left(3.334C_r - 3.334\right)\frac{\Delta T_L}{T_{avg}} + \left[\left(0.748NTU_{H,cl} + 2.472\right)\left(C_r - 1\right)\right] \quad (6.5a)$$

$$c_{f,cd} = \left(0.977C_r - 0.977\right)\frac{\Delta T_L}{T_{avg}} + \left(aC_r^2 + bC_r + c\right) \tag{6.5b}$$

where

$$a = -0.164NTU_{H,cl}^2 + 1.467NTU_{H,cl} + 1.268$$
$$b = 0.308NTU_{H,cl}^2 - 2.775NTU_{H,cl} + 0.412$$
$$c = -0.144NTU_{H,cl}^2 + 1.308NTU_{H,cl} - 0.856$$

In this section, we have seen that it is possible to provide fitted equations to determine the constants needed to predict properties and performance parameters under fouled conditions for a reverse CA cycle. Based on this, it may be said that all air-conditioning and refrigeration systems with internal irreversibilities that are built upon the concept of this system (such as the simple vapor compression cycle), can have such constants fitted for practical use.

6.3.5 Curzon-Ahlborn cycle

Data was generated for NTU ranging from 0.6 to 1 ($\varepsilon \approx 0.45 - 0.63$) and thermal capacitance ratio (C_r) from 0.13 to 0.04 for the three cases mentioned in 6.2.1. The clean conditions consist of varying the power from 700 W to 1200 W in 100 W steps. In the endoreversible case, the pump does not exist and, therefore, for simulating the performance case, the condenser temperature, corresponding to the normalized power ($\dot{W}'$), is kept constant for each of the three cases. Here, we will fit thermal efficiency and

boiler temperature. The same procedure was followed as in section 6.3.4 and in the fitted equations for the boiler temperature (T_{bl}) are:

$$c_{f,bl} = -1.375\dot{W}' + 0.167 \tag{6.6a}$$

$$c_{f,cd} = \left(-45C_r + 3.887\right)\dot{W}' + \left(35.8333C_r^2 - 9.753C_r + 0.837\right) \tag{6.6b}$$

The fitted equations for the thermal efficiency (η_{th}) are:

$$c_{f,bl} = \left(85.2C_r - 5.2177\right)\dot{W}' + \left(9.167C_r^2 - 3.835C_r + 0.2437\right) \tag{6.7a}$$

$$c_{f,cd} = \left(117.123C_r - 5.661\right)\dot{W}' + \left(51.944C_r^2 - 17.94C_r + 1.074\right) \tag{6.7b}$$

In this section, we have seen that it is possible to provide fitted equations to determine the constants needed to predict properties and performance parameters under fouled conditions for a CA cycle. Based on this, it may be said that all power systems with internal irreversibilities that are built upon the concept of this system (such as the Rankine cycle), can have such constants fitted for practical use.

Now, we will apply the proposed model to real systems simulated using verified models as opposed to ideal systems where refrigerant properties did not play a role and the cycle was internally reversible. For this, the simple vapor compression cycle and Rankine cycle are used after data generation. The purpose here is to show that the presence of internal irreversibilities do not hinder the same dimensionless quantities in predicting the constants (c_f).

6.3.6 Vapor compression system

Now, in this section, we will apply what has been established in section 6.3.3 and see if Eq. (6.1) can be used especially the fouling constants to a simple vapor compression cycle. In the system that was modeled, R134a was used as the working fluid. In these simulations, the following conditions were used: $T_{in,cd} = 40\ ^{o}C, T_{in,ev} = 0\ ^{o}C,\ \dot{C}_{\min} = 12\ kW.K^{-1}$ which are the same as were used in the endoreversible case. The isentropic efficiency of the compressor was taken as 0.65 in all the results. For the purpose of demonstration, two performance parameters (i.e. COP and $\dot{Q}_L$) and two properties (i.e. T_{cd} and T_{sup}) were modeled for their behavior under fouled conditions.

The same method, which was outlined in section 6.3.3, was used for the vapor compression cycle. One difference which was noticed was that while evaporator-side constants could be fitted with straight lines, generating minimum error for the condenser-side constants would require a second-degree polynomial fit for all four quantities mentioned above (See Figs. 6.4(a) and (b) as a sample). The reason for this seems to be the internal irreversibilities.

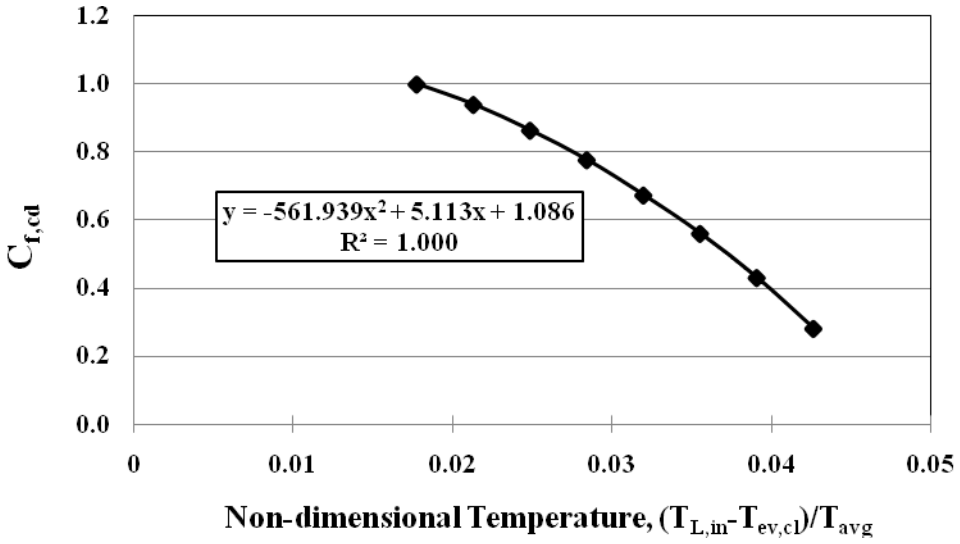

Figure 6.4(a). Determining fouling data constants for T_{cd} variation for Case 1 (for C_r=1): SVCC

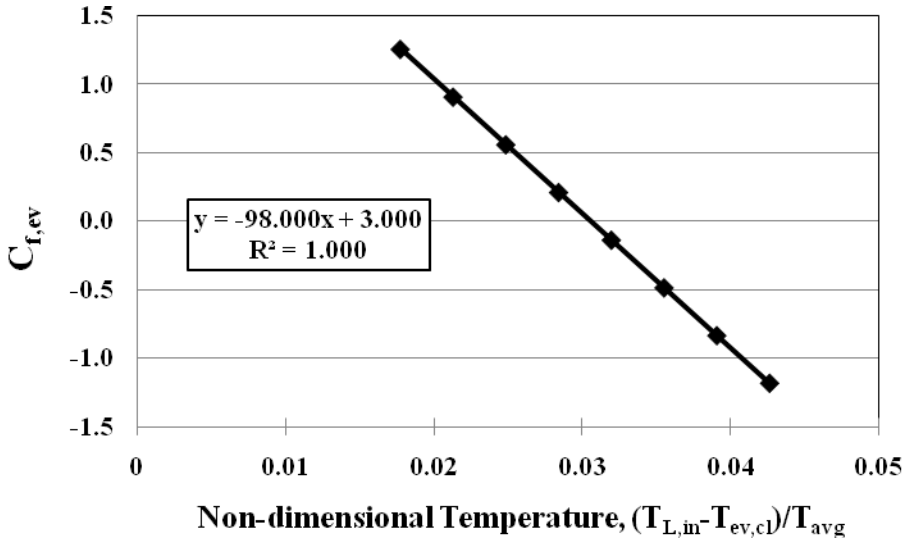

Figure 6.4(b). Determining fouling data constants for T_{cd} variation Case 2 (for C_r=1): SVCC

It was found that all quantities could be fitted within an error of 1.15% without the effect of the NTU being considered. Since this afforded a great deal of simplification in the prediction equations without significant loss in accuracy, this was accepted. It should be noted that this error above 1% typically occurred at the 40-50% range of decrease in UA-value. The final curve-fits for the constants (c_f) of COP were determined as:

$$c_{f,ev} = 54\frac{\Delta T_L}{T_{avg}} + \left[0.233C_r - 0.936\right] \tag{6.8a}$$

$$c_{f,cd} = 961.708\left(\frac{\Delta T_L}{T_{avg}}\right)^2 - 78.196\left(\frac{\Delta T_L}{T_{avg}}\right) + 2.363 \tag{6.8b}$$

The final curve-fits for the constants (c_f) of $\dot{Q}_L$ were determined as:

$$c_{f,ev} = \left(-69.1C_r + 89\right)\frac{\Delta T_L}{T_{avg}} + \left(C_r + 0.2\right) \tag{6.9a}$$

$$c_{f,cd} = a\left(\frac{\Delta T_L}{T_{avg}}\right)^2 + b\left(\frac{\Delta T_L}{T_{avg}}\right) + c \tag{6.9b}$$

where

$$a = -6122.7\,C_r^2 + 9771.4C_r - 2873.7$$
$$b = 300\,C_r^2 - 380C_r + 27$$
$$c = -3.7\,C_r^2 + 4.332C_r - 0.09$$

The final curve-fits for the constants (c_f) of T_{cd} were determined as:

$$c_{f,ev} = \left(-23.954C_r - 74.046\right)\frac{\Delta T_L}{T_{avg}} + \left(0.426C_r + 2.574\right) \tag{6.10a}$$

$$c_{f,cd} = a\left(\frac{\Delta T_L}{T_{avg}}\right)^2 + b\left(\frac{\Delta T_L}{T_{avg}}\right) + c \tag{6.10b}$$

where

$$a = -1723.846C_r + 1161.907$$
$$b = 77.676C_r - 72.563$$
$$c = -0.675C_r^2 + 0.445C_r + 1.317$$

The final curve-fits for the constants (c_f) of T_{sup} were determined as:

$$c_{f,ev} = -79.5\frac{\Delta T_L}{T_{avg}} + 4 \tag{6.11a}$$

$$c_{f,cd} = -630.296\left(\frac{\Delta T_L}{T_{avg}}\right)^2 + 44.865\left(\frac{\Delta T_L}{T_{avg}}\right) + 0.134 \tag{6.11b}$$

In this last property i.e. T_{sup}, it is noted that even the effect of C_r may be ignored within the specified error.

These calculations were repeated for R22 at an NTU of 1.609 and it was found that the nature of the equations did not change when checked for the COP and T_{sup} but rather only the constants used.

6.3.7 Rankine power cycle

Now, in this section, we will apply what has been established in section 6.3.3 and see if Eq. (6.1) can be used especially the fouling constants to a simple Rankine cycle. In these simulations, the following conditions were used some of which were taken from The Babcock & Wilcox Company [90]: $T_{in,cd} = 25\ ^{o}C, T_{in,bl} = 3560\ ^{o}C$, $\dot{m}_{fg} = 40.84\ kg.s^{-1}$. The isentropic efficiency of the pump and turbine were taken as 0.8 and 0.85, respectively. For the purpose of demonstration, two quantities (i.e. $\dot{Q}_H$ and $\dot{m}_{st}$) were fitted for their behavior under fouled conditions. The same method, which was outlined in section 6.3.3, was used for the Rankine power cycle to determine the fitting constants. Majority of the fitting equations were found to be linear. (See Figs. 6.5(a) and (b) as a sample).

It was found that all quantities could be fitted within an error of 1.1%. The effect of the NTU was considered for $\dot{Q}_H$ but not for $\dot{m}_{st}$. It should be noted that this error above 1% typically occurred at the 45-50% range of decrease in UA-value. The final curve-fits for the constants (c_f) of the boiler heat transfer rate ($\dot{Q}_H$) were determined as:

$$c_{f,ev} = \left(aC_r + b\right)\dot{W}' + \left(cC_r + d\right) \tag{6.12a}$$

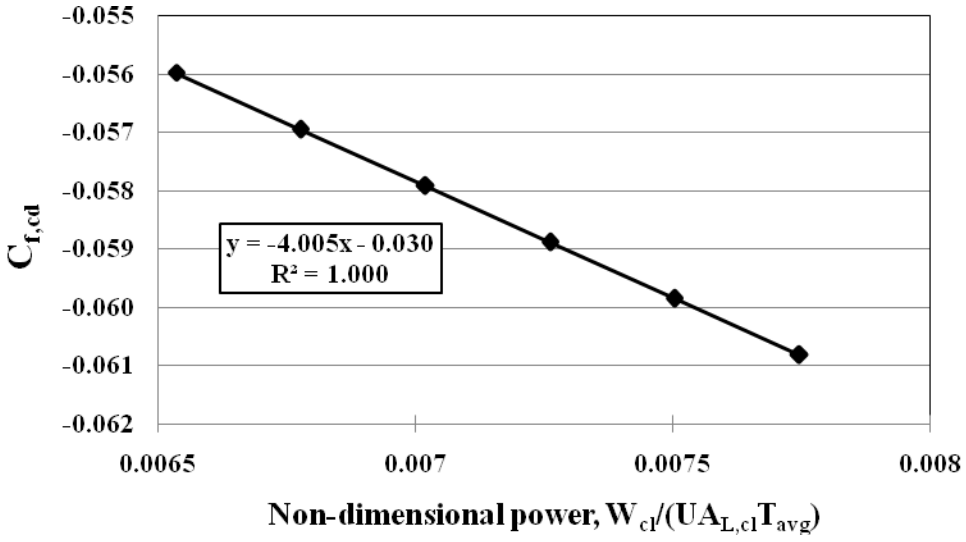

Figure 6.5(a). Determining fouling data constants for $\dot{m}_{st}$ variation for Case 1 (for C_r=0.04): RPC

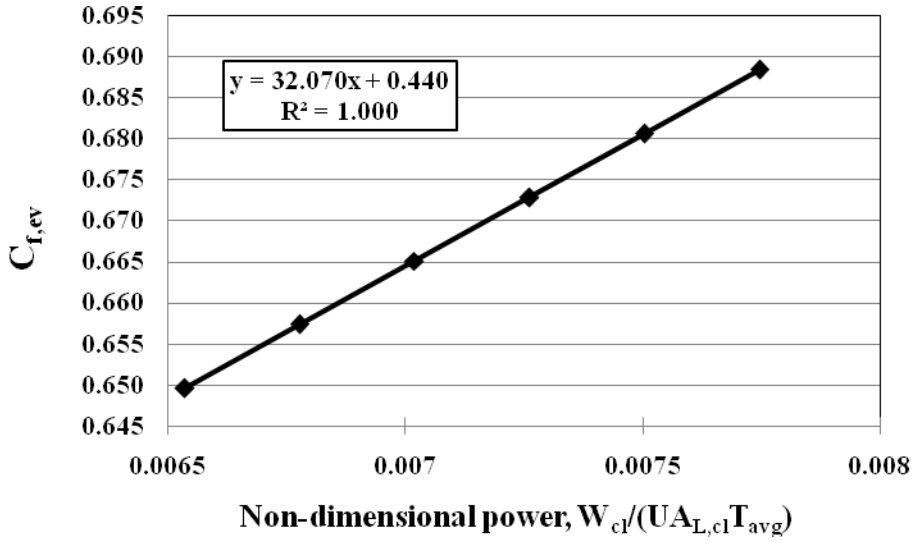

Figure 6.5(b). Determining fouling data constants for $\dot{m}_{st}$ variation Case 2 (for C_r=0.04): RPC

where

$$a = 3026NTU_{L,cl} + 4.2$$
$$b = -196.055NTU_{L,cl} - 0.203$$
$$c = -10.25NTU_{L,cl} - 20.15$$
$$d = 0.685NTU_{L,cl} + 2.412$$

$$c_{f,cd} = \left(aC_r + b\right)\dot{W}' + \left(cC_r + d\right) \tag{6.12b}$$

where

$$a = -21407.75NTU_{L,cl} - 20.8$$
$$b = 1385.5NTU_{L,cl} + 1.037$$
$$c = 106.5NTU_{L,cl} + 110.6$$
$$d = -8.785NTU_{L,cl} - 5.544$$

The final curve-fits for the constants (c_f) of steam mass flow rate $\dot{m}_{st}$ were determined as:

$$c_{f,cd} = \left(1065C_r - 46.605\right)\dot{W}' + \left(111C_r^2 - 16.81C_r + 0.465\right) \tag{6.13a}$$

$$c_{f,ev} = \left(13.5C_r + 31.53\right)\dot{W}' + \left(4.7C_r + 0.252\right) \tag{6.13b}$$

CHAPTER 7

COST OPTIMIZATION IN POWER AND REFRIGERATION SYSTEMS

There are four sections in this chapter; one for each system. These contain thermoeconomic optimization for a: i) vapor compression refrigeration system, ii) Carnot representation of mechanical subcooling cycles, iii) mechanical subcooling systems using thermodynamic models, and iv) Carnot power cycle with one feedwater heater.

7.1 Thermoeconomic Optimization of a Vapor Compression Refrigeration System

As mentioned above, some of the results of Antar and Zubair [26] will be checked by application to a SVCC. These results are related to two cost functions i.e. one determined based on a constant cooling load ($\dot{Q}_L$) and the other based on constant power consumption ($\dot{W}$). These are reproduced here for convenience:

$$F_1 = \frac{\Gamma}{\gamma_L \dot{W}} T_H = \frac{1}{1-\Phi}\left[\frac{G}{\theta - 1} + \frac{\Phi}{\xi - \Phi\theta}\right] \tag{7.1}$$

$$F_2 = \frac{\Gamma}{\gamma_L \dot{Q}_L} T_H = \frac{1}{\Phi}\left[\frac{G}{\theta - 1} + \frac{\Phi}{\xi - \Phi\theta}\right] \tag{7.2}$$

where $G = \frac{\gamma_H}{\gamma_L}, \theta = \frac{T_{HC}}{T_H}, \Phi = \frac{T_{01}}{T_{HC}}$ *and* $\xi = \frac{T_L}{T_H}$.

The general form of the cost functions (i.e. LHS of Eqs. (7.1) and (7.2)) were integrated with a model for SVCC. To check this, variation of one of the cost functions, F_2, was determined with changes in the compressor efficiency. Fig. 7.1 shows that, as the efficiency of the compressor increases, the cost decreases, which is a logical conclusion. It should be noted that designating the values of Φ, θ and ξ fixes the value of the same cost function in the endoreversible case.

An important minimum mentioned by the authors was with respect to θ. Antar and Zubair [26] determined that θ_{min} exists though they did not plot it. See Fig. 7.2 where a sample of this variation has now been plotted. The equation for determining the minimum value of θ is given below [26]:

$$\theta_{\min,th} = -\frac{1}{\Phi}\left[\frac{\Phi - G\xi + \sqrt{G}\Phi - \sqrt{G}\xi}{G - 1}\right] \tag{7.3}$$

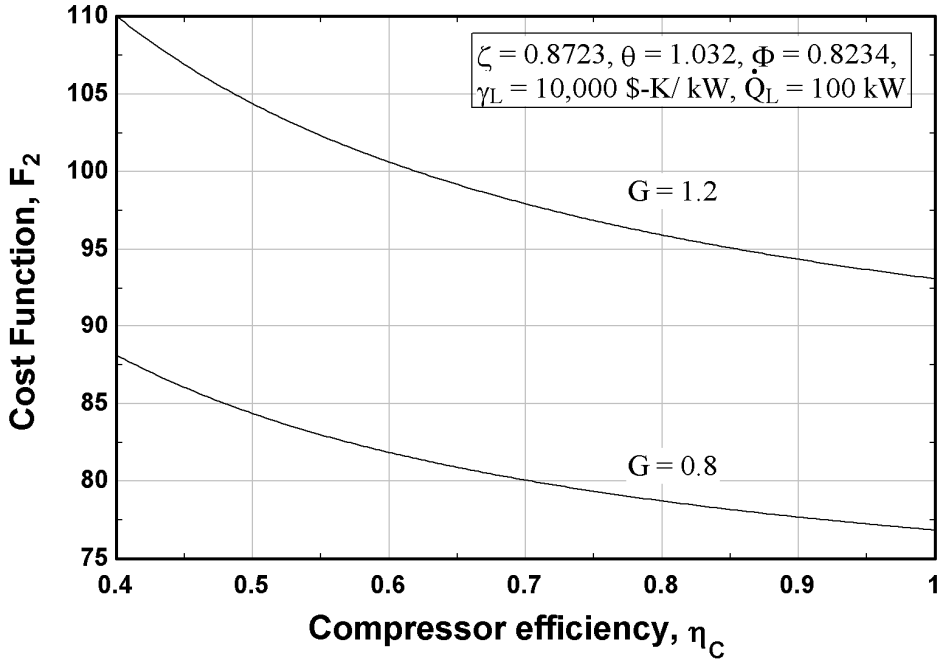

Figure 7.1. Effect of compressor efficiency on cost function F_2

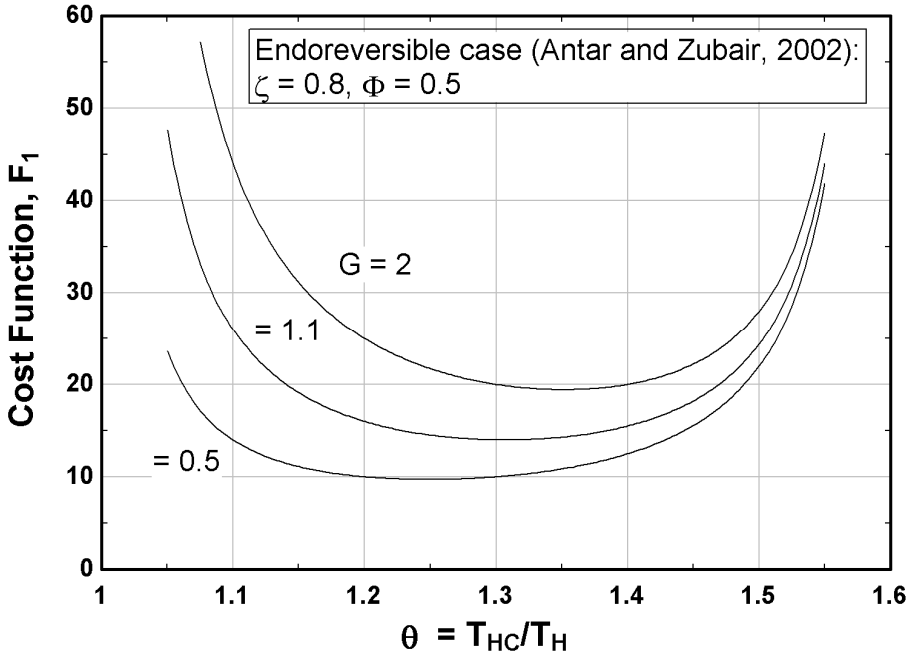

Figure 7.2. θ versus the cost function F_1 from Antar and Zubair [26]

It was found that F versus θ has a minimum similar to that found by Morales [37]. The variation of both cost functions, F_1 and F_2, with respect to θ were checked to see how closely it follows the endoreversible case. Figs. 7.3 and 7.4 show the variation of F_1 against θ at compressor efficiencies of 0.65 and 1, respectively. It should be noted that θ contains the condenser temperature which is based on refrigerant properties as well as system conditions.

It is seen that a minimum is reached as in the endoreversible case. Also, it is noted that actual minimum for SVCC is greater than the endoreversible one and that increasing the compressor efficiency reduces the difference between them. These behaviors are now checked for the cost function F_2. Figs. 7.5 and 7.6 show the variation of F_2 against θ at compressor efficiencies of 0.65 and 1, respectively. It is found that the above-mentioned behaviors are repeated for F_2 with the difference that the effect of increasing the compressor efficiency is more pronounced in this case. The closeness of the true and theoretical values in the case of F_2 was checked for a large range of G. Table 7.1 shows the results for G = 0.1 to 10 and we see that this closeness remains for the complete range.

This is a point of interest because it indicates that the prediction of θ_{min} is, in general, possible for the case of SVCC by using the compressor efficiency and the factors Φ and ξ. This may be expressed by the following equation:

$$\theta_{\min,act} = f(G, \zeta, \Phi, \eta_C, I_{throt}) \tag{7.4}$$

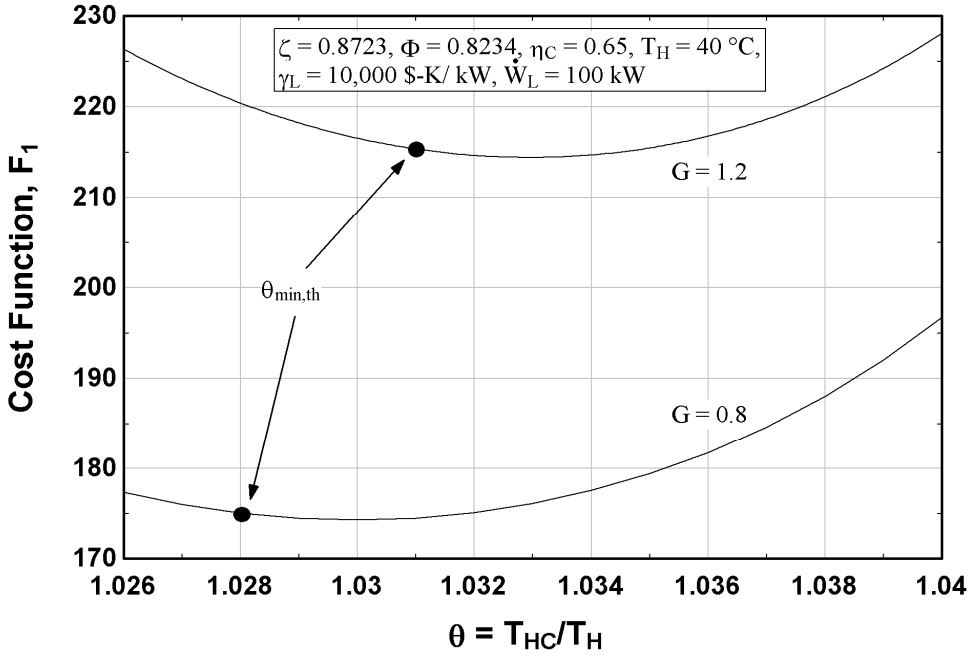

Figure 7.3. Variation of cost function F_1 with respect to θ [$\eta_c = 0.65$]: SVCC

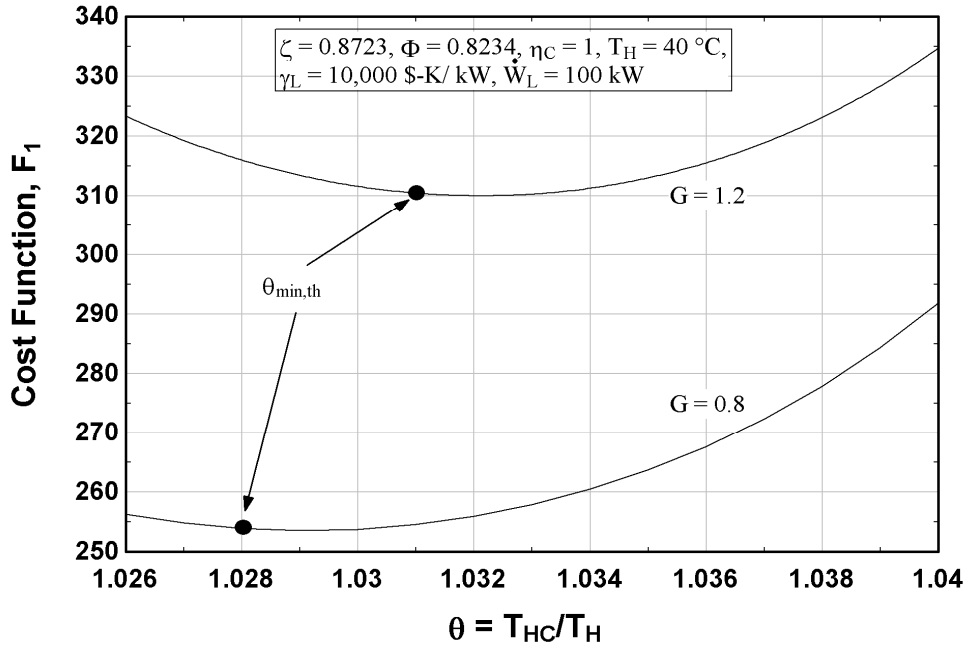

Figure 7.4. Variation of cost function F_1 with respect to θ [$\eta_c = 1$]: SVCC

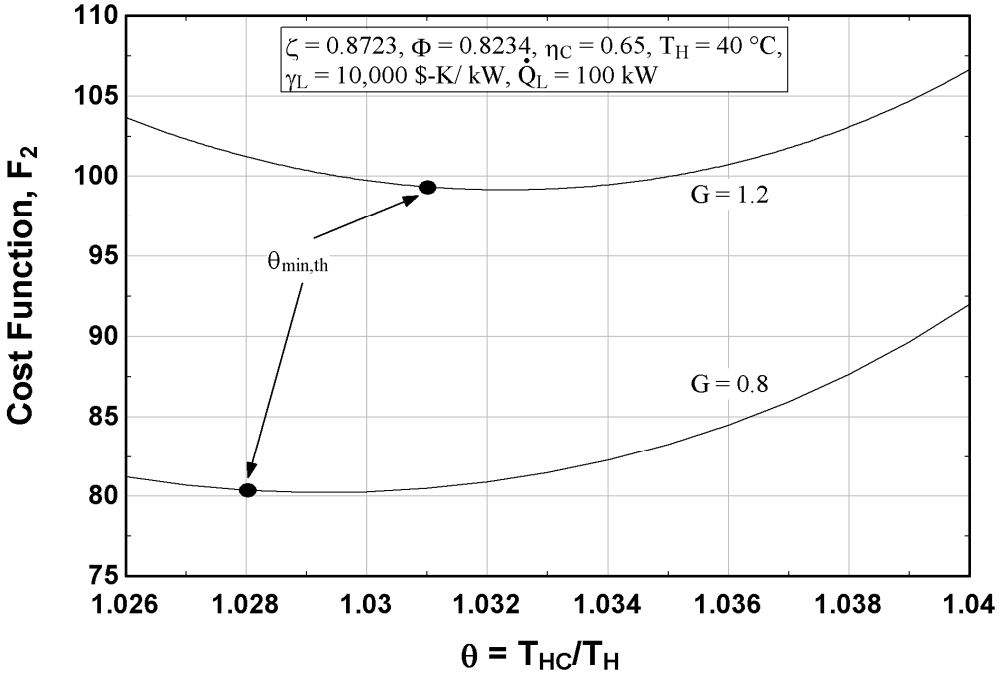

Figure 7.5. Variation of cost function F_2 with respect to θ [η_c = 0.65]: SVCC

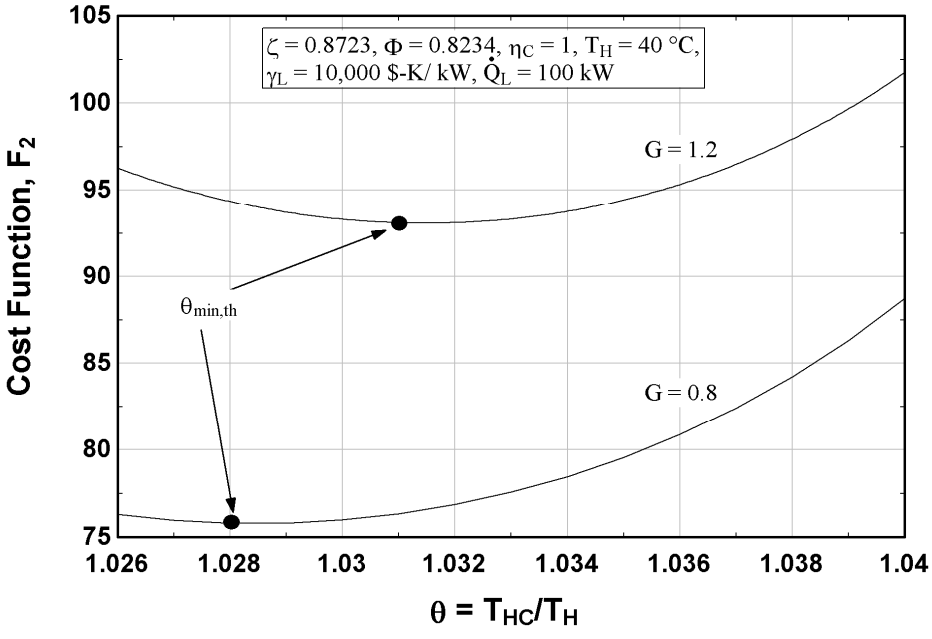

Figure 7.6. Variation of cost function F_2 with respect to θ [η_c = 1]: SVCC

Table 7.1: Comparison of θ_{min} in SVCC and endoreversible case [$\eta_c = 1$]

G	$\theta_{min,act}$	$\theta_{min,th}$
0.1	1.0146	1.0143
0.3	1.0218	1.0210
0.5	1.0250	1.0246
0.9	1.0293	1.0289
3	1.0380	1.0377
5	1.0414	1.0410
6	1.0425	1.0422
7	1.0434	1.0431
10	1.0454	1.0451

Keeping the above plots in mind, one possible form of this can be:

$$\theta_{\min,act} = \theta_{\min,th} + \Im \tag{7.5}$$

where $\Im = f(G, \zeta, \Phi, \eta_C, I_{throt})$ as well. For the case of F_2, it may be practically reduced to

$$\theta_{\min,act} = \theta_{\min,th} + f(\eta_C) \tag{7.6}$$

where $f(\eta_C)$ represents the main reason why there is a difference between the endoreversible and true values.

Antar and Zubair [26] showed variation of the total conductance (UA) against changes in the conductance unit cost ratio *G*. They determined this variation for optimum conditions i.e. at θ_{min} for each *G*. These θ_{min} values were first determined for different values of G with a compressor efficiency of 0.65 and are summarized in Table 7.2. Fig. 7.7 shows skewness in contrast to the symmetry found by Antar Zubair [26] around G=1

for UA_H and UA_L as they do not cross each other where UA minimizes. The UA curve itself is almost symmetrical with a minor difference of 0.07 kW/K at the ends.

Table 7.2: Comparison of θ_{min} in SVCC and endoreversible case [$\eta_c = 0.65$]

G	$\theta_{min,act}$
0.1	1.0152
0.3	1.0226
0.5	1.0258
0.9	1.0301
1	1.0310
1.1	1.0317
2	1.0360
3	1.0388
5	1.0421
6	1.0432
7	1.0440
10	1.0460

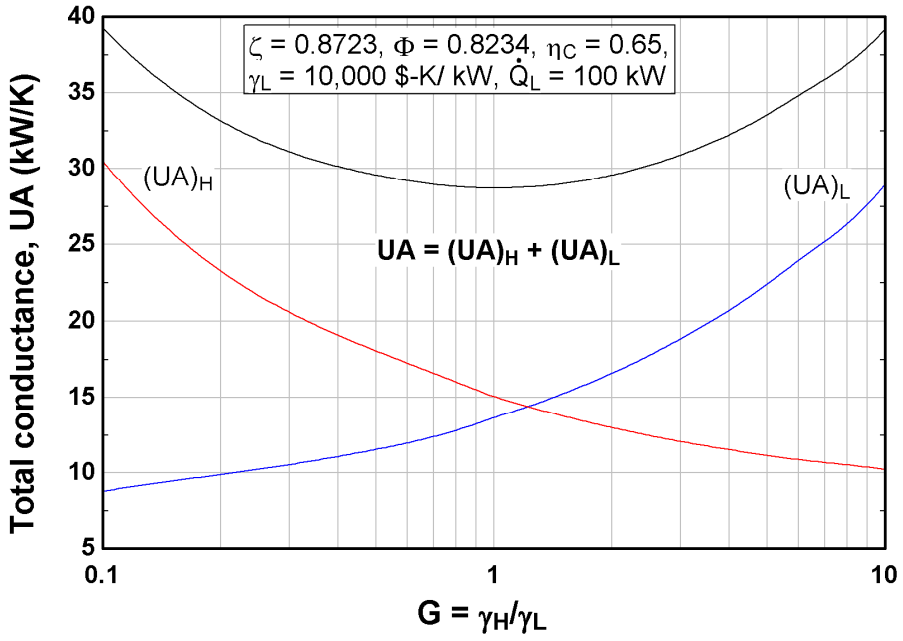

Figure 7.7. Total conductance versus the unit cost ratio for a SVCC with specified cooling capacity

7.2 Thermoeconomic Optimization for a Carnot Representation of Mechanical Subcooling Cycles

As mentioned before, one type of mechanical subcooling cycle is the dedicated mechanical subcooling system (See Fig. 1.1). The T-s diagram of the Carnot representation of this cycle is shown below in Fig. 7.8. Refer to Appendix F, for a discussion on how to best represent this system in an endoreversible manner.

The work of Morales [37] showed that θ_{min} was the same for all cost functions. Therefore, it is possible that the same may be found in the dedicated reversed Carnot cycle modeled in the previous section. It should be noted that, in these systems, the refrigerant may or may not be the same in both the cycles. Therefore, the general case of dissimilar refrigerants has been considered. The objective in the present investigation is to find minimum total cost of conductance (UA) for constant rate of work, cooling, heat rejection as well as subcooler heat transfer. Neglecting the costs of the compressors, piping system and expansion devices, the HEICE can be written as in terms of unit cost parameters of the heat exchangers as:

$$\Gamma = \gamma_{H,m}(UA)_{H,m} + \gamma_{H,d}(UA)_{H,d} + \gamma_{L}(UA)_{L} + \gamma_{sc}(UA)_{sc} \tag{7.7}$$

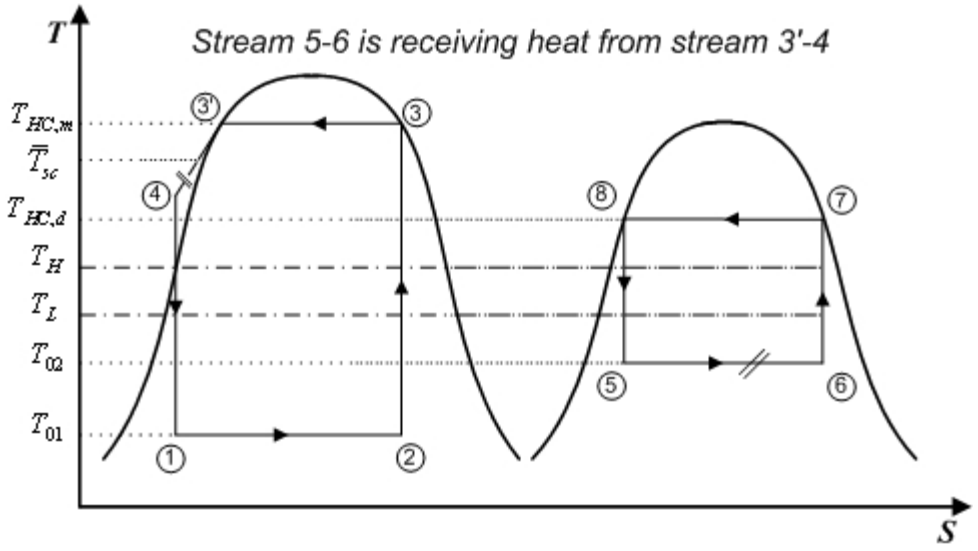

Figure 7.8. T-s diagram of Carnot representation of dedicated subcooling system

where $\gamma_{H,m}$, $\gamma_{H,d}$, γ_L, and γ_{sc} are unit cost of conductance for the condenser of the main cycle, sub-cooling cycle condenser, the evaporator and the sub-cooler, respectively, making Γ a parameter with units of dollars. Now, we know that

$$\dot{Q}_{H,m} = (UA)_{H,m}(T_{HC,m} - T_H) \tag{7.8}$$

$$\dot{Q}_{H,d} = (UA)_{H,d}(T_{HC,d} - T_H) \tag{7.9}$$

$$\dot{Q}_L = (UA)_L(T_L - T_{01}) \tag{7.10}$$

$$\dot{Q}_{sc} = (UA)_{sc}(\overline{T}_{sc} - T_{02}) \tag{7.11a}$$

where $\overline{T}_{sc}$ is the average subcooling temperature and may be defined as:

$$\overline{T}_{sc} = T_{HC,m} - \Delta T_{sc,avg} \tag{7.11b}$$

where $\Delta T_{sc,avg}$ is the average amount of subcooling and can be understood as half of the total amount of subcooling achieved. Substituting Eqs. (7.8) – (7.11) in Eq. (7.7), we get

$$\Gamma = \gamma_{H,m}\frac{\dot{Q}_{H,m}}{T_{HC,m} - T_H} + \gamma_{H,d}\frac{\dot{Q}_{H,d}}{T_{HC,d} - T_H} + \gamma_L\frac{\dot{Q}_L}{T_L - T_{01}} + \gamma_{sc}\frac{\dot{Q}_{sc}}{T_{HC,m} - \Delta T_{sc,avg} - T_{02}} \tag{7.12}$$

Dividing throughout by $\gamma_{H,m}$, we get

$$\frac{\Gamma}{\gamma_{H,m}} = \frac{\dot{Q}_{H,m}}{T_{HC,m} - T_H} + \frac{\gamma_{H,d}}{\gamma_{H,m}}\frac{\dot{Q}_{H,d}}{T_{HC,d} - T_H} + \frac{\gamma_L}{\gamma_{H,m}}\frac{\dot{Q}_L}{T_L - T_{01}} + \frac{\gamma_{sc}}{\gamma_{H,m}}\frac{\dot{Q}_{sc}}{T_{HC,m} - \Delta T_{sc,avg} - T_{02}} \tag{7.13}$$

Let $\frac{\gamma_{H,d}}{\gamma_{H,m}} = G_d$; $\frac{\gamma_L}{\gamma_{H,m}} = G_L$; $\frac{\gamma_{sc}}{\gamma_{H,m}} = G_{sc}$, then

$$\frac{\Gamma}{\gamma_{H,m}} = \frac{\dot{Q}_{H,m}}{T_{HC,m} - T_H} + G_d \frac{\dot{Q}_{H,d}}{T_{HC,d} - T_H} + G_L \frac{\dot{Q}_L}{T_L - T_{01}} + G_{sc} \frac{\dot{Q}_{sc}}{T_{HC,m} - \Delta T_{sc,avg} - T_{02}} \tag{7.14}$$

Factoring out $\dot{Q}_{sc}$, we get

$$\frac{\Gamma}{\gamma_{H,m}} = \dot{Q}_{sc} \left[\frac{\dot{Q}_{H,m}/\dot{Q}_{sc}}{T_{HC,m} - T_H} + G_d \frac{\dot{Q}_{H,d}/\dot{Q}_{sc}}{T_{HC,d} - T_H} + G_L \frac{\dot{Q}_L/\dot{Q}_{sc}}{T_L - T_{01}} + G_{sc} \frac{1}{T_{HC,m} - \Delta T_{sc,avg} - T_{02}} \right] \tag{7.15}$$

Now, from Fig. 7.8, we see that

$$\dot{Q}_{sc} = \dot{m}_m \overline{T}_{sc} (s_3' - s_4) \tag{7.16a}$$

$$\dot{Q}_{5-6} = \dot{m}_d T_{02} (s_6 - s_5) \tag{7.16b}$$

and

$$\dot{Q}_L = \dot{m}_m T_{01} (s_2 - s_1) \tag{7.16c}$$

But $\dot{Q}_{sc} = \dot{Q}_{5-6}$ as these are two streams exchanging heat in the same heat exchanger i.e. the subcooler.

$$\frac{\dot{Q}_{sc}}{\dot{Q}_L} = \frac{\dot{m}_d T_{02} (s_6 - s_5)}{\dot{m}_m T_{01} (s_2 - s_1)} \tag{7.17}$$

Now, it is also clear from Fig. 7.8 that, in general, $(s_2 - s_1) = k_1(s_6 - s_5)$ where k_1 can be any number greater than zero. It should be noted that it has been found in previous research [87], for the case of same refrigerants in both cycles, that $T_{HC,m}$ and $T_{HC,d}$ are very close in simulated systems probably due to the fact that both condensers exchange heat with a common environment. In such cases, k_1 may be taken as unity. Therefore, Eq. (7.17) becomes

$$\frac{\dot{Q}_L}{\dot{Q}_{sc}} = k_1 \frac{\dot{m}_m T_{01}}{\dot{m}_d T_{02}} \tag{7.18}$$

As the main cycle is internally reversible, applying the Clausis' inequality, we get

$$\frac{\dot{Q}_{H,m}}{T_{HC,m}} + \frac{\dot{Q}_{sc}}{\bar{T}_{sc}} = \frac{\dot{Q}_L}{T_{01}} \tag{7.19a}$$

$$\Rightarrow \qquad \frac{\dot{Q}_{H,m}}{\dot{Q}_{sc}} + \frac{1}{1 - \Delta T_{sc,avg} / T_{HC,m}} = \frac{\dot{Q}_L}{\dot{Q}_{sc}} \frac{T_{HC,m}}{T_{01}}$$

Substituting Eq. (7.18), we get

$$\frac{\dot{Q}_{H,m}}{\dot{Q}_{sc}} = k_1 \frac{\dot{m}_m T_{HC,m}}{\dot{m}_d T_{02}} - \frac{1}{1 - \Delta T_{sc,avg} / T_{HC,m}} \tag{7.19b}$$

Applying Clausis' inequality to the dedicated subcooling cycle, we get

$$\frac{\dot{Q}_{H,d}}{\dot{Q}_{sc}} = \frac{T_{HC,d}}{T_{02}} \tag{7.20}$$

Substituting Eqs. (7.18) – (7.20) in Eq. (7.15), and dividing the right hand side by T_H/T_H, we get

$$\frac{\Gamma}{\gamma_{H,m}} = \frac{\dot{Q}_{sc}}{T_H}\left[\frac{k_1 \dfrac{\dot{m}_m T_{HC,m}}{\dot{m}_d T_{02}} - \dfrac{1}{1-\Delta T_{sc,avg}/T_{HC,m}}}{\dfrac{T_{HC,m}}{T_H}-1} + G_d \frac{\dfrac{T_{HC,d}}{T_{02}}}{\dfrac{T_{HC,d}}{T_H}-1} + \right.$$
$$\left. G_L \frac{k_1 \dfrac{\dot{m}_m T_{01}}{\dot{m}_d T_{02}}}{\dfrac{T_L}{T_H}-\dfrac{T_{01}}{T_H}} + G_{sc} \frac{1}{\dfrac{T_{HC,m}}{T_H}-\dfrac{\Delta T_{sc,avg}}{T_H}-\dfrac{T_{02}}{T_H}}\right] \tag{7.21}$$

Introducing the following non-dimensional ratios below:

$$\theta_1 = \frac{T_{HC,m}}{T_H} \tag{7.22a}$$

$$\theta_2 = \frac{T_{HC,d}}{T_H} \tag{7.22b}$$

$$\theta_3 = \frac{\Delta T_{sc,avg}}{T_H} \tag{7.22c}$$

$$\Phi_1 = \frac{T_{01}}{T_{HC,m}} \tag{7.22d}$$

$$\Phi_2 = \frac{T_{02}}{T_{HC,m}} \tag{7.22e}$$

$$\xi = \frac{T_L}{T_H} \tag{7.22f}$$

$$K = k_1 \frac{\dot{m}_m}{\dot{m}_d} \tag{7.22g}$$

Substituting Eqs. (7.22a) – (7.22g) in Eq. (7.21), and multiplying both sides by T_H, we get

$$\frac{\Gamma}{\gamma_{H,m}} T_H = \dot{Q}_{sc} \left[\frac{K \frac{1}{\Phi_2} - \frac{1}{1-\theta_3/\theta_1}}{\theta_1 - 1} + G_d \frac{\frac{\theta_2}{\theta_1}\frac{1}{\Phi_2}}{\theta_2 - 1} + G_L \frac{K \frac{\Phi_1}{\Phi_2}}{\xi - \Phi_1 \theta_1} + G_{sc} \frac{1}{\theta_1(1-\Phi_2) - \theta_3} \right] \tag{7.23}$$

In the next section, starting from Eq. (7.23), the cost functions for constant work rate, constant heating (in the main and dedicated cycle), cooling and subcooling rate will now be determined. It should be noted that, in all cases, the unit cost conductance ratios are taken constant as unity. Therefore, it is understood that $(UA)_{tot}$ will also be minimum when the dimensionless HEICE is at a minimum. We introduce the following three dimensionless groups to facilitate presentation of the results:

$$\Omega = K \frac{1}{\Phi_2} - \frac{1}{1-\theta_3/\theta_1} + \frac{\theta_2}{\theta_1}\frac{1}{\Phi_2} - K \frac{\Phi_1}{\Phi_2} \tag{7.24a}$$

$$\Psi = \theta_1(1-\Phi_2) - \theta_3 \tag{7.24b}$$

$$\Theta = 1 - \theta_3/\theta_1 \tag{7.24c}$$

7.2.1 Constant Work Rate

Dividing Eq. (7.23) by the work rate results in a non-dimensional equation. This translates into applying the HEICE to a cycle with constant work rate.

$$F_a = \frac{\Gamma}{\gamma_{H,m}\dot{W}} T_H = \frac{\dot{Q}_{sc}}{\dot{W}} \left[\frac{K\dfrac{1}{\Phi_2} - \dfrac{1}{\Theta}}{\theta_1 - 1} + G_d \frac{\dfrac{\theta_2}{\theta_1}\dfrac{1}{\Phi_2}}{\theta_2 - 1} + G_L \frac{K\dfrac{\Phi_1}{\Phi_2}}{\xi - \Phi_1\theta_1} + G_{sc}\frac{1}{\Psi} \right] \tag{7.25}$$

Applying the First Law of Thermodynamics (See Fig. 1.1) gives us

$$\dot{W} = \dot{Q}_{H,m} + \dot{Q}_{H,d} - \dot{Q}_L \tag{7.26}$$

where $\dot{W}$ is the sum of work done by both compressors. Dividing both sides by $\dot{Q}_{sc}$, we get

$$\frac{\dot{W}}{\dot{Q}_{sc}} = \frac{\dot{Q}_{H,m}}{\dot{Q}_{sc}} + \frac{\dot{Q}_{H,d}}{\dot{Q}_{sc}} - \frac{\dot{Q}_L}{\dot{Q}_{sc}} \tag{7.27}$$

Substituting Eqs. (7.18) – (7.20) in above equation, we get

$$\frac{\dot{W}}{\dot{Q}_{sc}} = k_1 \frac{\dot{m}_m T_{HC,m}}{\dot{m}_d T_{02}} - \frac{1}{1 - \Delta T_{sc,avg}/T_{HC,m}} + \frac{T_{HC,d}}{T_{02}} - k_1 \frac{\dot{m}_m T_{01}}{\dot{m}_d T_{02}} \tag{7.28a}$$

Substituting Eqs. (7.22a) – (7.22e) and (7.24a) in Eq. (7.17), we get

$$\frac{\dot{Q}_{sc}}{\dot{W}} = \frac{1}{\Omega} \tag{7.28b}$$

Substituting Eqs. (7.28b) and (7.24b) into Eq. (7.25) gives

$$F_a = \frac{1}{\Omega}\left[\frac{K\dfrac{1}{\Phi_2}-\dfrac{1}{\Theta}}{\theta_1 - 1} + G_d\frac{\dfrac{\theta_2}{\theta_1}\dfrac{1}{\Phi_2}}{\theta_2 - 1} + G_L\frac{K\dfrac{\Phi_1}{\Phi_2}}{\xi - \Phi_1\theta_1} + G_{sc}\frac{1}{\Psi}\right] \tag{7.29}$$

This is the non-dimensional HEICE for a dedicated subcooling Carnot cycle with constant work rate. It is clear that there is an inverse relationship between F_a and ξ as well as θ_2 and no minimum point exists with respect to these parameters. It is unclear whether minima exist with respect to Φ_1, Φ_2, θ_1 and θ_3. Taking the derivative of F_a with respect to Φ_1 and setting it equal to zero gives the following equation after simplification:

$$\begin{aligned}\frac{\partial F_a}{\partial \Phi_1} = \frac{1}{\Omega^2}&\left[\frac{K\dfrac{1}{\Phi_2}-\dfrac{1}{\Theta}}{\theta_1 - 1} + G_d\frac{\dfrac{\theta_2}{\theta_1}\dfrac{1}{\Phi_2}}{\theta_2 - 1} + G_L\frac{K\dfrac{\Phi_1}{\Phi_2}}{\xi - \Phi_1\theta_1} + G_{sc}\frac{1}{\Psi}\right] \\ &+ \frac{1}{\Omega}\left[G_L\frac{\xi}{\left(\xi - \Phi_1\theta_1\right)^2}\right] = 0\end{aligned} \tag{7.30}$$

Since $T_L > T_{01}$, $T_L > T_{02}$, $T_{HC,m} > T_H$ and $T_{HC,d} > T_H$, then $(\xi - \Phi_1\theta_1)$, $\theta_1(1 - \Phi_2)$, $(\theta_1 - 1)$ as well as $(\theta_2 - 1)$ are greater than zero. Also, it should be noted that θ_3 is typically two order of magnitudes smaller than θ_1. This shows that Ψ and Θ are positive quantities. Therefore, the quantity $1/\Omega$ must be negative in order for $\partial F_a/\partial \Phi_1$ to be zero. This is not possible since the right hand side of Eq. 7.28(b) must be positive. Therefore, there is no practical minimum with respect to Φ_1. Now, taking the derivative of F_a with respect to Φ_2

provides a lengthy expression and it was unclear whether a minimum existed or not. Therefore, F_a was plotted against Φ_2 and the trend indicated that the only possibility of a minimum existing in this case would be if Φ_2 was negative. This is impractical and, thus, it was concluded that no minimum exists in this case. Similarly, θ_3 does not give a practical minimum either.

The function F_a does appear to have a minimum with respect to the parameter θ_1. Setting $\partial F_a/\partial\theta_1 = 0$ yields

$$\frac{\partial F_a}{\partial \theta_1} = \left[\frac{\frac{\theta_3}{\theta_1^2}}{(\theta_1 - 1)\Theta^2} - \frac{K\frac{1}{\Phi_2} - \frac{1}{\Theta}}{(\theta_1 - 1)^2} - G_d \frac{\frac{\theta_2}{\theta_1^2}\frac{1}{\Phi_2}}{(\theta_2 - 1)} + G_L \frac{K\frac{\Phi_1^2}{\Phi_2}}{(\xi - \Phi_1\theta_1)^2} - G_{sc}\frac{1-\Phi_2}{\Psi^2} \right] + \frac{\frac{\theta_2}{\theta_1^2}\frac{1}{\Phi_2} - \frac{\theta_3}{\theta_1^2}\frac{1}{\Theta^2}}{\Omega} \left[\frac{K\frac{1}{\Phi_2} - \frac{1}{\Theta}}{(\theta_1 - 1)} + G_d \frac{\frac{\theta_2}{\theta_1}\frac{1}{\Phi_2}}{(\theta_2 - 1)} + G_L \frac{K\frac{\Phi_1}{\Phi_2}}{(\xi - \Phi_1\theta_1)} + G_{sc}\frac{1}{\Psi} \right] = 0 \tag{7.31}$$

Fig. 7.9(a) shows that the minimum value of θ_1 shifts to a higher value as Φ_1 decreases. This indicates that, if all other quantities remains constant, lowering the main cycle evaporator temperature may result in a lower cost. Fig. 7.9(b) indicates that K has little effect on $\theta_{1,min}$ over a practical range of K = 8 to 10. It should be noted that this range of K was chosen on the basis that the mass flow rate ratio of the main to dedicated cycle is typically found to be in this range and since the factor k_1 acts as a multiplier only, it is conveniently chosen to be unity.

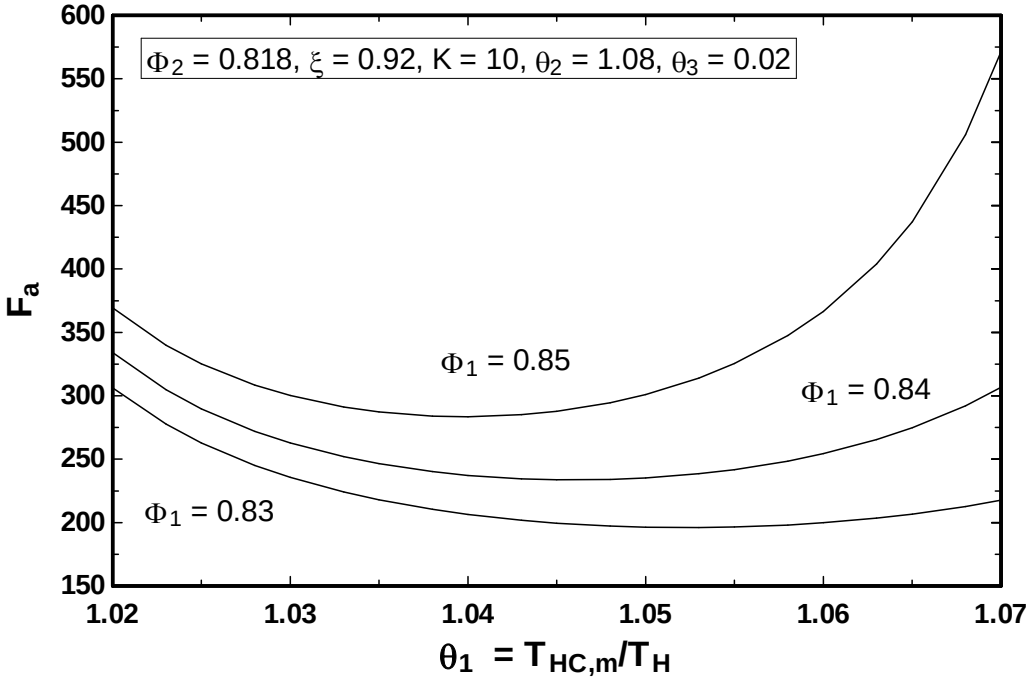

Figure 7.9(a). Dimensionless HEICE for constant work rate vs. θ: Effect of varying Φ_1

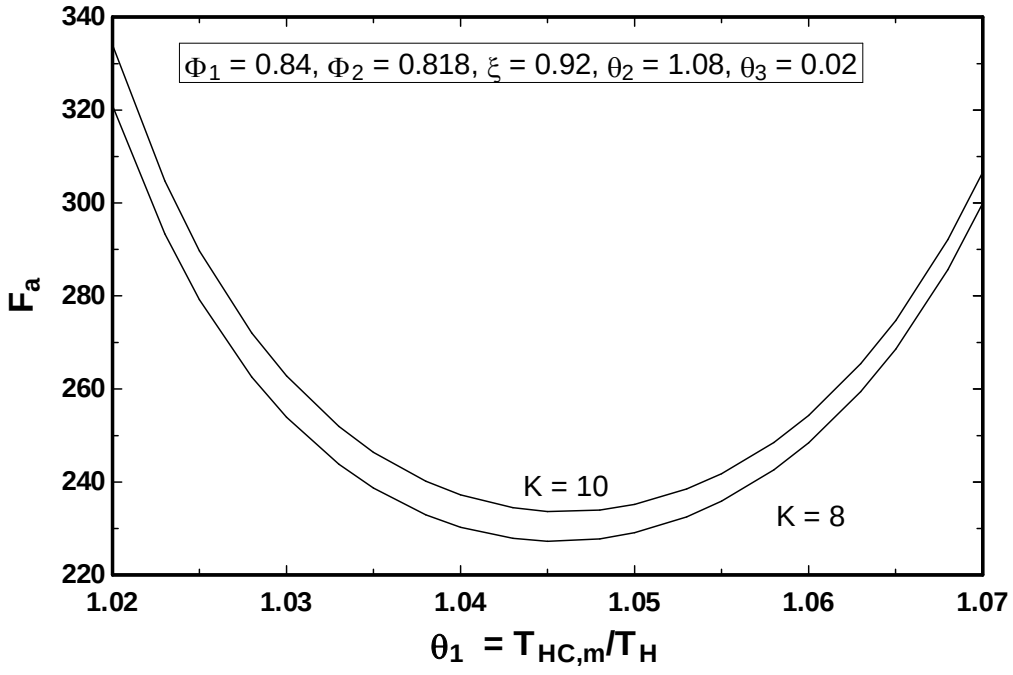

Figure 7.9(b). Dimensionless HEICE for constant work rate vs. θ: Effect of varying K

7.2.2 Constant Cooling Rate

Dividing Eq. (7.23) by the heat transfer in the evaporator results in a non-dimensional equation.

$$F_b = \frac{\Gamma}{\gamma_{H,m}\dot{Q}_L} T_H = \frac{\dot{Q}_{sc}}{\dot{Q}_L}\left[\frac{K\frac{1}{\Phi_2}-\frac{1}{\Theta}}{\theta_1 - 1} + G_d \frac{\frac{\theta_2}{\theta_1}\frac{1}{\Phi_2}}{\theta_2 - 1} + G_L \frac{K\frac{\Phi_1}{\Phi_2}}{\xi - \Phi_1\theta_1} + G_{sc}\frac{1}{\Psi}\right] \tag{7.32}$$

This translates into applying the HEICE to a cycle with constant heat transfer in the evaporator which, after the appropriate substitutions, gives

$$F_b = \frac{1}{K}\frac{\Phi_2}{\Phi_1}\left[\frac{K\frac{1}{\Phi_2}-\frac{1}{\Theta}}{\theta_1 - 1} + G_d \frac{\frac{\theta_2}{\theta_1}\frac{1}{\Phi_2}}{\theta_2 - 1} + G_L \frac{K\frac{\Phi_1}{\Phi_2}}{\xi - \Phi_1\theta_1} + G_{sc}\frac{1}{\Psi}\right] \tag{7.33}$$

This scenario deals with a constant cooling rate in the evaporator. The purpose is to determine whether the function F_b has a minimum with respect to ξ, Φ_1, Φ_2, θ_1, θ_2 and θ_3. F_b is clearly inversely proportional to ξ and θ_2, therefore, no minima exist with respect to these two variables. As before, taking the derivative of F_b with respect to θ_3 does not give a practical minimum as negative values of θ_3 are required. Taking the derivative of F_b with respect to Φ_1 and setting it equal to zero gives the following equation:

$$\frac{\partial F_b}{\partial \Phi_1} = \frac{(\Phi_2 - K\Theta)(\theta_1 - 1)}{K\Theta\left(\Phi_1(\theta_1 - 1)\right)^2} - G_d \frac{\theta_1\theta_2(\theta_2 - 1)}{K\left(\theta_1\Phi_1(\theta_2 - 1)\right)^2} + G_L \frac{\theta_1}{\left(\xi - \Phi_1\theta_1\right)^2} - G_{sc} \frac{\Phi_2\Psi}{K\left(\Phi_1\Psi\right)^2} = 0 \tag{7.34}$$

Fig. 7.10(a) shows that, as the value of θ_1 decreases, the minimum value of Φ_1 shifts to higher values. It is also noted that these minima are occurring at values less than that of Φ_2 and that the cost function is insensitive to a large extent, near the minima, for any particular value of θ_1. This indicates that, if all other quantities remain constant, variation in the evaporator temperature has very little effect on the cost near the minima.

Taking the derivative of F_b with respect to Φ_2 and setting it equal to zero gives the following equation:

$$\frac{\partial F_b}{\partial \Phi_2} = \frac{1}{K\Phi_1}\left[-\frac{1}{(\theta_1 - 1)\Theta} + G_{sc}\frac{\theta_1 - \theta_3}{\Psi^2}\right] = 0 \tag{7.35}$$

Fig. 7.10(b) illustrates that these minima are occurring at values less than that of Φ_1. For a particular value of θ_1, the cost function seems to be insensitive in the region of the minimum point and there seems to be little effect of θ_1. The line at $\theta_1 = 1.04$ was not below the line for $\theta_1 = 1.05$ but this type of reverse behavior was suspected as it had been observed by Morales [37] as well. The reason for the opposing behavior seems to be the fact that, for the given conditions, the minimum of θ_1 occurs at 1.045, which can be seen from Fig. 7.9(a). This indicates that once the minimum point for θ_1 is crossed, the behavior of the cost function reverses.

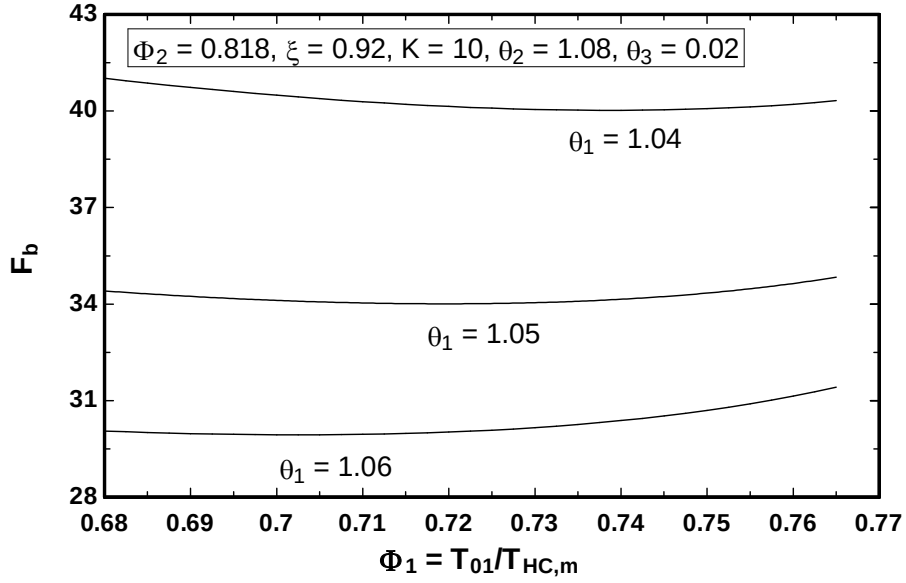

Figure 7.10(a). Dimensionless HEICE for constant cooling rate vs. Φ_1: Effect of varying θ_1

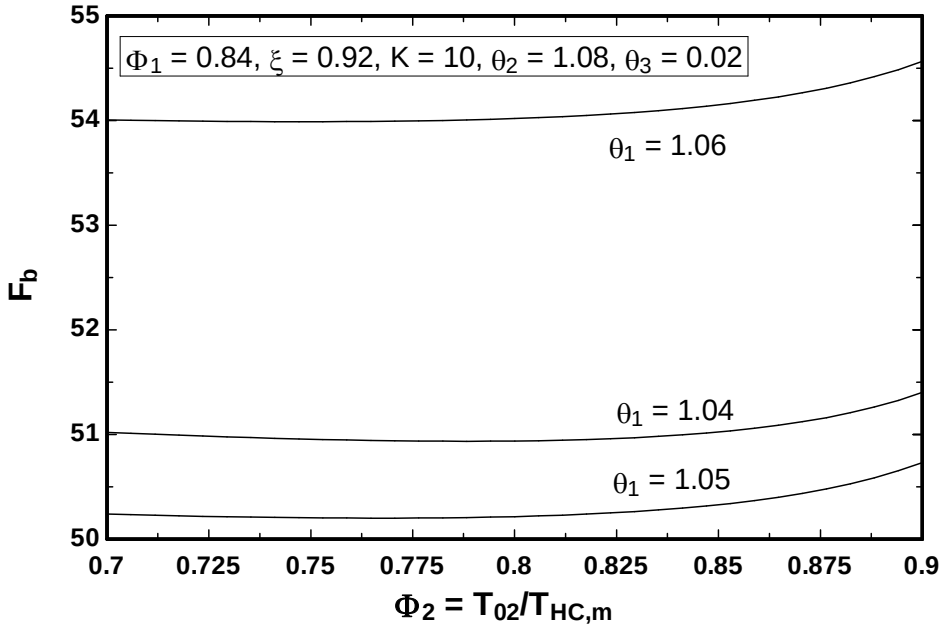

Figure 7.10(b). Dimensionless HEICE for constant cooling rate vs. Φ_2: Effect of varying θ_1

Taking the derivative of F_b with respect to θ_1 and setting it equal to zero results in the first term of Eq. (7.31) as can be seen below in Eq. (7.36), implying that $\theta_{1,min}$ is not exactly the same for F_a and F_b.

$$\frac{\partial F_b}{\partial \theta_1} = \frac{\frac{\theta_3}{\theta_1^2}}{(\theta_1 - 1)\Theta^2} - \frac{K\frac{1}{\Phi_2} - \frac{1}{\Theta}}{(\theta_1 - 1)^2} - G_d \frac{\frac{\theta_2}{\theta_1^2}\frac{1}{\Phi_2}}{(\theta_2 - 1)} + G_L \frac{K\frac{\Phi_1^2}{\Phi_2}}{(\xi - \Phi_1\theta_1)^2} - G_{sc}\frac{1-\Phi_2}{\Psi^2} = 0 \qquad (7.36)$$

Therefore, F_b is plotted against θ_1 to ascertain the possible difference in behavior (See Fig. 7.11). A comparison of Fig. 7.11 with Fig. 7.9(a) shows that the general behavior of θ_1 is still the same even though the values of F_b are much smaller than F_a due to the presence of the second term in Eq. (7.31). Also, before the minimum (for example, at $\theta_1 = 1.02$), the lines are closer together in Fig. 7.11 as compared to Fig. 7.9(a).

7.2.3 Constant Heat Rejection Rates – Both Condensers

Dividing Eq. (7.23) by the heat transfer in the main cycle condenser results in a non-dimensional equation. This translates into applying the HEICE to a cycle with constant heat transfer in the main cycle condenser.

$$F_c = \frac{\Gamma}{\gamma_{H,m}\dot{Q}_{H,m}}T_H = \frac{\dot{Q}_{sc}}{\dot{Q}_{H,m}}\left[\frac{K\frac{1}{\Phi_2} - \frac{1}{\Theta}}{\theta_1 - 1} + G_d\frac{\frac{\theta_2}{\theta_1}\frac{1}{\Phi_2}}{\theta_2 - 1} + G_L\frac{K\frac{\Phi_1}{\Phi_2}}{\xi - \Phi_1\theta_1} + G_{sc}\frac{1}{\Psi}\right] \qquad (7.37)$$

which, after the appropriate substitutions, gives

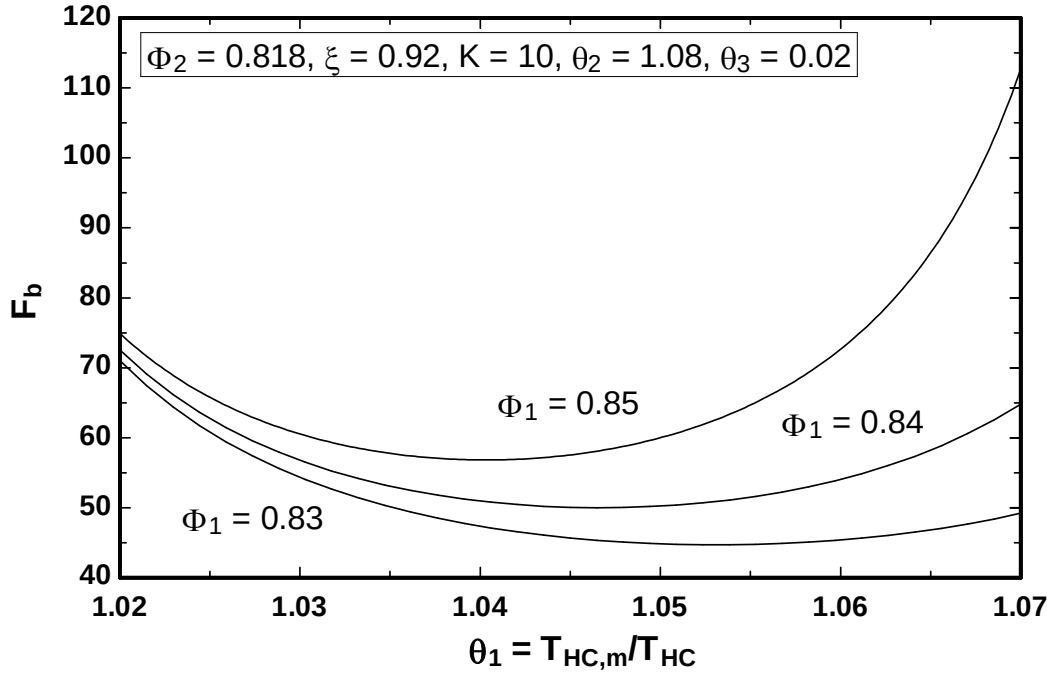

Figure 7.11. Dimensionless HEICE for constant cooling rate vs. θ_1: Effect of varying Φ_1

This scenario deals with a constant heat rejection rate in the main cycle condenser. As with the other cost functions, it was found that F_c has no minima with respect to ξ and θ_2. Taking the derivative of F_c with respect to Φ_1 and setting it equal to zero gives the following equation:

$$\frac{\partial F_c}{\partial \Phi_1} = \frac{K\xi}{\left(\xi - \Phi_1\theta_1\right)^2} = 0 \tag{7.39}$$

As the equation is clearly positive, therefore, no minimum exists. For the same reason, θ_3 was also not found to have a minimum in this case. The derivative with respect to Φ_2 was plotted as the possibility of a minimum existed but it was again found that it is only possible with a negative value of Φ_2. Taking the derivative of F_c with respect to θ_1 and setting it equal to zero results in a different expression when compared to Eq. (7.36). Still, it was noticed that the behavior was exactly the same as in Fig. 7.11 and only the function values encountered were different by a small amount.

Now, dividing Eq. (7.23) by $\dot{Q}_{H,d}$ corresponds to the HEICE of a cycle with constant heat transfer in the dedicated subcooling cycle condenser as shown below:

$$F_d = \frac{\Gamma}{\gamma_{H,m}\dot{Q}_{H,d}} T_H = \frac{\dot{Q}_{sc}}{\dot{Q}_{H,d}} \left[\frac{K\dfrac{1}{\Phi_2} - \dfrac{1}{\Theta}}{\theta_1 - 1} + G_d \frac{\dfrac{\theta_2}{\theta_1}\dfrac{1}{\Phi_2}}{\theta_2 - 1} + G_L \frac{K\dfrac{\Phi_1}{\Phi_2}}{\xi - \Phi_1\theta_1} + G_{sc}\frac{1}{\Psi} \right] \tag{7.40}$$

which, after the appropriate substitutions, gives

$$F_d = \frac{\theta_1}{\theta_2}\Phi_2\left[\frac{K\dfrac{1}{\Phi_2}-\dfrac{1}{\Theta}}{\theta_1-1}+G_d\frac{\dfrac{\theta_2}{\theta_1}\dfrac{1}{\Phi_2}}{\theta_2-1}+G_L\frac{K\dfrac{\Phi_1}{\Phi_2}}{\xi-\Phi_1\theta_1}+G_{sc}\frac{1}{\Psi}\right] \tag{7.41}$$

As with the other cost functions, F_d is found to have no minimum with respect to ξ and θ_2. The derivative of F_d with respect to θ_3 was found to be the same as for F_b and, thus, no minimum exists. Taking the derivative of F_d with respect to Φ_1 and setting it equal to zero gives the same result as Eq. (7.39). On the other hand, taking the derivative of F_d with respect to Φ_2 and setting it equal to zero gives the same result as that shown in Eq. (7.35). Taking the derivative of F_d with respect to θ_1 and setting it equal to zero results in a different derivative as shown below:

$$\frac{\partial F_d}{\partial \theta_1} = -\frac{K-\dfrac{1-2\theta_3/\theta_1+\theta_3}{\Theta^2}\Phi_2}{\left(\theta_1-1\right)^2}+G_L\frac{K\xi\Phi_1}{\left(\xi-\Phi_1\theta_1\right)^2}-G_{sc}\frac{\theta_3\Phi_2}{\Psi^2}=0 \tag{7.42}$$

Clearly, a minimum with respect to θ_1 may exist. Even though Eq. (7.41) is different when compared to Eq. (7.36), the behavior was exactly the same as in Fig. 7.11 and only the function values encountered were different.

7.2.4 Constant Heat Transfer Rate in Subcooler

Dividing Eq. (7.23) by the heat transfer rate in the sub-cooler results in a non-dimensional equation, which translates into applying the HEICE to a cycle with constant heat transfer rate in the sub-cooler.

$$F_e = \frac{\Gamma}{\gamma_{H,m}\dot{Q}_{sc}} T_H = \left[\frac{K\dfrac{1}{\Phi_2} - \dfrac{1}{\Theta}}{\theta_1 - 1} + G_d \frac{\dfrac{\theta_2}{\theta_1}\dfrac{1}{\Phi_2}}{\theta_2 - 1} + G_L \frac{K\dfrac{\Phi_1}{\Phi_2}}{\xi - \Phi_1\theta_1} + G_{sc}\frac{1}{\Psi} \right] \tag{7.43}$$

The function F_e is also found to have no minimum with respect to ξ and θ_2 as it is clearly inversely proportional to them. The derivative of F_e with respect to θ_3 was determined to be the same as for F_b and, thus, no minimum exists. Taking the derivative of F_e with respect to Φ_1 and setting it equal to zero provides no minimum as all quantities are positive. On the other hand, taking the derivative of F_e with respect to Φ_2 and setting it equal to zero gives:

$$\frac{\partial F_e}{\partial \Phi_2} = -\frac{K}{(\theta_1 - 1)} - G_d \frac{\dfrac{\theta_2}{\theta_1}}{(\theta_2 - 1)} - G_L \frac{K\Phi_1}{(\xi - \Phi_1\theta_1)} + G_{sc}\frac{\theta_1\Phi_2^2}{\Psi^2} = 0 \tag{7.44}$$

A minimum may exist and must be checked (See Fig. 7.12). Fig. 7.12 shows that, for all values of θ_1, the minimum value of Φ_2 stays approximately the same. It is also noted that this minimum occurs at a value greater than Φ_1. A reversal of behavior is seen here as it was seen in Fig. 7.10(b) but the insensitivity of the cost function near the minima is not noticed. Finally, $\partial F_e / \partial \theta_1$ was found to be the same as in Eq. (7.36).

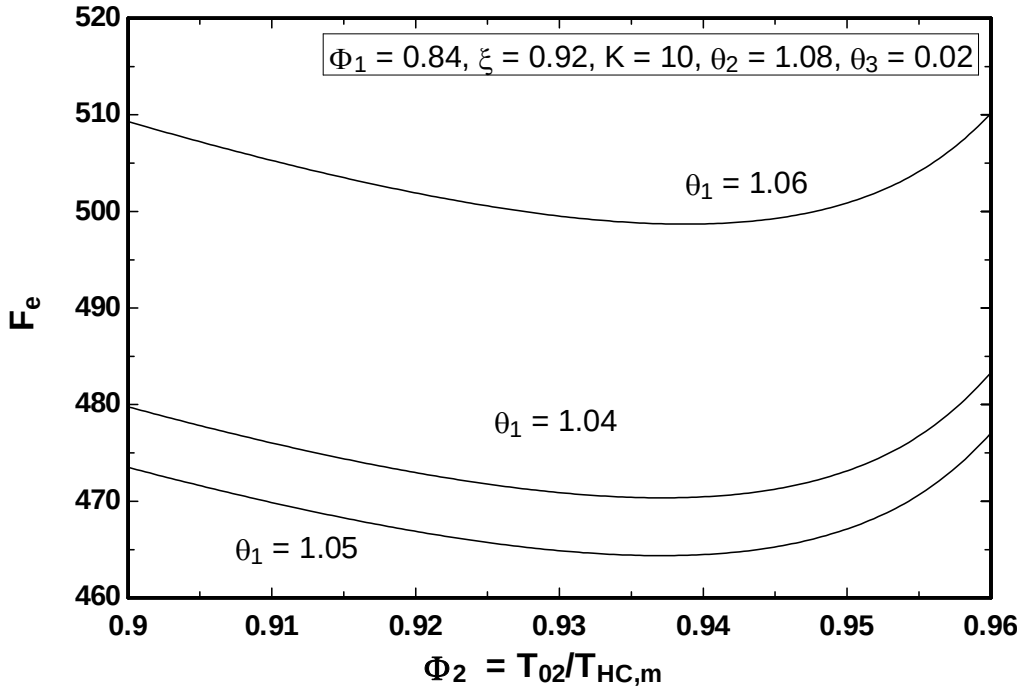

Figure 7.12. Dimensionless HEICE for heat transfer rate in the subcooler vs. Φ_2: Effect of varying θ_1

Some simplification of the cost analysis is possible based on recent research into refrigerant combinations [87] in these systems. From the models used in it, the maximum difference in the condenser temperatures of both cycles was found to be 22 °C i.e. $T_{HC,m}$ = 52 °C and $T_{HC,d}$ = 74 °C where the ambient temperature investigated was 45 °C for the case of R134a in the main cycle and R407C in the dedicated subcooling cycle. Then the temperature ratios θ_1 and θ_2 become 1.02 and 1.09, respectively, which shows that even when $T_{HC,m}$ is not equal to $T_{HC,d}$, $\theta_1 \simeq \theta_2$ and, thus, Eq. (7.23) may be written as

$$\frac{\Gamma}{\gamma_{H,m}} T_H = \dot{Q}_{sc} \left[\frac{K \dfrac{1}{\Phi_2} - \dfrac{1}{1-\theta_3/\theta}}{\theta - 1} + G_d \frac{\dfrac{1}{\Phi_2}}{\theta - 1} + G_L \frac{K \dfrac{\Phi_1}{\Phi_2}}{\xi - \Phi_1 \theta} + G_{sc} \frac{1}{\theta(1-\Phi_2) - \theta_3} \right] \tag{7.45}$$

The previous analysis was repeated for the above case but there was no major finding.

As far as the integrated mechanical subcooling system is concerned (See Figs. 7.13(a)-(b)), a close look at the cycle shows that the analysis shown above for the dedicated cycle is valid for this system as well but with the following modifications:

- The unit cost conductance ratio G_d (as well as the cost function F_d) will become zero as there are only three heat exchangers and the condenser is common in this case.
- The high-side absolute temperature ratios will become identical i.e. $\theta_1 = \theta_2 = \theta$ since the condenser temperatures will be the same i.e. $T_{HC,m} = T_{HC,d} = T_{HC}$.

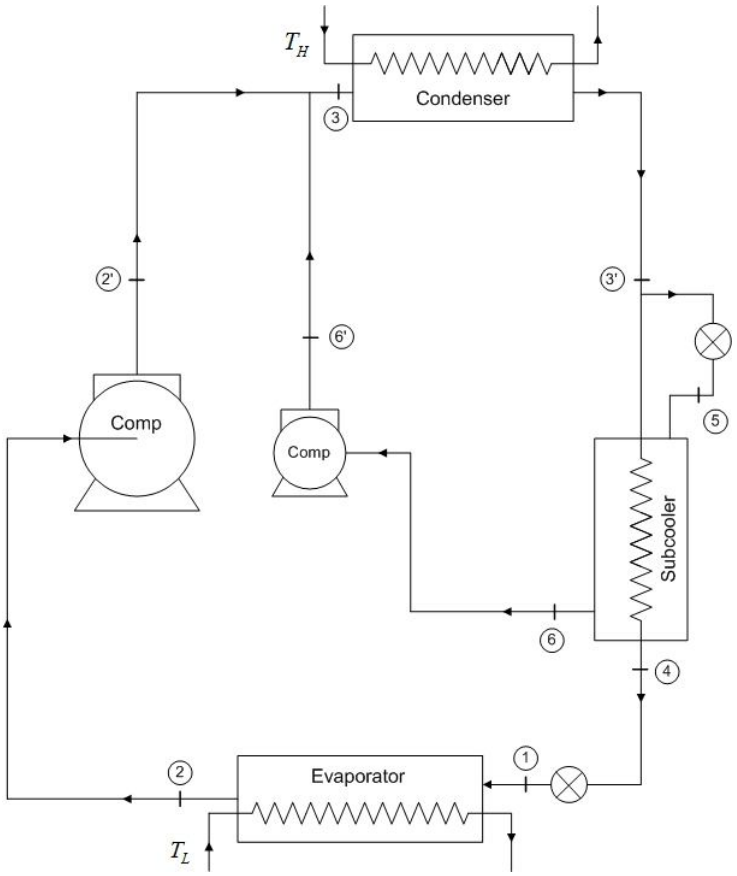

Figure 7.13(a). Schematic of an integrated mechanical subcooling system

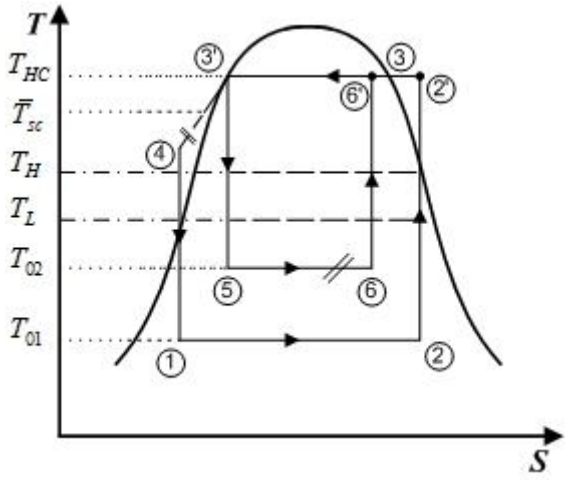

Figure 7.13(b). Integrated Carnot cycle with subcooler

- The symbol $\dot{m}_d$ will be replaced by $\dot{m}_i$ referring to the mass flow rate through the integrated subcooling cycle. Furthermore, it should be noted that the sum of $\dot{m}_m$ and $\dot{m}_i$ will now pass through the main condenser.
- In Eq. 7.22(g), K will now become K_1 and k_1 will be greater than unity. This is due to the fact that the system has a common refrigerant and $(s_2 - s_1) > (s_6 - s_5)$ (See Fig. 7.13(b)).
- Two further equations are introduced below due to the fact that, in contrast to the dedicated subcooling cycle, many of the entropy differences are not equal in this system:

$$K_2 = k_2 \frac{\dot{m}_m}{\dot{m}_i} \tag{7.46a}$$

$$K_3 = k_3 \tag{7.46b}$$

where $k_2 = \frac{s_3 - s_4}{s_6 - s_5}$, $k_3 = \frac{s_3 - s_3'}{s_6 - s_5}$ and both are greater than one (See Fig. 7.13(b)).

- It may be shown that the counterpart to Eq. 7.19(a) for integrated subcooling cycles can be written as (See Appendix G for derivation):

$$\frac{\dot{Q}_{H,m}}{T_{HC,m}} + \frac{\dot{Q}_{sc}}{\bar{T}_{sc}} = \frac{k_2}{k_1}\frac{\dot{Q}_L}{T_{01}} + k_3 \frac{\dot{Q}_{sc}}{T_{02}} \tag{7.47}$$

Applying the above modifications results in the following equation and is the counterpart to Eq. (7.23) for integrated subcooling cycles:

$$\frac{\Gamma}{\gamma_{H,m}} T_H = \dot{Q}_{sc} \left[\frac{K_4 \frac{1}{\Phi_2} - \frac{1}{1-\theta_3/\theta}}{\theta - 1} + G_L \frac{K_1 \frac{\Phi_1}{\Phi_2}}{\xi - \Phi_1 \theta} + G_{sc} \frac{1}{\theta(1-\Phi_2) - \theta_3} \right] \tag{7.48}$$

where $K_4 = K_2 + K_3$ and $K_2 < K_1$ since $k_2 < k_1$. Furthermore, the counterpart to Eq. (7.28b) required for the case of constant work was found to be as follows:

$$\frac{\dot{Q}_{sc}}{\dot{W}} = \frac{1}{K_4 \frac{1}{\Phi_2} - \frac{1}{1-\theta_3/\theta} - K_1 \frac{\Phi_1}{\Phi_2}} \tag{7.49}$$

It is important to note that the overall form of the equations has not changed. The analysis and cases performed for the dedicated subcooling cycle above were repeated for the integrated subcooling cycle. It was found that applying the modifications mentioned above to the derivatives of the various cost functions for the dedicated subcooling cycle and removing any derivative terms generated due to the G_d term resulted in the corresponding derivative for the integrated subcooling cycle. Furthermore, it was noticed that the figures qualitatively remain the same and only the value of the dimensionless cost functions change.

7.3 Thermoeconomic Optimization of Mechanical Subcooling Systems using Thermodynamic Models

Some of the results from sections 7.2.1 and 7.2.2 will be checked by application with a thermodynamic model for dedicated mechanical subcooling. The general form of the cost functions (i.e. LHS of Eqs. (7.25) and (7.32)) were integrated with the model. To check this, variation of one of the cost functions, F_2, was determined with changes in the compressor efficiency of the main cycle. Fig. 7.14 shows that as the efficiency of the main compressor increases, the cost decreases, which is a logical conclusion. It should be noted that designating the values of Φ, θ and ξ fixes the value of the same cost function in the endoreversible case.

The variation of both cost functions, F_1 and F_2, with respect to θ were checked to see how closely they follows the endoreversible case. Figs. 7.15 and 7.16 show the variation of F_1 against θ at compressor efficiencies of 0.65 and 1, respectively. It is seen that a minimum is reached as in the endoreversible case. Also, it is noted that, as in the SVCC case, actual minimum for this system is greater than the endoreversible one and that increasing the compressor efficiency reduces the difference between them. These behaviors are now checked for the cost function F_2. Figs. 7.17 and 7.18 show the variation of F_2 against θ at compressor efficiencies of 0.65 and 1, respectively. It is found that the above-mentioned behaviors are repeated for F_2 and is not pronounced in this case. Increasing the efficiency of the subcooling cycle compressor to unity as well did not have any further significant effect.

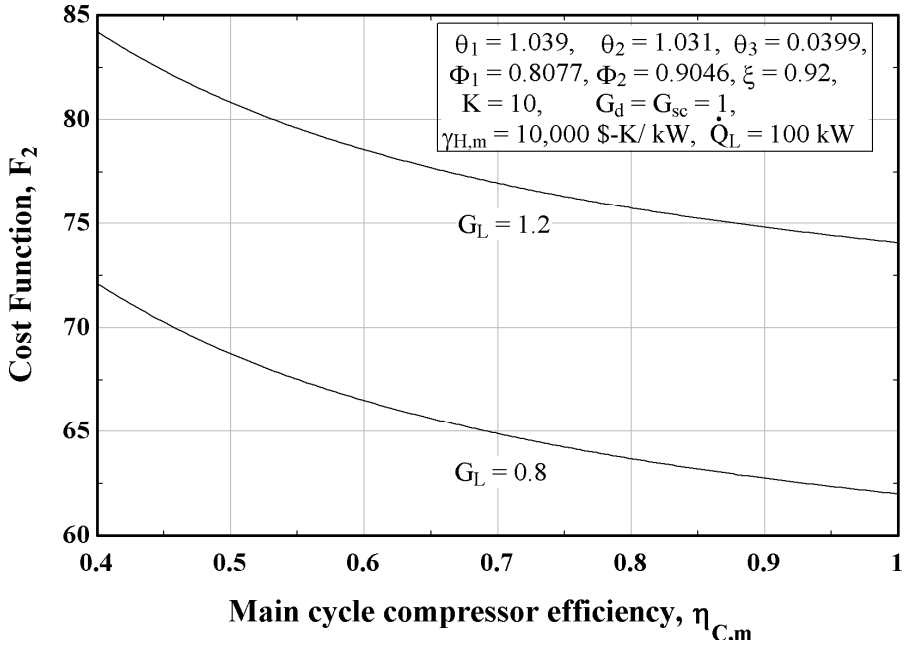

Figure 7.14. Effect of main compressor efficiency on cost function F_2

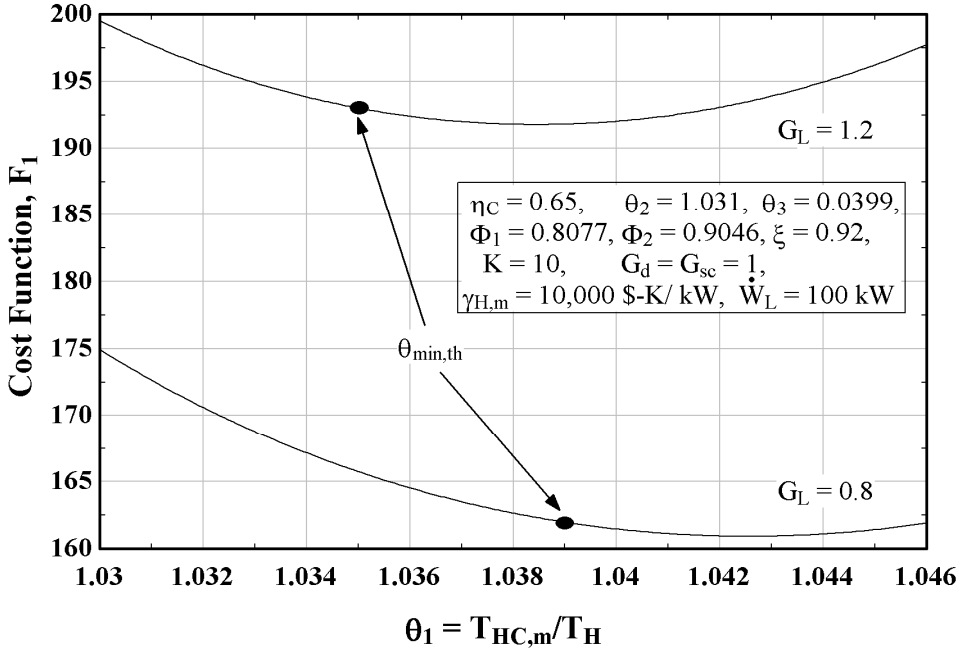

Figure 7.15. Variation of cost function F_1 with respect to θ_1 [$\eta_c = 0.65$]: VCC-DMS

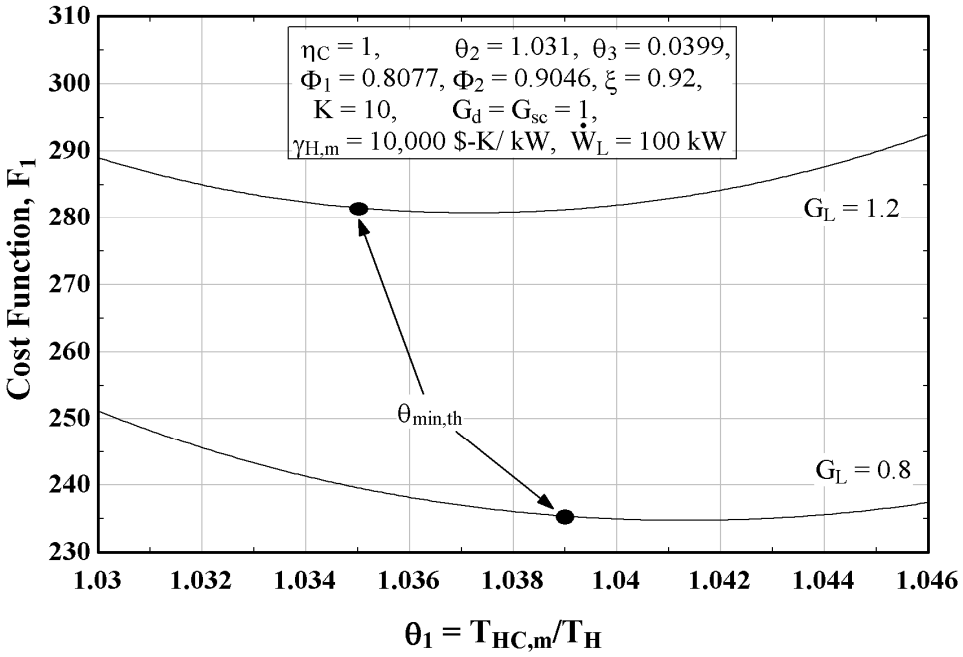

Figure 7.16. Variation of cost function F_1 with respect to θ_1 [$\eta_c = 1$]: VCC-DMS

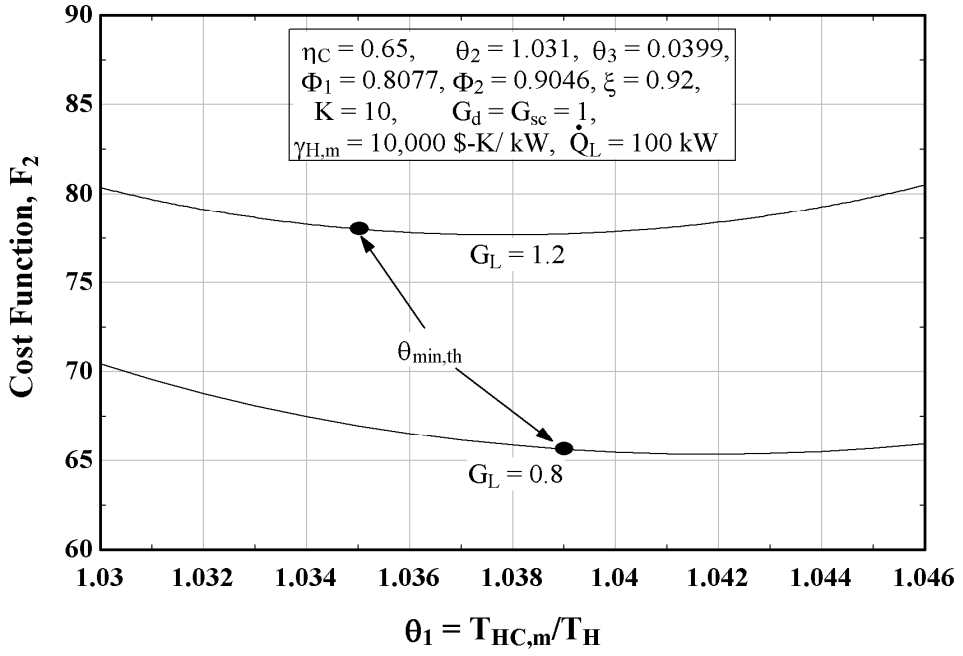

Figure 7.17. Variation of cost function F_2 with respect to θ_1 [$\eta_c = 0.65$]: VCC-DMS

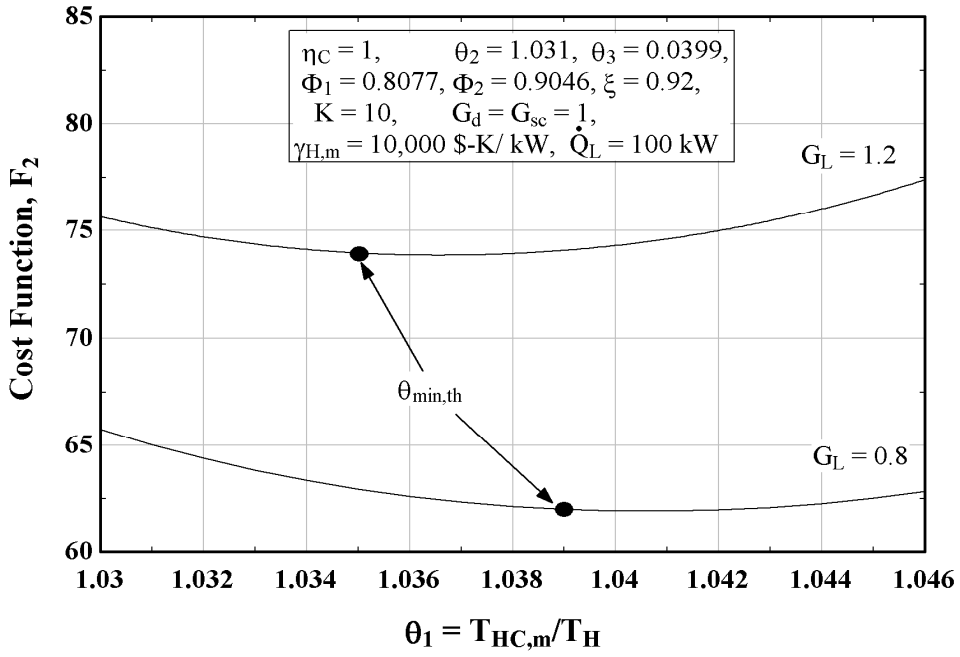

Figure 7.18. Variation of cost function F_2 with respect to θ_1 [$\eta_c = 1$]: VCC-DMS

This indicates that equations similar to Eqs. (7.1) and (7.2) can be used to determine the actual value of $\theta_{1,\min}$ for a dedicated mechanical subcooling cycle. This may be expressed by the following equation:

$$\theta_{1,\min,act} = f(G_L, G_d, G_{sc}, \zeta, \theta_2, \theta_3, \Phi_1, \Phi_2, \eta_{C,m}, \eta_{C,sc}, I_{throt,m}, I_{throt,sc}) \tag{7.50}$$

Keeping the above plots in mind, one possible form of this can be:

$$\theta_{1,\min,act} = \theta_{1,\min,th} + \Im \tag{7.51}$$

where $\Im = f(G_L, G_d, G_{sc}, \zeta, \theta_2, \theta_3, \Phi_1, \Phi_2, \eta_{C,m}, \eta_{C,sc}, I_{throt,m}, I_{throt,sc})$. The analysis indicates that $\eta_{C,m}$ is a major factor while $\eta_{C,sc}$ is a minor factor.

7.4 Thermoeconomic Optimization for a Carnot Power Cycle with one Feedwater Heater

Using feedwater heaters to enhance efficiency of power cycles is a standard practice in industry and, therefore, thermoeconomic analysis of such systems becomes important. For this purpose, the methodology of Bejan [14], Antar and Zubair [29] and Morales [37] is followed. The schematic of system under consideration is shown in Fig. 7.19(a) while the T-s diagram of the Carnot representation of this cycle is shown below in Fig. 7.19(b).

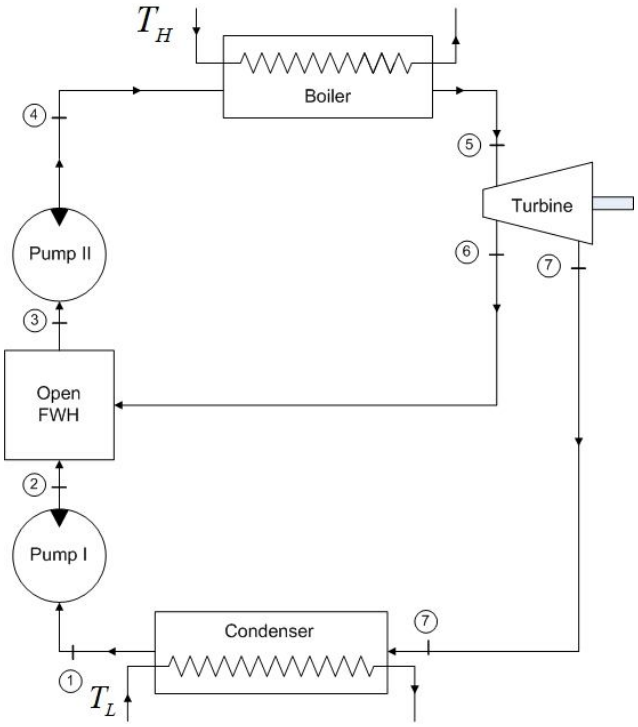

Figure 7.19(a). Schematic of an endoreversible power cycle with an open feedwater heater

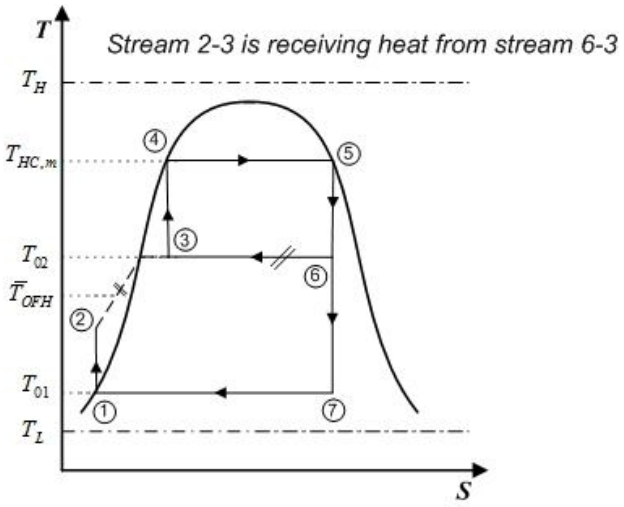

Figure 7.19(b). T-s diagram of an endoreversible power cycle with one open feedwater heater

The objective in the present investigation is to find minimum total cost of conductance (UA) for constant rate of work, heat addition and rejection capacities as well as heat transfer in the preheater. Neglecting the costs of the compressors, piping system and expansion devices, the HEICE can be written as in terms of unit cost parameters of the heat exchangers as:

$$\Gamma = \gamma_H (UA)_H + \gamma_L (UA)_L + \gamma_{OFH} (UA)_{OFH} \tag{7.52}$$

where γ_H, γ_L, and γ_{OFH} are unit cost of conductance for the boiler, the condenser and the preheater, respectively, making Γ a parameter with units of dollars. Now, we know that

$$\dot{Q}_H = (UA)_H (T_H - T_{HC}) \tag{7.53}$$

$$\dot{Q}_L = (UA)_L (T_{01} - T_L) \tag{7.54}$$

$$\dot{Q}_{OFH} = (UA)_{OFH} (T_{02} - \bar{T}_{OFH}) \tag{7.55a}$$

where $\bar{T}_{OFH}$ is the average preheating temperature and may be defined as:

$$\bar{T}_{OFH} = T_{02} - \Delta T_{OFH,avg} \tag{7.55b}$$

where $\Delta T_{OFH,avg}$ is the average amount of preheating and can be understood as half of the total amount of preheating achieved. Substituting Eqs. (7.53) – (7.55) in Eq. (7.52), we get

$$\Gamma = \gamma_H \frac{\dot{Q}_H}{T_H - T_{HC}} + \gamma_L \frac{\dot{Q}_L}{T_{01} - T_L} + \gamma_{OFH} \frac{\dot{Q}_{OFH}}{\Delta T_{OFH,avg}} \tag{7.56}$$

Dividing throughout by γ_H, we get

$$\frac{\Gamma}{\gamma_H} = \frac{\dot{Q}_H}{T_H - T_{HC}} + \frac{\gamma_L}{\gamma_H} \frac{\dot{Q}_L}{T_{01} - T_L} + \frac{\gamma_{OFH}}{\gamma_H} \frac{\dot{Q}_{OFH}}{\Delta T_{OFH,avg}} \tag{7.57}$$

Let $\frac{\gamma_L}{\gamma_H} = G_L$; $\frac{\gamma_{OFH}}{\gamma_H} = G_{OFH}$, then Eq. (7.57) can be written as

$$\frac{\Gamma}{\gamma_H} = \frac{\dot{Q}_H}{T_H - T_{HC}} + G_L \frac{\dot{Q}_L}{T_{01} - T_L} + G_{OFH} \frac{\dot{Q}_{OFH}}{\Delta T_{OFH,avg}} \tag{7.58}$$

Factoring out $\dot{Q}_H$, we get

$$\frac{\Gamma}{\gamma_H} = \dot{Q}_H \left[\frac{1}{T_H - T_{HC}} + G_L \frac{\dot{Q}_L / \dot{Q}_H}{T_{01} - T_L} + G_{OFH} \frac{\dot{Q}_{OFH} / \dot{Q}_H}{\Delta T_{OFH,avg}} \right] \tag{7.59}$$

Now, from Fig. 7.19(b), we see that

$$\dot{Q}_{OFH} = \dot{m}_{01} \overline{T}_{OFH} (s_3 - s_2) \tag{7.60a}$$

$$\dot{Q}_{3-6} = \dot{m}_{02} T_{02} (s_6 - s_3) \tag{7.60b}$$

$$\dot{Q}_L = \dot{m}_{01} T_{01} (s_7 - s_1) \tag{7.60c}$$

But $\dot{Q}_{OFH} = \dot{Q}_{3-6}$ as these are two streams exchanging heat in the same heat exchanger i.e. the feedwater heater. Therefore,

$$\frac{\dot{Q}_{OFH}}{\dot{Q}_L} = \frac{\dot{m}_{02} T_{02} (s_6 - s_3)}{\dot{m}_{01} T_{01} (s_7 - s_1)} \tag{7.61}$$

Now, it is also clear from Fig. 7.19(b) that, in general, $(s_6 - s_3) = k_1(s_7 - s_1)$ where k_1 can be any number less than one. Now, Eq. (7.61) becomes

$$\frac{\dot{Q}_{OFH}}{\dot{Q}_L} = k_1 \frac{\dot{m}_{02} T_{02}}{\dot{m}_{01} T_{01}} \tag{7.62}$$

As the cycle is internally reversible, applying the Clausis' inequality, we get

$$\frac{\dot{Q}_H}{T_{HC}} = \frac{\dot{Q}_L}{T_{01}}$$

$$\Rightarrow \qquad \frac{\dot{Q}_L}{\dot{Q}_H} = \frac{T_{01}}{T_{HC}} \tag{7.63}$$

Combining Eqs. (7.62)-(7.63), we get

$$\frac{\dot{Q}_{OFH}}{\dot{Q}_H} = k_1 \frac{\dot{m}_{02} T_{02}}{\dot{m}_{01} T_{HC}} \tag{7.64}$$

Substituting Eqs. (7.63)-(7.64) in Eq. (7.59), and dividing the right hand side by T_H/T_H, we get

$$\frac{\Gamma}{\gamma_H} = \frac{\dot{Q}_H}{T_H}\left[\frac{1}{1-\dfrac{T_{HC}}{T_H}} + G_L\,\frac{\dfrac{T_{01}}{T_{HC}}}{\dfrac{T_{01}}{T_H}-\dfrac{T_L}{T_H}} + G_{OFH}\,\frac{k_1\dfrac{\dot{m}_{02}T_{02}}{\dot{m}_{01}T_{HC}}}{\dfrac{\Delta T_{OFH,avg}}{T_H}}\right] \tag{7.65}$$

Introducing the following non-dimensional ratios below:

$$\theta_1 = \frac{T_{HC}}{T_H} \tag{7.66a}$$

$$\theta_2 = \frac{\Delta T_{OFH,avg}}{T_H} \tag{7.66b}$$

$$\Phi_1 = \frac{T_{01}}{T_{HC}} \tag{7.66c}$$

$$\Phi_2 = \frac{T_{02}}{T_{HC}} \tag{7.66d}$$

$$\xi = \frac{T_L}{T_H} \tag{7.66e}$$

$$K = k_1\frac{\dot{m}_{02}}{\dot{m}_{01}} \tag{7.66f}$$

Now, substituting Eqs. (7.66a) – (7.66f) in Eq. (7.65), and multiplying both sides by T_H, we get

$$\frac{\Gamma}{\gamma_H}T_H = \dot{Q}_H\left[\frac{1}{1-\theta_1} + G_L\,\frac{\Phi_1}{\Phi_1\theta_1-\xi} + G_{OFH}\,\frac{K\Phi_2}{\theta_2}\right] \tag{7.67}$$

In the next section, starting from Eq. (7.67), the cases for constant rate of work, heat addition and rejection capacities as well as heat transfer rate in the open feedwater heater will be discussed one by one. It should be noted that, in all cases, the unit cost conductance ratios are taken constant as unity. Therefore, it is expected that $(UA)_{tot}$ will also be minimum when the dimensionless HEICE is at a minimum.

7.4.1 Constant work rate

Dividing Eq. (7.67) by the work rate results in the non-dimensional equation given below:

$$F_a = \frac{\Gamma}{\gamma_H \dot{W}} T_H = \frac{\dot{Q}_H}{\dot{W}} \left[\frac{1}{1-\theta_1} + G_L \frac{\Phi_1}{\Phi_1 \theta_1 - \xi} + G_{OFH} \frac{K\Phi_2}{\theta_2} \right] \tag{7.68}$$

Applying the First Law of Thermodynamics (See Fig. 7.19(a)) gives us

$$\dot{W} = \dot{Q}_H - \dot{Q}_L \tag{7.69}$$

where $\dot{W}$ is the sum of work done by both pumps. Dividing both sides by $\dot{Q}_H$, we get

$$\frac{\dot{W}}{\dot{Q}_H} = 1 - \frac{\dot{Q}_L}{\dot{Q}_H} \tag{7.70}$$

Substituting Eqs. (7.63) in the above equation, we get

$$\frac{\dot{W}}{\dot{Q}_H} = 1 - \frac{T_{01}}{T_{HC}} \tag{7.71a}$$

Taking the reciprocal of the result, we get

$$\frac{\dot{Q}_H}{\dot{W}} = \frac{1}{1-\frac{T_{01}}{T_{HC}}} \tag{7.71b}$$

Substituting Eq. 7.71(b) into Eq. (7.68) gives

$$F_a = \frac{1}{1-\Phi_1}\left[\frac{1}{1-\theta_1} + G_L \frac{\Phi_1}{\Phi_1\theta_1 - \xi} + G_{OFH}\frac{K\Phi_2}{\theta_2}\right] \tag{7.72}$$

This is the non-dimensional HEICE for a dedicated subcooling Carnot cycle with constant work rate. It is clear that there is a direct relationship between F_a and ξ as well as Φ_2 and an inverse one with respect to θ_2. Thus, no minimum point exists with respect to these parameters. It is unclear whether minima exist with respect to Φ_1 and θ_1. Taking the derivative of F_a with respect to Φ_1 and setting it equal to zero gives the following equation after simplification:

$$\frac{\partial F_a}{\partial \Phi_1} = \frac{1}{1-\Phi_1}\left[\frac{1}{1-\theta_1} + G_L \frac{\Phi_1}{\Phi_1\theta_1 - \xi} + G_{OFH}\frac{K\Phi_2}{\theta_2}\right] - \left[G_L \frac{\xi}{\left(\Phi_1\theta_1 - \xi\right)^2}\right] = 0 \tag{7.73a}$$

or

$$\Phi_{1,\min} = \frac{c\xi + \sqrt{\xi\left(1+c-c\xi\right)}}{\left(1+c\right)\theta_1} \tag{7.73b}$$

where

$$c = \left[\frac{1}{1-\theta_1} + G_{OFH} \frac{K\Phi_2}{\theta_2} \right] \frac{1}{G_L}$$

It is noted that putting G_{OFH} equal to zero will result in the respective derivative for the system analyzed by Antar and Zubair [29]. Fig. 7.20(a) shows a plot of the cost function F_a against Φ_1 for different values of ξ. It is found that the minimum value of Φ_1 as well as the cost rise as ξ increases. The reason for the cost increasing is evident from Eq. (7.72) where ξ is seen in the second term inside the brackets only. As ξ increases, this term increases in value and, thus, F_a as well. Regarding the minimum value of Φ_1 (that provides a minimum cost), it can be seen from Eq. (7.73b) that this is due to the fact that $\Phi_{1,min}$ is directly proportional to ξ. Furthermore, this shows that, if all other quantities remain constant, a lower ambient temperature may result in a lower cost. Fig. 7.20(b) shows a plot of the cost function F_a against Φ_1 for different values of θ_1. It is found that the minimum value of Φ_1 decreases as θ_1 increases but the cost rises. The reason for the cost increasing is understood from Eq. (7.72) where θ_1 is seen in the first and second terms inside the brackets. The first term containing θ_1 is the dominant term, therefore, as θ_1 increases, this term increases in value and, thus, F_a as well. Regarding the minimum value of Φ_1, it can be seen from Eq. (7.73b) that this is due to the fact that $\Phi_{1,min}$ is inversely proportional to θ_1. Also, the (1+c) term, which contains θ_1 as well, dominates the quantities containing 'c' in the numerator. Furthermore, this shows that a higher furnace temperature may result in a lower cost if all other quantities remained the same.

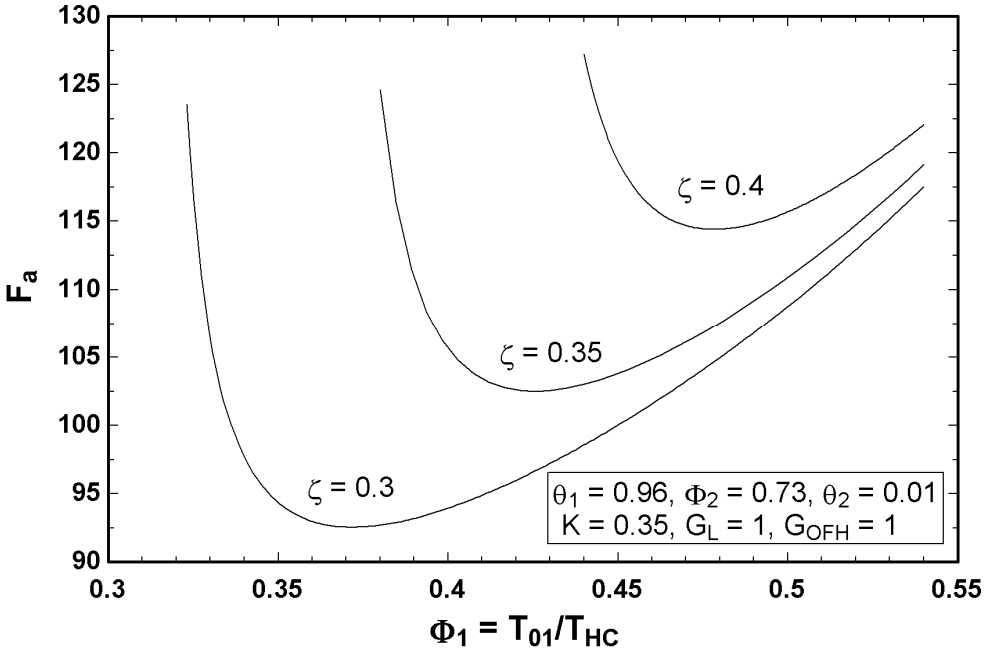

Figure 7.20(a). Dimensionless HEICE for constant work rate vs. Φ_1: Effect of varying ξ

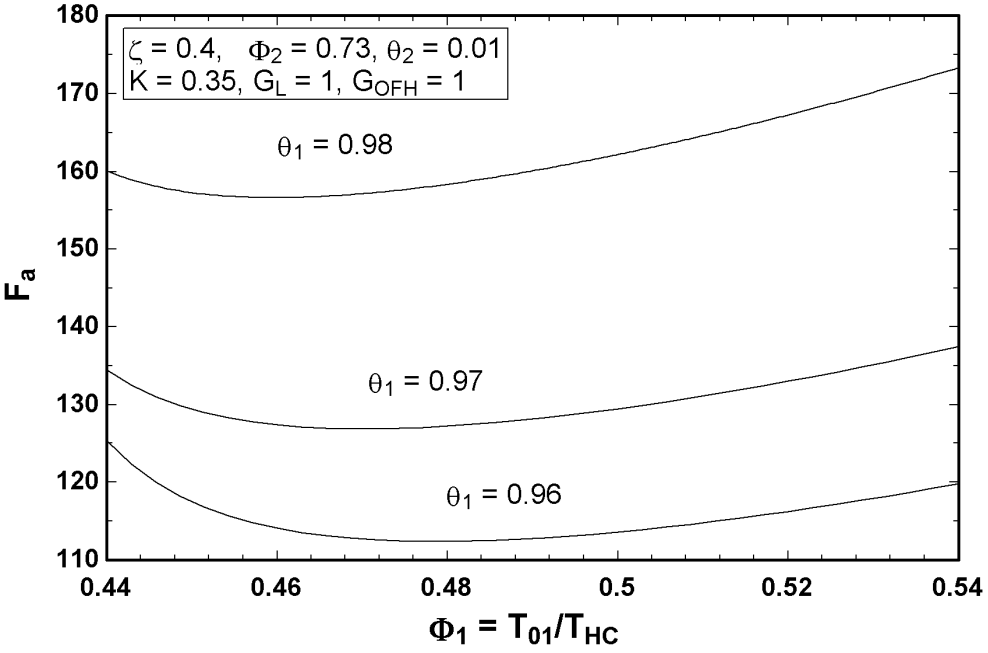

Figure 7.20(b). Dimensionless HEICE for constant work rate vs. Φ_1: Effect of varying θ_1

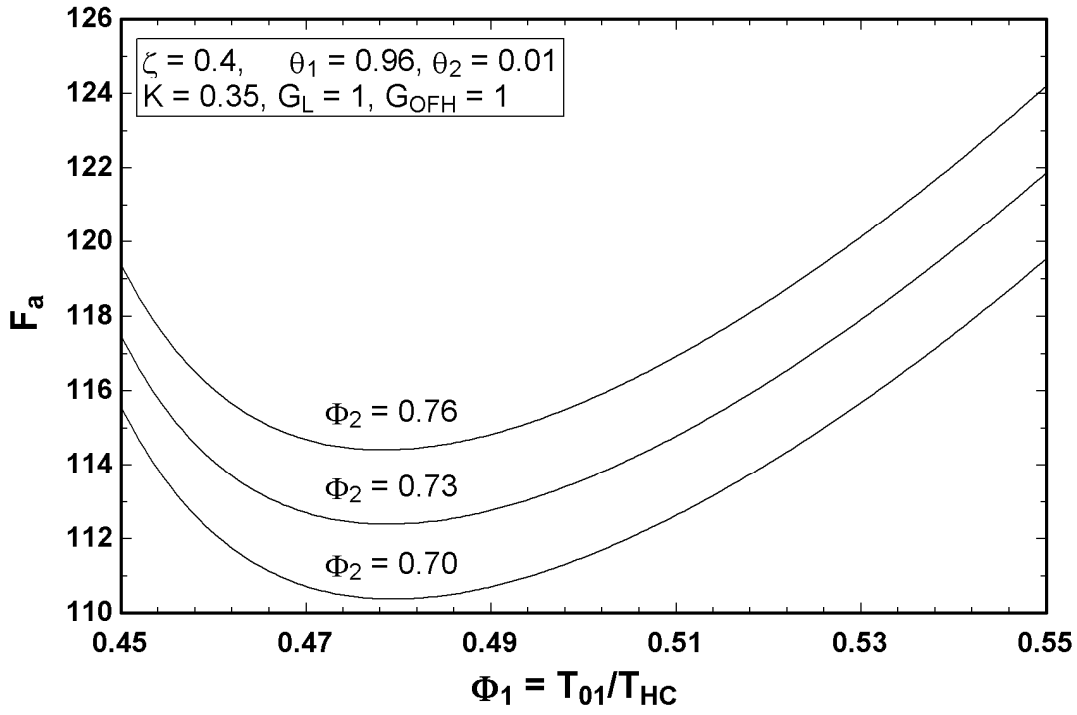

Figure 7.20(c). Dimensionless HEICE for constant work rate vs. Φ_1: Effect of varying Φ_2

Fig. 7.20(c) shows a plot of the cost function F_a against Φ_1 for different values of Φ_2. It was noted that lower values of Φ_2 produced lower costs while the minimum value of Φ_1 was not affected by change in Φ_2. The reason for the cost decreasing is understood from Eq. (7.72) where Φ_2 is seen in the last term inside the bracket only and directly proportional to F_a. Regarding the minimum value of Φ_1 not changing significantly, the reason is that the effect of variation in Φ_2 is very small on 'c'. Furthermore, this shows that, if all other quantities remain constant, a lower feedwater heater extraction temperature (T_{02}) may result in a lower cost.

The function F_a does appear to have a minimum with respect to the parameter θ_1. Setting $\partial F_a/\partial\theta_1 = 0$ yields

$$\theta_{1,\min} = \frac{1}{\Phi_1}\left[\frac{\xi(\sqrt{G_L}-1)+\Phi_1(G_L-\sqrt{G_L})}{G_L-1}\right] \tag{7.74}$$

It should be noted that Eq. (7.74) is identical to the respective derivative found by Antar and Zubair [29] though they did not plot it. Fig. 7.21(a) shows the effect of different values of ξ as F_a varies against θ_1. It is found that the minimum value of θ_1 shifts to a higher value as ξ increases as well as the cost. This behavior is similar to that found in Fig. 7.20(a). As can be seen from Eq. (7.74), this is simply due to the fact that ξ is directly proportional to $\theta_{1,\min}$. Fig. 7.21(b) shows the effect of different values of Φ_1 as F_a varies against θ_1. It is seen that the cost function and $\theta_{1,\min}$ shift to a lower value as Φ_1 increases and this is because Φ_1 is inversely proportional to $\theta_{1,\min}$ (See Eq. (7.74)).

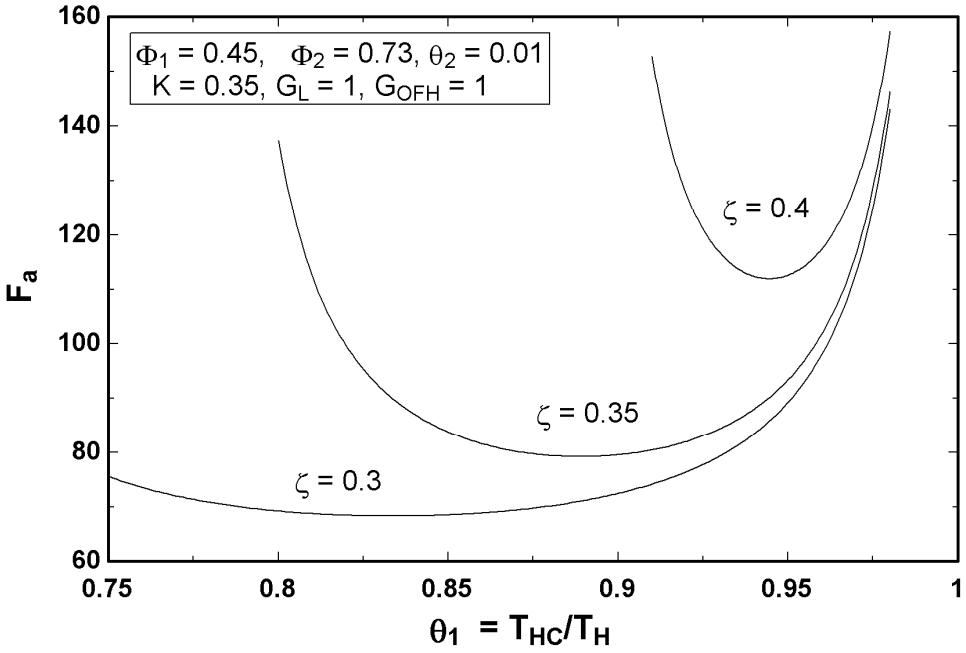

Figure 7.21(a). Dimensionless HEICE for constant work rate vs. θ_1: Effect of varying ξ

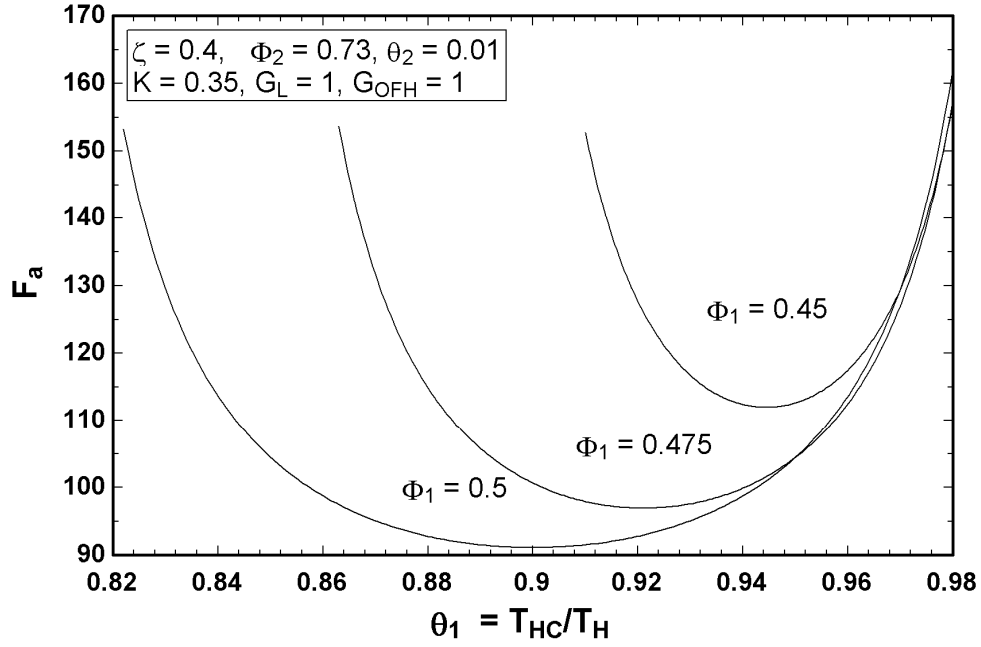

Figure 7.21(b). Dimensionless HEICE for constant work rate vs. θ_1: Effect of varying Φ_1

As far as the cost is concerned, the reason is that, in Eq. (7.72), the second term inside the brackets is dominant and the term outside is not significantly affected by the variation in Φ_1. It shows that, if all other quantities remain constant, increasing the condenser temperature may result in a lower cost since a larger temperature difference would be available and, thus, a heat exchanger of smaller size (or UA) would be needed. Fig. 7.21(c) shows a plot of the cost function F_a against θ_1 for different values of Φ_2. It is found that the minimum value of Φ_1 is not affected by change in Φ_2 and this is because the term Φ_2 does not exist in the expression for $\theta_{1,min}$. It was noted that higher values of Φ_2 produced higher costs and the reasons are the same as was explained for Fig. 7.20(c). This indicates that, if all other quantities remain constant, a lower feedwater heater extraction temperature may result in a lower cost.

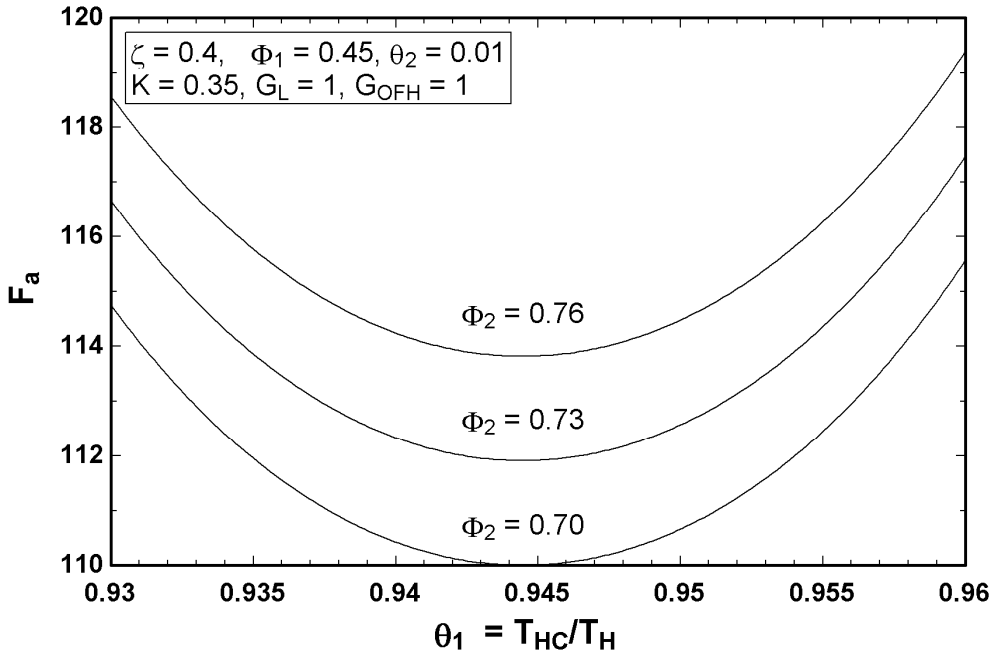

Figure 7.21(c). Dimensionless HEICE for constant work rate vs. θ_1: Effect of varying Φ_2

7.4.2 Constant heating rejection rate

Dividing Eq. (7.67) by the heat transfer in the condenser results in the non-dimensional equation shown below:

$$F_b = \frac{\Gamma}{\gamma_H \dot{Q}_L} T_H = \frac{\dot{Q}_H}{\dot{Q}_L}\left[\frac{1}{1-\theta_1} + G_L \frac{\Phi_1}{\Phi_1\theta_1 - \xi} + G_{OFH}\frac{K\Phi_2}{\theta_2}\right] \tag{7.75}$$

This translates into applying the HEICE to a cycle with constant heat transfer in the condenser which, after the appropriate substitution, gives

$$F_b = \frac{1}{\Phi_1}\left[\frac{1}{1-\theta_1} + G_L \frac{\Phi_1}{\Phi_1\theta_1 - \xi} + G_{OFH}\frac{K\Phi_2}{\theta_2}\right] \tag{7.76}$$

This scenario deals with a constant heat rejection rate in the condenser. The purpose is to determine whether the function F_b has a minimum with respect to ξ, Φ_1, Φ_2, θ_1 and θ_2. F_b is directly proportional to ξ as well as Φ_2 and inversely proportional to θ_2. Therefore, no minima exist with respect to these three variables. Taking the derivative of F_b with respect to Φ_1 and setting it equal to zero gives the following equation:

$$\frac{\partial F_b}{\partial \Phi_1} = \frac{1}{\Phi_1}\left[\frac{1}{1-\theta_1} + G_L \frac{\Phi_1}{\Phi_1\theta_1 - \xi} + G_{OFH}\frac{K\Phi_2}{\theta_2}\right] + \left[G_L \frac{\xi}{\left(\Phi_1\theta_1 - \xi\right)^2}\right] = 0 \tag{7.77}$$

It is again noted that putting G_{OFH} equal to zero will result in the respective derivative for the system analyzed by Antar and Zubair [29]. In the above equation, all terms are positive and, therefore, a practical minimum is not possible. The result of taking the derivative of F_b with respect to θ_1, in this case, is identical to Eq. (7.74).

Figs. 7.22(a)-(c) are plotted for conditions identical to those of Figs. 7.21(a)-(c). It is found that the behavior for this cost function is qualitatively the same as F_a and the only difference is in the values. The reason for this is that the terms inside the brackets for both the cost functions are identical while there is a minor difference in the term outside it.

7.4.3 Constant heat addition rate

Dividing Eq. (7.67) by the heat transfer in the condenser results in a non-dimensional equation. This translates into applying the HEICE to a cycle with constant heat transfer in the condenser.

$$F_c = \frac{\Gamma}{\gamma_H \dot{Q}_H} T_H = \left[\frac{1}{1-\theta_1} + G_L \frac{\Phi_1}{\Phi_1 \theta_1 - \xi} + G_{OFH} \frac{K\Phi_2}{\theta_2} \right] \tag{7.78}$$

This scenario deals with a constant heat addition rate in the condenser. As with the other cost functions, it was found that F_c has no minima with respect to ξ, Φ_2 and θ_2. Taking the derivative of F_c with respect to Φ_1 and setting it equal to zero gives the following equation:

$$\frac{\partial F_c}{\partial \Phi_1} = \frac{\xi}{\left(\xi - \Phi_1 \theta_1\right)^2} = 0 \tag{7.79}$$

As all terms in the equation are clearly positive on one side, therefore, no minimum exists. The result of taking the derivative of F_c with respect to θ_1, in this case, is identical to Eq. (7.74).

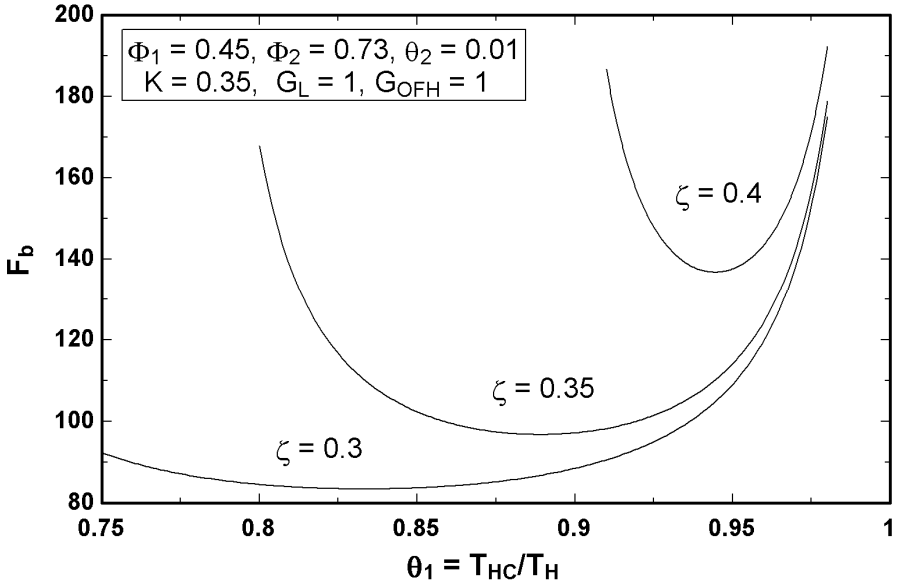

Figure 7.22(a). Dimensionless HEICE for constant heat rejection rate vs. θ_1: Effect of varying ξ

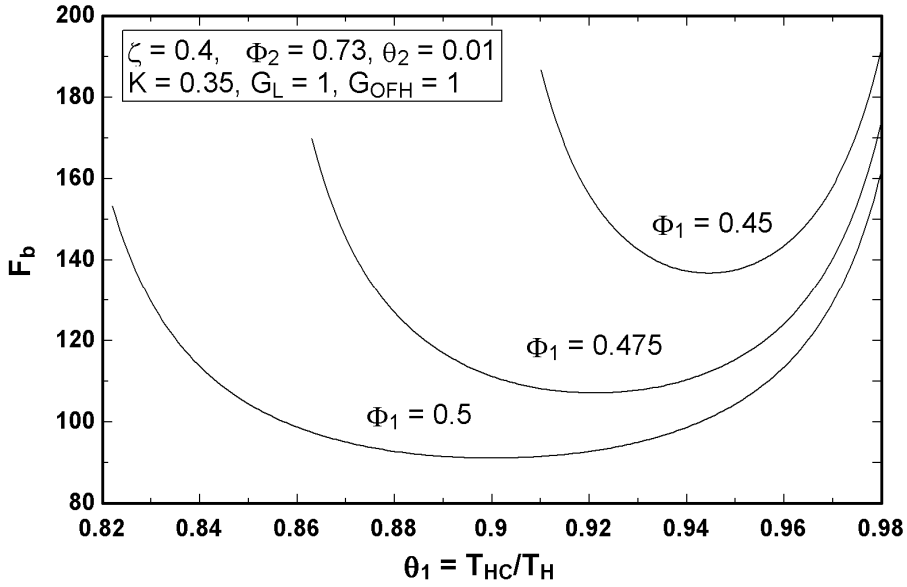

Figure 7.22(b). Dimensionless HEICE for constant heat rejection rate vs. θ_1: Effect of varying Φ_1

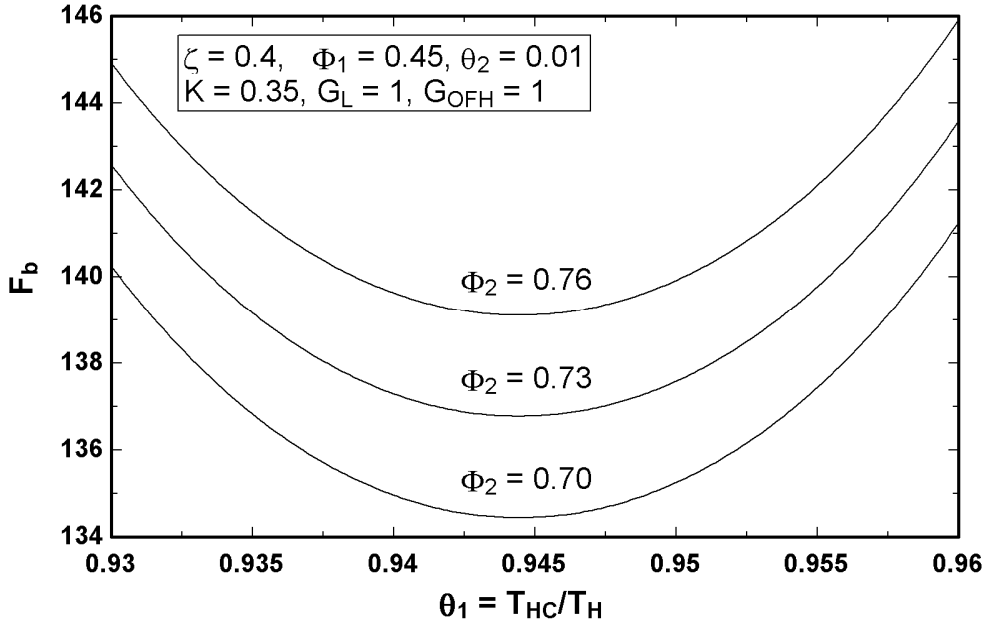

Figure 7.22(c). Dimensionless HEICE for constant heat rejection rate vs. θ_1: Effect of varying Φ_2

Figs. 7.23(a)-(c) are plotted for conditions identical to those of Figs. 7.21(a)-(c). It is found that the behavior for this cost function is qualitatively the same as F_a and the only difference is in the values. The reason for this is that the quantities inside the brackets for both the cost functions (i.e. F_a and F_c) are identical while there is a small difference outside it which is a multiplying factor only.

7.4.4 Constant heat transfer rate in the feedwater heater

Dividing Eq. (7.67) by $\dot{Q}_{OFH}$ results in a non-dimensional equation which corresponds to applying the HEICE to a cycle with constant heat transfer rate in the open feedwater heater (See Eq. (7.80) below).

$$F_d = \frac{\Gamma}{\gamma_H \dot{Q}_{OFH}} T_H = \frac{\dot{Q}_H}{\dot{Q}_{OFH}} \left[\frac{1}{1-\theta_1} + G_L \frac{\Phi_1}{\Phi_1 \theta_1 - \xi} + G_{OFH} \frac{K\Phi_2}{\theta_2} \right] \tag{7.80a}$$

which, after the appropriate substitution, gives

$$F_d = \frac{\Gamma}{\gamma_H \dot{Q}_{OFH}} T_H = \frac{1}{K\Phi_2} \left[\frac{1}{1-\theta_1} + G_L \frac{\Phi_1}{\Phi_1 \theta_1 - \xi} + G_{OFH} \frac{K\Phi_2}{\theta_2} \right] \tag{7.80b}$$

The function F_d is also found to have no minimum with respect to ξ and θ_2 as it is clearly inversely proportional to them. Taking the derivative of F_d with respect to Φ_1 and setting it equal to zero results in Eq. (7.74) and, therefore, no minimum exists. On the other hand, taking the derivative of F_d with respect to Φ_2 and setting it equal to zero gives:

$$\frac{\partial F_d}{\partial \Phi_2} = G_{OFH} \frac{1}{\theta_2 \Phi_2} - \frac{1}{K\Phi_2^2} \left[\frac{1}{1-\theta_1} + G_L \frac{\Phi_1}{\Phi_1 \theta_1 - \xi} + G_{OFH} \frac{K\Phi_2}{\theta_2} \right] = 0 \tag{7.81a}$$

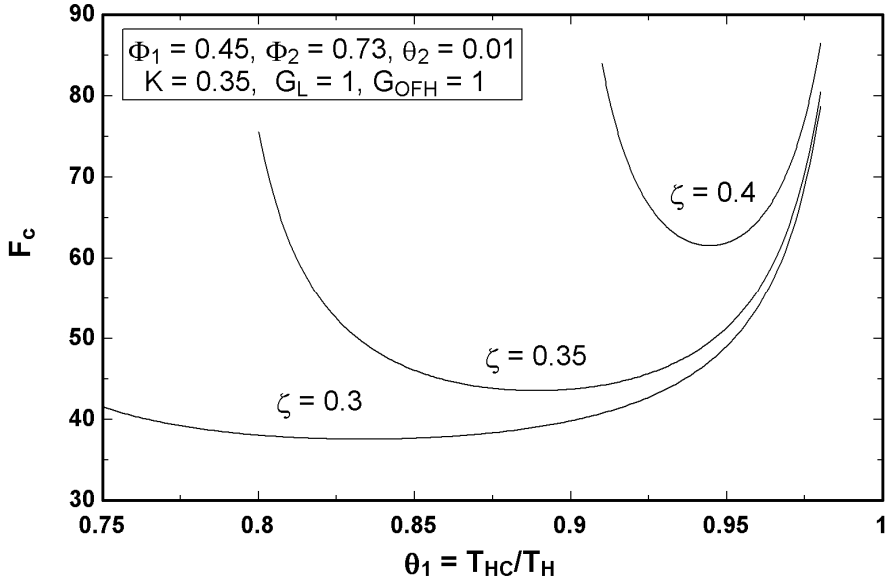

Figure 7.23(a). Dimensionless HEICE for constant heat addition rate vs. θ_1: Effect of varying ξ

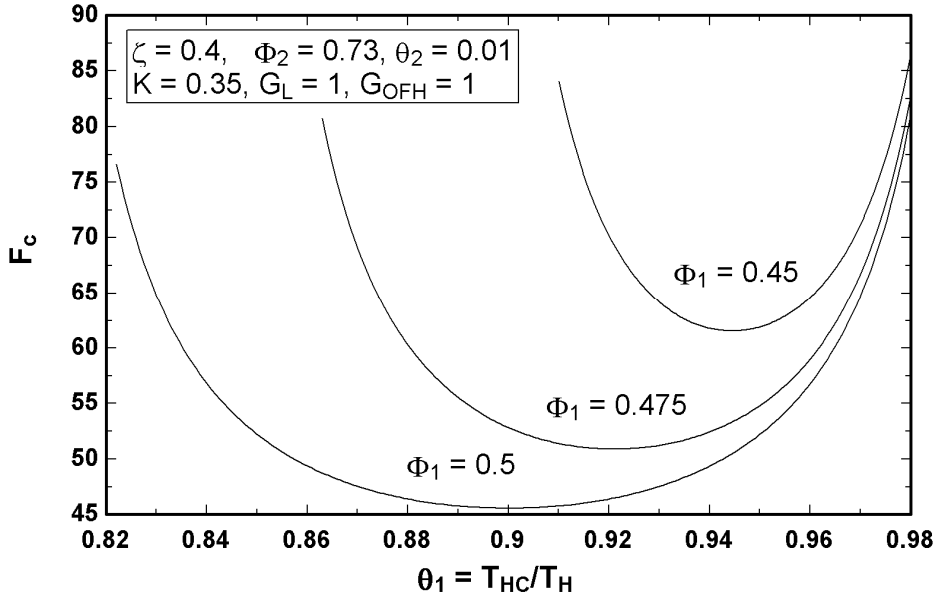

Figure 7.23(b). Dimensionless HEICE for constant heat addition rate vs. θ_1: Effect of varying Φ_1

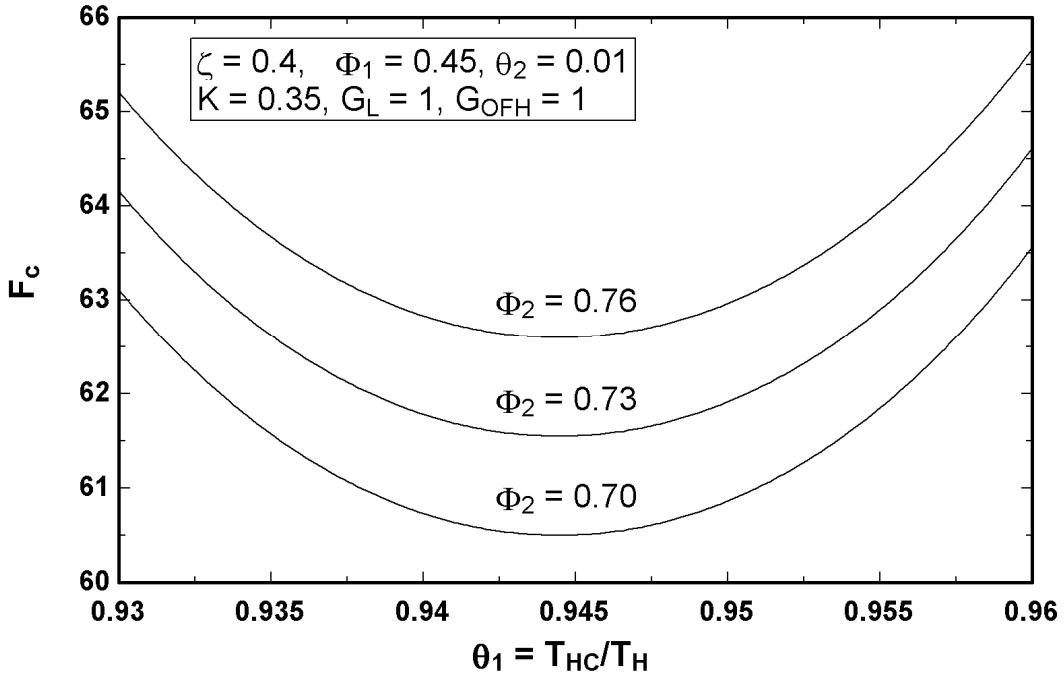

Figure 7.23(c). Dimensionless HEICE for constant heat addition rate vs. θ_1: Effect of varying Φ_2

or, after simplification, gives

$$\frac{\partial F_d}{\partial \Phi_2} = \frac{1}{1-\theta_1} + G_L \frac{\Phi_1}{\Phi_1\theta_1 - \xi} = 0 \qquad (7.81b)$$

As all terms in the equation are clearly positive, therefore, no minimum exists. Finally, $\partial F_d / \partial \theta_1$ was found to be the same as in Eq. (7.74). Figs. 7.24(a)-(c) are plotted for conditions identical to those of Figs. 7.21(a)-(c). It is found that the behavior for this cost function is qualitatively the same as F_a and the only difference is in the values. This is due to the fact that the quantities inside the brackets for both the cost functions (i.e. F_a and F_d) are the same and, although the term outside it is different, it only acts a multiplying factor resulting in a change of value but not behavior.

7.4.5 Effect of unit cost ratios

The purpose of the analysis in this section is determining the minimum of the total conductance for specified power production and this scenario is chosen due to its practical nature. Optimum values for Φ_1 and θ_1 will be determined from Eqs. (7.73b) and (7.74), respectively.

In order to provide an illustrative example for the purpose of showing model applicability, it is required that ratios of the conductance costs of each heat exchanger to the total cost be determined. For the sake of brevity, only the final expressions are shown below:

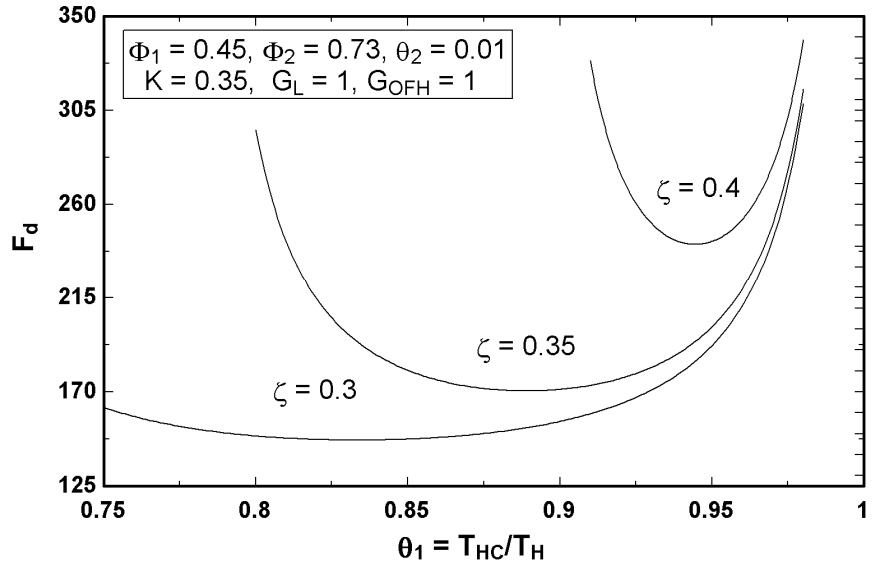

Figure 7.24(a). Dimensionless HEICE for constant heat transfer rate in the feedwater heater vs. θ_1: Effect of varying ξ

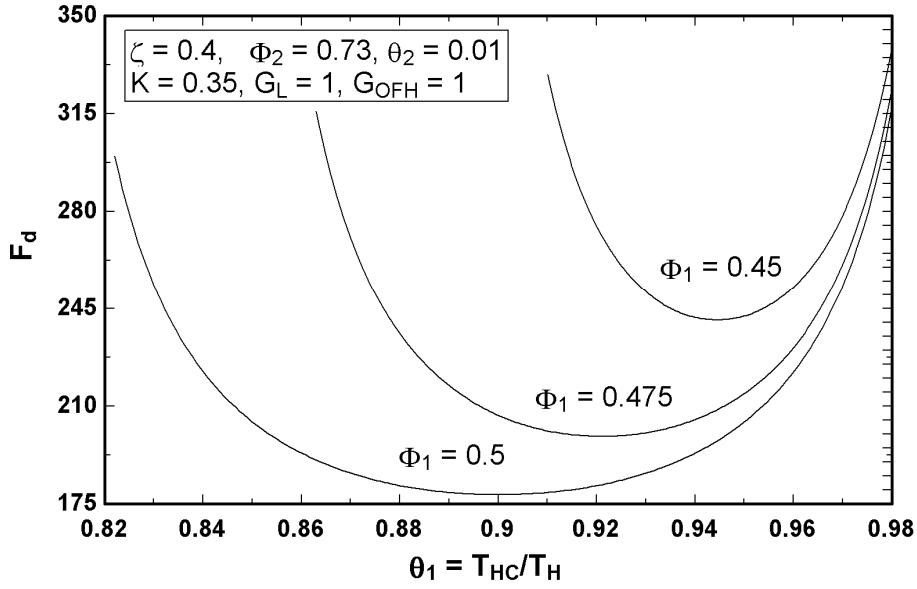

Figure 7.24(b). Dimensionless HEICE for constant heat transfer rate in the feedwater heater vs. θ_1: Effect of varying Φ_1

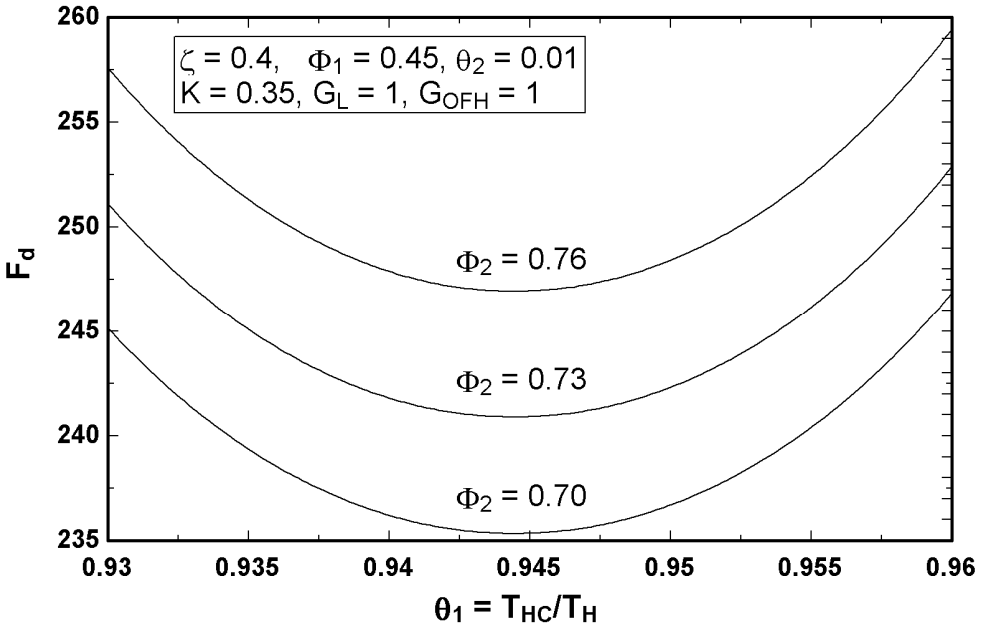

Figure 7.24(c). Dimensionless HEICE for constant heat transfer rate in the feedwater heater vs. θ_1: Effect of varying Φ_2

$$\frac{\gamma_H (UA)_H}{\Gamma} = \left[1 + G_L \frac{\Phi_1 (1-\theta_1)}{\Phi_1 \theta_1 - \xi} + G_{OFH} \frac{K\Phi_2 (1-\theta_1)}{\theta_2} \right]^{-1} \tag{7.82}$$

$$\frac{\gamma_L (UA)_L}{\Gamma} = \left[\frac{1}{G_L} \frac{\Phi_1 \theta_1 - \xi}{\Phi_1 (1-\theta_1)} + 1 + \frac{G_{OFH}}{G_L} \frac{K\Phi_2}{\theta_2} \frac{\Phi_1 \theta_1 - \xi}{\Phi_1} \right]^{-1} \tag{7.83}$$

$$\frac{\gamma_{OFH} (UA)_{OFH}}{\Gamma} = \left[\frac{1}{G_{OFH}} \frac{\theta_2}{K\Phi_2 (1-\theta_1)} + \frac{G_L}{G_{OFH}} \frac{\theta_2}{K\Phi_2} \frac{\Phi_1}{\Phi_1 \theta_1 - \xi} + 1 \right]^{-1} \tag{7.84}$$

A comparison of the above equations with the work of Antar and Zubair [29] clearly shows that, due to the presence of the feedwater heater unit conductance ratio (G_{OFH}) term, Eqs. (7.82) and (7.83) do not reduce to mere dependence on G_L. Now, we use the same values for T_H, γ_L, ξ and $\dot{W}$, as used by Antar and Zubair [29], for our example (See Figs. 7.25(a)-(c)). It should be noted that, in power systems, the unit cost of the boiler (γ_H) would be higher than the other heat exchangers. Therefore, it is appropriate to focus on values less than unity for G_{OFH} in our investigation. It is noted that, in Figs. 7.25(a)-(c), compared to Antar and Zubair [29], the total conductance curve is slightly asymmetric. This is due to the fact that the conductance of the feedwater heater is larger than the other heat exchangers and varies non-linearly with G_L. The difference at the ends is 1.32 kW/K when G_{OFH} is unity; though it increase to 4.25 kW/K at G_{OFH} = 0.1.

It is seen that when all unit cost ratios are unity, the minimum total conductance is also obtained at unity. The reason is that the unit cost of each heat exchanger becomes the same which results in all conductances influencing the total cost, Γ, by equal weightage.

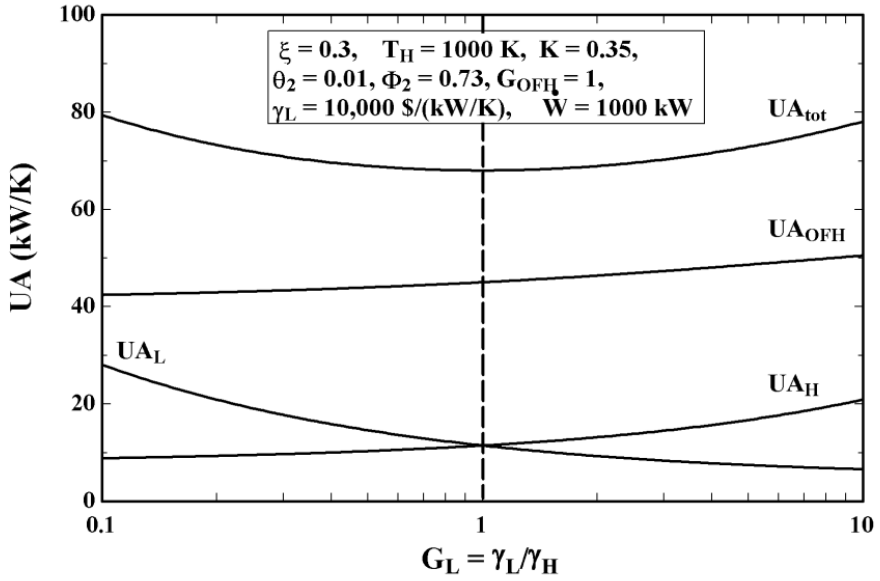

Figure 7.25(a). Example of all conductances versus unit cost ratio of cold to hot end at

$G_{OFH} = 1$

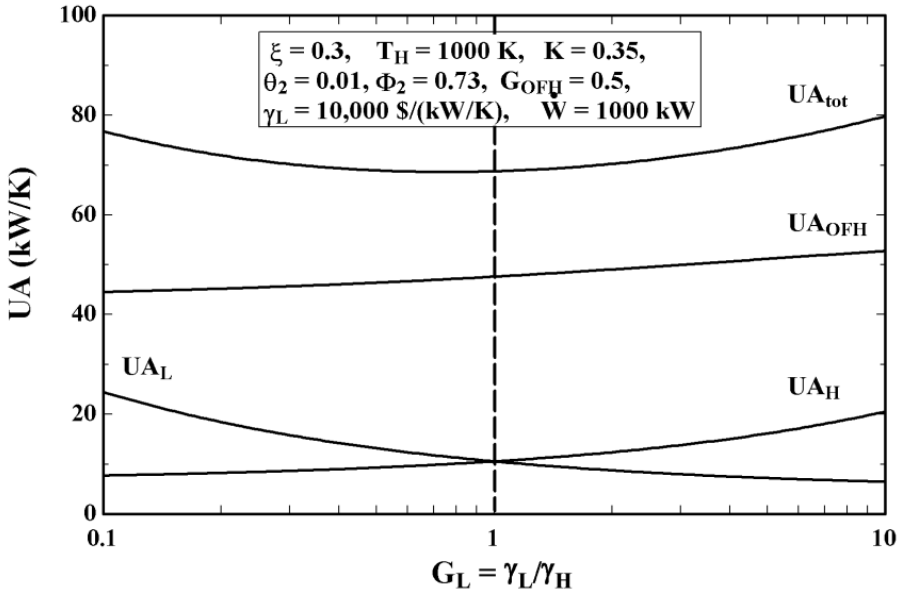

Figure 7.25(b). Example of all conductances versus unit cost ratio of cold to hot end at

$G_{OFH} = 0.5$

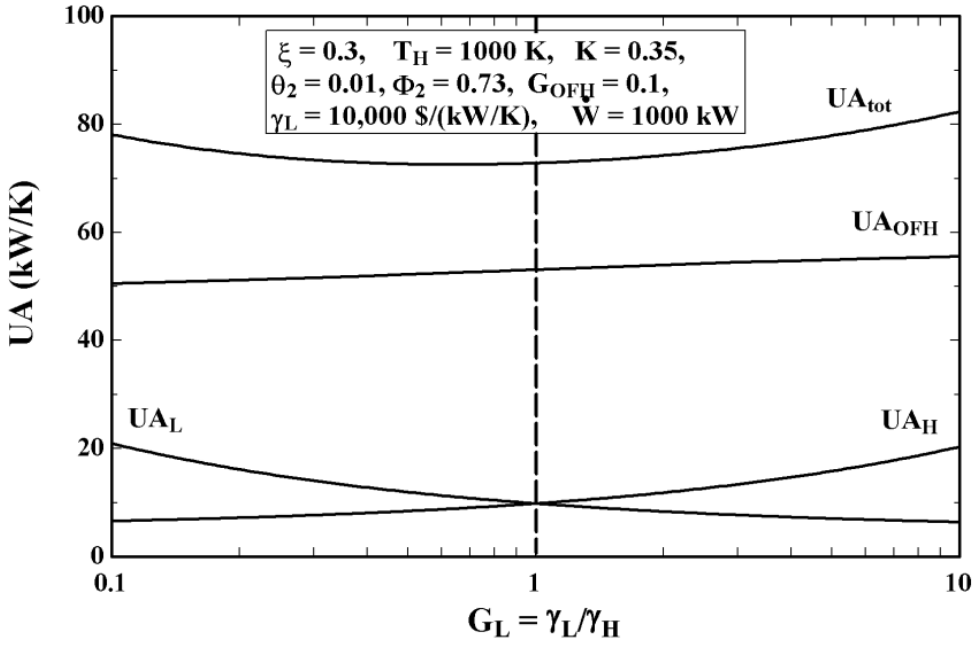

Figure 7.25(c). Example of all conductances versus unit cost ratio of cold to hot end at $G_{OFH} = 0.1$

Another observation is that, as G_{OFH} decreases, the minimum of the total conductance required increases and that it is obtained at lower values of G_L. These variations are found to be non-linear such that when G_{OFH} decreases from 1 to 0.5, there is only a 0.88% increase in the minimum total conductance while it increases by 5.7% when G_{OFH} decreases from 0.5 to 0.1.

7.5 Holistic View of Thermoeconomic Optimization in Power and Refrigeration Systems

If we compare the cost functions derived in Antar and Zubair [26], Morales [37] and those in section 7.2, a holistic picture begins to appear. It can be seen that just as the cost equations for the integrated subcooling cycle can be derived from the dedicated subcooling cycle, all the cost equations can be reduced to the reversed Carnot cost equations when all the irrelevant quantities are removed. This can be done by comparing Eqs. (7.1) with (7.29) and Eqs. (7.2) and (7.33). A similar situation is seen when comparing the cost equations derived by Antar and Zubair [29] with the corresponding ones in section 7.4 such as the cost function for constant power production given by Eq. (7.72). This also indicates that a generalized cost equation can be determined which can be used based upon the components in the system.

Cost optimization theory can be generalized in another way by comparing cost functions determined for the base cases of CA and reversed CA cycles by Antar and Zubair [26, 29]. It is found that if we take the cost functions of any one case, we can get

the cost functions for the other cycle by simply multiplying a minus sign on one side. This method can be generalized providing a shortcut to determining cost equations and this can be done if reversing the direction of one cycle results in the other. The discussion in this section can be represented by the diagram in Fig. 7.26.

For power cycles, considering the work of Antar and Zubair [29] and that done in section 7.4, the following general cost function can be presented:

$$F = \frac{1}{\mathbb{Z}_P}\left[\frac{1}{1-\theta_1} + G_L\,\frac{\Phi_1}{\Phi_1\theta_1 - \xi} + G_{OFH}\,\frac{K\Phi_2}{\theta_2}\right] \tag{7.85}$$

Eq. (7.85) can be used to generate any of the cost functions from these works. Furthermore, keeping Fig. 7.26 in mind, this can also be used to generate the cost functions for the endoreversible refrigeration cycle with the help of the minus sign as explained above. To achieve this, we need to keep the following rules in mind regarding how to determine $\mathbb{Z}_P$:

1. Numerators of all heat exchanger terms (inside the brackets) must be used except for those that represent internal heat exchange.
2. Each term in $\mathbb{Z}_P$ must be separated by a minus or plus sign. For power cycles, if the numerator term belongs to a heat exchanger that is taking in heat, then a plus sign should be used but if it is rejecting heat, then a minus sign should be used. On the other hand, the opposite is true for refrigeration cycles.

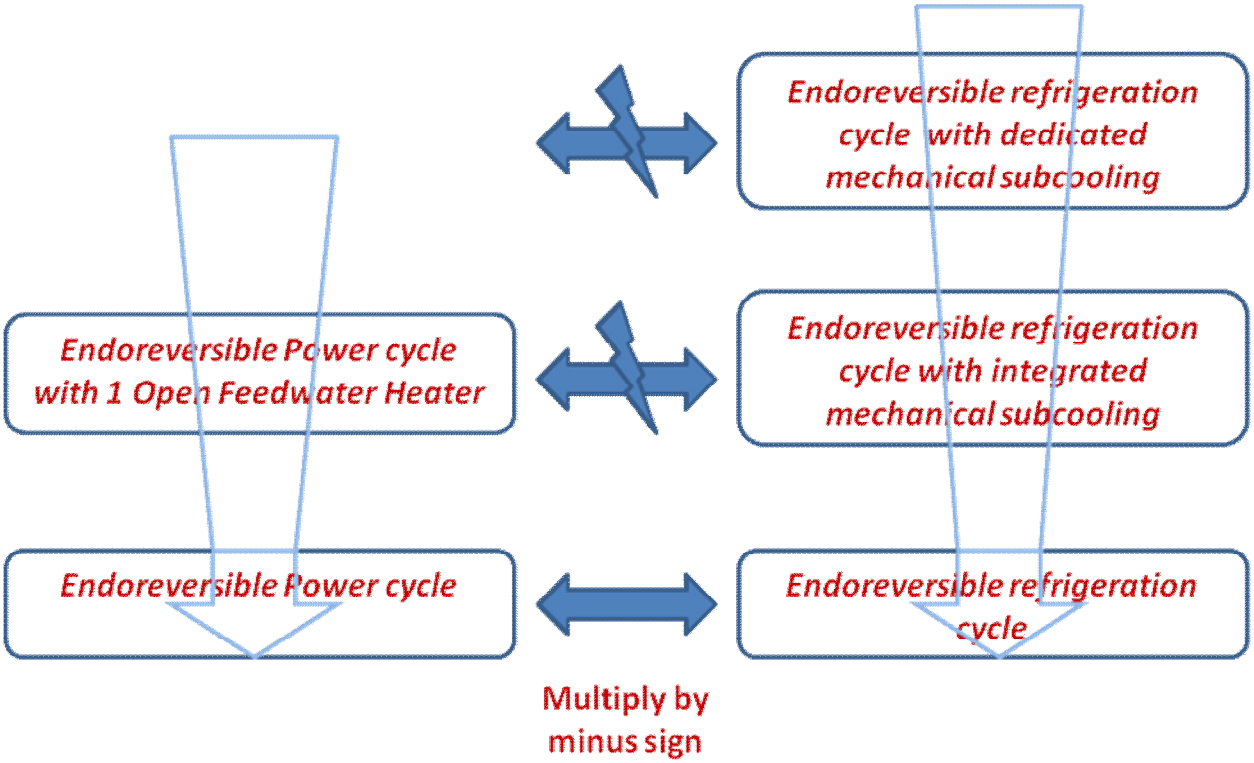

Figure 7.26. Holistic view of thermoeconomic optimization

To demonstrate this, let us take Eq. (7.85) and generate the cost function for constant power case for the endoreversible refrigeration cycle. The first thing to do is to remove the heat exchanger terms in the brackets that do not exist for the system under consideration. This means that the G_{OFH} term will vanish. Now, to determine what constitutes $\mathbb{Z}_P$, we apply the two rules above and we see that both the numerator terms i.e. 1 and Φ_1 are to be used since they both represent heat exchangers that exchange heat from outside the system. The '1' term will be positive since it is connected to the heat exchanger that is absorbing heat and the Φ_1 will be negative since it is connected to the condenser, which rejects heat. This results in the following equation:

$$F = \frac{1}{1-\Phi_1}\left[\frac{1}{1-\theta_1} + G_L \frac{\Phi_1}{\Phi_1\theta_1 - \xi}\right] \tag{7.86}$$

Now, since this is the cost equation for constant power case, the subscript 'a' may be written with the 'F' on the left hand side. Furthermore, as there is only one heat exchanger rejecting and absorbing heat in the system, the '1' subscript in Eq. (7.86) should be removed. Finally, keeping Fig. 7.26 in mind, we multiply a minus sign on right hand side only as we want to convert the power cycle cost equation into a refrigeration cycle one. Thus, we get

$$F_a = \frac{1}{1-\Phi}\left[\frac{1}{\theta - 1} + G_L \frac{\Phi}{\xi - \Phi\theta}\right] \tag{7.87}$$

This equation is essentially identical to that determined by Antar and Zubair [26] with the only difference being that the ‘G’ term is present in the first term in the brackets. This is simply due to the fact that the definition of ‘G’ used by Antar and Zubair [26] was the reciprocal of that used in this work. Making the definition same in both cases results in identical equations.

This shows that Eq. (7.85) can be used as a general cost equation as proposed. A similar cost equation was derived for the refrigeration cycles mentioned in Fig. 7.26 and is shown below.

$$F = \frac{1}{\mathbb{Z}_R}\left[\frac{1}{\theta_1 - 1} + G_d \frac{\left(\frac{\Theta}{K\Theta - \Phi_2}\right)\frac{\theta_2}{\theta_1}}{\theta_2 - 1} + G_L \frac{\left(\frac{K\Theta}{K\Theta - \Phi_2}\right)\Phi_1}{\xi - \Phi_1\theta_1} + G_{sc} \frac{\left(\frac{\Theta}{K\Theta - \Phi_2}\right)\Phi_2}{\Psi}\right] \quad (7.88)$$

CHAPTER 8

CONCLUSIONS AND RECOMMENDATIONS

There are two sub-sections in this chapter. The first sub-section deals with the conclusions of the thesis and the second sub-section is related to recommendations.

8.1 Conclusions

The following conclusions were made:

8.1.1 Experimental Work

The first work experimentally demonstrates the nature of the effect of fouling on performance parameters (such as compressor power consumption and coefficient of performance (COP)) as well as properties (such as condenser pressure and superheat temperature at the compressor exit) using a simple vapor compression cycle in order to augment theoretical studies found in the open literature. The results of the experiments indicate that the above-mentioned quantities demonstrate a logarithmic behavioral change when the ambient (i.e. environmental) and room temperatures are kept constant. It is

understood that this is inherently due to the governing equation for the phase change occurring in the condenser.

The other work demonstrates an experimental comparison between a simple vapor compression system and the improvement experienced by using a dedicated mechanical subcooling cycle in order to augment theoretical studies done in the past. The outcomes of the experiments indicate that the amount of subcooling is consistently larger in value when the outside ambient temperature is lower. Subcooling was found to approximately range between 5 to 8 °C, which helps to improve the cooling capacity of the evaporator during the day time.

The power consumption of the compressor is consistently greater in value whenever the subcooler cycle is used. The increase in the cooling capacity results in an increase in the COP of the system proven through the use of the second-law efficiency. The percentage increase in this efficiency increases as the ambient temperature decreases. This shows that dedicated subcooling can be used in daylight hours when ambient temperature is high, which is the time when it is most needed. Experiments on larger systems need to be performed to demonstrate the percentage increase in COP (or second-law efficiency) to be higher compared to small size systems.

8.1.2 Predicting the effect of fouling

It has been established through the use of the Curzon-Ahlborn and reversed Curzon-Ahlborn cycles that the effect of fouling on thermodynamic properties and

performance parameters of these systems can be predicted but that this is possible through combining data under specific conditions. The fact that real power and refrigeration cycles are based upon these cycles points to the conclusion that this can be used on actual industrial and residential systems. This has been demonstrated through application upon simulated models of a simple vapor compression cycle and a Rankine power cycle. The advantage provided by the fouling prediction model is the saving of time and money as it will reduce the amount of simulations and/or experimental work needed. Checking the results using a different refrigerant indicated that the nature of the equations did not change but only the values of the constants.

8.1.3 Thermoeconomic optimization

The cost function values, since they are based on endorevesible refrigeration cycles, make a prediction of what the minimum initial cost of the heat exchangers would be at the given temperatures and heat transfer parameter values. The optimization problem explored for dedicated and integrated mechanical subcooling cycles has three possible parameters with minima of significance: θ_1, Φ_1 and Φ_2. The following conclusions were made:

- $\theta_{1,min}$ for all functions exists and behavior is the same even though more than one expression was found. The minimum value of θ_1 shifts to a higher value as Φ_1 decreases.

- When the work rate is constant, Φ_1 and Φ_2, only provide a theoretical minimum since that minimum only occurs for negative values of the function F_a, which is impractical.
- For a constant $\dot{Q}_{H,m}$, no minimum exists with respect to Φ_1 and Φ_2.
- For a constant $\dot{Q}_L$, at a particular value of θ_1, the cost functions seem to be insensitive to Φ_1 and Φ_2 in the region of the minimum point.
- For a constant $\dot{Q}_{sc}$, for all values of θ_1, the minimum value of Φ_2 stays approximately the same. It is also noted that this minimum occurs at a value greater than Φ_1.
- For the mechanical subcooling systems investigated, none of the cost functions displayed a minimum with respect to θ_3.
- The derivatives for the integrated subcooling cycle can be generated from the derivatives of the dedicated subcooling cycle.
- For the mechanical subcooling systems investigated, the cost functions of one system qualitatively display the same behavior as the other.

The cost optimization problem explored for an endoreversible power cycle with an open feedwater heater resulted in the following important conclusions:

- For the system investigated, none of the cost functions displayed a minimum with respect to ξ, θ_2 and Φ_2.

- $\theta_{1,min}$ for all functions exists and is the same for all cases. It is found that the behavior for all cost functions is qualitatively the same with respect to θ_1.

Other conclusions include:

- The cost functions for simpler cycles can be derived from those of its respective higher systems.
- If the only difference between a power and refrigeration cycle is that the cycle is running in the opposite direction, then multiplying a minus sign on one side of the resulting cost equations of one system would provide the cost equations for the other system.
- Eqs. (7.4) and (7.50) constitute a step forward in thermoeconomic optimization theory development of an important aspect that establishes the connection between Carnot-based and thermodynamic cycles.
- Eqs. (7.82) and (7.85) constitute a step forward in thermoeconomic optimization theory as they provide generalized equations to determine all cost functions.

8.2 Recommendations and Future Work

The following recommendations are made:

8.2.1 Predicting the effect of fouling

The prediction of fouling model may be improved by performing the following:

- Effect of $T_{H,in}$ and $T_{L,in}$ should be checked to ascertain its effect on the prediction of the fouling constants.
- Effect of internal irreversibilities, such as the isentropic efficiency of the compressor and choice of refrigerant, should be ascertained.
- The complete investigation may be repeated for higher systems such as those with dedicated mechanical subcooling to ascertain how more than two heat exchangers may be incorporated into the fouling prediction model.

8.2.2 Cost optimization

The following line of research may be pursued to improve the current work:

- Following the same methodology as used in section 7.2 and 7.4, perform thermoeconomic analysis on more complex power and refrigeration systems. This will help to move towards a general equation from which cost equations for any system can be extracted and, thus, improve upon Eqs. (7.82) and (7.85).
- The work of Morales [37] can be added to Eq. (7.85) once a common basis for all definitions is established.
- Solution/modeling for Eqs. (7.5) and (7.51) should be completed based on a sensitivity analysis.
- Existence of a similar solution to $\theta_{1,min,act}$ should be checked for power systems as well.

NOMENCLATURE

A	area (m^2)
$\dot{C}$	thermal capacitance rate (kW K^{-1})
COP	coefficient of performance (-)
COP_N	normalized coefficient of performance (-)
ER	endoreversible (-)
F	non-dimensional cost ratio (-)
FPI	fins per inch (-)
G	unit cost conductance ratio (-)
h	specific enthalpy (kJ kg^{-1})
HEICE	Heat Exchanger Inventory Cost Equation
HX	heat exchanger
K	non-dimensional quantity defined by Eq. 7.22(g) or 7.66(f) (-)
K_2	non-dimensional quantity defined by Eq. 7.46(a) (-)
K_3	non-dimensional quantity defined by Eq. 7.46(b) (-)
k_1	ratio of evaporator/feedwater heater to subcooler/condenser entropy change (-)
k_2	ratio of main condenser plus subcooler to subcooler entropy change (-)
k_3	ratio of main condenser to subcooler entropy change (-)
$\dot{m}$	refrigerant mass flow rate (kg s^{-1})
P	pressure (Pa or kPa)

P_N	normalized pressure (-)
$\dot{Q}$	rate of heat transfer (kW)
R	ratio of the clearance volume to the displacement volume (-)
RPC	Rankine power cycle
s	specific entropy (kJ kg^{-1} K^{-1})
SVCC	simple vapor compression cycle
t	time (min)
T	temperature (K)
T_N	normalized superheat temperature at compressor exit (-)
TC	thermocouple
U	overall heat transfer coefficient (W m^2 K^{-1})
UA	overall conductance (kW K^{-1})
v	specific volume (m^3 kg^{-1})
VCC-DMS	vapor compression cycle using dedicated mechanical subcooling
VCC-IMS	vapor compression cycle using integrated mechanical subcooling
$\dot{V}$	volumetric flow rate (m^3 s^{-1})
W	work done (kJ kg^{-1})
$\dot{W}$	power requirement (W or kW)
W_N	normalized compressor power consumption (-)
$\dot{W}'$	normalized pumping power (-)

Greek symbols

ε	heat exchanger effectiveness
η	efficiency
η_{II}	second-law efficiency
Γ	total cost ($)
γ	unit conductance cost ($ W^{-1} K)
Φ_1	non-dimensional quantity defined in Eq. (7.22d) or (7.66c)
Φ_2	non-dimensional quantity defined in Eq. (7.22e) or (7.66d)
Ω	non-dimensional quantity defined in Eq. (7.24a)
Ψ	non-dimensional quantity defined in Eq. (7.24b)
Θ	non-dimensional quantity defined in Eq. (7.24c)
θ_1	non-dimensional quantity defined in Eq. (7.22a) or (7.66a)
θ_2	non-dimensional quantity defined in Eq. (7.22b) or (7.66b)
θ_3	non-dimensional quantity defined in Eq. (7.22c)
ξ	absolute temperature ratio ($=T_L/T_H$)

Subscripts

01	at low-temperature evaporator/condenser
02	at high-temperature evaporator/condenser
amb	ambient
avg	average
bl	boiler
C	reversible compartment

cd	condenser
cl	clean condition
cp	compressor
d	dedicated cycle
dl	discharge line
ev	evaporator
h	high-side
H	hot end
i	integrated cycle
in	entering
is	isentropic
l	low-side
L	cold end
m	main cycle
max	maximum
min	minimum
net	net
p	percentage change
pp	pump
rev	for reversible cycle
room	room
sc	sub-cooler or sub-cooler cycle

sl	suction line
sup	superheat
t	turbine
tot	total
v	volumetric
w	working fluid
wsc	with sub-cooler cycle
wosc	without sub-cooler cycle

APPENDIX A: Calibration of Thermocouples

Sixteen thermocouples were calibrated by comparing with a calibrated thermocouple. The calibration of the sixteen thermocouples was done using a heating bath to raise the temperature while a separate ice-water mixture was used for measurement at 0 °C. The temperature readings were recorded using the data logger of data acquisition software. Fig. A.1 shows the calibration curve of the used thermocouples.

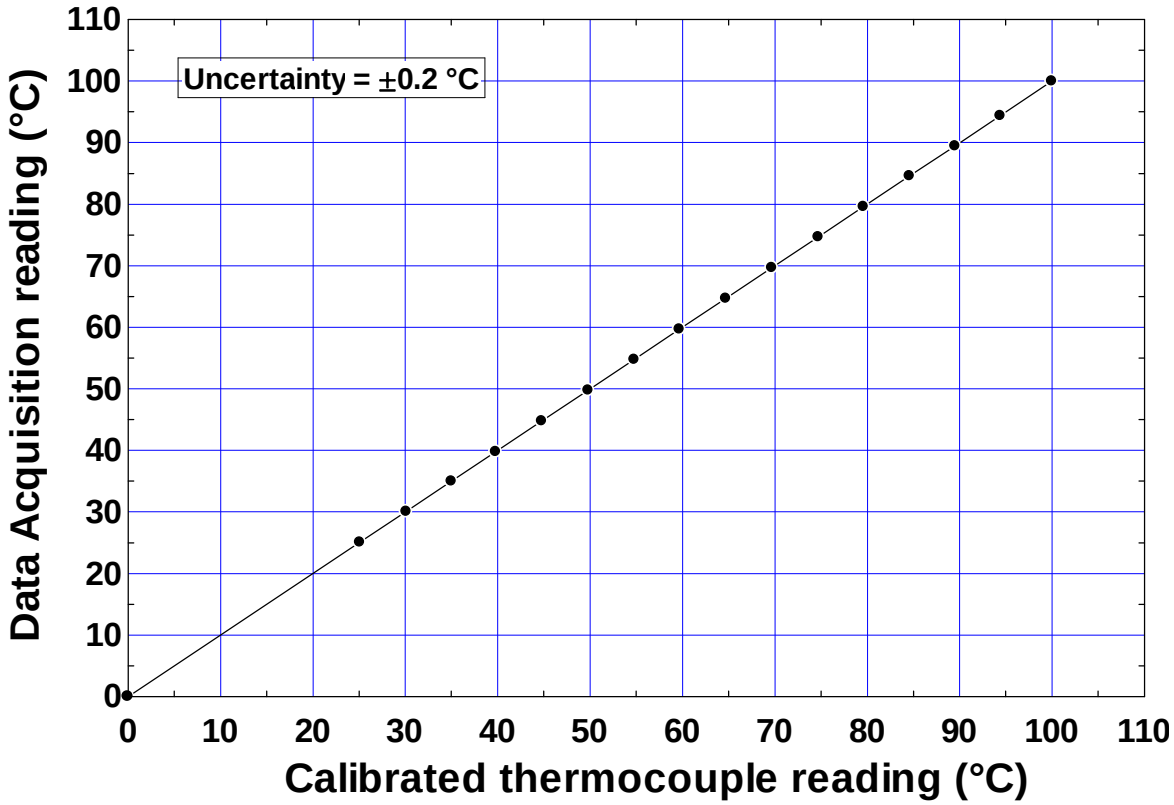

Figure A.1. Calibration curve of thermocouples

APPENDIX B: Calibration of Pressure Transducers

Four pressure transducers were calibrated by comparing with calibrated Bourdon tube gauges. This was done by installing the transducers and gauges on the experimental setup and operating it under typical conditions in the day time. The pressure transducer readings were recorded using the data acquisition (DAQ) software while the Bourdon tube gauge readings were recorded manually every 30 minutes. Figs. (B.1) through (B.4) show the calibration curves of the used pressure transducers. In Fig. (B.1), the difference between the Bourdon tube and pressure transducer readings was less than 1 psig while it was less than 2 psig in Figs. (B.2) through (B.4).

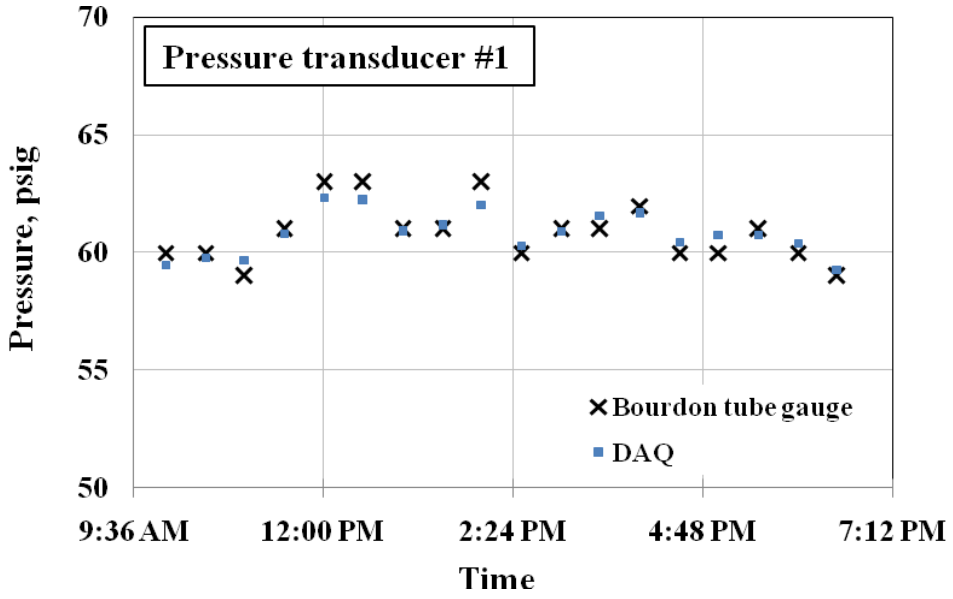

Figure B.1. Calibration curve of pressure transducer #1

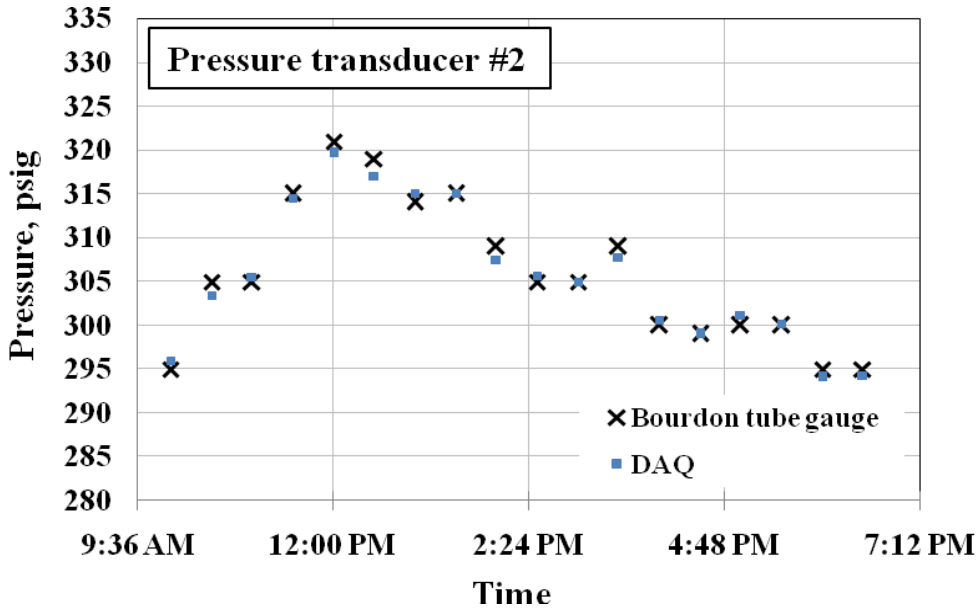

Figure B.2. Calibration curve of pressure transducer #2

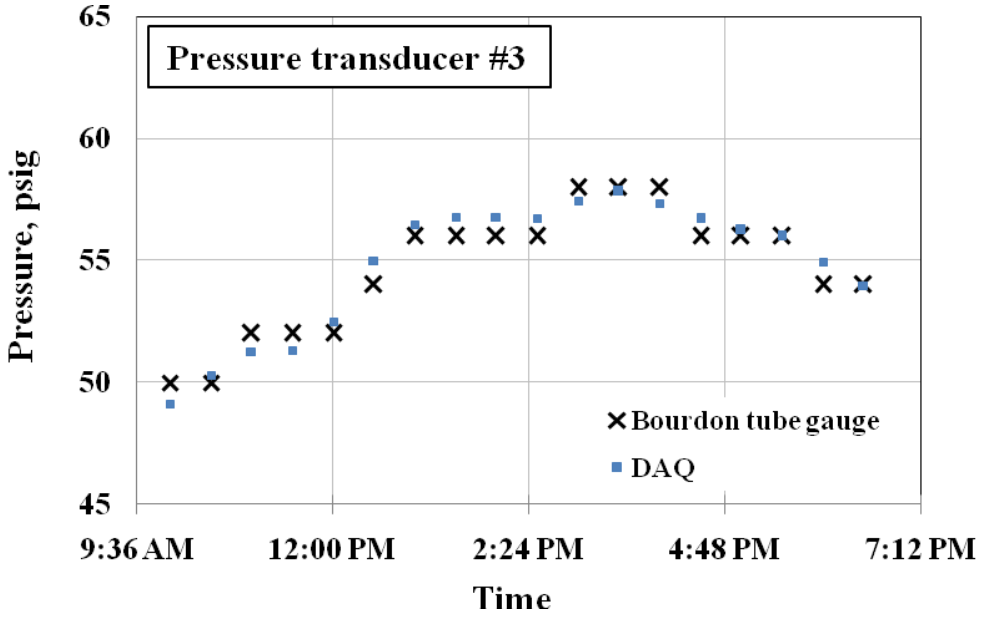

Figure B.3. Calibration curve of pressure transducer #3

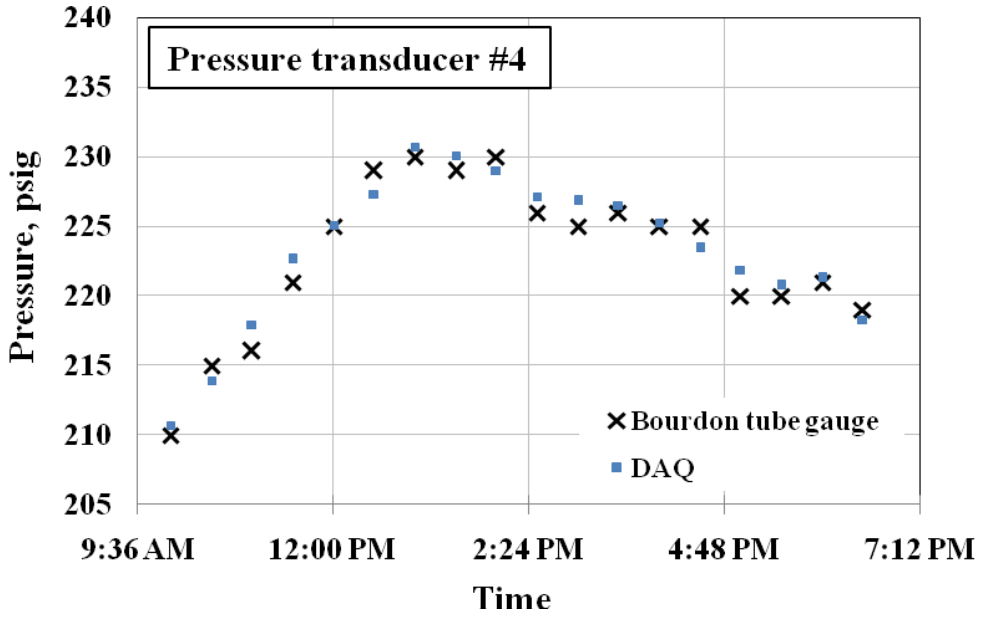

Figure B.4. Calibration curve of pressure transducer #4

APPENDIX C: Experimental Data for SVCC

At clean condition:

Time (min)	T_{sup} (°C)	T_{amb} (°C)	T_{room} (°C)	P_{cd} (kPa)	$\dot{W}$ (W)
45.0	75.1	32.4	21.2	2001.7	2106.4
45.5	75.1	31.4	21.3	2002.4	2123.5
46.0	75.0	31.7	21.0	1989.6	2097.8
46.5	75.1	31.6	21.3	2003.2	2107.0
47.0	74.9	30.7	21.3	1986.9	2115.7
47.5	75.0	31.7	21.0	1993.3	2114.9
48.0	74.9	31.6	21.5	1976.0	2117.7
48.5	74.9	31.8	21.1	2008.6	2115.0
49.0	74.9	31.8	21.0	1990.6	2115.6
49.5	74.9	31.4	21.1	1991.6	2112.2
50.0	74.9	32.1	21.2	2003.0	2108.8
50.5	74.8	31.6	21.2	1993.5	2093.6
51.0	74.7	31.3	21.1	1994.4	2085.2
51.5	74.8	31.7	21.1	1976.7	2099.5
52.0	74.7	31.5	21.2	1971.9	2100.6
52.5	74.8	31.4	21.1	1999.7	2117.9
53.0	74.8	31.7	21.3	1980.6	2099.3
53.5	74.8	31.9	21.0	1997.6	2108.8
54.0	74.9	32.0	20.9	1978.1	2114.2
54.5	74.9	32.4	21.2	1985.2	2116.2
55.0	74.8	32.2	20.7	1987.4	2116.7
55.5	74.8	31.1	20.9	1961.3	2101.7
56.0	74.7	31.4	21.1	1990.2	2109.8
56.5	74.7	31.2	21.2	1976.8	2094.8
57.0	74.6	31.1	21.0	1998.5	2111.2
57.5	74.7	31.4	20.9	1987.2	2089.6
58.0	74.8	31.8	20.8	1985.2	2112.2
58.5	74.7	31.6	20.9	1963.7	2060.1
59.0	74.7	31.4	21.0	1988.6	2091.3
59.5	74.6	31.7	20.9	1971.7	2109.8
60.0	74.6	31.9	21.1	1995.9	2091.1
60.5	74.7	31.4	21.0	1975.0	2097.6
61.0	74.6	31.6	21.0	1966.1	2099.3
61.5	74.6	32.3	21.1	1990.7	2091.3
62.0	74.6	31.7	21.0	1984.5	2102.5

62.5	74.5	31.7	21.0	1976.7	2103.9
63.0	74.6	32.4	20.9	1998.3	2087.4
63.5	74.5	31.9	21.1	1969.2	2099.2
64.0	74.6	30.9	21.1	1982.4	2103.0
64.5	74.6	31.9	21.0	1975.3	2098.0
65.0	74.7	31.9	21.1	1977.9	2100.4
65.5	74.7	31.6	20.9	1982.4	2107.6
66.0	74.6	31.6	21.0	1978.9	2101.9
66.5	74.6	31.9	21.0	1985.7	2095.4
67.0	74.7	32.2	20.8	2012.1	2095.2
67.5	74.6	31.8	20.9	1997.6	2109.8
68.0	74.6	32.1	20.9	1987.5	2088.6
68.5	74.5	31.8	21.0	1966.3	2088.5
69.0	74.5	31.6	20.9	1959.2	2086.3
69.5	74.7	31.9	20.8	2011.0	2112.8
70.0	74.6	31.5	21.1	1967.8	2092.6
70.5	74.6	31.8	20.9	1961.1	2093.5
71.0	74.7	31.8	20.8	1979.6	2106.1
71.5	74.6	31.7	20.9	1983.4	2091.0
72.0	74.5	31.5	20.9	1967.7	2108.2
72.5	74.6	31.5	20.9	1978.8	2085.7
73.0	74.5	31.5	21.0	1988.6	2092.5
73.5	74.6	32.3	20.9	1986.6	2113.5
74.0	74.7	32.0	20.8	1992.0	2086.9
74.5	74.7	31.7	20.8	1995.2	2090.7
75.0	74.6	31.5	21.1	1967.5	2109.9
75.5	74.5	31.7	20.9	1967.4	2093.7
76.0	74.6	31.6	20.9	1982.6	2101.9
76.5	74.6	31.0	20.9	1979.6	2099.1
77.0	74.6	31.4	21.0	1966.4	2103.2
77.5	74.7	31.8	21.0	1988.3	2112.1
78.0	74.7	32.5	21.0	1983.3	2089.7
78.5	74.7	32.1	20.8	1993.1	2114.2
79.0	74.6	31.6	21.0	1989.5	2107.9
79.5	74.6	31.5	20.8	1982.0	2095.3
80.0	74.6	32.1	21.0	1981.6	2094.8
80.5	74.6	31.5	20.8	1987.4	2110.6
81.0	74.5	31.1	20.9	1968.9	2095.5
81.5	74.6	31.3	20.7	1995.2	2101.5
82.0	74.6	31.4	20.8	1960.8	2105.8
82.5	74.5	31.3	20.8	1984.7	2102.2

83.0	74.6	31.7	20.9	1966.1	2093.5
83.5	74.6	31.8	20.7	1992.4	2084.9
84.0	74.5	31.3	20.7	1961.1	2103.6
84.5	74.5	32.2	20.6	1983.0	2098.5

At 10% fouling condition:

Time (min)	T_{sup} (°C)	T_{amb} (°C)	T_{room} (°C)	P_{cd} (kPa)	$\dot{W}$ (W)
97	75.7	31.2	20.9	2028.0	2140.2
97.5	75.9	31.7	21.2	2019.0	2093.6
98	75.7	31.7	21.0	2010.4	2113.7
98.5	75.7	31.4	20.7	2023.2	2107.9
99	75.7	31.2	20.8	2003.0	2109.0
99.5	75.8	31.7	21.0	2039.4	2135.0
100	75.7	31.7	20.7	1992.8	2122.2
100.5	75.7	31.5	20.7	1996.3	2118.1
101	75.7	32.5	21.0	2019.1	2129.1
101.5	75.8	32.6	21.0	2025.0	2131.3
102	75.7	32.5	21.1	2020.1	2127.3
102.5	75.7	31.8	21.0	2015.5	2118.4
103	75.6	31.7	21.0	2021.8	2118.9
103.5	75.5	31.9	21.1	2028.8	2093.0
104	75.7	29.9	20.8	2005.5	2132.4
104.5	75.7	31.4	20.9	2044.7	2141.2
105	75.7	30.8	21.0	2008.7	2121.1
105.5	75.7	32.0	21.0	2009.3	2093.9
106	75.6	31.8	21.0	2016.3	2113.5
106.5	75.5	31.0	20.9	2000.7	2117.0
107	75.4	31.8	20.7	1990.7	2111.4
107.5	75.4	31.4	20.8	2012.5	2111.4
108	75.5	32.0	20.8	2002.5	2112.9
108.5	75.5	31.8	20.8	2032.6	2123.5
109	75.4	31.5	21.0	2013.2	2114.2
109.5	75.2	31.7	20.9	1990.2	2100.9
110	75.4	31.8	20.7	1999.3	2119.6
110.5	75.3	31.9	20.8	2001.3	2111.6
111	75.3	30.3	21.1	2001.5	2065.2
111.5	75.2	31.5	20.9	1993.1	2104.9
112	75.2	30.7	20.8	1998.0	2112.1
112.5	75.2	31.8	20.6	1995.9	2115.7
113	75.1	29.1	20.8	1981.9	2099.2

113.5	75.1	31.7	20.8	1994.4	2100.3
114	75.1	31.7	20.7	1996.6	2104.2
114.5	75.0	31.8	20.6	1992.0	2111.4
115	74.9	31.7	20.7	2003.9	2122.7
115.5	75.0	30.0	20.8	2000.4	2121.3
116	75.0	31.1	20.6	1986.2	2106.7
116.5	75.2	31.8	20.9	2015.5	2109.0
117	75.2	28.1	21.0	1989.5	2104.7
117.5	75.0	32.0	20.7	1996.5	2112.1
118	75.1	31.0	20.9	2011.1	2127.8
118.5	75.1	31.3	20.7	2009.0	2115.6
119	75.1	30.5	20.9	1976.0	2115.0
119.5	75.0	31.2	21.0	1999.7	2108.8
120	75.1	32.0	21.0	2007.3	2118.3
120.5	75.2	31.9	20.9	1994.2	2107.6
121	75.1	30.8	21.1	2002.1	2117.4
121.5	75.1	31.9	20.7	2010.8	2127.9
122	75.1	31.8	20.7	2010.0	2123.7
122.5	75.1	31.7	20.9	1988.9	2116.0
123	75.1	30.9	20.8	2001.1	2093.8
123.5	75.1	31.6	20.7	1993.3	2128.2
124	75.2	31.3	20.6	2017.2	2130.7
124.5	75.2	31.2	20.8	1998.2	2124.6
125	75.2	32.5	20.7	2008.3	2107.0
125.5	75.1	31.8	20.6	2007.5	2099.5
126	75.0	30.8	20.6	1987.5	2116.7
126.5	75.1	30.6	20.7	2020.0	2105.3
127	75.1	31.6	20.6	1994.9	2110.3
127.5	75.1	30.7	20.7	1990.2	2122.7
128	75.0	31.4	20.8	1985.7	2102.1
128.5	75.0	31.2	20.9	2006.6	2100.4
129	75.0	31.0	20.8	1998.0	2065.0
129.5	75.0	30.3	20.8	1998.2	2120.0
130	75.0	31.2	20.8	1994.9	2123.3
130.5	74.8	30.5	20.8	1983.8	2117.7
131	75.0	32.2	20.6	1993.7	2115.5
131.5	75.0	31.8	20.8	1993.0	2110.6
132	75.0	30.0	20.8	2009.4	2103.9
132.5	75.1	30.2	20.8	1998.2	2120.9
133	75.1	32.2	20.8	1999.2	2109.0
133.5	75.1	32.0	20.7	2007.9	2119.5

134	74.9	31.2	20.6	1992.8	2122.1
134.5	74.9	30.3	20.8	1983.7	2100.4
135	75.0	31.0	20.9	1993.7	2114.8
135.5	75.0	31.7	20.8	2008.7	2117.2
136	75.0	30.0	20.4	1984.4	2107.5
136.5	74.8	31.8	20.9	1982.3	2101.0

At 20% fouling condition:

Time (min)	T_{sup} (°C)	T_{amb} (°C)	T_{room} (°C)	P_{cd} (kPa)	$\dot{W}$ (W)
44.0	76.5	31.3	20.8	2059.7	2141.1
44.5	76.5	31.5	20.9	2062.3	2114.4
45.0	76.6	31.5	21.0	2030.6	2130.3
45.5	76.5	31.0	21.1	2045.7	2131.2
46.0	76.5	30.9	21.0	2034.6	2136.4
46.5	76.4	31.1	20.8	2059.7	2131.4
47.0	76.3	31.3	20.8	2024.7	2133.5
47.5	76.4	31.3	20.8	2038.9	2120.9
48.0	76.4	31.5	20.9	2037.0	2136.8
48.5	76.3	31.2	20.7	2034.7	2130.2
49.0	76.3	32.0	20.9	2039.6	2126.8
49.5	76.3	31.4	20.7	2028.4	2129.7
50.0	76.3	31.6	20.9	2027.6	2137.8
50.5	76.4	31.8	20.8	2040.6	2137.3
51.0	76.4	31.9	20.7	2068.6	2127.7
51.5	76.3	31.6	20.8	2057.4	2122.7
52.0	76.4	31.7	20.7	2051.3	2113.8
52.5	76.3	31.1	20.8	2034.7	2142.3
53.0	76.4	31.8	20.6	2039.5	2129.1
53.5	76.4	32.5	20.8	2043.3	2140.0
54.0	76.4	31.8	20.8	2046.7	2148.4
54.5	76.5	31.9	20.8	2062.3	2134.1
55.0	76.5	31.6	20.9	2044.1	2101.4
55.5	76.5	31.9	21.0	2048.8	2133.1
56.0	76.6	32.0	20.7	2067.5	2153.1
56.5	76.7	32.0	21.4	2066.2	2130.7
57.0	76.7	31.5	20.8	2038.9	2131.2

57.5	76.7	32.1	20.8	2073.4	2123.3
58.0	76.7	31.4	21.1	2036.8	2133.8
58.5	76.6	31.7	20.6	2054.4	2140.0
59.0	76.7	31.2	20.8	2066.6	2138.4
59.5	76.5	31.5	21.0	2062.4	2128.5
60.0	76.7	31.4	20.8	2070.0	2153.8
60.5	76.8	32.1	21.2	2065.8	2146.2
61.0	76.8	32.4	20.8	2061.4	2131.1
61.5	76.6	31.8	21.0	2055.4	2152.9
62.0	76.8	32.4	21.1	2057.1	2134.6
62.5	76.7	31.8	20.8	2066.9	2146.3
63.0	76.8	32.6	20.8	2070.0	2148.6
63.5	76.8	31.4	20.6	2068.5	2143.7
64.0	76.8	31.4	20.7	2043.0	2144.0
64.5	76.9	32.5	21.0	2083.9	2131.2
65.0	76.8	31.8	20.8	2048.6	2146.7
65.5	76.8	32.0	20.9	2061.7	2127.7
66.0	76.8	31.8	20.8	2067.2	2142.2
66.5	76.7	31.3	20.6	2032.6	2138.0
67.0	76.8	31.6	20.6	2047.2	2139.8
67.5	76.7	31.2	20.8	2063.0	2089.9
68.0	76.8	31.7	20.8	2039.8	2132.3
68.5	76.8	31.9	20.8	2063.3	2137.0
69.0	76.7	31.7	20.9	2048.1	2123.2
69.5	76.7	31.5	20.6	2054.8	2138.3
70.0	76.9	31.3	21.0	2051.6	2135.0
70.5	76.8	32.4	20.7	2051.5	2146.7
71.0	76.6	31.9	20.7	2047.5	2142.0
71.5	76.7	32.1	20.8	2061.9	2145.8
72.0	76.6	32.1	20.8	2054.5	2146.2
72.5	76.7	31.7	20.7	2055.0	2148.5
73.0	76.8	32.3	20.7	2059.7	2134.5
73.5	76.6	31.4	20.7	2035.8	2126.2
74.0	76.7	31.8	20.9	2053.7	2130.6
74.5	76.7	31.3	20.8	2051.7	2130.6
75.0	76.6	31.6	20.9	2035.6	2131.4
75.5	76.6	31.4	20.7	2032.6	2140.9
76.0	76.7	31.6	20.6	2055.0	2141.2
76.5	76.7	31.8	20.8	2054.0	2144.7
77.0	76.6	31.2	20.7	2047.7	2146.4
77.5	76.6	31.8	20.7	2052.7	2138.4

78.0	76.7	32.2	20.4	2055.0	2130.0
78.5	76.7	31.7	20.6	2043.4	2129.4
79.0	76.6	31.3	20.9	2045.5	2104.7
79.5	76.7	32.5	20.7	2066.5	2143.1
80.0	76.6	32.2	20.7	2045.0	2151.9
80.5	76.7	32.2	20.6	2069.2	2141.1
81.0	76.7	31.6	20.5	2055.0	2133.0
81.5	76.8	32.1	20.8	2070.9	2157.0
82.0	76.8	32.3	20.7	2063.7	2101.5
82.5	76.8	31.5	20.5	2064.0	2147.0
83.0	76.8	31.6	20.7	2051.0	2147.0
83.5	76.8	31.5	20.6	2054.1	2124.4

At 30% fouling condition:

Time (min)	T_{sup} (°C)	T_{amb} (°C)	T_{room} (°C)	P_{cd} (kPa)	$\dot{W}$ (W)
112.0	79.0	32.2	20.7	2133.8	2164.7
112.5	79.0	32.0	20.9	2122.0	2168.8
113.0	79.0	32.2	20.8	2150.9	2165.9
113.5	79.1	32.4	21.0	2142.7	2169.1
114.0	78.9	32.4	20.9	2126.1	2158.3
114.5	78.9	32.0	21.0	2103.6	2157.7
115.0	78.9	32.0	20.9	2128.6	2153.4
115.5	79.0	32.1	20.8	2136.8	2155.9
116.0	78.9	32.1	20.9	2117.4	2157.9
116.5	78.9	32.6	20.8	2109.5	2153.1
117.0	78.8	32.5	20.8	2099.8	2148.4
117.5	78.8	32.4	20.9	2124.3	2155.6
118.0	78.9	31.1	20.9	2115.1	2154.2
118.5	78.8	32.1	20.9	2119.2	2159.6
119.0	78.7	32.1	20.9	2105.4	2158.3
119.5	78.8	32.2	21.0	2109.5	2157.8
120.0	78.9	32.1	20.8	2121.5	2162.2
120.5	78.9	32.0	20.7	2105.6	2168.9
121.0	78.8	31.1	21.1	2120.6	2161.3
121.5	78.7	32.0	20.9	2129.5	2149.3
122.0	78.6	32.2	21.0	2125.4	2156.4

122.5	78.7	32.0	20.9	2103.2	2168.4
123.0	78.7	32.3	20.9	2131.3	2155.0
123.5	78.7	32.2	20.6	2101.2	2157.8
124.0	78.7	32.0	20.8	2107.3	2155.5
124.5	78.6	31.1	20.8	2097.8	2152.2
125.0	78.5	31.2	20.9	2101.9	2149.7
125.5	78.7	32.3	20.9	2112.3	2149.4
126.0	78.7	31.4	20.7	2116.5	2155.7
126.5	78.7	31.3	20.9	2103.7	2154.0
127.0	78.6	32.1	20.9	2099.1	2157.9
127.5	78.6	31.0	20.9	2125.4	2158.5
128.0	78.6	32.4	20.4	2116.8	2148.3
128.5	78.5	32.0	20.7	2101.4	2157.7
129.0	78.7	32.1	20.6	2132.4	2159.7
129.5	78.7	31.1	20.6	2118.7	2152.2
130.0	78.6	31.1	20.8	2114.7	2151.8
130.5	78.5	31.0	20.7	2122.0	2159.8
131.0	78.6	31.4	20.9	2120.1	2153.6
131.5	78.5	30.2	20.7	2095.2	2149.8
132.0	78.5	32.1	21.0	2120.1	2149.0
132.5	78.5	32.1	20.5	2105.6	2152.3
133.0	78.5	32.1	20.6	2097.8	2149.9
133.5	78.4	31.0	20.9	2105.7	2152.9
134.0	78.3	32.1	20.7	2082.4	2149.3
134.5	78.3	31.4	20.7	2093.9	2145.6
135.0	78.3	31.4	20.7	2102.2	2156.8
135.5	78.3	31.1	20.7	2117.4	2152.3
136.0	78.3	31.5	20.5	2119.4	2150.1
136.5	78.2	31.1	20.8	2112.2	2155.7
137.0	78.4	32.2	21.0	2113.5	2160.3
137.5	78.3	32.0	20.7	2111.2	2157.9
138.0	78.4	32.4	20.6	2115.0	2157.0
138.5	78.4	32.5	20.8	2115.8	2164.2
139.0	78.4	32.2	20.8	2108.8	2162.3
139.5	78.2	32.4	20.6	2110.1	2162.1
140.0	78.4	32.0	20.9	2102.2	2153.6
140.5	78.5	32.8	21.0	2115.7	2157.4
141.0	78.5	31.1	20.8	2126.4	2165.9
141.5	78.3	31.3	21.0	2112.5	2162.2
142.0	78.3	31.0	21.0	2108.2	2159.3
142.5	78.3	30.9	20.8	2089.7	2157.6

143.0	78.4	31.1	20.9	2124.6	2152.4
143.5	78.4	31.3	20.7	2098.8	2154.3
144.0	78.4	32.0	21.0	2099.5	2150.3
144.5	78.3	30.3	20.6	2080.6	2159.2
145.0	78.3	32.1	20.8	2115.7	2162.2
145.5	78.3	31.8	20.9	2096.0	2152.3
146.0	78.2	31.9	21.2	2104.9	2151.9
146.5	78.2	32.0	21.1	2075.5	2155.8
147.0	78.2	30.5	21.0	2104.0	2150.7
147.5	78.3	31.5	20.8	2112.2	2158.6
148.0	78.3	32.1	20.9	2097.1	2165.1
148.5	78.2	32.1	20.6	2113.5	2166.6
149.0	78.2	31.6	20.8	2095.9	2161.2
149.5	78.1	31.1	20.6	2112.3	2155.9
150.0	78.1	31.1	20.7	2088.4	2158.6
150.5	78.2	30.8	20.8	2109.4	2167.8
151.0	78.2	30.9	20.9	2114.7	2166.0
151.5	78.3	31.1	20.7	2114.0	2170.4

At 40% fouling condition:

Time (min)	T_{sup} (°C)	T_{amb} (°C)	T_{room} (°C)	P_{cd} (kPa)	$\dot{W}$ (W)
93	80.9	31.8	20.8	2213.0	2200.8
93.5	80.7	32.0	20.9	2218.6	2201.3
94	80.5	31.1	20.7	2209.2	2191.1
94.5	80.5	31.1	20.8	2176.7	2175.9
95	80.7	31.6	20.6	2211.2	2217.6
95.5	80.8	31.8	20.6	2223.6	2217.2
96	80.9	31.8	20.9	2215.1	2191.7
96.5	80.9	32.3	20.6	2191.1	2200.0
97	80.7	32.8	20.7	2209.6	2201.2
97.5	80.9	32.2	20.6	2220.3	2213.5
98	80.6	31.6	20.8	2184.7	2187.0
98.5	80.6	31.7	20.7	2224.3	2206.1
99	80.5	31.1	20.7	2198.7	2197.2
99.5	80.8	31.4	20.8	2202.3	2181.0
100	80.9	31.6	20.6	2203.0	2201.1

100.5	80.9	31.8	20.8	2211.7	2193.4
101	80.5	31.8	20.7	2220.3	2181.1
101.5	80.5	31.7	20.8	2219.1	2196.0
102	80.6	32.0	21.0	2208.9	2191.5
102.5	80.6	31.7	20.7	2197.7	2204.5
103	80.9	32.4	20.7	2230.7	2216.7
103.5	80.9	32.5	20.6	2236.2	2215.7
104	81.0	31.9	20.6	2219.1	2193.4
104.5	80.8	31.3	20.7	2198.4	2171.1
105	80.6	30.9	20.6	2175.0	2173.6
105.5	80.8	30.5	20.8	2199.5	2223.2
106	81.0	31.2	20.6	2209.2	2225.1
106.5	80.9	31.1	20.8	2210.6	2203.8
107	80.8	31.4	20.6	2207.5	2201.0
107.5	80.4	31.5	20.7	2189.8	2175.4
108	80.6	31.3	20.7	2169.7	2172.8
108.5	80.8	31.8	21.2	2221.3	2195.0
109	80.5	32.3	21.1	2188.0	2169.4
109.5	80.7	32.0	20.8	2203.3	2192.1
110	80.6	31.7	21.0	2186.8	2157.4
110.5	80.8	32.3	20.7	2231.3	2191.8
111	80.8	32.0	20.8	2192.1	2205.3
111.5	80.9	32.1	20.6	2230.6	2203.6
112	80.9	32.1	20.8	2220.0	2212.9
112.5	80.8	32.1	20.9	2212.3	2202.8
113	80.8	32.1	21.1	2213.3	2186.7
113.5	80.7	32.1	21.0	2232.8	2201.2
114	80.7	32.3	21.0	2220.0	2200.8
114.5	80.8	32.0	20.9	2224.1	2202.4
115	80.9	31.5	21.0	2219.6	2199.4
115.5	80.7	31.6	21.1	2211.2	2181.2
116	80.9	31.8	20.9	2240.9	2185.1
116.5	81.0	31.9	21.0	2246.5	2186.3
117	81.0	31.7	21.0	2243.7	2210.0
117.5	80.8	31.5	21.1	2209.8	2200.6
118	80.8	32.0	20.9	2211.9	2217.4
118.5	80.8	32.0	21.1	2204.6	2201.0
119	81.0	32.2	21.0	2227.8	2206.2
119.5	81.0	31.1	21.0	2218.2	2199.5
120	80.9	31.5	21.0	2224.1	2219.5
120.5	80.9	31.4	21.2	2197.4	2180.0

121	81.0	31.3	21.1	2222.7	2225.3
121.5	80.8	31.3	21.0	2204.0	2186.3
122	81.0	31.7	21.0	2200.9	2205.1
122.5	81.0	31.1	21.1	2200.8	2217.8
123	80.7	30.9	21.1	2192.8	2180.3
123.5	80.8	31.7	21.0	2191.2	2211.6
124	80.9	31.4	21.2	2219.6	2197.3
124.5	81.0	31.9	21.2	2224.1	2225.1
125	80.9	32.1	21.0	2225.0	2187.0
125.5	80.8	32.3	21.0	2220.3	2227.5
126	80.8	31.9	20.9	2196.7	2174.7
126.5	80.8	31.8	20.9	2215.5	2194.0
127	80.9	31.5	20.9	2203.9	2202.3
127.5	81.0	31.5	21.0	2216.4	2232.0
128	81.0	31.6	21.2	2229.7	2226.6
128.5	81.0	31.5	20.8	2217.9	2196.6
129	81.0	31.8	21.0	2201.1	2195.2
129.5	80.9	31.3	20.9	2222.7	2202.4
130	80.8	31.3	20.8	2211.0	2184.5
130.5	80.7	31.2	21.1	2209.2	2200.5
131	80.8	32.2	20.9	2209.1	2186.2
131.5	80.9	32.3	20.8	2214.8	2186.1
132	80.9	32.3	21.0	2243.2	2223.7
132.5	81.1	32.5	20.8	2245.6	2202.5

At 50% fouling condition:

Time (min)	T_{sup} (°C)	T_{amb} (°C)	T_{room} (°C)	P_{cd} (kPa)	$\dot{W}$ (W)
314.0	84.1	31.9	20.9	2352.8	2264.3
314.5	84.1	32.2	20.8	2356.9	2274.6
315.0	84.1	30.7	20.8	2363.4	2266.6
315.5	84.1	31.7	20.8	2352.4	2257.6
316.0	84.1	31.7	20.8	2341.1	2253.2
316.5	83.9	28.8	20.8	2342.3	2265.0
317.0	84.3	32.1	21.0	2358.4	2294.7
317.5	84.2	32.1	20.8	2338.9	2267.4
318.0	84.1	31.4	20.9	2326.8	2280.3

318.5	83.9	31.7	20.7	2330.4	2276.0
319.0	83.9	31.6	20.7	2333.8	2258.7
319.5	84.1	31.1	20.7	2336.4	2282.8
320.0	84.1	32.0	20.8	2334.5	2260.7
320.5	84.0	32.5	20.7	2359.6	2265.0
321.0	84.2	31.3	20.7	2355.2	2255.4
321.5	84.2	32.4	20.9	2356.0	2288.0
322.0	84.0	32.0	20.7	2356.3	2264.8
322.5	84.2	31.7	21.0	2338.3	2278.1
323.0	84.3	31.6	21.1	2356.9	2269.1
323.5	84.6	32.1	20.9	2371.9	2285.4
324.0	84.5	31.8	20.9	2353.8	2271.1
324.5	84.3	31.4	20.7	2334.8	2263.3
325.0	84.1	30.3	20.8	2325.4	2262.0
325.5	84.1	31.6	20.8	2345.2	2285.8
326.0	84.0	31.8	20.8	2343.7	2287.3
326.5	84.1	31.7	20.9	2366.7	2291.8
327.0	84.1	31.5	20.8	2372.8	2280.6
327.5	84.3	31.7	20.7	2352.4	2260.1
328.0	84.3	31.5	20.7	2356.0	2269.1
328.5	84.0	31.5	20.8	2341.8	2261.7
329.0	84.2	31.4	20.8	2351.3	2276.0
329.5	84.0	31.7	20.9	2348.6	2283.7
330.0	84.3	32.3	21.0	2356.0	2271.4
330.5	84.1	31.6	21.0	2312.3	2248.4
331.0	83.9	31.9	20.9	2301.3	2257.4
331.5	83.9	31.7	20.8	2321.7	2235.7
332.0	84.0	32.0	20.7	2335.1	2255.7
332.5	84.0	31.6	21.0	2317.6	2256.5
333.0	84.0	31.8	20.7	2320.6	2226.2
333.5	84.1	32.3	20.8	2338.5	2251.8
334.0	83.9	32.0	20.6	2328.3	2230.2
334.5	83.9	32.2	20.7	2313.0	2234.8
335.0	83.8	32.1	20.7	2320.6	2237.8
335.5	83.9	32.3	20.8	2326.2	2266.8
336.0	83.9	31.7	20.6	2313.0	2250.6
336.5	83.9	31.9	20.7	2340.0	2253.6
337.0	84.1	31.9	20.8	2338.2	2257.1
337.5	83.9	32.0	20.7	2334.2	2246.1
338.0	83.9	31.8	20.6	2347.9	2233.8
338.5	84.1	32.4	20.8	2336.6	2263.9

339.0	84.0	31.7	21.0	2344.2	2264.3
339.5	83.7	31.8	20.6	2327.1	2244.2
340.0	83.7	31.3	20.6	2327.4	2239.2
340.5	83.8	31.8	20.6	2336.4	2262.9
341.0	83.8	31.5	20.6	2326.5	2247.2
341.5	83.9	31.6	20.7	2359.6	2259.2
342.0	83.8	31.0	20.7	2349.7	2271.9
342.5	83.7	31.2	20.9	2315.3	2259.6
343.0	83.6	31.3	20.9	2337.3	2265.5
343.5	83.7	31.2	20.7	2327.4	2273.6
344.0	83.7	30.6	20.9	2347.0	2270.6
344.5	84.0	31.7	21.0	2342.3	2278.6
345.0	84.0	31.8	21.2	2363.2	2267.4
345.5	84.0	31.6	21.1	2328.6	2261.6
346.0	83.9	31.7	21.0	2332.6	2260.2
346.5	83.7	31.7	21.1	2308.5	2229.4
347.0	83.8	31.6	21.1	2339.2	2255.4
347.5	83.9	31.4	20.8	2328.9	2258.1
348.0	84.0	31.6	21.0	2318.3	2253.9
348.5	84.0	31.5	20.9	2338.0	2250.1
349.0	83.8	31.6	20.6	2295.8	2240.5
349.5	83.7	31.6	20.9	2316.4	2240.9
350.0	83.5	31.7	20.8	2318.3	2218.4
350.5	83.5	31.7	20.6	2297.5	2264.5
351.0	83.6	31.5	20.5	2307.2	2245.8
351.5	83.6	31.5	20.7	2305.1	2228.2
352.0	83.5	31.4	20.6	2300.9	2259.3
352.5	83.6	31.4	20.8	2286.1	2217.9
353.0	83.5	31.5	20.8	2320.6	2242.5
353.5	83.4	31.4	20.6	2302.2	2223.2

APPENDIX D: Experimental Data for VCC-DMS

With subcooling:

t (min)	TC1 (°C)	TC4 (°C)	TC5 (°C)	TC8 (°C)	TC9 (°C)	TC10 (°C)	TC12 (°C)	TC15 (°C)	TC17 (°C)	TC18 (°C)	P1 (Pa)	P2 (Pa)	P3 (Pa)	P4 (Pa)	$\dot{W}_{sc}$ (W)	$\dot{W}_{m}$ (W)
0	126.4	51.9	46.1	10.4	13.1	107.0	54.6	43.7	38.9	22.0	404.4	1999.6	249.4	1379.0	236.4	2024.9
6	127.0	53.2	46.8	11.0	13.3	108.1	55.3	44.3	40.0	22.4	413.5	2030.4	255.1	1381.7	235.7	2084.5
12	126.9	52.3	45.9	11.0	13.6	108.5	55.1	43.8	40.2	22.3	400.7	1996.1	256.4	1384.5	238.8	2016.3
18	126.8	52.6	46.5	10.1	11.9	109.4	55.6	44.3	39.6	22.1	404.8	2015.5	258.1	1387.2	236.4	2023.0
24	126.3	51.9	45.4	11.5	13.4	109.3	54.2	43.6	38.8	22.2	410.4	1984.0	249.0	1390.0	232.3	1998.1
30	126.8	52.9	46.5	10.7	13.2	110.3	55.8	44.4	39.5	22.0	413.6	2051.3	263.1	1392.7	234.3	2047.2
36	126.6	52.8	45.9	9.2	12.2	110.6	55.3	43.8	39.5	21.7	421.0	2041.6	266.4	1403.7	242.8	2055.8
42	127.0	53.6	47.8	10.9	12.8	111.4	56.5	45.3	39.7	22.3	410.6	2045.7	279.9	1414.8	248.7	2060.0
48	127.1	53.7	46.9	9.5	12.8	111.8	56.9	44.5	40.9	21.7	423.7	2101.8	280.8	1425.8	248.4	2088.8
54	127.2	53.4	48.0	9.4	11.6	112.1	56.4	45.5	39.6	21.8	413.6	2059.6	274.9	1436.9	247.4	2041.1
60	127.2	53.3	47.6	11.1	12.7	112.1	56.3	45.3	40.9	21.8	402.7	2027.7	279.6	1447.9	245.0	2031.5
66	127.8	54.3	47.3	9.2	12.6	113.1	57.9	45.0	40.9	21.2	424.2	2094.3	286.6	1458.9	246.1	2129.1
72	127.6	53.7	47.7	9.7	11.7	112.7	56.7	45.4	40.9	21.6	404.0	2059.3	286.7	1470.0	248.4	2051.9
78	127.5	54.1	46.9	10.2	12.9	113.5	57.8	44.7	41.4	21.9	430.1	2105.9	291.6	1481.0	251.5	2104.9
84	127.8	53.7	48.0	9.6	12.1	113.8	57.5	45.6	41.0	21.1	411.2	2089.4	292.6	1492.1	252.0	2055.2
90	127.6	53.7	47.4	9.6	11.8	114.1	57.2	45.2	40.4	21.6	417.7	2088.1	288.7	1503.1	250.7	2080.1
96	127.8	54.5	48.3	10.5	12.8	114.5	57.1	45.8	40.6	22.1	420.4	2123.6	292.3	1507.2	249.1	2112.2
102	127.4	53.6	47.9	9.6	11.6	114.8	57.4	45.4	41.3	20.9	410.3	2079.6	299.0	1511.3	259.2	2041.0
108	127.7	54.9	48.9	8.1	11.9	115.2	58.4	45.9	42.0	21.3	437.3	2110.2	302.2	1515.5	263.4	2156.2
114	127.4	53.5	47.7	9.9	12.5	114.8	56.8	45.3	40.5	21.4	410.3	2047.7	296.4	1519.6	256.3	2039.2
120	127.3	53.8	47.6	9.3	11.6	115.2	57.0	45.3	41.2	20.8	414.0	2071.1	301.1	1523.7	255.9	2064.5
126	127.0	54.0	46.6	10.0	12.6	115.5	58.2	44.4	41.2	21.5	422.0	2071.8	308.6	1529.2	261.1	2089.0
132	127.2	54.1	47.6	8.4	11.9	115.5	57.9	44.9	40.7	20.9	422.0	2081.1	308.6	1534.7	261.7	2087.5
138	126.6	53.6	46.8	8.8	11.4	115.3	57.1	44.5	41.5	21.3	408.6	2052.6	304.5	1540.3	258.7	2072.0

144	126.7	54.4	48.1	9.6	12.0	115.7	58.7	45.2	41.0	21.5	425.9	2087.7	314.8	1545.8	265.5	2105.1
150	126.8	53.9	47.2	3.9	11.6	115.4	56.8	44.7	40.8	21.2	429.2	2103.6	309.2	1551.3	255.9	2088.2
156	126.5	53.9	47.1	8.7	11.1	115.5	57.2	44.8	40.8	21.0	412.5	2058.9	312.7	1545.8	261.4	2065.9
162	126.2	53.6	47.2	9.8	12.2	115.1	57.0	44.5	40.5	21.5	419.7	2068.7	315.0	1540.3	262.1	2069.8
168	126.3	53.5	47.3	8.1	11.0	114.9	57.2	44.8	40.2	21.1	409.7	2050.7	318.8	1534.7	260.9	2050.4
174	125.8	53.4	47.1	9.1	10.3	114.5	55.8	44.6	40.7	20.7	413.6	2032.5	316.9	1529.2	262.7	2037.9
180	125.9	53.6	47.0	9.7	12.2	115.3	56.9	44.6	40.9	21.1	412.1	2060.2	319.4	1523.7	258.3	2052.2
186	126.1	53.8	47.6	7.2	9.7	115.3	57.8	44.9	41.4	20.2	417.7	2096.3	323.1	1529.2	261.2	2080.3
192	126.0	54.3	48.0	9.1	10.0	115.5	57.4	45.2	40.9	21.0	423.4	2103.0	320.6	1534.7	267.1	2093.6
198	125.8	53.1	46.5	9.6	12.2	115.1	55.8	44.1	40.2	20.6	411.4	2063.1	318.9	1540.3	259.8	2051.8
204	125.9	53.5	47.5	3.3	9.3	115.7	57.3	44.7	40.8	20.3	424.1	2047.8	325.3	1545.8	266.3	2066.8
210	125.6	53.8	47.6	9.3	11.2	115.5	56.1	45.0	40.8	21.0	416.5	2092.6	323.3	1551.3	264.5	2066.8
216	125.6	53.5	46.8	3.6	10.9	115.2	57.3	44.0	40.9	20.5	427.7	2041.8	327.2	1554.1	265.4	2079.2
222	125.1	53.4	46.9	7.2	8.3	115.0	56.6	44.3	40.7	20.6	420.2	2030.5	327.3	1556.8	268.3	2039.4
228	124.9	53.1	46.5	9.0	11.8	115.3	56.7	43.9	40.5	21.0	421.6	2052.6	328.2	1559.6	269.6	2066.4
234	124.9	52.8	46.1	7.6	10.8	115.2	56.1	43.6	40.3	20.4	418.5	2045.1	326.1	1562.3	265.8	2034.4
240	124.9	53.8	47.2	3.9	9.7	115.1	57.4	44.4	41.2	20.9	428.5	2061.7	333.8	1565.1	273.7	2082.3
246	125.2	53.4	46.6	8.7	11.7	115.3	56.6	44.1	40.0	20.9	419.7	2045.7	329.9	1569.2	269.6	2050.4
252	125.1	53.4	47.2	2.7	8.0	115.7	56.8	44.5	41.0	20.4	413.8	2074.6	331.0	1573.4	266.7	2060.3
258	124.6	53.8	47.6	8.9	9.8	116.2	57.2	44.8	41.0	21.2	417.0	2064.9	335.3	1577.5	269.0	2068.4
264	124.9	53.3	46.5	7.0	11.5	116.2	56.5	43.8	40.3	20.4	425.7	2080.3	331.8	1581.7	273.9	2063.6
270	124.8	53.3	46.2	2.9	8.9	116.5	57.2	43.7	40.7	20.1	409.7	2054.7	336.7	1585.8	275.9	2042.6
276	124.4	53.2	46.4	9.2	11.3	116.1	56.2	43.8	39.5	21.0	415.6	2051.6	333.7	1581.7	271.2	2052.8
282	124.4	52.5	46.2	8.5	10.1	115.8	55.5	43.7	39.7	20.2	396.6	1986.6	332.3	1577.5	272.4	1997.9
288	123.9	52.8	46.3	3.1	7.9	116.5	56.5	43.4	39.7	20.8	416.8	2018.0	335.8	1573.4	276.2	2035.8
294	123.7	52.6	45.7	9.3	11.4	115.7	55.7	43.0	40.0	20.7	409.3	1998.0	335.4	1569.2	272.4	2027.0
300	123.8	52.4	45.9	5.6	9.4	115.7	55.7	43.2	40.1	20.2	413.9	2039.2	334.6	1565.1	270.2	2020.8
306	123.2	52.5	45.1	8.5	10.2	115.4	55.0	42.6	40.1	20.4	415.3	2004.6	333.0	1561.0	272.4	2025.5

312	123.2	51.8	45.1	8.9	11.2	115.1	55.0	42.5	39.7	20.0	407.6	1981.2	334.3	1556.8	266.0	2002.6
318	123.1	51.9	45.2	3.9	8.4	114.5	54.8	42.4	39.3	19.9	408.0	1980.2	334.2	1552.7	270.1	2003.6
324	122.6	52.0	45.1	8.8	10.3	114.3	55.0	42.4	39.5	20.6	412.1	1996.5	335.1	1548.5	272.0	2007.3
330	122.9	52.0	44.8	3.3	10.7	114.1	55.3	42.1	39.5	20.1	421.6	2009.1	337.1	1544.4	272.8	2021.5
336	122.5	51.7	45.1	7.4	8.0	114.0	54.9	42.3	39.2	20.2	402.6	1956.1	339.8	1538.9	273.4	2002.8
342	122.5	51.6	43.9	7.9	11.4	113.7	54.1	41.4	39.1	20.0	414.5	1975.3	334.8	1533.4	265.8	2014.6
348	122.1	51.4	44.4	3.1	9.1	113.7	54.4	41.6	39.2	19.9	406.1	1946.6	339.3	1527.8	271.7	1984.3
354	121.9	51.4	44.2	9.1	10.8	113.5	54.2	41.6	39.1	20.6	411.2	1945.9	337.3	1522.3	268.9	1993.6
360	121.9	51.2	43.9	4.8	9.4	113.5	54.2	41.3	39.1	19.9	405.8	1953.9	337.6	1516.8	266.6	1993.5
366	121.3	50.8	43.8	8.3	10.2	113.0	53.7	41.0	38.7	19.9	408.5	1953.2	334.6	1516.8	269.4	1987.1
372	121.3	50.7	43.7	8.7	11.1	112.6	53.6	41.0	38.2	20.5	402.9	1936.3	333.4	1516.8	264.6	1989.0
378	121.2	50.5	43.4	5.5	9.1	112.7	53.6	40.8	38.5	19.9	395.2	1906.1	333.7	1516.8	266.0	1977.9
384	120.8	50.5	43.2	8.8	10.9	112.1	53.5	40.6	38.2	20.6	397.3	1904.1	333.8	1516.8	269.5	1980.4
390	120.7	50.0	42.8	8.4	10.7	112.0	53.0	40.3	38.1	20.3	396.5	1897.4	329.6	1516.8	264.5	1957.5
396	120.5	50.0	42.8	8.2	9.4	111.8	53.0	40.2	38.1	20.0	402.7	1916.8	330.5	1516.8	264.0	1964.3
402	120.4	50.1	42.6	8.9	11.4	111.8	52.9	39.9	37.9	20.4	400.5	1897.7	330.2	1516.8	267.5	1963.3
408	120.4	50.3	43.1	6.8	9.4	111.6	53.5	40.3	38.4	19.5	405.5	1914.5	334.7	1516.8	269.4	1980.1
414	120.3	50.2	42.7	8.9	11.2	111.6	52.9	39.8	38.2	20.3	402.3	1925.8	331.9	1516.8	265.8	1979.6
420	120.3	49.8	42.6	7.9	10.1	111.2	52.7	40.0	38.0	19.9	390.8	1864.1	330.5	1516.8	268.0	1943.4
426	119.9	49.8	42.4	8.2	10.2	111.5	52.6	39.6	37.8	20.3	396.3	1907.1	335.4	1514.1	272.5	1950.8
432	120.0	49.8	42.2	8.9	11.1	110.9	52.3	39.5	37.7	20.4	403.7	1908.2	326.4	1511.3	264.6	1948.6
438	120.0	49.6	42.4	7.9	10.4	110.7	52.3	39.7	37.4	20.1	392.7	1857.6	328.5	1508.6	268.9	1932.6
444	119.6	49.4	42.2	6.9	8.7	110.5	52.0	39.5	37.6	20.0	393.5	1883.8	329.4	1505.8	264.7	1929.6
450	119.6	49.7	42.1	8.9	11.0	111.0	52.4	39.3	37.7	20.2	402.9	1906.4	329.3	1503.1	264.3	1963.6
456	119.6	49.4	42.2	8.7	11.1	110.5	52.1	39.4	37.6	19.9	400.1	1894.3	326.6	1501.7	266.3	1936.8
462	119.7	49.3	42.1	7.0	9.0	111.0	52.1	39.4	37.7	19.8	389.5	1850.2	329.8	1500.3	266.0	1937.1
468	119.1	49.4	41.4	8.1	10.2	110.5	51.8	38.9	37.7	19.9	397.6	1862.6	325.6	1499.0	267.9	1939.3
474	119.2	49.3	41.6	8.9	11.1	110.5	51.9	38.9	37.7	20.3	396.1	1854.1	328.0	1497.6	263.5	1954.1

480	119.4	49.2	42.0	6.4	10.0	110.6	51.9	39.2	37.7	19.8	394.4	1886.7	328.5	1496.2	263.8	1952.7

Without subcooling:

t (min)	TC1 (°C)	TC4 (°C)	TC5 (°C)	TC8 (°C)	TC9 (°C)	TC17 (°C)	TC18 (°C)	P1 (Pa)	P2 (Pa)	$\dot{W}_m$ (W)
0	131.1	49.9	49.2	11.8	13.9	37.3	23.1	346.5	1861.3	1830.7
6	131.2	50.4	49.8	12.2	14.5	38.2	23.4	347.0	1915.8	1846.7
12	131.6	50.3	50.0	11.3	13.6	37.7	22.9	344.8	1881.1	1841.7
18	131.8	50.6	50.3	12.0	13.8	37.0	23.4	350.1	1906.5	1830.0
24	131.6	50.0	49.6	12.1	14.5	36.6	23.2	344.4	1908.4	1826.6
30	131.9	50.5	50.3	11.1	13.5	38.4	23.1	344.5	1927.9	1835.4
36	132.3	51.2	50.9	12.1	13.9	37.3	23.2	348.7	1910.8	1851.3
42	132.4	51.1	50.7	12.2	14.4	37.9	23.4	360.2	1947.4	1854.4
48	132.7	50.9	50.7	10.8	13.3	37.4	23.0	348.3	1898.7	1838.9
54	133.0	50.9	50.5	12.0	14.2	38.9	23.2	353.4	1955.9	1858.9
60	133.1	51.2	50.9	12.2	14.5	38.6	23.5	348.0	1939.6	1869.7
66	134.5	52.1	51.8	11.0	13.3	39.1	22.8	352.0	1967.8	1916.1
72	133.9	51.6	51.3	11.6	13.8	38.4	23.1	360.5	1968.0	1850.5
78	133.4	51.1	51.0	12.7	14.5	37.4	23.3	344.6	1951.8	1823.9
84	133.9	52.7	52.4	13.3	13.3	38.6	22.6	366.5	1992.1	1888.0
90	133.2	51.5	51.4	10.7	13.3	38.3	22.3	347.4	1981.4	1872.9
96	133.0	52.0	51.7	10.6	12.9	37.6	22.1	360.9	1975.1	1887.4
102	133.0	51.8	51.4	11.2	13.8	38.1	22.5	358.0	1987.1	1879.0
108	133.7	52.5	52.3	11.0	13.8	39.0	22.4	367.9	1994.4	1913.3
114	133.6	52.2	51.9	10.2	13.1	39.0	21.8	354.3	1997.5	1895.3
120	133.1	51.8	51.5	11.1	13.6	38.3	22.3	362.5	1979.5	1874.6
126	133.5	52.5	52.2	11.5	13.9	38.8	22.7	361.2	2004.6	1910.6
132	133.6	52.4	51.8	10.2	13.3	37.8	22.2	362.6	2021.9	1918.4
138	133.3	52.3	51.9	10.8	13.3	38.8	22.4	357.7	1999.3	1887.6
144	133.4	52.4	52.0	11.3	14.0	39.3	22.6	374.6	2022.6	1892.2
150	133.6	52.2	51.9	10.7	13.7	37.5	22.4	364.8	2014.9	1898.9
156	133.2	51.9	51.7	10.3	13.0	38.8	22.0	351.3	1986.2	1860.1
162	133.1	52.2	51.8	11.4	13.8	38.7	22.6	371.4	2019.1	1885.3
168	133.1	51.9	51.7	11.6	14.1	38.8	22.7	359.7	1955.3	1873.8
174	133.3	51.8	51.7	10.6	13.4	38.7	22.2	357.2	1966.7	1879.9
180	132.7	51.5	51.2	10.7	13.0	38.4	22.1	350.4	1939.1	1850.5
186	132.6	51.8	51.6	11.7	13.9	38.7	22.7	360.7	1946.0	1871.9
192	132.5	51.6	51.4	11.5	14.3	37.7	22.5	359.4	1976.7	1879.0

198	132.6	51.8	51.6	10.3	13.1	38.3	22.3	354.7	1953.2	1857.2
204	132.5	51.3	51.0	11.5	13.7	37.8	22.5	352.3	1954.0	1847.1
210	132.4	51.7	51.3	11.6	14.2	38.7	22.7	358.7	1968.5	1872.1
216	132.3	51.0	51.0	11.0	13.6	38.4	22.4	353.0	1932.8	1850.7
222	132.1	51.2	51.0	11.3	13.5	38.4	22.6	358.6	1937.5	1827.5
228	132.0	51.3	50.9	11.8	14.3	38.3	22.8	357.3	1929.3	1839.4
234	132.0	51.4	50.9	10.6	13.6	38.3	22.2	360.4	1968.1	1837.2
240	131.6	51.3	50.7	10.9	13.2	37.8	22.4	355.5	1921.3	1848.6
246	131.2	50.7	50.5	11.9	14.2	37.0	22.8	348.4	1929.4	1830.5
252	131.4	50.8	50.6	10.9	13.7	36.8	22.2	347.2	1904.1	1810.3
258	131.1	50.3	50.0	10.7	13.2	37.5	22.4	347.3	1920.4	1814.2
264	131.3	50.9	50.6	11.8	14.0	38.2	22.8	349.2	1920.9	1829.2
270	131.2	50.9	50.5	11.0	13.8	38.4	22.5	354.3	1908.8	1827.8
276	131.0	50.7	50.3	10.4	13.1	38.2	22.3	343.3	1943.2	1820.1
282	130.7	50.3	50.0	11.9	14.1	38.3	22.6	344.8	1913.8	1809.8
288	130.7	50.2	49.8	11.1	13.9	37.5	22.5	346.9	1911.6	1800.4
294	130.5	49.8	49.5	10.6	13.1	37.4	22.1	349.5	1899.9	1781.6
300	130.3	50.2	49.9	11.8	14.0	37.5	22.6	347.7	1876.2	1805.1
306	130.4	50.2	49.7	10.9	13.6	36.4	22.4	347.3	1875.2	1794.9
312	130.2	49.8	49.5	10.5	13.1	36.7	22.4	338.5	1889.5	1796.5
318	130.0	49.4	49.1	11.9	14.0	36.3	22.8	341.6	1876.2	1773.2
324	130.1	49.5	49.2	11.4	13.9	37.4	22.6	339.4	1859.7	1797.4
330	130.0	49.7	49.4	10.5	13.1	37.1	22.3	343.5	1855.5	1789.0
336	129.8	49.5	49.1	11.9	14.1	37.0	22.7	339.8	1888.1	1778.0
342	129.9	49.5	49.1	11.3	13.9	36.7	22.7	338.8	1882.5	1781.1
348	129.9	49.6	49.0	11.1	13.3	37.7	22.7	345.1	1890.2	1799.1
354	129.8	49.4	49.0	11.7	14.2	37.6	22.6	342.3	1864.2	1773.0
360	129.7	49.2	49.0	10.9	13.4	36.9	22.3	334.8	1859.6	1766.9
366	129.6	49.2	48.8	11.8	13.9	36.9	22.7	339.1	1843.0	1791.4
372	129.6	49.2	48.7	11.4	14.0	37.2	22.7	338.8	1869.6	1764.5
378	129.6	49.2	48.7	11.0	13.3	36.4	22.4	342.1	1854.3	1792.6
384	129.5	49.0	48.8	12.1	14.2	35.9	22.8	336.1	1861.4	1776.7
390	129.6	49.0	48.7	11.5	14.1	37.1	22.6	342.1	1867.5	1763.5
396	129.4	48.6	48.3	10.9	13.3	37.0	22.4	336.4	1843.7	1762.0
402	129.3	48.8	48.4	12.0	14.1	36.3	22.7	335.7	1806.8	1774.5
408	129.4	49.1	48.6	11.9	14.4	36.6	22.7	336.7	1848.4	1773.3
414	129.4	48.8	48.6	11.0	13.5	36.6	22.5	335.0	1815.6	1773.0
420	129.1	48.6	48.2	11.7	13.7	37.0	22.7	326.4	1806.2	1763.7
426	129.2	48.7	48.1	12.1	14.5	36.3	23.0	331.3	1843.2	1758.1
432	129.2	48.5	48.1	11.1	13.7	36.4	22.5	336.0	1806.9	1755.4
438	129.0	48.3	47.8	12.0	14.1	36.2	22.8	332.4	1806.1	1753.6

444	129.1	48.4	48.0	11.8	14.2	36.7	23.0	325.7	1840.3	1750.9
450	128.9	48.3	47.9	10.3	13.0	36.2	22.8	333.5	1819.0	1757.6
456	128.6	48.0	47.7	11.2	13.3	36.4	22.8	332.9	1816.3	1741.3
462	128.5	48.1	47.8	11.3	13.5	35.9	23.1	318.6	1818.4	1741.1
468	128.4	48.1	47.6	10.0	12.7	35.7	22.6	331.1	1822.5	1750.0
474	128.1	48.0	47.6	10.4	12.5	35.0	23.1	319.2	1777.8	1735.4
480	127.9	47.7	47.4	10.8	13.0	36.1	23.0	328.5	1767.7	1722.4

APPENDIX E: Steps for Buckingham Pi Theorem

The following steps were followed while applying the Buckingham Pi theorem [105-106]:

i) Clearly define the problem and think about which variables are important. Identify which is the main variable of interest i.e. $q_1 = f(q_2,\ldots q_n)$. It is important to think physically about the problem. Are there any constraints; *i.e.* 'can I vary all of these variables independently'; e.g. $F_w = \rho g l^3$ weight of an object (only two of these are independent, unless g is also variable). If all the pertinent parameters are not included, a relation may be obtained, but it will not give the complete story. If parameters that actually have no effect on the physical phenomenon are included, either the process of dimensional analysis will show that these do not enter the relation sought or one or more dimensionless groups will be obtained that experiments will show to be extraneous.

ii) Express each of n variables in terms of its fundamental dimensions, $\{MLtT\}$ and $\{FLtT\}$ both. This is done to check $k = r$ condition from each set where r is the number of primary dimensions in each set used to express the variables and k is the rank of the dimensional matrix.

iii) Select r *(or* k*)* repeating parameters. All primary dimensions should be represented by the selection. Typically pick variables which characterize the fluid properties, flow geometry, flow rate. They should not form a Pi product. No two

repeating parameters may have the same net dimensions differing by only a single exponent; e.g. don't include both length (L) and moment of inertia of an area (L^4) as repeating parameters. Do not include the dependent parameter among the selection.

iv) Determine the number of Pi groups, $j = n - k$. Form j dimensionless Π groups and check that they are all indeed dimensionless. This is done by combining repeating parameters with each of the other parameters one by one and solving the dimensional equations.

v) Express result in form $\Pi_1 = \varphi(\Pi_2,\ldots\Pi_{n-k})$ where Π_1 contains the quantity of interest and interpret your result physically!

vi) Make sure that your groups are indeed independent; i.e. can I vary one and keep others constant. A Π group is not independent if it can be formed from other Π groups. For example, $\Pi_4 = 2\ \Pi_2/\ \Pi_3$.

APPENDIX F: Cost Optimization Representation for VCC-DMS

To ascertain which of the two models shown in Figs. 7.8 and F.1 is more appropriate for representing dedicated mechanical subcooling systems, we should keep the following points in mind:

1. For a cycle to be considered in line with the Carnot model, the heat transfers occurring in it must be reversible and isothermal.
2. In actual mechanical subcooling systems, the condenser and the subcooler are two different heat exchangers. The average temperature at which heat transfer takes place is also different in each of them.

In Fig. F.1, the first point is clearly satisfied as both heat exchangers function inside the two-phase region. On the other hand, both heat exchangers are transferring heat at the same temperature, which goes against the second point mentioned above. In Fig. 7.8, the condenser exchanges heat inside the two-phase region and, thus, it is understood to satisfy the first point. In a real subcooler, the temperature decreases below the saturation temperature of the condenser and there is a finite temperature drop (See dashed line in Fig. 7.8). In order to represent this in a reversible manner, an average value for the subcooler temperature ($\overline{T}_{sc}$) is considered. It can be understood that the heat transfer is taking place reversibly at this average temperature. Thus, both points mentioned are

satisfied. The same methodology was, thus, followed in representing the integrated subcooling cycle as can be seen in Fig. 7.13(b).

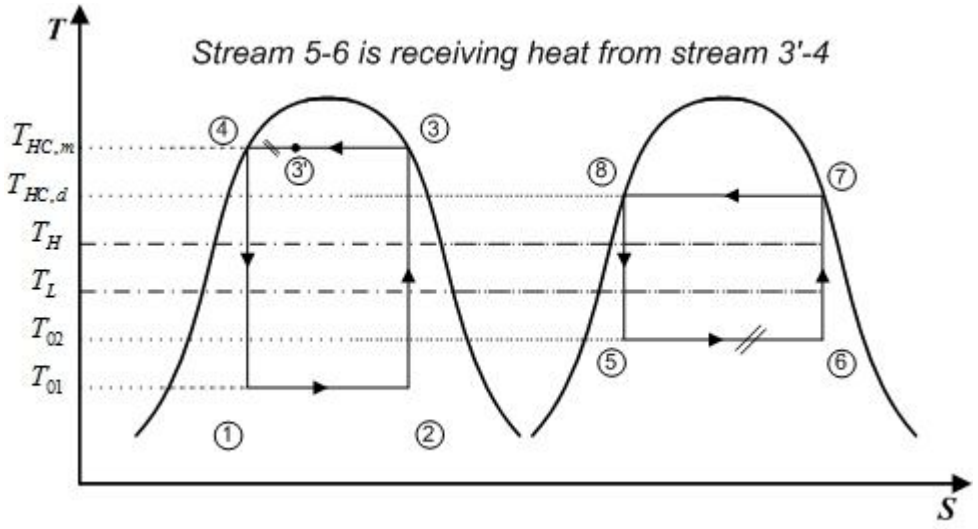

Figure F.1. Dedicated Carnot cycle with subcooler - Alternative

APPENDIX G: VCC-IMS Cost Optimization Equation Derivation

To derive Eq. (7.47), keeping Fig. 7.13 in mind, consider that

$$\dot{Q}_{H,m} = (\dot{m}_m + \dot{m}_i) T_{HC,m} (s_3 - s_3^{/}) \tag{G.1}$$

Using the above equation and Eq. (7.16a), we see that

$$\frac{\dot{Q}_{H,m}}{T_{HC,m}} + \frac{\dot{Q}_{sc}}{\overline{T}_{sc}} = (\dot{m}_m + \dot{m}_i)(s_3 - s_3^{/}) + \dot{m}_m (s_3^{/} - s_4) \tag{G.2}$$

The above equation can be manipulated such that we get

$$\frac{\dot{Q}_{H,m}}{T_{HC,m}} + \frac{\dot{Q}_{sc}}{\overline{T}_{sc}} = \dot{m}_m (s_3 - s_4) + \dot{m}_i (s_3 - s_3^{/}) \tag{G.3}$$

On the right hand side of Eq. (G.3), multiplying and dividing the first term by $(s_2 - s_1)$ and the second term by $(s_6 - s_5)$. Therefore, we get

$$\frac{\dot{Q}_{H,m}}{T_{HC,m}} + \frac{\dot{Q}_{sc}}{\overline{T}_{sc}} = \frac{(s_3 - s_4)}{(s_2 - s_1)} \dot{m}_m (s_2 - s_1) + \frac{(s_3 - s_3^{/})}{(s_6 - s_5)} \dot{m}_i (s_6 - s_5) \tag{G.4}$$

From the definition of k_1, k_2, k_3 and the heat transfers defined by Eqs. (7.16b) and (7.16c), we finally get

$$\frac{\dot{Q}_{H,m}}{T_{HC,m}} + \frac{\dot{Q}_{sc}}{\bar{T}_{sc}} = \frac{k_2}{k_1}\frac{\dot{Q}_L}{T_{01}} + k_3\frac{\dot{Q}_{sc}}{T_{02}} \tag{G.5}$$

REFERENCES

[1] Tribus, M., Evans, R., The thermoeconomics of seawater conversion, UCLA Report No.62-63, August 1962.

[2] Gaggioli, R. (Editor), Thermodynamics: Second-Law Analysis, ACS Symposium Series 122, 1980.

[3] Gaggioli, R. (Editor), Efficiency and Costing, ACS Symposium Series 235, 1983.

[4] De Vos, A., Endoreversible Thermodynamics of Solar Energy Conversion. Oxford University Press, Oxford, 1992.

[5] De Vos, A., 1995. Endoreversible thermodynamics. Energy Conversion and Management, 36(1), 1-5.

[6] Klein, S.A., Engineering Equation Solver. Academic Professional, Version 8 and 9. URL http://www.fchart.com/ees/ees.shtml

[7] Valero, A., Lozano, M.A., Munoz, M., A general theory of exergy saving. Part I: On the exergetic cost, Part II: On the thermoeconomic cost. Part III: Energy saving and thermoeconomics. In Computer-Aided Engineering of Energy Systems, Vol. 3 - Second Law Analysis and Modelling, ed. R. A. Gaggioli, 1-22. ASME, New York, 1986.

[8] Valero, A., Torres, C., Lozano, M.A., On the unification of thermoeconomic theories. In Simulation of Thermal Energy Systems, ed. R. F. Boehm and Y. M. El-Sayed, 63-74. ASME, New York, 1989.

[9] Lozano, M.A., Valero, A., Serra, L., Theory of exergetic cost and thermoeconomic optimization, Proceedings: Energy Systems and Ecology, ed. J. Szargut and G. Tsatsaronis. Cracow, Poland, 1993.

[10] d'Accadia, M.D., de Rossi, F., 1998a. Thermoeconomic analysis and diagnosis of a refrigeration plant. Energy Conversion Management, 39(12), 1223–1232.

[11] d'Accadia, M.D., de Rossi, F., 1998b. Thermoeconomic Optimization of a Refrigeration Plant, International Journal of Refrigeration, 21(1), 42–54.

[12] Bejan, A., 1988. Theory of heat transfer-irreversible power plants. International Journal of Heat Mass Transfer, 31(6), 1211-1219.

[13] Bejan, A., 1989. Theory of heat transfer-irreversible refrigeration plants. International Journal of Heat Mass Transfer, 32(9), 1631-1639.

[14] Bejan, A., 1993. Power and refrigeration plants for minimum heat exchanger inventory. Journal of Energy Resources Technology, 115, 148-150.

[15] Bejan, A., Vargas, J.V.C., Sokolov, M., 1995. Optimal allocation of heat exchanger inventory in heat driven refrigerators. International Journal of Heat Mass Transfer, 38(16), 2997-3004.

[16] Chen, L., Sun, F., Wu, C., 2004. Optimal allocation of heat-exchanger area for refrigeration and air-conditioning plants. Applied Energy, 77, 339–354.

[17] Klein, S.A., 1991. Design considerations for refrigeration cycles. International Journal of Refrigeration, 15(3), 181-185.

[18] Wu, C., 1995. Maximum obtainable specific cooling load of a refrigerator. Energy Conservation and Management, 36(1), 7-10.

[19] Chen, L., Sun, F., Chen, W., 1995. Optimization of the specific rate of refrigeration in combined refrigeration cycles. Energy, 20(10), 1049-1053.

[20] Sahin, B., Kodal, A., 1995. Steady-State thermodynamic analysis of a combined Carnot cycle with internal irreversibility. Energy: The International Journal, 20(12), 1285-1289.

[21] Wall, G., 1990. Optimization of refrigeration machinery, International Journal of Refrigeration, 14, 336-340.

[22] Wu, C., Chen, L., Sun, F., 1998. Effect of heat transfer law on finite-time exergoeconomic performance of Carnot heat pump. Energy Conservation and Management, 39(7), 579–588.

[23] E1-Sayed, Y.M., 1999. Thermoeconomics of some options of large mechanical vapor-compression units. Desalination, 125, 251-257.

[24] Sahin, B., Kodal, A., 1999. Finite time thermoeconomic optimization for endoreversible refrigerators and heat pumps. Energy Conversion and Management, 40, 951-960.

[25] Kodal, A., Sahin, B., Yilmaz, T., Effects of internal irreversibility and heat leakage on the finite time thermoeconomic performance of refrigerators and heat pumps, Energy Conversion and Management, 2000; 41, 607-619.

[26] Antar, M.A., Zubair, S.M., 2002. Thermoeconomic considerations in the optimum allocation of heat transfer inventory for refrigeration and heat pump systems. Journal of Energy Resources Technology, 124, 28-33.

[27] Klein, S.A., Reindl, D.T., 1998. The relationship of optimum heat exchanger allocation and minimum entropy generation rate for refrigeration cycles. Journal of Energy Resources Technology, 120, 172-178.

[28] Sahin, B., Kodal, A., 2001. Performance analysis of an endoreversible heat engine based on a new thermoeconomic optimization criterion. Energy Conversion and Management, 42, 1085-1093.

[29] Antar, M.A., Zubair, S.M., 2001. Thermoeconomic considerations in the optimum allocation of heat exchanger inventory for a power plant. Energy Conversion and Management, 42, 1169-1179.

[30] Kodal, A., Sahin, B., 2003. Finite size thermoeconomic optimization for irreversible heat engines. International Journal of Thermal Sciences, 42, 777–782.

[31] Bandyopadhyay, S., Bera, N.C., Bhattacharyya, S., 2001. Thermoeconomic optimization of combined cycle power plants. Energy Conversion & Management, 42, 359-371.

[32] Rovira, A. Sánchez, C., Muñoz, M., Valdés, M., Durán, M.D., 2011. Thermoeconomic optimisation of heat recovery steam generators of combined cycle gas turbine power plants considering off-design operation. Energy Conversion and Management, 52, 1840–1849.

[33] Silveira, J.L., Tuna, C.E., 2004. Thermoeconomic analysis method for optimization of combined heat and power systems—part II. Progress in Energy and Combustion Science, 30, 673–678.

[34] Abusoglu, A., Kanoglu, M., 2009. Exergoeconomic analysis and optimization of combined heat and power production: A review. Renewable and Sustainable Energy Reviews, 13, 2295–2308.

[35] Sahin, B., Kodal, A., Koyun, A., 2001. Optimal performance characteristics of a two-stage irreversible combined refrigeration system under maximum cooling

load per unit total cost conditions. Energy Conversion and Management, 42, 451-465.

[36] Sahin, B., Kodal, A., 2002. Thermoeconomic optimization of a two stage combined refrigeration system: A finite-time approach. International Journal of Refrigeration, 25, 872–877.

[37] Morales, M., Optimization of heat exchanger inventory of a two-stage vapor compression refrigeration cycle, M.Sc. thesis, University of Florida, Florida, 2003.

[38] Misra, R.D., Sahoo, P.K., Sahoo, S., Gupta, A., 2003. Thermoeconomic optimization of a single effect water/LiBr vapour absorption refrigeration system. International Journal of Refrigeration, 26, 158–169.

[39] Misra, R.D., Sahoo, P.K., Gupta, A., 2006. Thermoeconomic evaluation and optimization of a aqua-ammonia vapour-absorption refrigeration system, International Journal of Refrigeration, 29, 47–59.

[40] Rosen, M.A., Dincer, I., 2003. Thermoeconomic analysis of power plants: An application to a coal fired electrical generating station. Energy Conversion and Management, 44, 2743–2761.

[41] Chen, J., Tyagi, S.K., Wu, C., 2003. Optimal design on the performance parameters of an irreversible Carnot heat engine based on the thermoeconomic approach. International Journal of Ambient Energy, 24, 201-206.

[42] Durmayaz, A., Sogut, O.S., Sahin, B., Yavuz, H., 2004. Optimization of thermal systems based on finite-time thermodynamics and thermoeconomics. Progress in Energy and Combustion Science, 30, 175–217.

[43] Chen, L., Sun, F., Wu, C., 2004. Maximum-profit performance for generalized irreversible Carnot-engines. Applied Energy, 79, 15–25.

[44] Tyagi, S.K., Chena, G.M., Wang, Q., Kaushik, S.C., 2006. A new thermoeconomic approach and parametric study of an irreversible regenerative Brayton refrigeration cycle. International Journal of Refrigeration, 29, 1167-1174.

[45] Selbas, R., Kizilkan, O., Sencan, A., 2006. Thermoeconomic optimization of subcooled and superheated vapor compression refrigeration cycle. Energy, 31, 2108–2128.

[46] Kotas, T.J., The Exergy Method of Thermal Plant Analysis, London: Butter-Worths, 1985.

[47] Kizilkan, O., Sencan, A., Kalogirou, S.A., 2007. Thermoeconomic optimization of a LiBr absorption refrigeration system. Chemical Engineering and Processing, 46, 1376–1384.

[48] Kim, D.J., 2010. A new thermoeconomic methodology for energy systems. Energy, 35, 410–422.

[49] Silveira, J.L., Tuna, C.E., de Queiroz Lamas, W., de Castro Villela, I.A., 2010. A contribution for thermoeconomic modelling: A methodology proposal. Applied Thermal Engineering, 30, 1734-1740.

[50] Sayyaadi, H., Nejatolahi, M., 2011. Multi-objective optimization of a cooling tower assisted vapor compression refrigeration system. International Journal of Refrigeration, 34, 243-256.

[51] Wouagfack, P.A.N., Tchinda, R., 2013. Finite-time thermodynamics optimization of absorption refrigeration systems: A review. Renewable and Sustainable Energy Reviews, 21, 524–536.

[52] Mumanachit, P., Comparative Analysis of Low Temperature Industrial Refrigeration Systems, M.Sc. thesis, University of Wisconsin-Madison, USA, 2009.

[53] Rezayan, O., Behbahaninia, A., 2011. Thermoeconomic optimization and exergy analysis of CO_2/NH_3 cascade refrigeration systems. Energy, 36, 888-895.

[54] Zare, V., Mahmoudi, S.M.S., Yari, M., Amidpour, M., 2012. Thermoeconomic analysis and optimization of an ammonia-water power/cooling cogeneration cycle. Energy, 47, 271-283.

[55] Xiong, J., Zhao, H., Zheng, C., 2012. Thermoeconomic cost analysis of a 600 MWe oxy-combustion pulverized-coal-fired power plant. International Journal of Greenhouse Gas Control, 9, 469–483.

[56] Bassily, A.M., 2012. Numerical cost optimization and irreversibility analysis of the triple-pressure reheat steam-air cooled GT commercial combined cycle power plants. Applied Thermal Engineering, 40, 145-160.

[57] Garrett-Price, A.B., Smith, S.A., Watts, R.L., Knudsen, J.G., Marner, W.J., Suitor, J.W., Overview of fouling, in: Fouling of Heat Exchangers,

Characteristics, Costs, Prevention, Control and Removal, Noyes Publications, Park Ridge, NJ, 9–19, 1985.

[58] Steinhagen, R., Muller-Steinhagen, H., Maani, K., 1993. Problems and costs due to heat exchanger fouling in New Zealand industries. Heat Transfer Engineering, 14, 19–30.

[59] Bott, T.R., Fouling Notebook, The Institution of Chemical Engineers, Rugby, England, 1990.

[60] Mwaba, M.G., Golriz, M.R., Gu, J., 2006. A semi-empirical correlation for crystallization fouling on heat exchange surfaces. Applied Thermal Engineering, 26, 440–447.

[61] Merheb, B., Nassar, G., Nongaillard, B., Delaplace, G., Leuliet, J.C., 2007. Design and performance of a low-frequency non-intrusive acoustic technique for monitoring fouling in plate heat exchangers. Journal of Food Engineering, 82, 518–527.

[62] Pahlavanzadeh, H., Jafari Nasr, M.R., Mozaffari, S.H., 2007. Experimental study of thermo-hydraulic and fouling performance of enhanced heat exchangers. International Communications in Heat and Mass Transfer, 34, 907–916.

[63] Cussac, F., Modelling of particulate fouling on heat transfer surfaces: The influence of bubbles on the deposition of Iron Oxide on Alloy-800 heater tubes, M.Sc., University of New Brunswick, Canada, 2007.

[64] Zhenhua, Q., Yongchang, C., Chongfang, M.A., 2008. Experimental study of fouling on heat transfer surface during forced convective heat transfer, Chinese Journal of Chemical Engineering, 16(4), 535-540.

[65] Perez, L., Ladevie, B., Tochon,P., Batsale, J.C., 2009. A new transient thermal fouling probe for cross flow tubular heat exchangers. International Journal of Heat and Mass Transfer, 52, 407–414.

[66] Lalot, S., Palsson, H., Detection of fouling in a cross-flow heat exchanger using a neural network based technique, International Journal of Thermal Sciences, 2010; 49, 675-679.

[67] Lim, E., A preliminary investigation of fouling in brazed plate heat exchangers, M.Sc., Oklahoma State University, USA, 2010.

[68] Sun, J., Surface coating of condenser tubing and CO_2 sparging for preventing fouling and water use reduction, M.Sc., West Virginia University, USA, 2010.

[69] Vessakosol, P., Charoensuk, J., 2010. Numerical analysis of heat transfer and flow field around cross-flow heat exchanger tube with fouling. Applied Thermal Engineering, 30, 1170–1178.

[70] Lei, C., Peng, Z., Day, T., Yan, X., Bai, X., Yuan, C., 2011. Experimental observation of surface morphology effect on crystallization fouling in plate heat exchangers. International Communications in Heat and Mass Transfer, 38, 25–30.

[71] Albert, F., Augustin, W., Scholl, S., 2011. Roughness and constriction effects on heat transfer in crystallization fouling. Chemical Engineering Science, 66, 499–509.

[72] Mohanty, D.K., Singru, P.M., 2011. Use of C-factor for monitoring of fouling in a shell and tube heat exchanger. Energy, 36, 2899-2904.

[73] Izadi, M., Experimental and numerical investigation of fouling in heat exchangers, Ph.D., Clarkson University, USA, 2011.

[74] Mayer, M., Bucko, J., Benzinger, W., Dittmeyer, R., Augustin, W., Scholl, S., 2012. The impact of crystallization fouling on a microscale heat exchanger. Experimental Thermal and Fluid Science, 40, 126–131.

[75] Pak, B.C., Groll, E.A., Braun, J.E., 2005 Impact of fouling and cleaning on plate fin and spine fin heat exchanger performance. ASHRAE Transactions, 111(1), 496-504.

[76] Yang, L., Braun, J.E., Groll, E.A., 2007a. The impact of fouling on the performance of filter-evaporator combinations. International Journal of Refrigeration, 30(3), 489-498.

[77] Yang, L., Braun, J.E., Groll, E.A., 2007b. The impact of evaporator fouling and filtration on the performance of packaged air-conditioners. International Journal of Refrigeration, 30(3), 506-514.

[78] Ali, A.H.H., Ismail, I.M., 2008. Evaporator air-side fouling: Effect on performance of room air conditioners and impact on indoor air quality. HVAC & R Research, 14(2), 209-219.

[79] Pu, H., Ding, G., Ma, X, Hu, H., Gao, Y., 2009. Effects of biofouling on air-side heat transfer and pressure drop for finned tube heat exchangers. International Journal of Refrigeration, 32, 1032-1040.

[80] Bell, I.H., Groll, E.A., 2010. Air-side particulate fouling of microchannel heat exchangers: experimental comparison of air-side pressure drop and heat transfer with plate-fin heat exchanger. Applied Thermal Engineering, 31, 742-749.

[81] Jonsson, G.R., Lalot, S., Palsson, O.P., Desmet, B., Use of extended Kalman filtering in detecting fouling in heat exchangers, International Journal of Heat and Mass Transfer, 2007; 50, 2643–2655.

[82] Siegel, J.A., Particle deposition on HVAC heat exchangers, Ph.D. thesis, University of California, Berkeley, 2002.

[83] Bultman, D.H., Burmeister, L.C., Bortone, V., 1995. Effects of condenser air-flow blockage on vapor-compression refrigerator performance. Journal of Energy Resources Technology, 117, 349-353.

[84] Yang, L., Li, Z.-Y., Shao, L.-L., Zhang, C.-L. Model-based dimensionless neural networks for fin-and-tube condenser performance evaluation. International Journal of Refrigeration, 2014; In Press.

[85] Qureshi, B.A., Zubair, S.M., 2011. Performance degradation of a vapor compression refrigeration system under fouled conditions, International Journal of Refrigeration, 34, 1016-1027.

[86] Qureshi, B.A., Zubair, S.M., 2012a. The impact of fouling on performance of a vapor compression refrigeration system with integrated mechanical subcooling. Applied Energy, 92, 750-762.

[87] Qureshi, B.A., Zubair, S.M., 2012b. The effect of refrigerant combinations on performance of a vapor compression refrigeration system with dedicated mechanical subcooling. International Journal of Refrigeration, 35(1), 47-57.

[88] Curzon, F.L., Ahlborn, B., 1975. Efficiency of a Carnot engine at maximum power. Applied Journal of Physics, 43, 22-24.

[89] Incropera, F. P., DeWitt, D. P., Bergman, T., Lavine, A., 2006. Fundamentals of Heat and Mass Transfer, sixth ed., John Wiley & Sons, Inc.

[90] The Babcock & Wilcox Company. (2005). Steam: its generation and use. (J. B. Kitto & S. C. Stultz, Eds.) 41st ed. The Babcock & Wilcox Company.

[91] Kelley, C.T., 1987. Solving Non-linear Equations with Newton's Method (Fundamentals of Algorithms), Society for Industrial Mathematics.

[92] Demirel, Y., 2007. Nonequilibrium Thermodynamics: Transport and Rate Processes in Physical, Chemical and Biological Systems, second ed., Elsevier Science & Technology Books.

[93] Cengel, Y.A., Boles, M.A., 2005. Thermodynamics: An Engineering Approach, McGraw-Hill., New York, USA.

[94] Kuehn, T.H., Ramsey, J.W., Threlkeld, J.L., 1998. Thermal Environmental Engineering, third ed., Prentice-Hall Inc., New Jersey, USA.

[95] Modera, M., Xu, T., Fesutel, H., *et al*. 1999. Efficient thermal distribution in commercial buildings, Lawrence Berkeley National Laboratory LBNL-41365.

[96] Stoecker, W.F., Jones, J.W., 1982. Refrigeration and Air Conditioning, McGraw-Hill., New York, USA.

[97] Aprea, C., Greco, A., 2003. Performance evaluation of R22 and R407C in a vapor compression plant with reciprocating compressor. Applied Thermal Engineering, 23, 215-227.

[98] Khan, J.R., Zubair, S.M., 2000. Design and rating of dedicated mechanical subcooling vapor-compression system. Proceedings of the Institute of Mechanical Engineers, 214: 455-471.

[99] Cabello, R., Torrella, E., Llopis, R., Sánchez, D., 2010. Comparative evaluation of the intermediate systems employed in two-stage refrigeration cycles driven by compound compressors. Energy, 35, 1274–1280.

[100] Dopazo, J.A., Fernández-Seara, J., 2011. Experimental evaluation of a cascade refrigeration system prototype with CO_2 and NH_3 for freezing process applications. International Journal of Refrigeration, 34, 257-267.

[101] Borges, B.N., Hermes, C.J.L., Gonçalves, J.M., Melo, C., 2011. Transient simulation of household refrigerators: A semi-empirical quasi-steady approach. Applied Energy, 88 (3), 748-754.

[102] Hermes, C.J.L., Melo, C., Knabben, F.T., Gonçalves, J.M., 2009. Prediction of the energy consumption of household refrigerators and freezers via steady-state simulation. Applied Energy, 86 (7-8), 1311-1319.

[103] Waltrich, M., Hermes, C.J.L., Melo, C., 2011. Simulation-based design and optimization of refrigeration cassettes. Applied Energy, 88 (12), 4756-4765.

[104] Federov, A.G., 2004. Personal Correspondence.

[105] Buckingham, E., 1914. On physically similar systems; Illustrations of the use of dimensional equations. Physical Review, 4, 345-376.

[106] Sabersky, R.H., Acosta, A.J., Hauptmann, E.G., Gates, E. M., 1999. Fluid Flow: A First Course in Heat Transfer, fourth ed., Prentice-Hall Inc., New Jersey, USA.

Vitae

Name:	Bilal Ahmed Qureshi
Nationality:	Pakistani
Date of Birth:	August 4th, 1978
Email:	baqureshi78@yahoo.com
Address:	H. # 4, St # 7, Safari Villas, Rawalpindi, PAKISTAN.
Academic Background:	B.E. (Mechanical Engineering), October 2000, NUST, Pakistan
	M.Sc. (Mechanical Engineering), April 2004, KFUPM, KSA
Work Experience:	Lecturer, 11/2005 – 12/2009, NUST, Pakistan

Publications:

1. **Qureshi**, **B.A.**, Zubair, S.M., The impact of fouling on the condenser of a vapor compression refrigeration system: An experimental observation, *Int. J. Refrigeration*, 38, pp. 260-266, **2014**.
2. **Qureshi**, **B.A.** et al. Experimental energetic analysis of a vapor compression refrigeration system with dedicated mechanical sub-cooling, *Applied Energy*, 102, pp. 1035-1041, **2013**.
3. **Qureshi**, **B.A.**, Zubair, S.M., Cost optimization of heat exchanger inventory for mechanical subcooling refrigeration cycles, *Int. J. Refrigeration*, 36, pp. 1243-1253, **2013**.
4. **Qureshi**, **B.A.**, Zubair, S.M., Mechanical sub-cooling vapor compression systems: Current status and future directions, *Int. J. Refrigeration*, 36, pp. 2097-2110, **2013**.
5. **Qureshi**, **B.A.** et al. Design and performance evaluation of reverse osmosis desalination systems: An emphasis on fouling modeling, *Applied Thermal Engineering*, 60, pp. 208-217, **2013**.
6. Al-Sarkhi, A., Sarica, C., **Qureshi, B.A.**, Modeling of droplet entrainment in co-current annular two-phase flow: A new approach, *Int. J. Multiphase Flow*, 39, pp. 21-28, **2012**.

7. **Qureshi, B.A.**, Zubair, S.M., The Effect of Refrigerant Combinations on Performance of a Vapor Compression Refrigeration System with Dedicated Mechanical Subcooling, *Int. J. Refrigeration*, 35, pp. 47-57, **2012**.
8. **Qureshi, B.A.**, Zubair, S.M., Performance Degradation of a Vapor Compression Refrigeration System with Integrated Mechanical Sub-Cooling under Fouled Conditions, *Applied Energy*, 92, pp. 750-762, **2012**.
9. **Qureshi**, **B.A.,** Zubair. S.M., A Unified Approach to Predict Evaporation Losses in Evaporative Heat Exchangers, *Int. J. Refrigeration*, 34, pp. 1866-1876, **2011**.
10. **Qureshi, B.A.**, Zubair, S.M., Performance Degradation of a Vapor Compression Refrigeration System under Fouled Conditions, *Int. J. Refrigeration*, 34, pp. 1016-1027, **2011**.
11. **Qureshi, B.A.**, Zubair, S.M., Prediction of Evaporation Losses in Evaporative Fluid Coolers, *Applied Thermal Engineering*, 27(2-3), pp. 520-527, **2007**.
12. **Qureshi, B.A.**, Zubair, S.M., Second-law-based Performance Evaluation Of Cooling Towers and Evaporative Heat Exchangers, *Int. J. Thermal Sciences*, 46(2), pp. 188-198, **2007**.
13. **Qureshi, B.A.**, Zubair, S.M., The Impact of Fouling on Performance Evaluation of Evaporative Coolers and Condensers, *Int. J. Energy Research*, 29(14), pp. 1313-1330, **2005**.
14. Zubair, S.M., **Qureshi, B.A.**, A Probabilistic Fouling and Cost Model for Plate-and-Frame Heat Exchangers, *Int. J. Energy Research*, 30(1), pp. 1-17, **2006**.
15. **Qureshi, B.A.**, Zubair, S.M., An Improved Non-dimensional Model of Wet Cooling Towers, *J. Process Mechanical Engineering*, 220(1), pp. 31-41, **2006**.
16. **Qureshi, B.A.**, Zubair, S.M., A Comprehensive Design and Rating Study of Evaporative Coolers and Condensers – Part I; Performance Evaluation, *Int. J. Refrigeration*, 29(4), pp. 645-658, **2006**.
17. **Qureshi, B.A.**, Zubair, S.M., A Comprehensive Design and Rating Study of Evaporative Coolers and Condensers – Part II; Sensitivity Analysis, *Int. J. Refrigeration*, 29(4), pp. 659-668, **2006**.
18. **Qureshi, B.A.**, Zubair, S.M., Prediction of Evaporation Losses in Wet Cooling Towers, *Heat Transfer Engineering*, 27(9), pp. 86-92, **2006**.
19. **Qureshi, B.A.**, Zubair, S.M., A Complete Model of Wet Cooling Towers with Fouling in Fills, *Applied Thermal Engineering*, 26(16), pp. 1982-1989, **2006**.
20. Khan, J.R., **Qureshi, B.A.**, Zubair, S.M., A Comprehensive Design and Performance Evaluation Study of Counter Flow Wet Cooling Towers, *Int. J. Refrigeration*, 27(8), pp. 914-923, **2004**.
21. **Qureshi, B.A.**, Zubair, S.M., Exergy Analysis of Various Psychrometric Processes, *Int. J. Energy Research*, 27(12), pp. 1079-1094, **2003**.

Conferences:

1. Fourth Saudi Scientific Conference held at Makkah, 29th April – 2nd May, 2013.